PALEOMAGNETIC CHARACTERISATION OF PRECAMBRIAN BASEMENT ROCKS AND THEIR ASSOCIATED OROGENIC EVENTS IN SOUTHWESTERN NIGERIA

BY

CYRIL CHIBUEZE, OKPOLI

Matric. No. 135997

B.Sc. Geology (Akungba - Akoko), M.Sc. Applied Geophysics (Ibadan)

A thesis in the Department of Geology,
Submitted to the Faculty of Science
In partial fulfilment of the requirements for the Degree of

DOCTOR OF PHILOSPHY

of the

UNIVERSITY OF IBADAN

September, 2021

CERTIFICATION

I certify that this work was carried out by Mr. C. C. Okpoli in the Department of Geology, University of Ibadan

…….

Supervisor
M. A. Oladunjoye
B.Sc. (Ado-Ekiti), M.Sc., Ph. D (Ibadan)
University of Ibadan, Nigeria

DEDICATION

This thesis is dedicated to the Father, the Son and the Holy Spirit

ACKNOWLEDGEMENTS

Inspite of all odds, I give all glory to God, because without HIS infinite wisdom and blessings this PhD programme would not be a success. Thank you Lord for your grace and sufficiency throughout this doctoral programme.

I want to sincerely give my thoughtful appreciation to my supervisor Dr. Michael Adeyinka Oladunjoye for his inspiring guidance, constant encouragement, and patiently supporting me with his knowledge and experience during the entire span of my doctoral research. Thanks to the HOD of Geology department Prof. O.A. Ehinola and the Subdean Postgraduate College Dr. A.S. Olatunji as well as coordinator of the postgraduate studies in the department Dr. I.A. Oyediran and Dr. O.O. Osinowo respectively. I am grateful to the following lecturers: Prof. A.I. Olayinka, Prof. G.O. Adeyemi, Prof. M.N. Tijani, Prof. O A. Okunlola, Prof. M.E. Nton, Dr. O.A. Boboye, Dr. A.T. Bolarinwa, Dr. O.O. Omitogun, Dr. O.C. Adeigbe, Dr. A.M. Adeleye, Dr. F.F. Ajayi, Dr. A. Jayeoba, Dr. J.A. Aladejana. Dr. O.K.Aromolaran and Miss Oluwatoyin Ajilore for their eagerness to serve during my presentation and for their priceless constructive critiques to the successful completion of this study. The non-teaching staff are highly acknowledged for their services.

Many thanks to eminent Professor of Paleomagnetism, Prof. Emilio Herrero-Bervera at University of Hawaii at Manoa (SOEST-HIGP), Honolulu, USA. During my PhD fellowship/internship, he ensured that I understand all the fundamentals of paleomagnetism; fortunate to having been associated with him here at the institute. Grateful for his participation in field trips to Makapou scenic points under National

science foundation grants. I owe my sincere appreciation to Prof. Shiv Sharma, Dr. Misra K. Anupam and Dr. Tayro Acosta-Maeda for exposure into Material Physics in the infrared and Raman spectroscopy. Many thanks to James Lau paleomagnetic laboratory technician for his expertise in Spinner magnetometer and AF demagnetizer, for maintaining a cheerful atmosphere in the laboratory for generating good data, swapping data sets among us; as well as being accommodating during my stay.I also wish to thank all other research scholars of SOEST-HIGP for helping me directly or indirectly during my stay at the institute.

Also said and unsaid blessings and homely support of Mrs. Amgrace Cyril, my wife, friend, sweetheart, confidant as well as her understanding during my PhD research work. Many thanks for my daughters Peaceful-Haven Cyril and Reighner-Crystal Cyril for their prayers, unflinching love and family members without whom I would not have achieved this goal. It is the constant sacrifice and ceaseless encouragements of my wife that made it possible for me to realize my goals and dreams.

I appreciate the management of Adekunle Ajasin University for awarding me with the NEEDS assessment grant and support of all my colleagues at the Department of Earth sciences and Faculty of Science. I would like to thank my pastors (Joseph and Adeyinka Ezire; Leafe and Florence Amosa) of Christ Embassy Akure and Hawaii, Deacon and Deaconess Ikuna, Bro and Sis Uzama, Bro and Sis Boman Avang, African American military folks at the Latin Hawaii FC and all my brethren from Loveworld Nation for all their care and support.

ABSTRACT

Paleomagnetic characteristics of iron-oxide in Precambrian Basement rocks documents orogenic events in those rocks and has been used to decipher the evolution of such rocks world-wide. Previous studies on paleomagnetism of rocks in Nigeria concentrated mainly on microstructures and Curie temperatures with little or no emphasis on continental drifts that are important for correlation of rocks globally, direction of movements and reconstruction of ancient continents. This work was aimed to determine the magnetic character, evolution, orientation of microstructures and paleomagnetic pole positions of Precambrian rocks associated with orogenic events in southwestern Nigeria.

Precambrian Basement rocks samples collected from 110 locations in southwestern Nigeria were cylindrically cored into 25 mm by 22 mm specimen. Eighty-two of these rock samples were cut into fabrics and polished sections for the determination of magnetic mineralogy using Raman spectroscopy, scanning electron microscopy and Electron Probe Microanalyzer (EPMA). The Curie temperatures of the rock specimens were measured using multifunctional Kappabridge. Anisotropy of Magnetic Susceptibility (AMS) measurements were carried out to determine the microstructures in the cored samples. The cored rocks were subjected to paleomagnetic measurements using Alternating Field (AF) and thermal demagnetisers. The poles direction of the demagnetised cored samples was determined using cryogenic and JR5 spinner magnetometer. Day plots, First Order Reversal Curves (FORCs), backfield remanence and hysteresis loops of the rock samples were determined using Princeton vibrating sample magnetometer.

The magnetic mineralogy of iron-oxide minerals in Precambrian Basement rocks (gneisses, schists and granites) revealed mostly maghemite, magnetite and titanomagnetite minerals with their Curie temperatures of 590-600°C, 575-585°C and 360-410°C, respectively. Iron oxide composition of maghemite which is the most predominant was 74.6%. Magnetic foliations were exhibited and striked dominantly in the NE-SW (32.9°-252.9°) direction with moderate to steep dip angles and lineation plunging 8° to 86° to the NE/ENE direction. The foliation poles defined a girdle pattern with a zone axis (52/11) close to the best line of the lineation (44/21). The microstructures of the rocks had suffered deformation from the magmatic state to the high temperature solid-state due to tectono-metamorphic events. A positive inclination in the northwest direction, which corresponded to the paleomagnetic pole of Pan-African was identified. Isolated locations with paleomagnetic discrepancies were observed at >530℃, which indicated Pan-African regional remagnetisation of the granitoids in the Trans- Saharan province. These suggested high mantle activity, a true polar Wander drifts towards the equator and the amalgamation of the Rodinia supercontinent. The Day plots and FORCs showed Pseudo-single domain and multi-domain phases. The backfield remanence and hysteresis loops showed narrow-waisted loops which, generally indicated ferromagnetic to paramagnetic Precambrian Basement rocks.

The ferromagnetic to paramagnetic maghemite, magnetite and titanomagnetite in the Precambrian Basement rocks of southwestern Nigeria bear evidences of tectono-metamorphic events in the Pan-African. The resultant microstructural deformation and orientation, remagnetisation and True Polar Wander drifts of the paleomagnetic pole move towards the equator.

Keywords: Precambrian rocks, Microstructures, Magnetic mineralogy, Remagnetisation, Paleomagnetic pole

Word count: 478

TABLE OF CONTENTS

Title page i

Certification ii

Dedication iii

Acknowledgements iv

Abstract vi

Table of contents vii

List of Tables xii

List of Figures xiii

Abbreviations xviii

CHAPTER ONE INTRODUCTION

1.1 Background to the study 1

1.2 Problem statement 3

1.3 Research Justification 4

1.4 Aim and objectives of study 4

1.5 Significance of Research 5

1.6 Scope of the thesis 5

1.7 Location map 6

CHAPTER TWO LITERATURE REVIEW

2.1 Review of the regional geological setting 8

2.2 Supercontinent paleogeographies 13

2.2.1 Rodinia reconstructions 13

2.2.2 Congo craton in Rodinia 14

2.2.3 The West African craton 17

2.2.4 Gondwana configuration 17

2.2.5 Precambrian basement complex of Nigeria 23

2.2.5.1 Structural geology 27

2.2.5.1.1 Folds 27

2.2.5.1.2 Joint 29

2.2.5.1.3 Foliation 29
2.2.5.1.4 Vugs 30
2.2.5.1.5 Lineation 30
2.2.5.6 Fractures 30

2.3 Literature reviews 32
2.3.1 Thermomagnetic/ temperature dependence 32
2.3.2 Emplacement directions and anisotropy of magnetic susceptibility 32
2.3.3 Raman infrared spectroscopy fingerprinting 33
2.3.4 Microstructures 33
1.8.5 Scanning Electron Microprobe 33
1.8.6 Electron Probe Microanalyser 34
1.8.7 Apparent polar wandering paths 34
1.8.8 Geocentric axial dipole in the Precambrian 34
1.8.9 Day plots, hysteresis loops and first order reversal curves 35
2.4 Theories of method used 36
2.4.1 Thermomagnetic/ temperature dependence 36
2.4.2 Emplacement direction, microstructures and magnetic susceptibility 37
2.4.3 Raman spectroscopy 39
2.4.4 Scanning electron microprobe, electron microprobe analysis and X-ray diffraction 39
2.4.5 Day plots, hysteresis loops and FORCs 41
2.4.6 Apparent polar wandering paths APWPs and GPTS 46
2.4.6.1 Demagnetization 46
2.4.6.2 Determination of paleomagnetic direction and pole 46
2.4.6.3 Field test and paleomagnetic stability 52
2.4.6.3.1 Reversal test 52
2.4.6.3.2 Baked contact test 52
2.4.6.3.3 Regional consistency 52
2.4.6.4 Paleolatitude reconstruction 53
2.4.6.4.1 Comparison between two cratons 54
2.4.6.5 Magnetism and Paleomagnetism 56

2.4.6.5.1 Types of magnetic materials 56
2.4.7 Magnetic methodology 59
2.4.7.1 Ferromagnetic phasesIdentification 59
2.4.7.1.1 Alternating field demagnetization (AF) 59
2.4.7.11.2 Acquisition of Isothermal Remanent Magnetization (IRM) 59
2.4.7.1.1.3 Thermal demagnetization of the magnetization (TD) 60

CHAPTER THREEMATERIALS AND METHODS 61

3.1 Materials used for the field sampling 61
3.2 Materials used for the laboratory analyses 61
3.3 Methods 61
3.3.1 Paleomagnetic sampling 65
3.3.2 Laboratory Methods 68
3.3.2.1 Micro-Raman spectroscopy 68
3.3.2.2 Geochemistry (XRF AND ICP-MS) 71
3.3.2.3 Scanning Electron Microscopy and Electron Probe Microanalyser 71
3.3.2.3.1 Sample preparation 72
3.3.2.4 XRD 72
3.3.2.5 AGICO MFK1-FA Kappabridge 75
3.3.2.5.1 Anisotropy of Magnetic Susceptibility (AMS) 75
3.3.2.5.2 Thermomagnetic 78
3.3.2.6 Shielded AF and Thermal Demagnetizer 80
3.3.2.6.1 Demagnetization techniques 82
3.3.2.6.1.1 Analysis of remanent magnetization components 83
3.3.2.7 Impulse magnetizer 83
3.3.2.8 Molspin Spinner magnetometers 86
3.3.2.7 Vibrating Sample Magnetometer (VSM) 90

CHAPTER FOURRESULTS AND DISCUSSION 93
4.0 Preamble 93
4.1 Mineral composition and Raman infrared spectroscopy of the study area 93
4.1.1 Petrofabric Mineralogy 107

4.1.1.1 X-ray fluorescence 107
4.1.1.2 Electron Probe Microanalyser analyses 107
4.1.1.3 Scanning Electron Microprobe 111
4.1.1.4 X-ray Diffractometry 111
4.2 Thermomagnetic (temperature dependence) 115
4.3 Microstructural Emplacement 123
4.3.1 Evolution of the tectono-metamorphic andImplications for emplacement of the plutons 149
4.4 Paleogeographic reconstructions using Palaeomagnetic Results 156
4.4.1 Alternating field and thermal demagnetizations 156
4.4.1.1 Occurrence of Exsolved Maghemite in whole rock Analysis 156
4.4.1.2 Paleomagnetic pole magnetic components 166
4.4.1.3 Southwestern Nigeria paleomagnetic pole age 169
4.4.1.4 Southwestern Nigeria Pan African apparent polar wander path (APWP) 172
4.4.1.5 Demagnetization behaviours 174
4.4.1.6 Remagnetization age 182
4.4.1.7 Geochronological and paleomagnetic mechanisms 184
4.5 Day plots, hysteresis loops, first order reversal curves (FORCs) 187
4.6 Discussions 199

CHAPTER FIVECONCLUSIONS AND RECOMMENDATIONS 207
5.1 Conclusions 207
5.2 Recommendations 211
5.3 Contributions to Knowledge 211
References 213
Appendix 238

LIST OF TABLES

Table 2.1	Characters of iron oxides	58
Table 3.1	Coordinates of rock samples used for AMS analysis	77
Table 3.2	Coordinates of rock samples used for thermomagnetic analysis	79
Table 3.3	Cored samples used for paleomagnetic analyses	88
Table 4.1	Raman Spectra of Biotite granite gneiss, granite and charnockite for Maghemite	96
Table 4.2	Interatomic potentials, estimated and observed properties, estimated and experimental wavenumbers for maghemite	97
Table 4.3	Chemical analysis of granitoids from southwestern Nigeria (XRF)	109
Table 4.4	Electron Probe Microanalyser of maghemite from Biotite granite gneiss and potassium feldspar and albite in Granitoids	110
Table 4.5	Anisotropy of magnetic susceptibility of Gneiss	126
Table 4.6	Anisotropy of magnetic susceptibility of Aplite dyke	129
Table 4.7	Anisotropy of magnetic susceptibility of Granite	132
Table 4.8	Anisotropy of magnetic susceptibility of Diorite	136
Table 4.9	Anisotropy of magnetic susceptibility of Granite gneiss	138
Table 4.10	Anisotropy of magnetic susceptibility of Charnockites	142
Table 4.11	Anisotropy of magnetic susceptibility of Granite	145
Table 4.12	Anisotropy of magnetic susceptibility of Banded gneiss	147
Table 4.13	Alternating field demagnetization results	159
Table 4.14	Thermal demagnetization results	160
Table 4.15	Tectono-metamorphic history of Nigerian shield	167
Table 4.16	Isochron ages of Nigerian shield	167
Table 4.17	Paleomagnetic results (AF) for Southwestern Nigeria granitoids	170
Table 4.18	Paleomagnetic results (Thermal) for Southwestern Nigeria granitoids	171
Table 4.19	Recalculated paleomagnetic results	173

LIST OF FIGURES

Figure 1.1	Location map of the study area	7
Figure 2.1	Regional geological map of Trans-saharan metacraton/shield	11
Figure 2.2	Geological map of southwestern Nigeria	12
Figure 2.3	Maps for Rodinia according to different models described in the text all in a North American reference frame	16
Figure 2.4	Gondwana map with its cratonic nuclei positions	21
Figure 2.5	West Africa Cratonic map with its neighbouring cratons and mobile belts in a pre-Atlantic fit	22
Figure 2.6	(a) Symmetrical (b) Asymmetrical and (c) Recumbent folds	28
Figure 2.7	(a) Parallel joint (b) Master joint(c) Foliation(d)solution hole	31
Figure 2.8	Examples of correlation by varied AMS measurements of magnetic parameters	38
Figure 2.9	Hysteresis loops measurements	42
Figure 2.10	Magnetic hysteresis	43
Figure 2.11	Characterization of magnetic hysteresis	45
Figure 2.12	Lambert *equal-area* stereographic in grey	49
Figure 2.13	3D Zijderveld diagram and vector	50
Figure 2.14	Probability of overlapped demagnetized spectra	51
Figure 2.15	West Africa craton reconstruction at 600±150 Ma with the Southwestern Nigeria pole	55
Figure 2.16	Schematic depiction of the net magnetization in ferromagnetic materials Behavior of paramagnetic and diamagnetic material	57
Figure 3.1	Location map of the study area and sampled points	62
Figure 3.2a	interpretation flowchart	63
Figure 3.2b	Flowchart of workflow	64
Figure 3.3	A: Sampling with a handy rock machine driller B: Orienting rock. C: Drilled rocks. D: cylindrical rocks E: Coring syenite dike	67
Figure 3.4.	A-B. Kaiser 785nm micro-Raman Microprobe.C-F: Renishaw inVia 830 nm	70
Figure 3.5	SEM instrument	74
Figure 3.6	(a-b) Multifunctional Kappabridge (MFKI-FA) in Liquid Nitrogen and Argon gas environment	76

Figure 3.7	Thermal Demagnetizer MMTD80A and shielded Molspin Alternating Field demagnetizer	81
Figure 3.8	Impulse Magnetizer	85
Figure 3.9	Spinner magnetometer and its auto manipulations of six directions	89
Figure 3.10	Vibrating Sample Magnetometer (VSM)	91
Figure 4.1	(a-b) Raman maps and phase distribution inferred from additional 2D map, ID lines and single point measurement studied on biotite granite gneiss (BGG) and (a) Photomicrograph of biotite granite gneiss under PPL (b) photomicrograph of biotite granite gneiss under XPL	95
Figure 4.2	Biotite granite gneiss with 830nm In Via Renishaw micro-Raman all scaled 3x for clarity	99
Figure 4.3	(a) Raman maps and phase distribution 2D map of granite (a) Photomicrograph of granite under PPL (b) Photomicrograph of granite under XPL	101
Figure 4.4	Granite with 785nm Micro-raman microprobe all scaled 3x for clarity	103
Figure 4.5	Photomicrograph of charnockite	105
Figure 4.6	Charnockite with 785nm Micro-raman microprobe all scaled 3x	106
Figure 4.7	SEM results of magnetic minerals (JEOLJSM-5900LV)	113
Figure 4.8	XRD of some basement rocks (a) Alagbaka granite (b) Owo-Ago panu gneiss(c) Oda road Charnockite from the study area	114
Figure 4.9	Thermomagnetic curves of granites	116
Figure 4.10	Thermomagnetic curves (a) Quartzite and (b) Gbede BIF(c) Porphyritic granite (d) Porphyritic granite (e) Augen gneiss (f) Augen gneiss	117
Figure 4.11	Thermomagnetic curves (a) Banded gneiss (b) Banded gneiss (c) Biotite granite gneiss (d) Phyllite	119
Figures 4.12	Thermomagnetic curves (a) Charnockite (b) Charnockite (c) Charnockite (d) Charnockite (e) Granite gneiss (f) Granite gneiss (g) Granite gneiss (h) Granite gneiss	122
Figure 4.13	(a-c) Granite gneiss exsolution of albite in microcline, slight and Strong bend in twin lamellae in plagioclase, (d-f) Hornblende	

grains showing twinned and untwined cluster, microcracks, in feldspar healed with quartz, microcracks in microcline (g-i) Gneiss cut perpendicular to foliation and parallel to magnetic Lineation and also cut parallel to foliation and lineation; perpendicular to foliation and lineation. 124

Figure 4.14 Foliation (equidistant, stereographic, orthographic and equal area), Lineation (equidistant, stereographic and orthographic) and equal area circular histogram of Gneiss microstructures 127

Figure 4.15 Foliation (equidistant, stereographic, orthographic and equal area), Lineation (equidistant, stereographic and orthographic) and equal area circular histogram of Aplite dyke microstructures 130

Figure 4.16 Foliation (equidistant, stereographic, orthographic and equal area), Lineation (equidistant, stereographic and orthographic) and equal area circular histogram of Granite 1 microstructures 133

Figure 4.17 Foliation (equidistant, stereographic, orthographic and equal area), Lineation (equidistant, stereographic and orthographic) and equal area circular histogram of diorite microstructures 135

Figure 4.18 Foliation (equidistant, stereographic, orthographic and equal area), Lineation (equidistant, stereographic and orthographic) and equal area circular histogram of Granite gneiss microstructures 139

Figure 4.19 Foliation (equidistant, stereographic, orthographic and equal area), Lineation (equidistant, stereographic and orthographic) and equal area circular histogram of Charnockite microstructures 141

Figure 4.20 Foliation (equidistant, stereographic, orthographic and equal area), Lineation (equidistant, stereographic and orthographic) and equal area circular histogram of Banded gneiss microstructures 148

Figure 4.21 (A) Model showing tectono-regional metamorphism relationship: Ridges and rift valleys- described by intense geothermal gradients contact and metamorphosed ocean floor. (B-C) Regions of magmatic movement; volcanic - plutonic complexes: greenschists amphibolites granulites. Regions of thickening of the crust and orogeny: greenschists amphibolites (MP+LT and MP+HT) granulites (HP+HT) and type B

eclogites 152
Figure 4.22 (a) Pre-orogenic setting: subduction/back-arc basin (1-0.640Ga) (b) Phase D1: crustal redoubling and thickening-early thrusting/nappe 1 (0.640-0.630Ga) 154
Figure 4.22 (c) Phase D2: Crustal shortening and thickening-upright to recline fold/Nappe2 (0.600Ga) (d) Phase D: Conjugate wrench movement at the prong front (0.585-0.580Ga 155
Figure 4.23 Site mean directions of Biotite granite gneiss, gneiss and granite gneiss 157
Figure 4.24 (A) African craton displayed in present position. (B) Spline Apparent pole wandering APW of Africa pole (c)VGP reconstruction of Africa database (B)fit with Africa, taking account of the opening of the south Atlantic. (d) The corrected NW Africa 163
Figure 4.25 (A) Plotted new VGP from SW Nigeria (B)Reconstructed VGP for SW Nigeria Merged with NW Africa (c) VGPs stereogram of SW Nigeria shield (d) Reconstructed to present Coordinates 164
Figure 4.26 Alternate field demagnetization showing zijdervield orthogonal vectorization using DAIE 175
Figure 4.27 Thermal demagnetization showing zijdervield orthogonal vectorization 176
Figure 4.28 Thermal demagnetization showing zijdervield orthogonal vectorization 178
Figure 4.29 AF demagnetization showing zijdervield orthogonal vectorization 180
Figure 4.30 AF demagnetization showing zijdervield orthogonal vectorization 181
Figure 4.31 Recent concordia plot of uranium-lead zircon data of Iwo syenite, southwestern Nigeria 186
Figure 4.32 (a) SD, PSD and MD plot after Day plot *et al*. (1970) 188
Figure 4.33 Narrow waisted hysteresis loops of (b)Amphibolite(c) biotite granitegneiss (d)charnockite(e) charnockite (f) granite (g) granite 189
Figure 4.34 (a) FORC diagrams of PSD behaviour; (b) linear and

Gaussian cumulative measurements respectively having dominance of decreasing magnetic grain size of maghemite and hematite and (c) Examples of chip and powder specimen for hysteresis loops after applying correction to a linear gradient of paramagnetism 191

Figure 4.35 Linear acquisition plot, gradient of acquisition plot and thermal demagnetization of isothermal remanent magnetization obtained dc fields of 3 T for (a,a1)granite and (b,b1) aplite intrusive rock. Specimens were treated with AF demagnetizer at 100 mT 193

Figure 4.36 Linear acquisition plot, gradient of acquisition plot and thermal demagnetization of isothermal remanent magnetization obtained dc fields of 3 T for (b,b1) aplite intrusive rock. specimens were treated with AF demagnetizer at 100 mT 195

Figure 4.37 First Order Reversal Curves (FORCs) (A) Amphibolite (B) Banded Gneiss (C) Biotite granite (D) Charnockite (E) Granite 197

Figure 4.41 First Order Reversal Curves (FORCs (C) Biotite granite (D) Charnockite (E) Granite 198

Abbreviations

AF -Alternating Field

AMS -Anisotropy of Magnetic Susceptibility

APWP- Apparent Polar Wander Path

ChRM -Characteristic Remanent Magnetization

CRM -Chemical Remanent Magnetization

GAD- Geocentric Axial Dipole

HC_HT -High Coercivity and High Temperature

IRM Isothermal Remanent Magnetization

LATEA-Laouni terrane Algeria

LC_LT -Low Coercivity and Low Temperature

LF -Lowrie-Fuller

MAD -Maximum Angular Deviation

MD -Multi-Domain

MDF- Median Destructive Field

NRM -Natural Remanent Magnetization

PCA Principal Component Analysis

PDF- Present-Day Earth's Magnetic Field

PDFs -Planar Deformation Features

PFs -Planar Fractures

PSD -Pseudosingle-Domain

REM -NRM/SIRM

SD -Single-Domain

SEM -Scanning Electron Microscope

SIRM -Saturation Isothermal Remanent Magnetization

SP -Superparamagnetic

TH -Thermal

TRM -Thermo-Remanent Magnetization

VGP -Virtual Geomagnetic Pole

VRM -Viscous Remanent Magnetization

XRD- X-ray Diffraction

XRF -X-ray Fluorescence

χ -Bulk Suseptibility

Ms -Saturation Magnetization

Mrs -Saturation Remanent Magnetization

Hc -Coercivity

Hcr -Coercivity of remanence

$\alpha 95$ -95% confidence limit

D -Declination

I -Inclination

Tc -Curie point

GPa -gigapascals

k -Fisher's precision parameter

ka -kiloannum

Ma -Million years

K_1 -Maximum susceptibility axes

K_2 -Intermediate susceptibility axes

K_3 -Minimum susceptibility axes

P/ -Corrected degree of anisotropy

T -Shape parameter

dc -Direct current

CHAPTER ONE
INTRODUCTION

1.1 Background to the study

Iron-oxide minerals are significant to geomagnetism, paleomagnetic and magnetic studies on the environment because of their existence in the magnetic phases on Earth and behave as vital recorders of the paleomagnetic activities (Lindsley, 1991; Rohrbach *et al*., 2007). The properties of iron–oxide minerals are magnetic, thermodynamic and electrical which are influenced by the concentration and distribution of Fe amid sites of different symmetry in the structure (Lindsley, 1976). Studies on rock magnetic properties are carried out, to see whether variation in their molecular structures, morphologies, Curie temperatures, mineral phases can be used for their identification. Recent innovations in integrated Raman spectroscopy, Scanning Electron Microscope (SEM), X-ray Diffractometry (XRD), temperature dependence, Electron Probe Microanalyser (EPMA) are rarely used for characterization of metamorphic and igneous rocks for rock magnetic studies. Globally, temperature dependence (Curie points) is generally utilized for measurements of their magnetic phases (Gehring *et al*., 2009). Nonetheless, Curie temperatures largely reveal bulk properties of the rock without understanding of the modifications of minute grains or intra-grain configuration in the rock specimen while SEM, electron backscatter diffraction, EPMA techniques and X-ray diffraction are capable of determining minute grains of iron oxides (Gehring *et al*., 2009).

The presence of iron-oxide in Neoproterozoic (Pan-African) time (1000 – 542 Ma) have been remarkable for its unfathomable and important Eras of Earth history in rock formation. The dynamism of Pan African times led to series of crust formation and the break-up of supercontinent Rodinia and formation of supercontinent Gondwana (Meert *et al*., 1995). It led to the Cambrian evolutionary explosion and the late Neoproterozoic rock

record contains evidence for the existence of granitoids and marine glaciers at low to near-equatorial palaeolatitudes (Evans, 2009).

The proven quantitative technique to examine the mobile nature of continents through geological time horizontally is Paleomagnetism. Paleomagnetic studies offer preliminary documents of the mobility of the continents over the surface of the Earth resulting in plate tectonics theory (Wingate and Giddings, 2000). These continents are borne out of sole continent called Pangea, which was believed to have been formed around 280 Ma. The non-existence of earlier oceanic margins and their magnetic anomalies, makes the position of the continents before the evolution of Pangea problematic. The plate tectonics resulted to the creation of supercontinents or numerous "single continents" as revealed by studies on paleomagnetism. Rodinia supercontinent evolved after Pangea and was formed during 1000 Ma (Neoproterozoic times). Archean supercontinent existence is hypothetical due to paucity of paleomagnetic dataset and the intricacies involved in acquiring characteristically-stable Precambrian rock paleomagnetic poles. Continental paleogeography and paleomagnetic evidence before Pangea are scarcely distributed despite vast researches by paleomagnetists recently.

Preliminary geochronology, petrology and structural studies on the Nigerian basement complex were studied in the 1900s by the following researchers: Snelling, 1964; Tougarinov *et al*., 1968; Oversby, 1975; Pidgeon *et al*., 1976; Tubosun *et al*., 1984; Rahaman, 1988; Lar, 1988; Dada *et al*., 1989; Dada and Respaut, 1989; Dada *et al*., 1993; Kuster, 1995; Ferre *et al*., 1996; Ekwueme and Kroner, 1998; Ferre *et al*., 2002 but there were no paleomagnetic studies carried out in Nigeria's southwestern basement complex. Their findings have significant impacts on the Nigeria's basement complex during the Paleoproterozoic (2500 – 1600 Ma), but lacks paleomagnetic data in the Precambrian; despite its large surface area.

The orogeny of granitoids in the Precambrian are connected in space and time as well as unravel levels of orogenic belts and their deformations through Pan African orogeny (500 ± 150 Ma). This correlation occurs in a several geologic terrains (Liegeois *et al*., 2003).

Controversies arise owing to the correlation between plate movement and Neoproterozoic intrusions than the recent paradigms. The Pan African rocks reveal sinistral or dextral sense of motion across the basement rocks in the southwestern Nigeria. The acquisition of Paleoproterozoic geomagnetic accounts in iron oxide minerals are of vital essence because it serves as magnetic recorder that retain the natural remanent magnetization (NRM) for billions of years.

The small differences (anisotropy) recorded in Precambrian rocks are unravelled through Anisotropy of Magnetic Susceptibility (AMS) studies. The structure and evolution of the southwestern Nigeria's Precambrian basement rocks; as well as occurrence and magnetic properties of iron-oxides within Pyroxenes and Plagioclases in Paleoproterozoic gneissic and Pan Africandirections could be due to episodes of tectono-metamorphism and remagnetizations in the terranes. Thermal and alternate frequency demagnetizations of the whole rock crystals, tiny magnetic crystal and rock fabrics and the constraints due to their remagnetizations could be reconstructed with the paleomagnetic data.

This study involves baseline rock magnetism characterization (varieties of remanence; low-field susceptibility measurements; iron-titanium oxide mineralogy based on its crystallization temperatures and alteration, composition of magma and viscosity processes) of Nigeria's southwestern basement complex in order to decipher its paleomagnetic characteristics.

1.2 Problem Statement

The Basement complex rocks of Southwestern Nigeria have not been studied adequately in respect to paleomagnetic characterization as evidenced in previous works. There are scarcity of information/data on: Raman infrared spectroscopy fingerprinting on iron-oxide of the Basement rocks; microstructural orientation direction of southwestern Precambrian rocks; temperature dependence of the studied rocks; continental drifts/Apparent polar wandering paths and the pole positions of their natural remanence and magnetic hysteresis and their phases.

Paleomagnetic studies on Precambrian rocks of Southwestern Nigeria are extremely

problematic because of its internal magnetic structures and remagnetizations. More so, the character of these magnetic minerals that serve in the positioning, orientation, microstructures and evolution of these Precambrian rocks is limited. Hence, there is need for: new insights into unlocking the rock magnetic characterization; magnetic susceptibility/behaviour and paleomagnetism/remanence of the Precambrian Basement rocks.

1.3 Research Justification

This research work will address the aforementioned problem statement. There are little information on preliminary investigation of Southwestern Nigeria Precambrian rocks as regards its paleomagnetic characterization; which is due to unequal distribution of rock samples. Previous studies in the region have not fully addressed the constraints on the genesis/evolution and paragenesis of these rocks as well as their pole positions during and after the formation of the rock in the Pan-African times.

The non-availability of adequate data, numerical data, instrumentation and assumptions that Precambrian rocks is not good or fit for paleomagnetic study poses problem in its geodynamics. Thus, the research work is to fill the knowledge gaps created by dearth of comprehensive data on paleomagnetic characterization of some Precambrian rocks of Southwestern Nigeria. In so doing, the need of this research is to study continental drifts/apparent wandering paths by characterising the paleomagnetism of some Precambrian rocks using multidisciplinary approach.

1.4 Aim and objectives of study

The aim of this research is to characterise the paleomagneticbehaviour of some Precambrian rocks in southwestern Nigeria granitoids through rock magnetic, palaeomagnetic and geochemical data in relation to its orogenic events. Specific objectives of the study are:

- Find out evidences of magnetic indicators using Raman spectroscopy
- Investigate the magnetic susceptibility of some basement rocks and orientations of microstructural direction

- Determine the Thermomagnetic-Temperature dependenceof Precambrian rocks
- Study the rock and mineral magnetic properties of some southwestern Nigeria basement rocks
- To test Natural Remanent Magnetization (NRM) hypothesis, magnetic fields and determine the mean palaeomagnetic pole positions
- Assess and understand the geochemical variations of rock specimen
- Determination of rock magnetic phases- Single Domain (SD), Pseudo-Single Domain (PSD), and Multi-Domain (MD) in relation to its remanence

1.5 Significance of Research

The significance of the research is a multi-disciplinary study that involves rock magnetism, paleomagnetism, petrology and geochronology to classify the granitoids in the southwestern Nigeria Pan-African rocks. The current study has played a key function in furthering our knowledge of continental drifts/apparent polar wandering paths, evolution of the Precambrian Basement rocks in southwestern Nigeria, orientation of microstructures, temperature dependence, magnetic hysteresis and their phases. Remanent records on rocks are significant in understanding the evolution of the southwestern Nigeria orogenic events, geodynamic processes and its relation to global Earth's magnetic field reference frame.

1.6 Scope of the thesis

Geological field mapping was carried out at southwestern Precambrian Basement Complex involving Ondo, Ogun, Oyo, Osun and Ekiti states between 2016 and 2017. The field characteristics and its rock relationship were studied. Rock samples were collected for thin sectioning and cored for laboratory analyses. Geological maps were generated from the field and petrographic.

The rocks were divided into two categories for petrographic and mineral analyses as well as paleomagnetism. Some rocks were prepared into polished sections using Electron Probe Microanalyser (EPMA) and mineralogical phases of powdered samples were carried out using X-ray diffraction method, while the pulverised rock were analysed for

major, minor and trace element and Inductively Coupled Plasma-Mass Spectrometry (ICP-MS) methods. Some of the rock grains were employed for Raman infrared spectroscopy analyses for iron-oxides examinations. The cored samples were analysed in the magnetic-proofed room by the use of spinner magnetometer, MOLSPIN shielded alternating Field and Eurotherm thermal demagnetizers, impule magnetizer and Direct Current -Superconducting Quantum Interference Device (SQUID-DC).AGICO MFK1-FA Kappabridge was used for Curie temperature and anisotropy and magnetic susceptibility determinations while Vibrating Sample Magnetometer (VSM) was employed for hysteresis loop, backfield remanence, Isothermal Remanent Magnetization (IRM) and First Order Reversal Curves (FORCS). Several softwares (Remasoft, Orient, Cureval 8, SURFAR, IAPD, Anisoft, GRAMS AI, GPLATES, Igor Pro,DAIE-v2015) were used to process and analyse the data.

1.7 Location map

Figure 1.1 shows the site description map of the area. The study area lies between Longitudes 2° 30’ E and 6° 00’ E and Latitudes 5° 30’ N and 9° 30’ N within the Precambrian Basement complex of southwestern Nigeria. The geographical location and extent is made up of Ondo, Ekiti, Osun, Oyo and Ogun states. Sometimes paths have to be created because of the vegetative shrubs in accessing some locations of the outcrops. The relief of the study area consist of rugged hills, plains, valleys and outcrops. The area falls within the rainforest and tropical guinea savannah with wet and dry climate. The annual rainfall in the southwestern Nigeria is usally above 2,000 mm for tropical rainforest and has temperature range of 18 °C to 36.5 °C. (Eludoyin *et al*., 2013).

Fig. 1.1. Location map of the study area

CHAPTER TWO

LITERATURE REVIEW

2.1 Review of the regional geological setting

The southwestern Nigeria granitoids is within the basement complex domain that was reopened in the Pan- African time of the Neoproterozoic period. This province was located around East Saharan, southeast Congo craton and west of West African craton (Fig. 2.1), and has a long stretch from Hoggar to Brazil which ranges from 4000 km to an extensive orogen in hundreds of kilometers (Caby *et al.*, 1989). The Trans-Saharan fold belt runs north-southerly and the reopening of this belt was due to East Saharan, Congo and West African cratons continental collision about 790 and 500 Ma (Ferre *et al*., 2002; Dada, 2006; Adetunji *et al*., 2018). Granitoids, growth of thrust-nappe, medium- to high-grade metamorphism, parallel orogen tectonics typifies this belt (Black and Liégeois, 1993). The Hoggar separated into Air, Eastern and Central polycyclic; but now called the Pharusian belt plus Laouni terrain Algeria(LATEA) micro continent (Liégeois *et al*., 2003). Aggregation of twenty-three micro terranes constitute eastern and polycyclic central Hoggar in the northern province (Caby, 2003) while in the southern block (Dahomeyide) we have the Aïr-Hoggar composed of various continental oblique collision (Ajibade and Wright, 1989).

Nigerian sector evolved by profuse magmatism at late Neoproterozoic times at the culmination of prior basin made up of depleted Archaean crust (Caby and Boesse, 2001). The Nigerian part of the Dahomeyide was separated into the eastern (granulite facies) and western (greenschist to amphibolites facies) domains on the basis of some petrological attributes (Ferre *et al*., 1996). The southwestern Precambrian granitoids is made up of migmatite-gneisses, schists, granites and dykes (Rahaman, 1988). Pan-African granitoids and unmetamorphosed dykes are assigned Neoproterozoic isochron (Tubosun *et al*., 1984; Dada 1998; Kröner *et al*., 2001; Okonkwo and Ganev, 2012; Adetunji *et al.*, 2018;

Salminen, 2019). The Archean crust characterized the supercrustals which closure at later times, interpreted to be deposited in diverse proto ocean floors (Ajibade and Wright, 1989; Rahaman *et al*., 1988).

Pan-African belt evolution was by Plate tectonism which led to the active margin colliding with the Pharusian belt and passive continental margin of the West-African craton about 600 Ma (Rahaman, 1976; Caby *et al*., 1981; Nzenti, 1988; Sayab *et al*., 2021). The existence of basic to ultra-basic rocks thought to be remnants of mantle diapers or paleo-oceanic crust is part of this facts and they have ophiolitic complex characteristic. Geochronological studies have been examined on some major magmatic complexes with their isochron ages varying from 557 ± 8 to 686 ± 17 Ma (Rb/Sr whole rock); 640 ± 15 Ma (U–Pb) was acquired in these complexes. Deformation of migmatite-gneisses and post-tectonic uplift typifies the Pan-African fold belt in southwestern Nigeria; which was made up of polycyclic orogen of Liberian (2700±200Ma), Eburnean (2000±200Ma), Kibaran (1100±200Ma), and Pan-African (600±150Ma) (Black *et al*., 1979; Caby *et al*., 1981). For the Liberian and Eburnean, the International Geological Time Scale (2002) has followed the following ages: "Paleoarchean to Mesoproterozoic (3600 to 1600 Ma)", "Mesoproterozoic to Neoproterozoic (1600 to 1000 Ma)", and "Neoproterozoic to Early Paleozoic (1000 to 545 Ma (Obiora, 2008).

Ferre *et al.* (2002) studied the northeastern Nigeria Pan-African continental collision, which resulted in high grade - high pressure and temperature (HP-HT) metamorphism up to granulite facies, migmatization in supracrustal units of the same tectonism as the southeastern Nigeria domain (Onyegocha and Ekwueme, 1990; Kalsbeek *et al*., 2012). The extensive Archean crust of northern Nigeria at diverse time modified and remelted during the Pan-African tectonometamorphic episode. The Pan-African nappe system appears as rejuvenation of older polyorogenic times (Rahaman, 1988; Black *et al*., 1994).

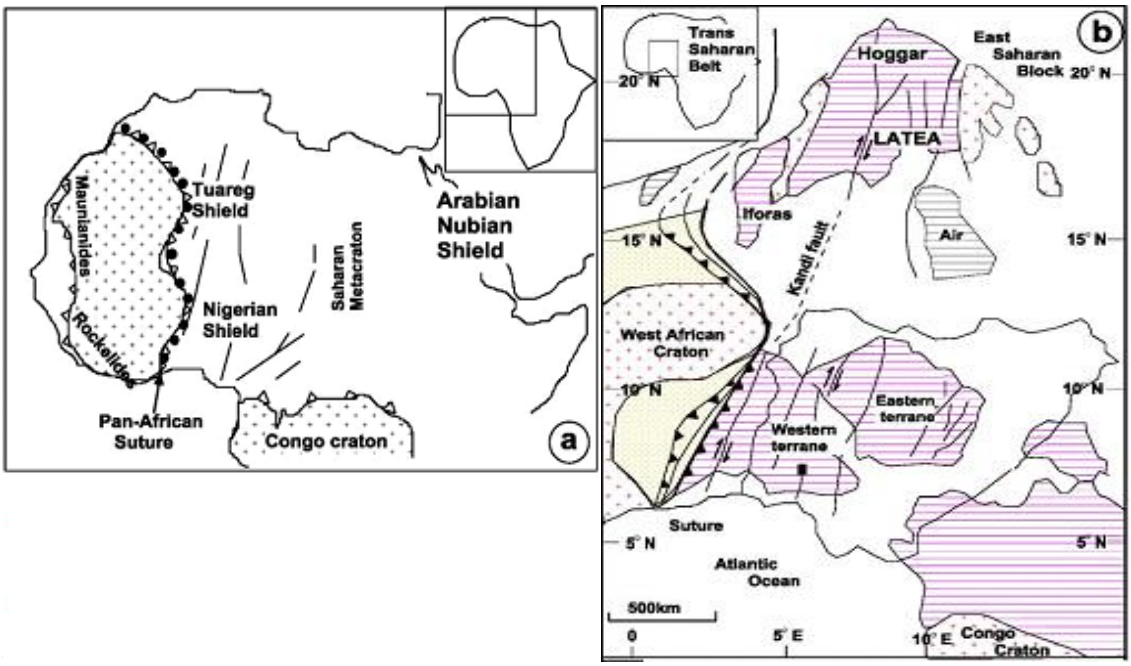

Fig. 2.1. Regional geological map of Trans-saharan metacraton/shield (Modified after Caby, 2003; Ferre *et al*., 2002)

Detailed geology of province as well as tectonometamorphic events in the whole of southwestern Nigerian shield is presented in Figure 2.2. with well pronounced granitoids.

Detail geological mapping of Iseyin-Oyan River, Ilesha-Ife, Igarra schist belts in southwestern Nigeria and the rest of the schist belts concentrating in the northwestern Nigeria have been conducted. Nonetheless, Dada (2006); Obaje (2009) subdivided the Precambrian basement rocks into four units: Migmatite-Gneiss (migmatites, gneisses, granite-gneisses); Schist zones (schists, phyllites, pelites, quartzites, marbles, amphibolites); Pan African Granitoids (granites, charnockite, granodiorites, diorite, monzonites, gabbro) and Undeformed Acid and Basic dykes (muscovite, tourmaline, pegmatites, aplites, syenites, basaltic, dolerites and lamprophyre dykes). They occur as small medium-grained rock with massive hills. This charnockites is made up of orthopyroxene, clinopyroxene, hornblende, plagioclase, alkali feldspar, magnetite, quartz and zircon. In some places, granite, porphyritic, augen, banded gneiss can be seen as low-lying outcrops and large hills.

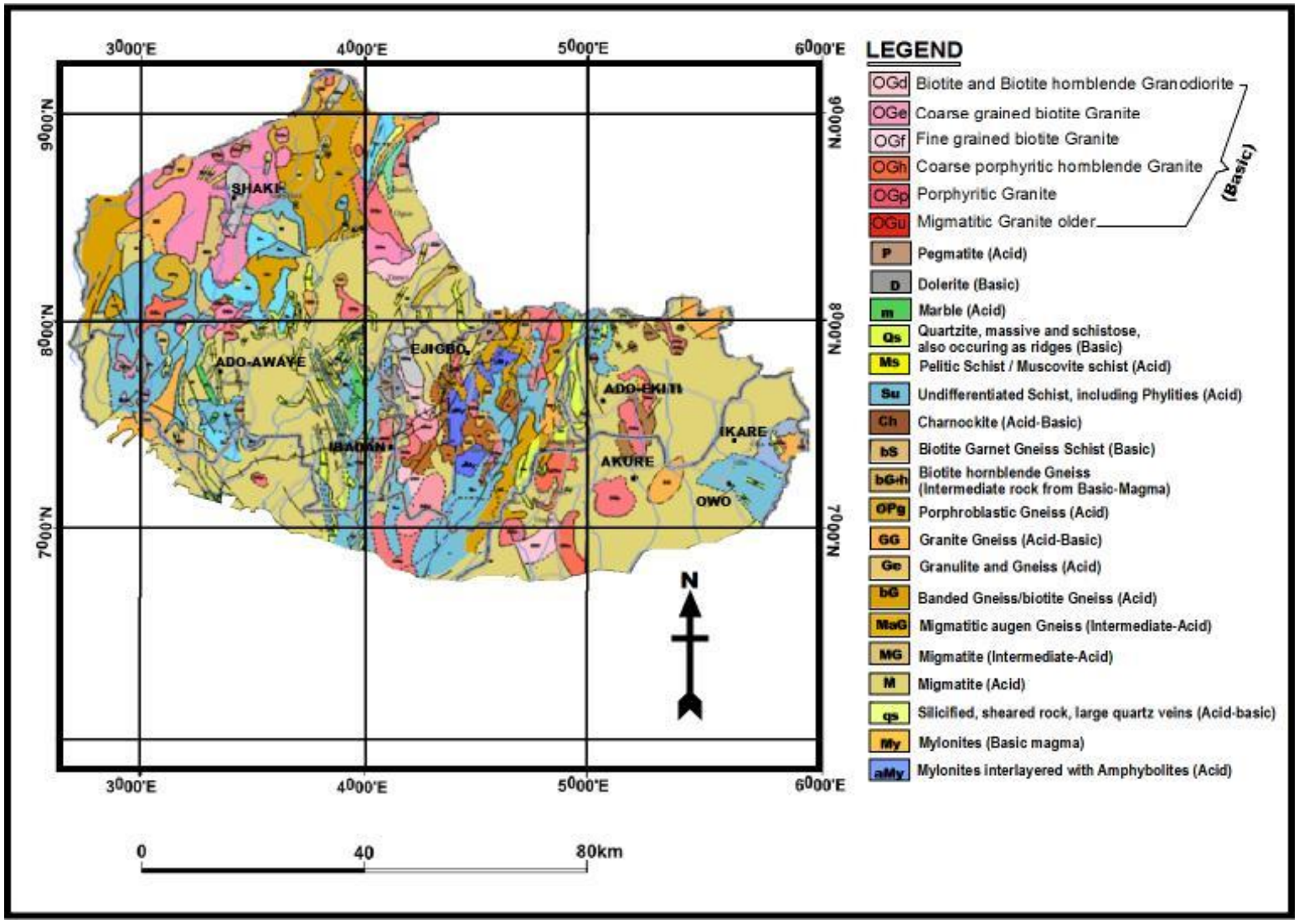

Fig. 2.2. Geological map of southwestern Nigeria (modified from NGSA, 2010)

2.2 Supercontinent palaeogeographies

Supercontinent palaeogeographies is imperative for understanding the mechanisms of continent recycling and more generally the geological evolution of the Earth's surface (Condie, 2002b). The supercontinent was formed when most of the continental crust collides to form a single landmass. The supercontinent Pangea was formed during the Palaeozoic by the amalgamation of Gondwana (which roughly consisted of Africa, South America, East Antarctica, India and Australia) and Laurasia (Laurentia and Eurasia) (Rogers, 1996). Reliable paleomagnetic constraints show three pre-existing continents in the (Precambrian): Arctica (Laurentia and Siberia) involved Baltica; Nena, Kalahari, India and Australia formed Ur; South America, linked to West Africa and Congo is termed Atlantica (Rogers, 1996). These "palaeo-continents" survived the supercontinental cycle and remained intact during separation of Columbia around 1.5 Ga (Condie, 2002a). Restructuring of these palaeo-continents generated another supercontinent termed Rodinia between ca. 1.3 and 1.0 Ga (Rogers and Santosh, 2002).

Neoproterozoic palaeogeographic reconstructions are dominated by models for the formation and successive collision of this supercontinent Rodinia, reconfiguration of the constituents and the amalgamation of Gondwana (ca. 530 Ma). The first geological models were based on the recognition and correlation of ca. 1.0 Ga orogenic belts found on Australia, Antarctica and Laurentia (Hoffman, 1991). These belts are called "Grenvilian" after their archetype, the Grenville Belt in eastern Canada (Gower, 1996). Some workers have used palaeomagnetic data to support geologically based reconstructions or have fully integrated palaeomagnetism with stratigraphical, geochronological and tectonic constraints (Evans, 2009).

2.2.1 Rodinia Reconstructions

The Laurentia Craton has played a key role in models for Rodinia following Weil *et al*.(1998) who interpreted Neoproterozoic tectonic subsidence curves from around the craton margins to suggest simultaneous rifting and formation of passive margins as a result of the supercontinent breaking up. As indicated in Figure 2.3, Laurentia was the only craton with a reasonably well established polar wander path, allowing comparisons

of coeval palaeopoles from other cratons. Southwestern Laurentian border lies adjacent to East Antarctica that form baseline Rodinia models, the so called ***SWEAT*** postulation (South-West U.S. - Antarctica; Moores, 1991). Figures 2.3a, b and c was primarily based on geological correlations of the North America western cordillera with the Eastern Pacific margin of the Antarctica craton and it's the central idea of many subsequent Rodinia reconstructions (Dalziel, 1997; Weil *et al*., 1998). Another model to ***SWEAT*** places Australia adjacent to southwestern Laurentia and was based on the alignment of several rift-transform fault systems on both cratons (Brookfield, 1993). This configuration was later called ***AUSWUS*** (Australia - Western U.S.; not shown in Fig. 2.3 Both the ***SWEAT*** and the ***AUSWUS*** models, however, appeared to disagree with a new, 1070 Ma palaeomagnetic key pole for Western Australia which led to the proposed ***AUSMEX*** (Australia - Mexico) assembly (Wingate *et al*., 2002). This fit was palaeomagnetically sound and still allows for most of the geological correlations that were part of the previous models. The ***AUSMEX*** fit was adopted by Pisarevsky *et al*. (2003) in Figure 2.3d. The role of the West Africa (i.e. the craton that form the focus of this study) in Rodinia is still subject to discussion. Evidence from both cratons to support or deny Rodinia participation are discussed below.

2.2.2 Congo Craton in Rodinia

The Congo Craton consists of several tectonic blocks of Archaean age which amalgamated during the Mesoproterozoic. The NE Congo-Uganda domain, Angola-Kasai and the Cameroon-Gabon-Sao Francisco Block are connected through the Kibaran belt with the Tanzania Block and the Bangweulu Block (Hanson, 2003). Kibaran belt was known with peak compressional tectonism where the Congo Craton was assembled at ca. 1.38 Ga (Tack *et al*., 2010). The evolution of the Atlantic Ocean in Cretaceous times, the Sao Francisco Craton in northern Brazil was associated with the Congo Craton, a continental link that has existed since the Palaeoproterozoic Era (Tack *et al*., 2010).

The Congo Craton has at several times been assumed to be part or separated from Rodinia. Based on age comparisons of the Kibaran and Irumide belts with the Grenvillian type mobile belt system in Amazonia and Laurentia, the Congo was considered to be part

of Rodinia in the reconstruction (Hoffman, 1991; Figure 2.3a). But it was not evident whether or not the Kibaran and Irumide belts represent Rodinia related late to Mesoproterozoic tectonics (De Waele *et al*., 2008).

Dalziel (1997) placed the Congo Craton with its western margin towards Laurentia (Fig. 2.3b) with the Kalahari and Congo cratons in their Gondwana-type configuration. Zambezi belt that was between the Congo and Kalahari was an intracratonic belt (Dalziel, 1997) and the two cratons have been connected since the Mesoproterozoic. First, two phases of extensional tectonism are recognized along this margin which resulted to the growth of a large passive margin (De Waele *et al*., 2008). The first phase was characterized by felsic volcanics with isotopic signatures recording continental extension which occurred between U-Pb age of 880 and 820 Ma (De Waele *et al*., 2008). The start of a second phase was marked by 765±5 Ma mafic volcanic rocks (zircon U-Pb ***SHRIMP***, Key *et al*., 2001) overlain by a passive margin type sedimentary sequence dated by a Sm-Nd isochron age of 595±10 Ma (John *et al.,* 2003). Another Neoproterozoic oceanic basin comes from pressure-temperature estimates of these eclogites-suture zone: a low geothermal gradient implying the existence of a cold subducted lithosphere (> 1000km) and associated oceanic basin (John *et al*., 2003).

Rodinia reconstructions partly based on palaeomagnetic data also question whether Congo was part of Rodinia (Figs. 2.3c and d) (Pisarevsky *et al*., 2003). Combining geological evidence with palaeomagnetic results led Pisarevsky *et al*. (2003) to suggest a scenario where the Congo Craton was independent from Rodinia (Fig. 2.3d). The authors constrain the Congo Craton palaeopoles at 795 and 748 Ma (Meert *et al*., 1995). Both poles require separation of the Congo from Laurentia and similarly ca. 1080 - 1020 Ma palaeomagnetic data from the Craton of Sao Francisco Craton require separation from Laurentia. Despite these results, the Congo was part of Rodinia as of ca. 1000 Ma. In this geological model (Fig. 2.3e) the craton was placed with its south-east margin facing Laurentia following Hoffman (1991)'s. Thus, reliability of these two poles could be questioned given the lack of field tests.

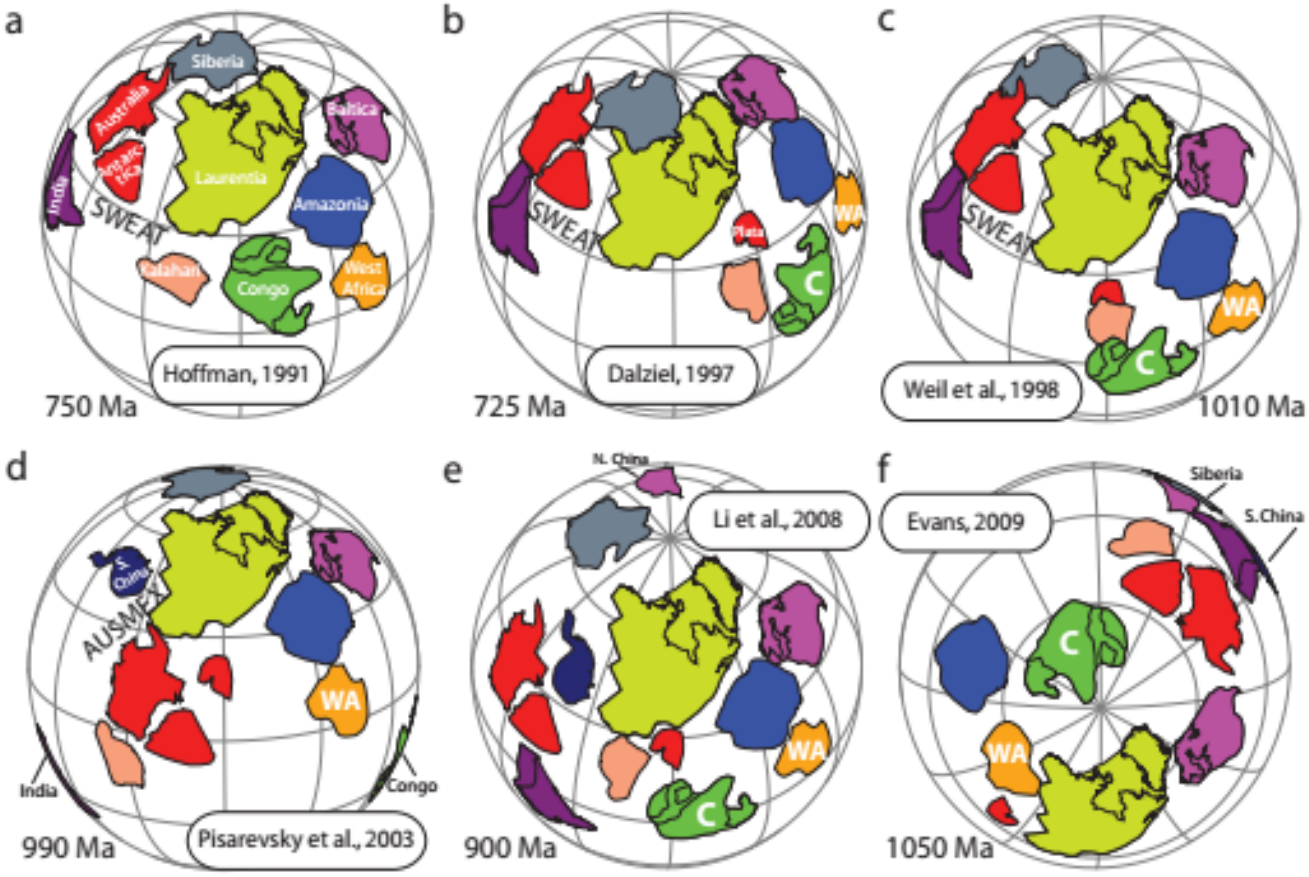

Fig. 2.3. Maps for Rodinia according to different models described in the text, reffered to North American setting. The cratons models are modified after Pisarevsky *et al*. (2003) Reconstructions are made using GPLATES software

2.2.3 The West African Craton

The West African Craton has formed a stable cratonic entity since a period of tectonic amalgamation around 2.0 Ga. After that the craton provides no evidence for any major tectonothermal event until formation of late Neoproterozoic Gondwana (Deynoux *et al*., 2006). Most of the margins of the West African Craton are marked by mid Neoproterozoic rifting but these events seem to be rifts of the back-arc kind that open and close quickly on themselves rather than record large continental break-up (Rogers, 1996). Palaeomagnetic data from West Africa are absent (for the Mesoproterozoic) or unreliable (Neoproterozoic).

If West Africa was part of Rodinia it would have had a passive role as part of a larger craton. Following the suggestion of Rogers (1996) for the existence of Mesoproterozoic Atlantic, West Africa could have been part of a stable continent from 2.0 Ga until incorporation in Gondwana (Trompette, 1994; Rogers and Santosh, 2002). This long term stability however remains to be confirmed. In the majority of Rodinia reconstructions, the West African Craton has been connected to Dahomeyide and Nigerian shield, based on the idea of Trompette (1994) and similar to their fit in West Gondwana (Figs. 2.3a-e, Hoffman, 1991; Weil *et al*., 1998; Pisarevsky *et al*., 2003).

Recently, a completely revised model for Rodinia was suggested by Evans (2009) positioning the Congo Craton in the north and Amazonia west of Laurentia with West Africa filling in a gap between Amazonia and Laurentia (Fig. 2.3f). The Congo-Laurentia connection would have lasted from 1235 to 755 Ma with a loop in their polar wander path between 800 and 750 Ma to account for palaeomagnetic poles from the Congo Craton. The position of West Africa implies a more active role for which evidence remains to be found.

2.2.4 Gondwana Configuration

Although different models exist for the absolute position of Gondwana (Pisarevsky *et al*., 2008) as well as the relative positioning of cratons can be done with small margins of error (Fig. 2.4; Eagles, 2007). The formation of Gondwana is often presented as a merger

of East Gondwana (Antarctica, Australia, and India) with West Gondwana (those currently in Africa and South America). Evidence especially from the eastern Gondwana cratons, however, indicates that it was not a simple unification of two halves, but rather a poly-phase amalgamation of cratons during the waning stages of the Proterozoic, as a result, that Gondwana was created (Meert and Lieberman, 2008).

The Congo and West Africa cratons both form part of West Gondwana and are connected through the Borborema Province in northern Brazil (Fig. 2.4). This province was essentially an assemblage of several terrains and comprises reworked Mesoproterozoic-Neoproterozoic metasedimentary rocks and Archean-Palaeoproterozoic crystalline basement (Dada, 2008). Reworking is the result of Neoproterozoic continent-continent collision which caused extensive deformation, migmatization, granitization and intrusive plutons. Geochronological constraints for the different stages of deformation in the Borborema Province are provided by U-Pb radiometric ages of the granitoid plutons (van Schmus *et al*., 2008). Ages for zircons from syn-tectonic I-type granitoids and zircons from migmatitic gneisses show that deformation started ca. 625 Ma and peaked at about 600 Ma (Neves *et al.,* 2008). Post-tectonic alkaline granitoids mark the final orogenic stage and U-Pb zircon ages show that deformation had ceased around 570 Ma (Neves *et al*., 2008). The Borborema Domain was correlated, predominantly on the basis of Sm-Nd model ages and U-Pb zircon ages of Archaean-Palaeoproterozoic basement rocks in conjunction with Neoproterozoic structural tectonic data, with the Central African fold belt (Fig. 2.4) and with the Nigerian Shield (Fig. 2.5) in NW Africa (van Schmus *et al*., 2008).

The Central African fold belt demonstrate a poly-stage geodynamic evolution of nappe emplacement onto the Congo Craton northwardly (Toteu *et al*., 2004). Geochronological constraints reveal a history of individual orogenic stages broadly coeval with those of the Borborema Province: high pressure metamorphism with granulite facies typified for syn-tectonic calc-alkaline and S-type granitoids and migmatization occurred at 640 - 610 Ma, as well as post-collisional phase of exhumation and late-tectonic calc-alkaline to sub-alkaline granitoid emplacement was dated at 610 - 570 Ma (Toteu *et al*., 2004). The exact

nature of the continental landmasses involved was still enigmatic. The belt could be entirely the consequence collision of the Congo Craton with the ill-defined Saharan Metacraton (Abdelsalam *et al.,* 2002).

Neoproterozoic intrusions within the Nigerian Shield show a history very similar to that of the Borborema Province (Dada, 2008). Combined structural data and U-Pb ages suggest that an early deformational phase took place at 640 - 620 Ma, peak metamorphism and syn-tectonic granitoids are positioned between 620 and 600 Ma and a post tectonic phase from 600 to 580 Ma (geochronological data synthesized by Dada, 2008). Geochronology of these plutons shows that the continental collision evolved diachronously between 620 and 580 Ma (Caby, 2003). The Nigerian Shield and the Tuareg Shield parted from the West African Craton by the Dahomeyide and Pharusian belts respectively (Fig. 2.5). Peak metamorphism in the Dahomeyides occurred approximately at 610±2 Ma (Attoh *et al*., 1991) to 603±5 Ma (Hirdes and Davis, 2002) premised on the basis of radiometric dating of U-Pb obtained from gneisses from granulite facies peak metamorphic zones. Post-collisional exhumation was dated by ^{40}Ar-^{39}Ar muscovite ages of 587±4.3 and 581.9±2.4 Ma (Attoh *et al*., 1997) which corresponds with rutile ages of 576±2 Ma which represent regional cooling below 400°C (Hirdes and Davis, 2002). The collision of Island Arc with the West African Craton around 620 and 580 Ma, simultaneous with the height of the tectonic events in the Tuareg Shield to the east (Caby, 2003). The Borborema domain evolved synchronous with the Central African Fold Belt, the Nigerian Shield (Dahomeyide Belt) and the Tuareg Shield (Pharusian Belt) strongly implies that this part of West Gondwana had amalgamated by 600 Ma and all tectonic activity had ceased by 570 Ma.

Archaean to Mesoproterozoic granite-gneiss-migmatite complexes, greenstone belts and metasedimentary and metavolcanic units are caught up in the Brasilia Belt involving the Sao Francisco Craton and Magmatic Arc of Goias (Valeriano *et al*., 2008). Observed data from the Paraguay-Araguaia belt which flanks the western side of the Goias Arc imply that the collision of Sao Francisco/Goias with Amazonia slightly post-dates the Brasilia event at ca. 550 Ma (Klein and Moura, 2008; Chaves, 2021). Biotite and muscovite ages

around 530 Ma from Archaean basement gneisses may record late-orogenic cooling in the Araguaia belt (K-Ar), (Klein and Moura, 2008).

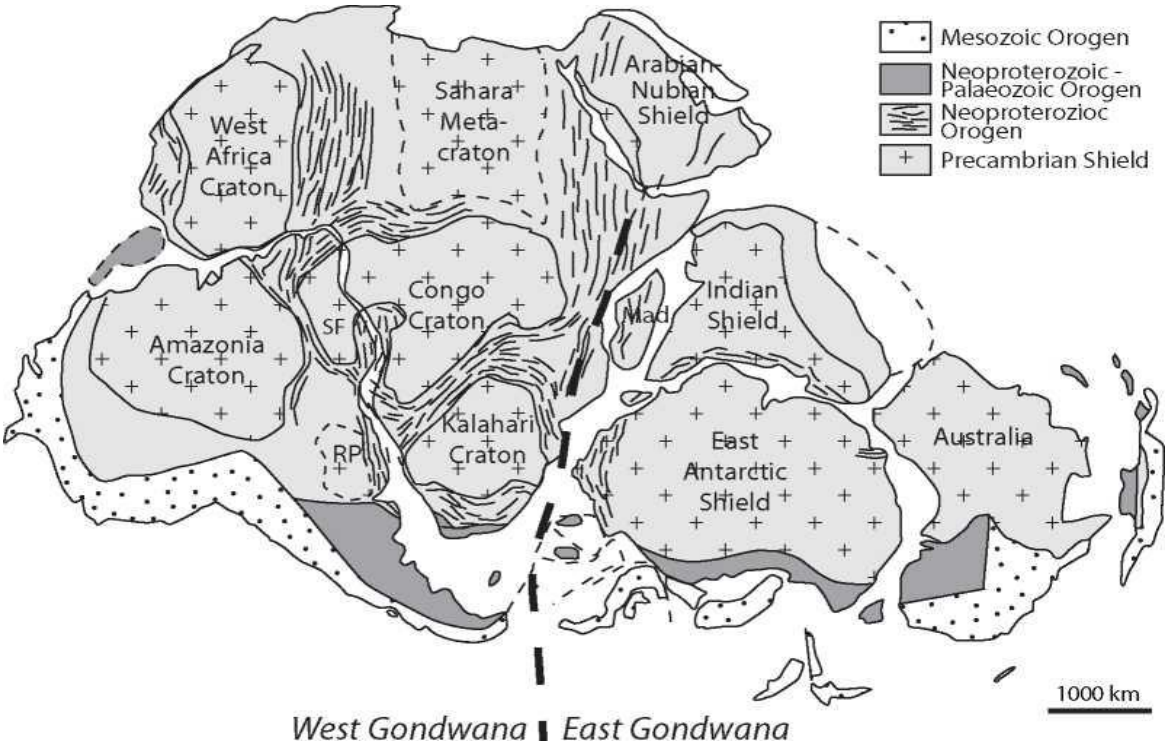

Fig. 2.4. Gondwana map with its cratonic nuclei positions (Adapted after Gray *et al.*, 2008). RP -Rio de la Plata Craton; SF- Sao Francisco Craton

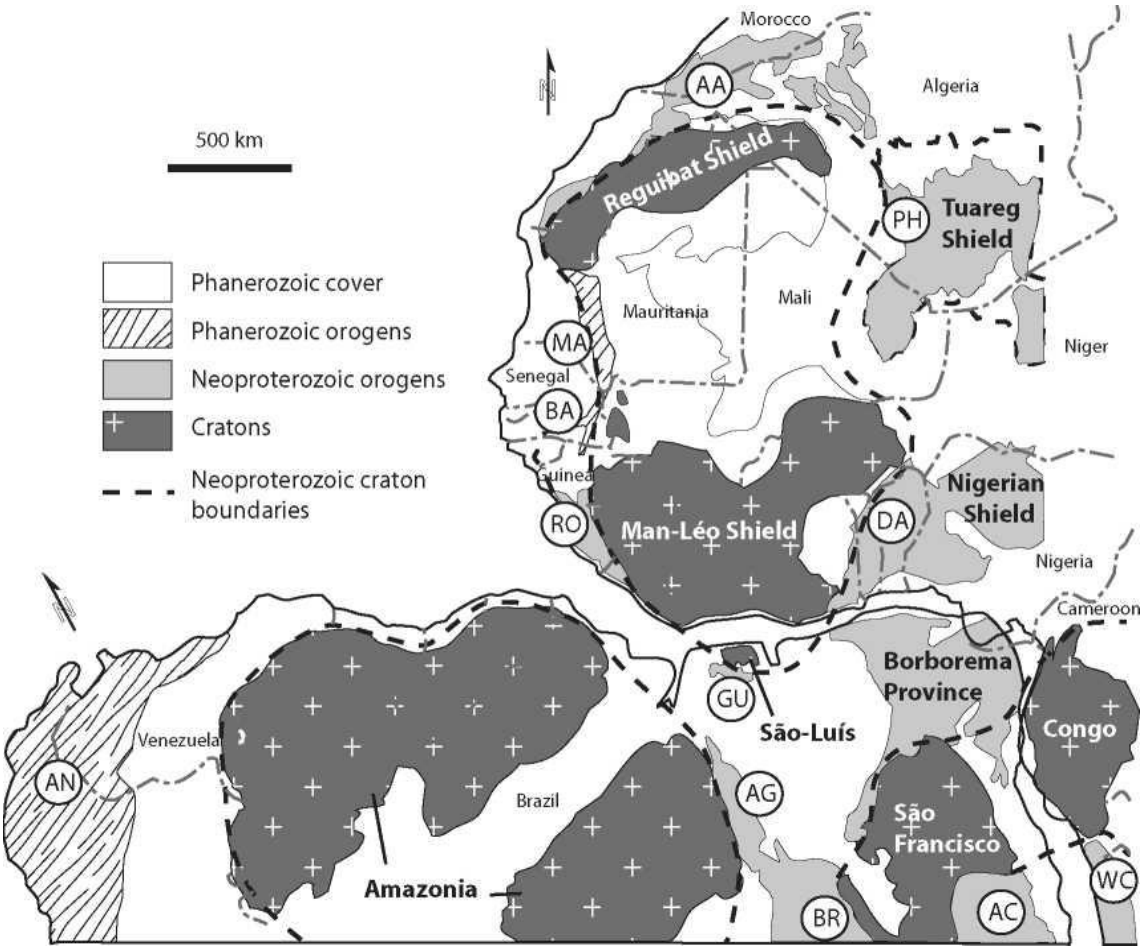

Fig. 2.5. West Africa Cratonic map with its neighbouring cratons and mobile belts in a preAtlantic fit (Modified after Klein and Moura, 2008). AA, Anti-Atlas Belt; AC, Araguaf Belt; AG, Araguaia Belt; AN, Andean Belt; BA, Bassaride Belt; BR, Brasilia Belt; DA, Dahomeyide Belt; GU, Gurupi Belt; MA, Mauritanide Belt; PH, Pharuside Belt; WC, West Congo Belt

All through the Neoproterozoic, the Adamastor Ocean separated the Kalahari cratons and southern Congo from the Rio de la Plata Craton while the Khomas Sea was flanked by the Kalahari and Congo cratons (Stern, 2008). The Adamastor Ocean enlarged south-wards from the Congo-Sao Francisco Cratonic Bridge and perhaps have been a continuation of the Macaubas Basin separating the Sao Francisco Craton from Congo Craton. Closure of the Adamastor and Khomas basins are documented in southern Africa by a triple junction of three fold belts: The Gariep, Kaoko and Damara belts (Fig. 2.4). The closing of the Adamastor Ocean yielded transpression as recognised by S-type granite intrusions and metamorphic mineral assemblages in the Kaoko belt (Goscombe *et al*., 2003b). Ages for granite orthogneisses range between 580 and 565 Ma and coincide with direct age peak metamorphic minerals interpretations from zircon and garnet (Goscombe *et al*., 2003b). The southern Kaoko belt experienced a younger deformational event at ca. 530 Ma which coeval with a deformation phase in the Damara belt flanked by the Kalahari and Congo cratons (Goscombe *et al*., 2003a; Gray *et al.*, 2008). This N-S crustal compression is prevalent in the Ifewara-Ilesha and Damara schist belts (Goscombe *et al*., 2003a), affected the Kaoko and Gariep belts as well as the Ribeira and Dom Feliciano (Gray *et al.*, 2008) belts between the Rio de la Plata Craton in South America (Fig. 2.4).

2.2.5 Precambrian basement complex of Nigeria

The Nigerian Precambrian Basement Complex outcropped in five major locations, viz.: southwestern sector, south-southeastern (the Oban Massif), southeastern sector (extension of the Bamenda Massif into Nigeria), northeastern zone (the Hawal massif) and northwestern sector (Obiora, 2005). Obaje (2009) classified the Basement Complex rocks into three main groups, viz.:

(a) The older metasediments, which he called the older rocks are composed of arkosic quartzite,calc-silicate and high grade schists found as lensoid relicts in regional gneisses or as paleosomes of the migmatites.

(b) Gneisses, migmatites, and older granites are also examples of this. The author identified two dominant gneisses in this group, namely banded gneiss and biotite gneiss.

He also distinguished between two groups of migmatites: lit-par-lit gneiss and migmatitic gneiss. According to the author, the paleosome (an old metasediment granulite or high grade schist) appears with quartz-feldspar veins and dykes in a parallel orientation in the lit-par-lit gneiss. The metasome is quartz-microcline veins in migmatitic gneiss, whereas the paleosome, which is biotite or banded gneiss, is split into irregular blocks. Gneisses and migmatites, according to Obaje (2009), are the product of silica-potash metasomatism. He suggested that the 'Older Granites', probably have a metasomatic origin and associated them with three other types of rocks namely; the coarse-grained, greenish fayalite-bearing rocks (Bauchites), pyroxene-quartz-diorite and pyroxene-amphibole syenite. At Toro in Jos Plateau, Obaje (2009) reported the presence of the pyroxene-quartz-diorite within the Basement Complex, typified by the blue-black 'charnockitic'quartz-diorite while he described the pyroxene-amphibole-syenite (a typically purplish rock) as zoned intrusion at Shaki, southwestern Nigeria (Oyawoye, 1972).

(c) The younger meta-sediments, to which he ascribed Paleozoic age

Cooray, (1974) reviews added another family of rocks (the intrusives) to the works of Oyawoye (1964). He further effected some changes in the conclusions of Oyawoye (1964) such as:

(a) The intrusives rather than metasomatic origin are: the Older granites and associated charnockitic rocks.

(b) Depending on the relative time of emplacements and deformation, Older granites and granodiorites are classed as syn-tectonic microcline-megacrystic, partly foliated granites and late-tectonic, less richly megacrystic, weakly foliated xenolithic granites and granodiorites with cross-cutting contacts and periodic thermal aureoles. (McCurry and Wright, 1971).

(c) The author pin- pointed the generally north-south to northeast-southwest structural pattern in the Basement Complex and suggested a polyphase metamorphism during the Eburnean, Kibaran, and Pan-African orogenic episodes, there were at least three plutonic

occurrences (Grant, 1978).

The Basement Complex rocks were defined in more classical terms by Rahaman (1976, 1988) and Rahaman and Ocan (1978). Obaje (2009) and Cooray (1974) identified three rock groups, which have now been subdivided into six major lithologic groups. There are some of them:

(a) A heterogeneous group of rocks known as the Migmatite-Gneiss Quartzite Complex. It is divided into sub-groups, which include:

(i) The Migmatite-Gneiss Quartzite Complex described as a heterogeneous group of rocks. It has sub-groups namely:

(i) Early (grey) gneiss, the oldest recognizable member of the migmatite-gneiss-quartzite complex, grey, hornblende gneiss of granodioritic to tonalitic composition and/ or foliated biotite,

(ii) mafic to ultramafic components which are usually amphiboles, biotite and biotite-hornblende schists and

(iii) felsic components, usually of granitic composition and aplitic, granitic to pegmatitic. The granite gneisses are interpreted as deformed intrusive granites and the other felsic components are either products of partial melting of the older basement or magmatic injection. Other subgroups are:

(iv) bodies of meta-sediments which are quartzites, calc-silicates and garnet-sillimanite-cordierite gneiss

(b) Newer Meta-sediments, also known as slightly Migmatized or Unmigmatized Paraschists and Metaigneous Rocks, according to Obaje (2009) younger metasediments (McCurry, 1976) or Schist Belt Rocks (Ajibade, 1976);

(c) Charnockitic, gabbroic, and dioritic rocks, which Rahaman (1988) divided into three types:

(i) charnockitic -gneissic rocks with planar penetrative fabric,

(ii) charnockitic foliation with migmatitic foliation due to feldspar megacrysts in platy parallelism and discrete concentrations of mafic minerals, and

(iii) massive porphyritic granulite facies mineral assemblages can be found in both of them. Because of the interaction association with granitic rocks, the rocks are considered

to be of igneous origin. Some are believed to be younger than granites.

d) Older granite suite,the following sub-members were identified by Rahaman (1988) depending on members textural characteristics : (i) Migmatitic granite; (ii) Granite gneiss; (iii) Early pegmatite and fine-grained granite; (iv) Slightly deformed pegmatites, aplites, and vein quartz; (v) Homogeneous to coarse porphyritic granite; and (vi) Non-deformed pegmatites, mica granites, and vein quartz; (v) Homogeneous to coarse porphyritic granite; (vii) Metamorphosed and un-metamorphosed hypabyssal and calc-alkaline volcanics; (viii) Unmetamorphosed dolerite and syenite dykes; (Rahaman 1988).. Early grey gneisses or quartzo-feldspathic gneisses made up of granodiorite to quartz-diorite or tonalite. The Migmatite-Gneiss complex consist of granite gneiss having felsic components (Rahaman, 1976) while the oldest rocks-grey gneisses comprises of pegmatitic and quartzo-feldspathic intrusions (Rahaman, 1976; Rahaman and Ocan, 1988).

The Schist belt's rocks are mostly metamorphosed pelitic to semi-pelitic rocks, granites, sandstones, polymict conglomerates, calcareous rocks, mafic to ultramafic rocks, with small concentrations of greywacke and acid to intermediate volcanic rocks, according to Rahaman (1988). Some of the southwestern Precambrian rocks in the study area are listed in Appendix 3-5. They are also documented in Rahaman, 1988 classification of southwestern Precambrian basement rocks.

According to Obiora (2005), the schistose components of the migmatitic terrain were designated, "the older metasediments" while "Low to high-grade mica-schists, quartz schists, quartzites, and concordant amphibolites, talc schists (meta-basites, meta-mafites/meta-volcanics) make up the younger meta-sediments.The Schist belts are mixed with marbles, dolomites, calc-silicate rocks (e.g. calc-silicate schists) and meta-conglomerates in some areas, especially in the south-western Basement Complex. They are the metamorphic properties of limestone, marls, calcareous sediments, and conglomerates, in that order. The Banded Iron Formation (BIF) has also been linked to schist belts, such as the Muro Schist belt (Anike *et al*., 1990). The schists and amphibolites of the Schist belts are the host rocks of Nigerian gold deposits, which occur primarily as alluvial deposits in some parts of the Basement Complex, in the Ilesha,

Sokoto, Minna, and Birnin-Gwari districts.

N-S synformal troughs pass through the Nigerian schist belts, and 17 of them have been found and defined (Obaje, 2009). The Schist belts of the Nigerian Precambrian Basement Complex are identical to the Archaean greenstone belts (Attoh *et al.,* 1997), they are thought to possess major mineral resources of commercial value. They're thought to be remnants of a once-wide cover that was deposited in a proto-basin and is now housed in synclinal keels. Ajibade (1988) was, on the other hand, opposed to the idea of deposition in a single basin.

2.2.5.1 Structural geology

The mapped areas characterized by hilly and undulating rocks; where the structures and geologic data acquired are principally from field observations and studies. Geological structures in rocks are caused by the following processes which include;

i. Folding
ii. Faulting
iii. Shearing
iv. Fracturing
v. Quartz intrusion

2.2.5.1.1 Folds

Permanent bent or curved deformations occurring as one or a stack of originally flat and planar surfaces. Adeoti and Okonkwo (2017) established the structures and shear zones of Iwaraja in southwestern Nigeria and characterized diverse folds - symmetrical fold, asymmetrical fold, and recumbent fold.

Symmetrical fold: Figure 2.6a illustrated a symmetrical fold with limbs that fall at about the same angle from the axial surface. Its axial plane is vertical and it passes through the crest or trough.

Asymmetrical fold: Figure 2.6b demonstrate symmetrical fold in which limbs have unequal angle of dip in opposite direction. In some cases, the axial plane is inclined and it may not necessarily pass through the crest line.

Recumbent fold: Figure 2.6c revealed that symmetrical fold exists in outcrops that have been subjected to intense deformation such that both limbs become almost horizontal while the lower limb becomes overturned. They have near horizontal or horizontal axial plane; and are products of highly ductile deformation. Field observation have demonstratedfold displacement from its original position by crustal activities.

Fig. 2.6. Grey gneiss from the study area (a) Symmetrical, (b) Asymmetrical and (c) Recumbent folds

2.2.5.1.2 Joint

Joints are fracture along which there has been no relative displacement. The joints are vertical, inclined or even horizontal.

Parallel joint: Joint that consist of large number of joint that lies parallel to one another (Fig. 2.7a).

Master joint: the joint runs in two directions, which are perpendicular to each other. One runs parallel to the dip direction whilst the other to the strike direction (Fig.2.7b). Of these, one set of joints is more strongly developed and extend for long distance than the other.

2.2.5.1.3 Foliation

Foliation is dominated throughout the area. In the gneisses, the most conspicuous was recognised by parallel layer comprising of alternate dark and minerals that are light. This foliation typically runs parallel to the colour banding seen in most outcrops. light minerals. This foliation is frequently parallel to the colour banding observed in most of the outcrops (Fig. 2.7c). The foliation trend in the migmatitic gneisses are predominately West-East direction. The foliation in general, is parallel to the limbs of the folds. The foliation is thought to forms as a result of tectonism illustrated through the presence of small, tight to straight limbs having isoclinals fold.

2.2.5.1.4 Solution hole

Vugs vary from small to medium size cavities found within the rock due to variety of processes. Irregular voids formed due to erosion or dissolution processes of mineral crystals within the rock matrix gives rise to solution hole (Fig. 2.7d)

2.2.5.1.5 Lineation

Mineral lineation is very clear on the metamorphosed rocks such as granite gneiss, grey gneiss. The mineral lineation owing to the preferred alignment of minerals, which are made up of quartz and biotite.

2.2.5.6 Fractures

The frequent presence of fractures is a signature characteristic of the basement complex tectonic. Fractures describe any break or rupture in a rock, and indicated by such lineament as silicified sheared rocks and zones. They also form dyke's ridges and straight channelled streams which exploit the weak zones of the earth.

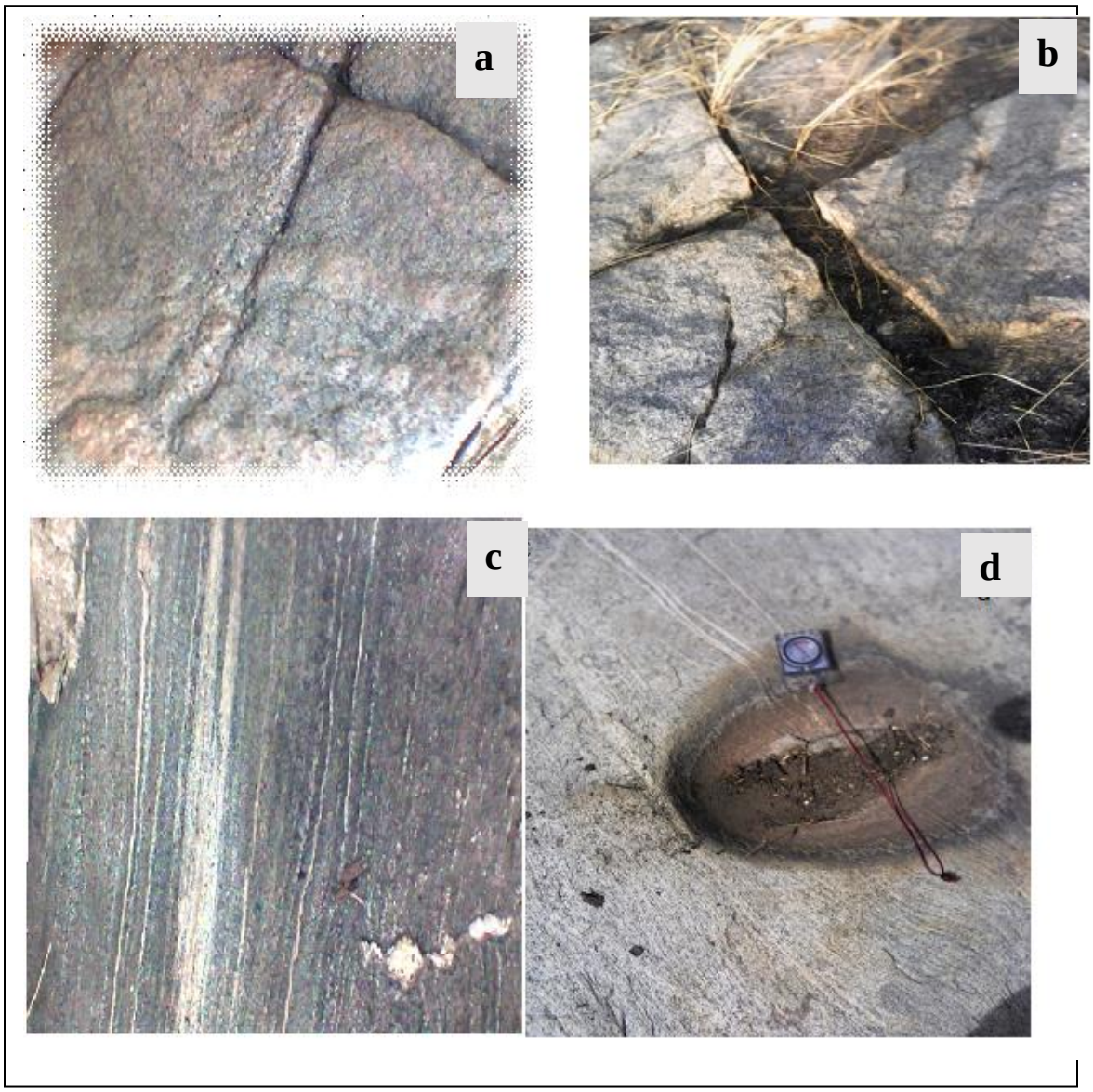

Fig. 2.7. Banded gneiss from the study area showing (a) Parallel joint (b) Master joint (c) Foliation (d) Solution hole

2.3 Literature Reviews

2.3.1 Thermomagnetic/ temperature dependence

Temperature dependence (Curie temperature) of rock fabrics is one of the easy approach to unravel the magnetomineralogy of earth materials. Osazuwa *et al.*(2008) worked on thermomagnetic/temperature dependence of magnetic susceptibility of granite rocks in Zaria, northwestern Nigeria, using Bartington MS2X/T system. Their study showed that the batholiths behaved paramagnetically except some few biotite minerals that have ferromagnet in them. There is no available literature on Curie temperature of magnetic susceptibility of some rocks in southwestern Nigeria Precambrian Basement Terrain using this method.

The temperature of rock material is slowly lowered under external field conditions –the domain will roughly align as it goes below the domain temperature. Different domain has different blocking temperature, as the temperature is lowered, more domains will align until a net magnetization is frozen in thermo-remanent magnetization (TRM) (stronger in cool rock, persist through geologic time) (Odeyemi, 2005; Osazuwa *et al*., 2008; Oniku *et al*., 2008; Salminen *et al*., 2019)

2.3.2 Emplacement directions and anisotropy of magnetic susceptibility

Anisotropy of magnetic susceptibility has proved its efficacy in determining its emplacement direction and magnetic susceptibility of granitoids globally without studying the macrostructures in the field but having to study it in the laboratory. Ferre *et al.,* 2002; Oniku *et.al.,* 2008 studied the granitoids in northeastern and northwestern Nigeria respectively. They used cored oriented samples for its laboratory measurement and the results showed predominance of north-south direction of Pan-African rock and clustering of tectonic axes. The magnetic fabric has its applications on diverse settings such as on plutons, dykes (Geoffroy *et al.,* 2002), lava flows and volcanic avalanches (Herrero-Bervera *et al.,* 2002). In northwestern and northeastern Nigeria (Ferre *et al.,* 2002; Oniku *et.al.,* 2008) studied the granitoids using this approach while (Ajaikaiye, 1989) used petrological and potential field techniques to study emplacement of plutons.

2.3.3 Raman infrared spectroscopy fingerprinting

Raman infrared microspectroscopy is a valuable tool for fingerprinting of granitoids of minute crystals in earth and planetary materials and incorportions in optically transmissive host stages (Zedgenizov *et al.*,2004). Studies on Raman spectroscopyby deFaria *et al*., 1997, Shebanova and Lazor, 2003 and Hanesh, 2009 to igneous and metamorphosed rock samples on: zircon and garnet as ultra-high pressure phases; iron – oxide phases as well as retrograded gneissic Precambrian basement terranes showed that low laser powered were used in studying iron oxides present in the granitoids in order to avoid destroying the minerals. The results also documented their crystal morphologies using the right laser caliberations and detected the exact iron oxide minerals present in the rock.

.

2.3.4 Microstructures

Cañón-Tapia and Herrero-Bervera, 2009 used Anisotropy of Magnetic Susceptibility (AMS) for microstructural studies of dyke walls and directions of magma flow of Koolau dyke complex in O'ahu in Hawaii, USA. They used theoretical hypothesis to predict field sampling of dykes. The result showed the first practical evidence that supported the occurrence of cyclic fabric acquisition and that significant percentage of the crystals are non-parallel to flow direction magma throughout the dyke emplacement in the rock fabric.

2.3.5 Scanning Electron Microprobe (SEM)

Brown and McEnroe (2015) studied iron oxide magnetic mineralogy and paleomagnetism of southern Norway igneous rocks, as collaborative research with thermomagnetic to unravel the magneto-mineralogy of sequences of magnetite-ulvospinel and hematite-ilmenite. McEnroe *et al*. (2004) similarly reported on the magnetization of hematite and ilmenite intergrowth: mineral chemistry, phase relationships and magnetic properties of micron- to nanometer-sized hemo-ilmenite ores from Allard Lake, Quebec which demonstrated oxidation-exsolution of the blocking temperature of the TRM of magnetite,

giving rise to magnetite, retaining its compositional blocking temperature. Thus, few studies subsist on SEM and X-ray diffractometer (XRD) in Nigerian Precambrian basement rocks on the presence of iron oxides (Oloche *et.al*., 2009; Abubakre *et.al*., 2009; Roberts *et al.,* 2017).

2.3.6 Electron microprobe analysis

Krasa and Herrero-bervera (2005) studied the modification initiated alterations of magnetic textures as typified by dykes of koolau volcanic series using electron microprobe analysis (EMPA) to corroborate the thermomagnetic analysis of hydrothermally altered titanomagnetites in the cracks and joints in the basalts. Observations show paramagnetic mineral behavior at room temperature as well as bulk susceptibility usually outweighed by the ferrimagnetic mineral as described by thermomagnetic analyses while EMPA quantitative result showed titanomaghemite as predominant mineral due to iron emigration model of maghemitization.

2.3.7 Apparent polar wandering paths

Previous studies carried out by McElhinny and Senanayake, 1982; Van der Voo, 1990; Reshetnyak and Pavlov, 2016; Veikkolainen *et al.*,2014 using fold test, the conglomerate test, and the baked contact test to study the Precambrian rocks were due to its ability to magnetized when exposed to a magnetic field and capacity to memorize its remanence and field direction.The results showed that the frequency analysis of the geocentric axial dipole (GAD) generated the normal and reverse polarities of the Precambrian rocks by the use of frequency analysis and comparison of normal and reverse polarities.

Globally- Opdyke and Channell (1996); Reshetnyak and Pavlov (2016); D'Agrella-Filho *et al*. (2016) worked on paleomagnetism for apparent polar wandering paths (APWPs) and the geomagnetic polarity timescale (GPTS) as chronological /
charts but none of these studies have been carried out in West Africa.

2.3.8 Geocentric axial dipole in the Precambrian

McElhinny *et al*., 1996 normalized adequate amount of virtual geomagnetic pole (VGP) from sampling locations in the Precambrian terrain with the aim of estimating the paleomagnetic pole position. The result showed that hundreds of sampling cored oriented rocks could estimate pole positions in the Precambrian using the geocentric axial dipole (GAD).

Evans (1976) said that to assess the GAD in Precambrian, we have to deploy frequency analysis of slopes estimated from the paleomagnetic dataset distribution throughout the world. Veikkolainen *et al*. (2014) suggested the region Precambrian was largely dual poles with minor influences of octupole (5%) and quadrupole (2%) constituents while Veikkolainen *et al*. (2014) compared the reverse and normal field polarities owing to latitudinal GAD dependency (such as the reversals test). This analysis was implemented and supports the GAD hypothesis in the Precambrian (Hyodo and Dunlop 1993; Wingate and Giddings, 2000).

According to Reshetnyak and Pavlov (2016), the development of magnetic convection courses in the liquid core as a result of the impact and solid core development of Precambrian rocks is linked to the development of magnetic convection courses in the liquid core. A conglomerate test inside the Kaapvaal craton by Tarduno and Mamajek. (2014) revealed the possibility of an earlier Earth magnetic field (ca. 3400 Ma) (Usui et al., 2009). The mantle thermal regime led to dynamic exchange of the core nucleation. However, paleomagnetic studies applied to the geological timing of rock formation in Nigeria is generally lacking.

2.3.9 Day plots, hysteresis loops and first order reversal curves

Studies have shown simple measurements of magnetic minerals but problematic identification of its domain state due to its systematic mineralogy. Despite standard procedures for the measurement of magnetic hysteresis of rock fabrics; there is still ambiquity in results interpretation. This is largely due to varied mineral composition, internal stress, grain size and magnetic interactions among the grains resulting to its magnetic behaviour. This is evident in universally adopted Day plot (Day *et al*., 1977)

that describes generally the magnetic hysteresis behaviour by measuring ratios of saturation, remanent magnetization and saturation magnetization Mrs/Ms versus coercivity of remanence and coercive force Hcr/Hc. For instance, magnetostatic interactions in numerical studies demonstrates ideal SD grains could bring about large hysteresis parameters of tests to plot within the MD locale of the Day plot (Muxworthy *et al*., 2003). Recently, studies by Dunlop (2002) resulted to the development of series of regions that be determined by the mixture of several magnetite grain sizes: SD-MD and SD-SP mixing lines, and the SP (superparamagnetic) saturation envelope.

In order to eliminate some of the imprecision inherent to standard hysteresis estimations; Roberts *et al*. (2000) established a technique of mineral and domain state [single domain (SD), multi domain (MD), pseudo-domain (PSD) and super-paramagnetic (SP)] of type of hysteresis curve called a first-order reversal curve (FORC). FORCs measurement offer suite of detailed information from the hysteresis loop that aids assessment and interpretation of the interchanging field distribution and interactive elements that support the hysteresis loop. Recently, sensitive alternating gradient magnetometers and vibrating sample magnetometers have the capacity to measure appropriate FORCs and its diagrams rapidly.Thus, studies by Roberts *et al*. (2000) and Muxworthy *et al*.(2003) in Europe and USA on hysteresis loops, Day plots, "first order reversal curves" (FORCs) showed the character of their domain phases, namely: Single domain (SD), multi domain (MD), pseudo-single domain (PSD) and superparamagnetic (SP).

2.4 THEORIES OF METHODS USED

2.4.1 Thermomagnetic/ temperature dependence

Magnetic phase transformations, effective magnetic grain sizes changes, oxidation state of minerals and internal stress are products of mineralogical alterations of laboratory heating of rocks. Successes of several magnetic studies were based on the presence or absence of such alterations.For instance, mineralogical alteration can cause errors during

thermal demagnetization, especially when the magnetic carrier of the latter had suffered lower temperature transformation.

Determination of curve of Curie temperature (i.e. susceptibility measurements depending on the temperature in low- high magnetic field) is veritable tool in identification of magnetic minerals (conversion from ferrimagnetic to paramagnetic phase). Increasing temperature on Curie curve demonstrate a significant drop in susceptibility, sometimes accompanied by a rise in susceptibility (Hopkinson peak). However, changes in mineralogy can increase or reduce susceptibility, making it difficult to distinguish Curie temperature and the Hopkinson peak from mineralogy changes. It's easy to distinguish reversible heating and cooling curves from the Curie curves shape ((Odeyemi, 2005; Osazuwa *et al*., 2008; Oniku *et al*., 2008).

2.4.2 Emplacement direction, microstructures and magnetic susceptibility

Figure 2.8 below illustrates emplacement directions, microstructures and magnetic susceptibilities of rock materials. Many of the various kinds of rocks can be calculated in the laboratory to investigate rock micro foliations and lineations through the measurement of the tensor axes in six directions.

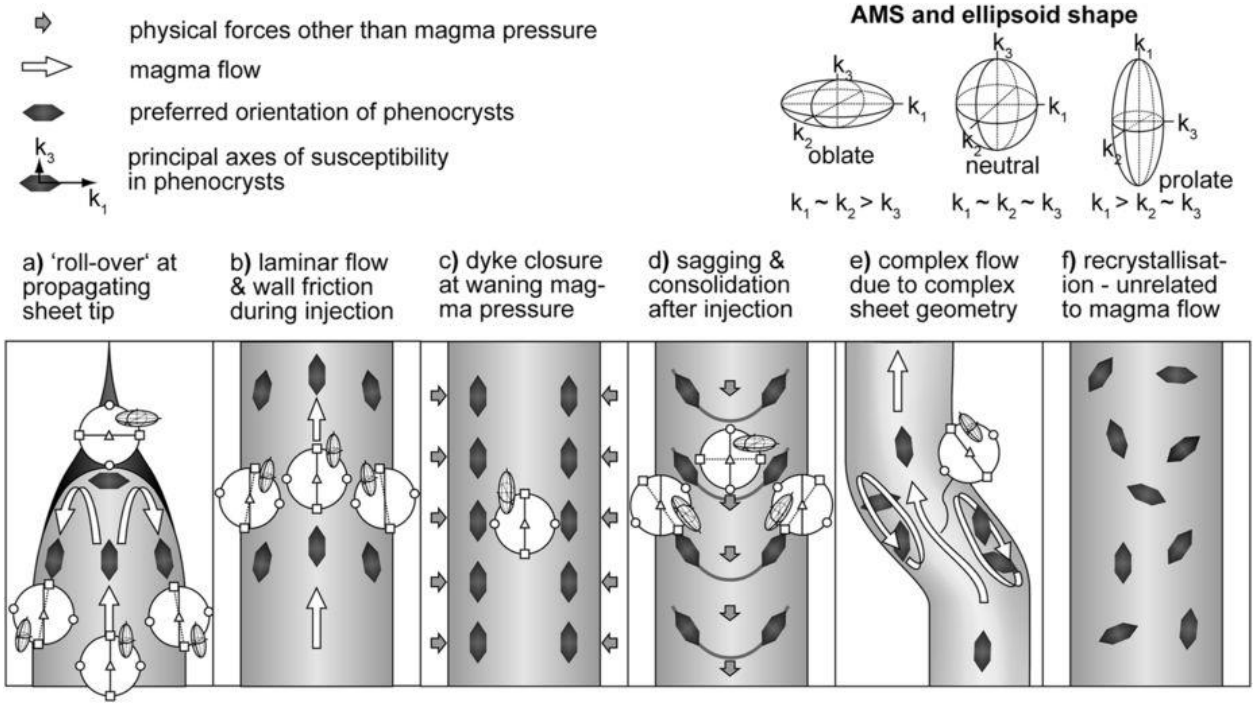

Fig. 2.8. Examples of correlation by varied AMS measurements of magnetic parameters. Intensely oblate magnetic ellipsoid induces high degrees of planar anisotropies (P' and F) and low degrees of linear anisotropies (L) (Adapted from Jelinek, 1981; Borradaile and Craig, 1987)

2.4.3 Raman spectroscopy

Raman spectroscopy is a precise tool for analysing iron-oxide minerals which are central in unravelling crustal magnetic phases that serves as paleomagnetic recorder and has extensive application in rockmagnetic studies (Rohrbach *et al*., 2007). Vibrational information and chemical bonds in molecules is commonly used in a Raman spectroscopy characterization. Raman microscopes have the capacity to map and expose the dispersion among different minerals using strong spectral and spatial resolutions, as well as a tool to identify minerals remotely in planetary research. (Zinin *et al*., 2007). Crustal and planetary materials can unravel the magnetism of iron oxide composition in them. In crustal work, thermomagnetic points are usually employed in the determination of these magnetic phases constituents. However, temperature dependence points in a sample typically represent whole rocks characters and do not provide information about specific grains or intra-grain composition variability. The structure of minute iron-titanium oxide grains can be determined using electron microprobe analysis, scanning electron microscopy with electron backscatter diffraction, and X-ray diffraction (Gehring et al., 2009).

2.4.4 Scanning Electron Microprobe (SEM), Electron Probe Microanalyser (EPMA) and X-ray diffraction (XRD)

By scanning a directed electron beam on the sample's surface, this type of electron microscope is unable to create an image. The primary beam used in the SEM commonly has an acceleration voltage between 15 and 30 keV (although lower values can also be used) and works under the conditions of high vacuum. The spatial resolution of SEM depends on multiple factors: 1) wavelength of the electrons in the primary beam (dependent on the energy), 2) the optical system used in the microscope (the type of electron gun and quality of the electron lenses), 3) the interaction volume of the electrons with sample (dependent on the electron energy and type of material analysed). The resolution of a SEM is up to few nm.

SEM images can be obtained by measuring electrons generated through two processes: back-scattered electrons (BSE) and secondary electrons (SE) are two different types of electrons. Secondary electrons are low-energy electrons (typically 2-5 eV) expelled from the K-orbitals of excited atoms by inelastic scattering of the beam electrons. They originate from the surface layer of the sample and because of this they provide information about topography of the sample. Back-scattered electrons are produced by elastic scattering of high-energy electrons from the beam by interaction with elements of the sample (of energies comparable to those of the primary electron beam). Elements with high atomic number tend to scatter more efficiently than those with lower atomic number (thus generating higher signal), and because of that they appear brighter in the resulting image. The BSE imaging mode allows graphical detection of areas of differing chemical composition (Brown and McEnroe, 2015; McEnroe *et al*., 2004; Salminen *et al.,* 2019).

An SEM equipped with an appropriate detector can be used to analyse X-rays produced due to interactions of the sample with a primary electron beam. Those X-rays can be used to acquire informative chemical constituents of the sample due to the fact that they are characteristic to particular elements and their intensity is equivalent to the element concentration in the sample. However, to quantify the measurement it is necessary to reference the wavelengths to the appropriate standards. The signature X-rays have two properties that can be measured: photon radiation (dispersive energy) spectrometer, EDS) or photon wavelengths (wavelength dispersive spectrometer, WDS); in SEM instruments EDS is used, whereas electron microprobes usually use the WDS method. Samples used for SEM analysis can include whole sample fragments, but they must be small enough to fit into the sample chamber, or thin sections prepared in the same way as for optical microscopy. Polishing a thin section before analysis makes the dispersal of X-rays more predictable, as under those conditions it depends only on the compositional variation. Samples analysed under SEM usually have to be coated with a conductive layer (most often carbon, gold or platinum) to avoid accumulation of charging on the surface of the sample (although working with uncoated samples is also possible, but no high-resolution images or analytical data can then be obtained).

As this electron configuration is unstable, one of the electrons from the outer orbital fills the newly free position. During this process, energy equal to the difference in energetic level between the "void" orbital and orbital from which the electron filling the void originates is released, forming secondary X-rays. Because each element is characterized by a set of specific allowed energies of fluorescent X-rays, it can be unequivocally identified. The contents of a certain element within the sample can be measured because the intensity of the specific X-ray wavelengths is proportionate to the intensity of certain element in the specimen. However, in order to quantify the results, the obtained information about wavelength and intensity of measured X-rays needs to be compared with data obtained for samples of known composition.

2.4.5 Day plots, hysteresis loops and First Order Reversal Curves (FORCs)

Pseudosingle-domain (PSD) and multidomain (MD) magnetite grains size have low relationship with magnetic susceptibility (Hartstra, 1982), as well as differential grain size alteration into SD to PSD or superparamagnetic (SP) to Single domain (SD). SD has finer grains and higher susceptibility than others (Stacey and Banerjee, 1974) and the homogenization of the distribution of crystals have substantial impacts in susceptibility of large grain size and domain wall rearrangement. Thus, inverting and placement of new cations in vacant sites inside the crystal lattice (Bina and Henry, 1990) yield meaningful susceptibility distinctions owing to comparatively low temperature heating.

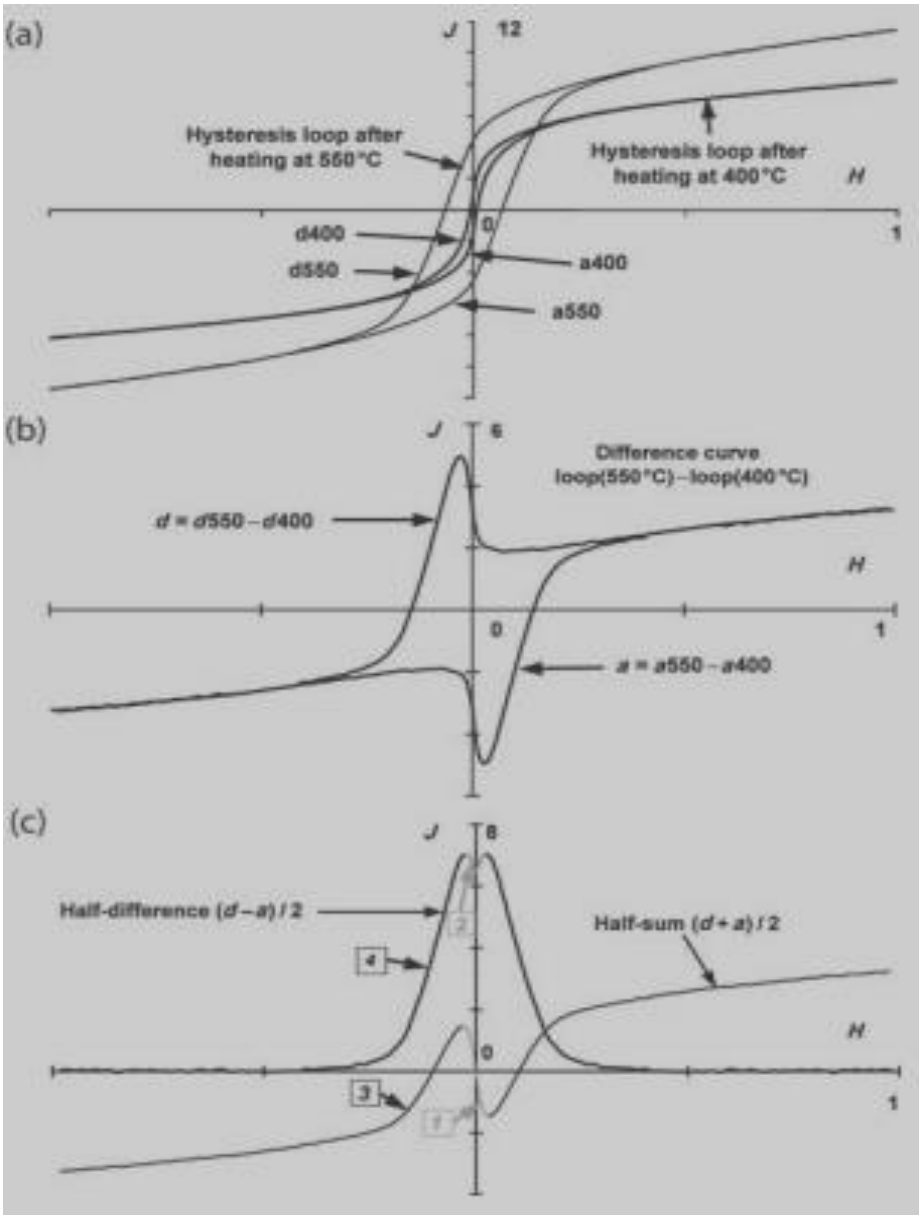

Fig. 2.9. Hysteresis loops measurements(After Henry *et al*., 2004)

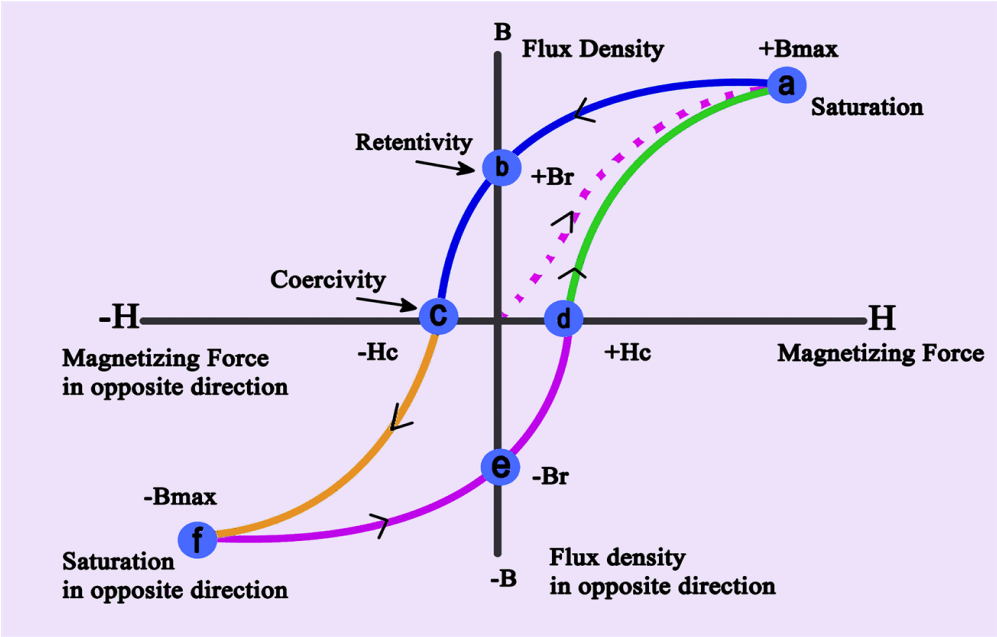

Fig. 2.10. Magnetic hysteresis (Adapted from www.theoretica.us)

Hysteresis loop investigation into magnetic mineral grain size and its coercivities in rock magnetism can be used to derive the saturation of the magnetization. Results of total magnetization saturation is obtained by gradual decrease and increase of fields in opposite course ("descending" curve d, Fig.2.9) while the "ascending" curve a is acquired by initiating continuous decrease and increase of fields in opposite course. Then, room temperature hysteresis loops measurements of altered minerals are acquired before and after heating (Fig. 2.9a). In curves d and a, different hysteresis loops (Jb–a) are obtained by subtracting the same field (H) value of the calculated magnetization value before (Jb) and after (Ja) heating. (Fig. 2.9b). Half-difference and half-sum separation techniques are comparatively complicated curves, yet the interpretation turn out to be much easier (Fig. 2.9c). Figures 2.10 and 2.11 demonstrate discrimination of characteristics of saturation of magnetic field coercivities are likely for receding and occurring magnetic minerals.

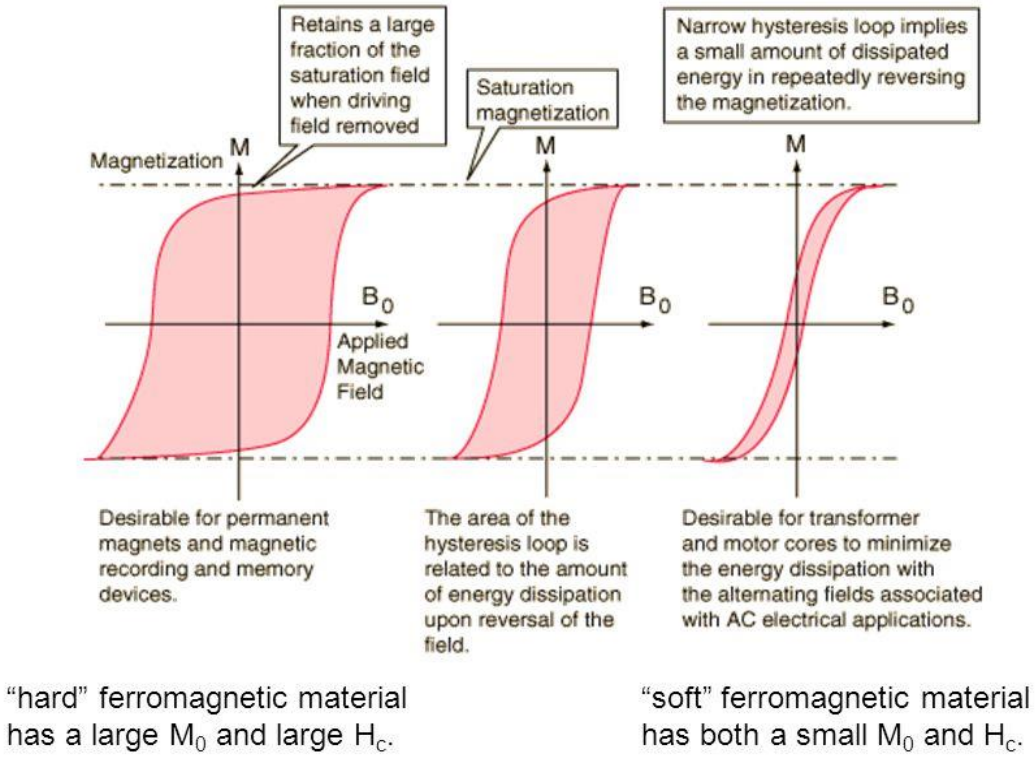

Fig. 2.11. Characterization of magnetic hysteresis (Adapted from Studfile.net)

2.4.6 Apparent polar wandering paths APWPs and Geomagnetic polarity time scale (GPTS)

2.4.6.1 Demagnetization

Separation of distinct natural remanent magnetization (NRM) components can be evaluated using Kirschvink's principal component analysis (PCA), which is driven by careful evaluation of orthogonal demagnetization plots and is used to approximate magnetization components (Zijderveld, 1967). The least squares fit method is used to define the points of linear trajectories, whereas the maximal angular deviation (MAD) approach is used to determine the fit correctness of straight projectories. Paleomagnetic directions with a MAD smaller than 10° are suitable. Fisher (1953)'s statistics are used to measure mean directions, since each direction is vector element to generate paleomagnetic poles in paleomagnetism. Fisher's probability density distribution uses statistical data to classify the goodness of the mean direction. The parametric quantity (K) measures the precised intensity distributive directions of data projections around the mean. Equation 2.1 yields the projected parametric quantity (K) in the Fisher's measurementsasa result, for well clustered directions, high values for the parametric quantity (K) are predicted.

The program generates a regular Zijderveld orthogonal vector map, an equal area stereoplot of directions, and a decay of strength as demagnetization progresses (Fig. 2.12). Equal field stereographic projections indicate the declination and inclination of each step of demagnetization, as well as the progress of magnetic components and directions. Observing the NRM frequency's decay behaviour is an easy way to estimate the magnetic minerals and their coercivities. Low coercivity minerals (MD magnetite) decay rapidly to zero, while high coercivity minerals (hematite, goethite) do not reach absolute magnetization even though an AF field is applied.

$$K = \frac{N-1}{N-R} \quad \text{Eq. 2.1}$$

where R is the length of the summation of N discrete unit vectors. The formula below is used to calculate where R is the length of the summation of N discrete unit vectors. The

formula below is used to calculate (α95) confidence limit for a given mean direction (equation 2.2)

$$\alpha 95 = \frac{140^{\circ}}{\sqrt{KN}} \quad \text{Eq. 2.2}$$

The implication of α95 is that accuracy of the mean direction is less than 16%.

The Zijderveld plot is a two-dimensional visualization of three-dimensional demagnetization data on a series of two vector projections. By projecting the vector onto two orthogonal planes, the Zijderveld plot will represent directional and intensity information on a single diagram. The Zijderveld diagram projections the magnetization vector's end point into two planes at the same time. Two planes are necessary because the vector is oriented in 3D-space. Any two orthogonal planes would do, but commonly the (geographic) horizontal and vertical planes are chosen, such that the horizontal plane shows a component corresponding to the declination and the vertical plane shows the vertical (upward or downward) component, which gives an indication of the inclination (Fig. 2.12). The horizontal and vertical projections have one horizontal axis in common, optimally the one to which the declination is closest. The successive end points obtained during demagnetization reflect the intensity of magnetization in their distance from the origin. From Zijderveld diagram, it is possible to distinguish the primary and secondary components present in an NRM direction along with their individual intensities and directions. However, such distinction is possible provided that demagnetization procedure gives rise to Zijderveld diagrams consisting of only straight line segments. On the other hand, if the diagrams show curves, it means that the direction undergoes a change at every demagnetization step, and difficult to pick out any stable direction. Recognizing that a high-stability NRM (ChRM) portion has been isolated requires observing a linear trajectory of the vector end point toward the origin.

Principal component analysis (Kirschvink, 1980), best-fit line over dispersed measurement points, with a total of three phases, is defined as palaeomagnetic components and a median angular deviation (MAD) of 6°. Directions of mean remanence are achieved when components of at least 3 specimens are the same. The component

level calculations are carried on, with all of the sites pointing in the same orientation. From demagnetization, this technique of investigation can be used to determine various palaeomagnetic components.

2.4.6.2 Determination of palaeomagnetic direction and pole

A site's mean direction of characteristic remanent magnetization (ChRM) is a record of the past direction of the geomagnetic field vector at the time it was acquired. The pole is determined (Fisher, 1953) from a specific site and virtual geographic pole (VGP) that forms the geocentric dipole of accounts for the observed magnetic field direction at one location and one point by specimen examination. The apparent polar wander path (APWP) shows the sequential placements of palaeomagnetic poles for each continent. Because the polarity of the Earth's magnetic field fluctuates, it's impossible to say whether the researched site region was in the northern or southern hemisphere.

Structural geology differs from paleomagnetism studies, due to the magnetic vector pointing down or up, denoting positive and negative inclinations respectively. To characterize this vector, Lambert *equal-area* projection was adopted (Fig. 2.13); due to its interest of the directional scatter in distributions of paleomagnetic directions.

The problematic issue with paleomagnetic studies is the overlapping coercivity spectra (Fig.2.14e); where arched sections are not determined (Fig.2.14f). Therefore, unconventional measurements of thermoremanent magnetization are estimated without cleaning the remagnetization episodes (Halls, 1978).

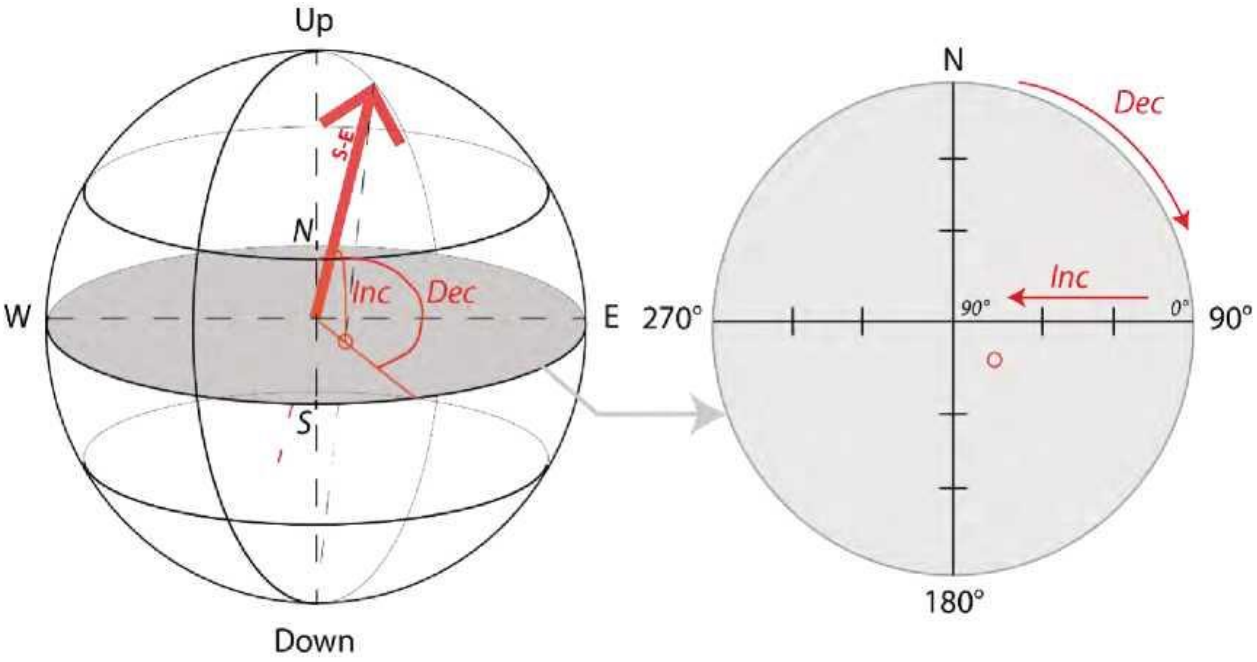

Fig. 2.12. Lambert stereographic in grey (Modified from Bispo-Santos *et al.*, 2012)

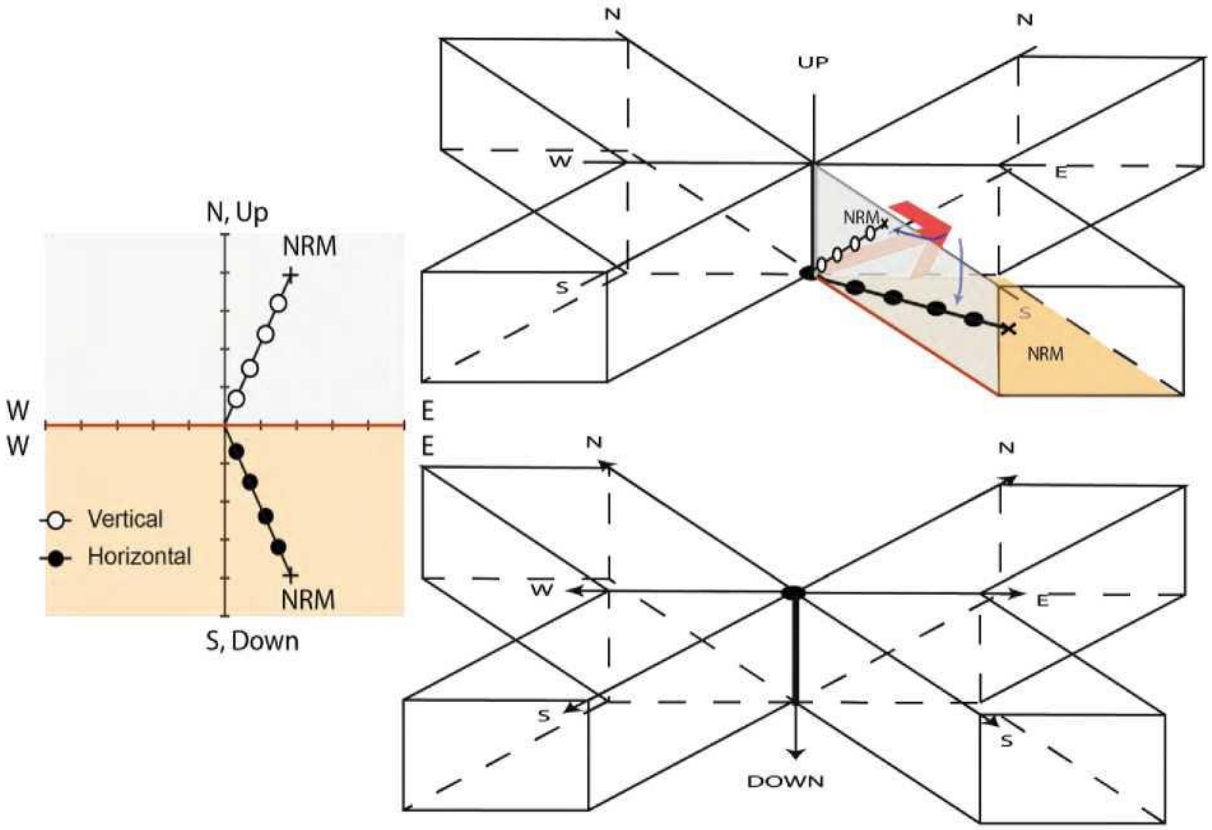

Fig. 2.13. 3D Zijderveld diagram and vector. Note the decomposition of two orthogonal planes

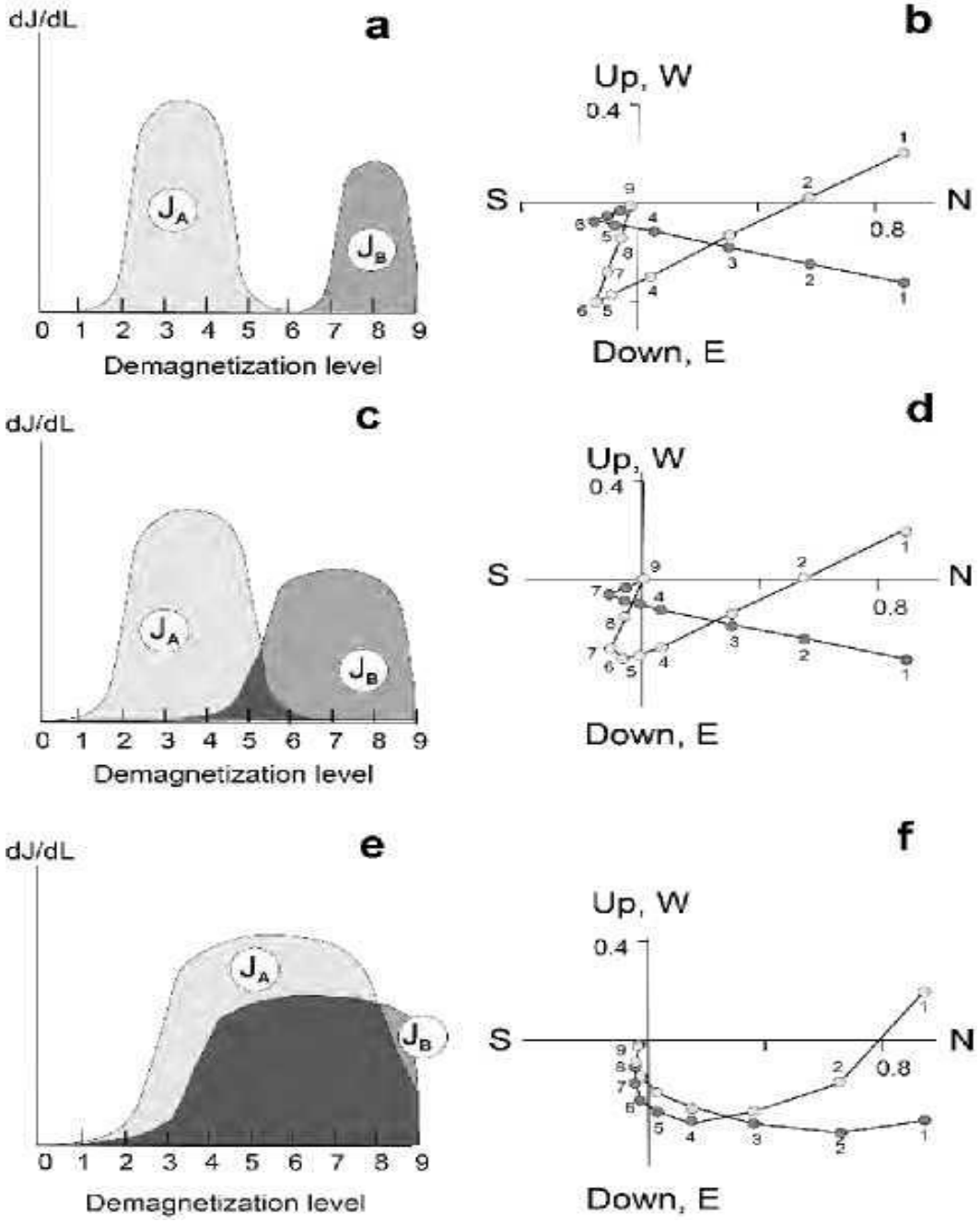

Fig. 2.14. Probability of overlapped demagnetized spectra (Hc or Tb) for 3 cases (a, c, e) and related Zijderveld plots (b, d, f) (Langereis *et al.*, 1989)

2.4.6.3 Field tests and paleomagnetic stability

During rock cooling, stable direction identification and isolation (ChRM) transmitted by ferrimagnetic minerals with high blocking temperatures and coercivities was obtained. Fold, reversals, baked contact, regional consistency tests are usually adapted to this study because of its relevance to its deformational history.

2.4.6.3.1 Reversals test

Reversion of the orientation of geomagnetic field varies by space of 180° between a normal and reverse polarity. Throughout lowering the temperature of the rocks, the magnetic minerals do document such occurences that yield location of normal and reverse polarities. Positive reversal test suggests the use of statistical examinations (McFadden and McElhinny, 1990). Thus, positive reversal test suggests stable specimen of averaged secular variation and secondary components cleaning.

2.4.6.3.2 Baked contact test

Baked contact test was used to study the igneous rocks. For example, perpendicular dike intruding an older rock (Fig.2.14); throughout the collison and deformation of the rock, the altered rock obtains thermal remanent magnetization (TRM) parallel to the dike. Furthermore, country rock far from contact (unaltered rock) retain previous directional trend separately. Thus, the dikes's ChRM direction is primary and positive.

2.4.6.3.3 Regional consistency

This criterion entails rationality in the successions of directions recorded in the study area, which implies that uniform units have same age and orientations. Thus, Precambrian rocks may possibly be remagnetized by tectonometamorphism; yet, substantial dataset is needed to determine the extent of remagnetization.

2.4.6.4 Paleolatitude reconstruction

Southwestern Nigeria Pan-African granites can be used to reconstruct the paleomagnetic pole (600±150 Ma,) using mean magnetic inclination of 60.2° and magnetic declination of 133.8° and the equivalent West Africa (28°S, 346°E) is the paleomagnetic pole. (Théveniaut *et al*., 2006) (Fig. 2.15)

Once the rock has been deposited in the Earth's area, the paleomagnetic pole corresponds to the geographic north/south pole using the geocentric axial dipole (GAD) principle. As a result, in paleogeographic reconstruction, a rotation pole (λ_ρ; λ_ρ) must be measured as long as the paleopole corresponds to the geographic pole. As a result, in paleogeographic reconstruction, a rotation pole must be determined in relation to the rotation angle. Typically, the Euler pole is employed to spin the continent back to its paleogeographic location.

The paleomagnetic pole's coordinates alongside the rotation angle (almost) are generally determined to ensure that the paleopole corresponds to geographic pole as well as rotate the globe to its paleogeographic position using Euler axis. As long as the paleomagnetic pole coordinates (λ_ρ; φ_ρ) are known, one can estimate the coordinates of the Euler pole **(λ_E; φ_E):**

$$\lambda_{E=}\varphi_p + 90°; \lambda_{E=}0° \quad \text{...Eq. 2.3}$$

The angle of rotation ((θ) is :

$$\theta = \lambda p - 90° \ (North\ pole) \quad \text{...Eq. 2.4}$$

Or

$$\theta = \lambda p \pm 90° \ (South\ pole) \quad \text{... Eq. 2.5}$$

The rotation (Euler) pole is (0°, 76°) for the western African pole and the rotation angle is 62° on a reconstruction of the northern Pole, the coordinates are (0°, 76°) and the angle of rotation is -118°. (Equations 2.3 - 2.5). Due to the GAD model's polarity ambiguity, this indicates polarity ambiguity (Fig. 2.15). The craton's position in the southern hemisphere (locations B, C, and D) or the northern hemisphere (locations A, B, C, and D) (locations E, F, G) can be reconstructed (Fig. 2.15). Nevertheless, paleolongitude is not restricted:

nevertheless, a full paleogeographic reconstruction requires additional data such as geological evidence (orogenic belts, mafic dike swarms)

2.4.6.4.1 Comparison between two cratons

For two ideal cratons for example X and Y, two different approaches can be adopted: First make use of two coeval paleomagnetic poles in their current positions for the two cratons. Then estimation of the rotation pole for each craton and reverse their paleolatitudinal positions to the poles on the geographical northern pole. Hence, both cratons in longitude around an Euler pole are allowed to move freely in their north pole positions, owing to their GAD symmetry model as well as alignment of coeval poles age.
Alternative methodology can be adopted in reconstructing the configuration and position of the cratons in latitude. But observing the cratons configuration we hypothesize that both cratons were together and the rotation pole can be moved to the second craton (craton B) in our first assumed shape. For example, the second paleomagnetic pole, the geographic North Pole can be reconstructed since the craton is close to the first paleomagnetic pole. This process allows us to test cratonic form models; for example, SAMBA or NENA models over time (D'Agrella-Filho *et al*., 2016).

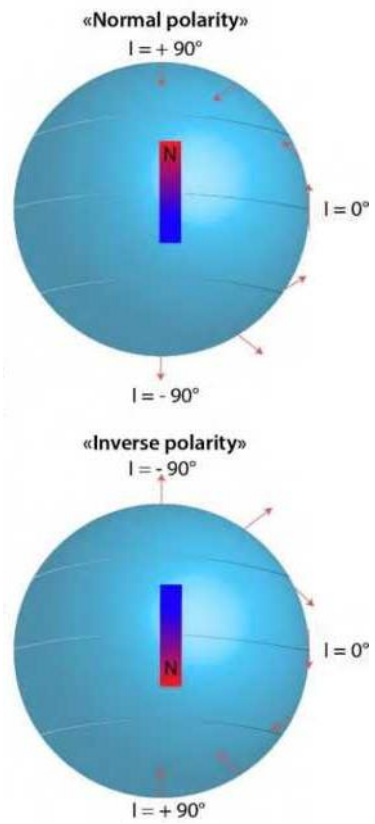

Fig. 2.15. West Africa craton reconstruction at 600±150 Ma with the Southwestern Nigeria pole (Adapted from D'Agrella-Filho *et al.*, 2016)

2.4.6.5 Magnetism and Paleomagnetism

Mobility of orbital electrons within the nucleus and their intrinsic electron spin emanates from magnetism from natural materials. The application of magnetic field (**H**) to a rock sample allows mobile electrons to be transformed, causing an induced magnetization (**M**). The correlation between **M** and **H** is Equation 2.6:

$$M = KH \qquad \text{……Eq 2.6}$$

2.4.6.5.1 Types of magnetic materials

The magnetic materials behave diamagnetically, ferromagnetic, paramagnetic, ferrimagnetic, antiferromagnetic and parasitic ferromagnetic (Figs. 2.16 and Table 2.1)

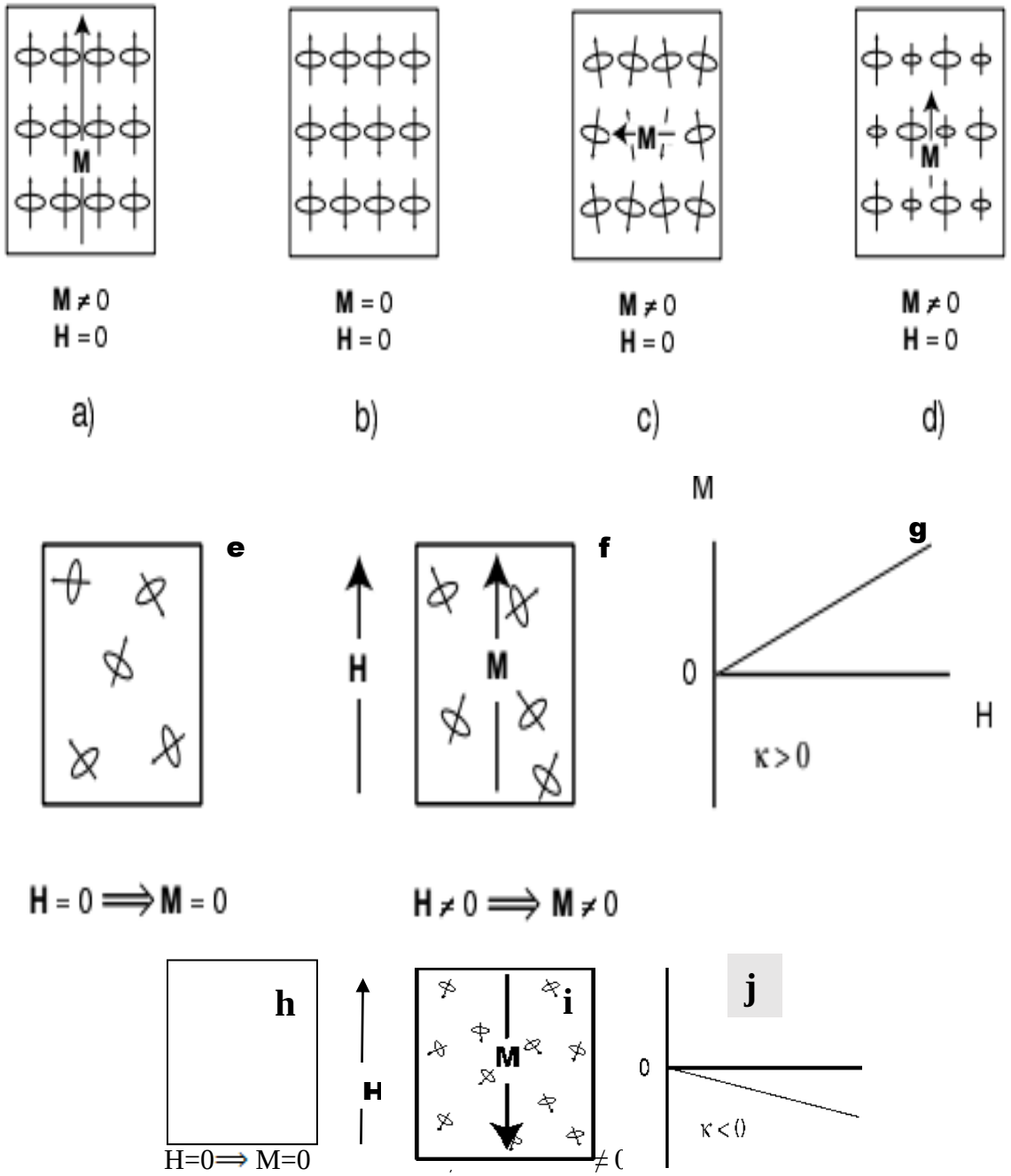

Fig. 2.16. Schematic depiction of the net magnetization in ferromagnetic materials (a) ferromagnetic (b) antiferromagnetic (c) parasitic and (d) ferrimagnetism. Behavior of paramagnetic material (e) no magnetic field and (f) presence of magnetic field; (g) the transformation of magnetization due to applied field strength. Behavior of a diamagnetic material (h) no magnetic field and (i) presence of magnetic field (j) the transformation of magnetization due to applied field strength (Modified from Lowrie, 2007)

Table 2.1Characters of iron oxides

Mineral/Oxides	Composition	Magnetic Order	T_c(°C)	(Am^2/kg)
Magnetite	Fe_3O_4	Ferrimagnetic	575-585	90-92
Ulvospinel	Fe_2TiO_2	Antiferromagnetic	-153	
Hematite	αFe_2O_3	Canted antiferromagnetic	675	0.4
Ilmenite	$FeTiO_2$	Antiferromagnetic	-233	
Maghemite	γFe_2O_3	Ferrimagnetic	~600	~80
Jacobsite	$MnFe_2O_4$	Ferrimagnetic	300	77
Trevorite	$NiFe_2O_4$	Ferrimagnetic	585	51
Goethite	$\alpha FeOOH$	Antiferromagnetic	120	21
Magnesioferrite	$MgFe_2O_4$	Ferrimagnetic	440	

2.4.7 Magnetic methodology

2.4.7.1 Ferromagnetic phases Identification

Rock materials are easily identified by measurement of the anisotropy of ferromagnetic phases present in the specimen. Majority of fine grain minerals with high coercivity is recognizable using state of the art microscopic tools (Butler, 1992; Raposo and Gastal, 2009). Methodologies employed are:

2.4.7.1.1 Alternating field demagnetization (AF*)*

Randomizing and tumbling of rock material in alternating field demagnetization removes antipodal magnetization at right angles to three mutual directions of the material. The material is subjected in a zero ambient and alternating fields and particles with lower coercivity spectra than the maximum peak field will be randomized and part of the magnetization of the sample will be annulled. By step-wisely increasing the fields, the remanence are progressively demagnetized and lower coercivities magnetic grains than the maximum peak field will be generated. Hence, hematite or goethite demagnetization practicability is not always possible (Lowrie and Fuller, 1971; Chaves, 2021).

2.4.7.1.2 Acquisition of Isothermal Remanent Magnetization (IRM*)*

Remanence obtained under stable temperature situations in a direct current field and saturation isothermal magnetization (SIRM) occurs when the concentration of the magnetization will climb in lockstep with the external field concentration until the magnetization reaches its maximum. The geometry is based on the presence of concentration and coercivities of magnetic mineral in a material (Dunlop and Özdemir, 1997; Lowrie, 2007; Chen *et al.*, 2017). Thermal demagnetization allows multicomponent IRM discrimination of which coercivity elements is being unblocked in a specific temperature range along their three axes.

2.4.7.1.3 Thermal demagnetization of the magnetization (TD*)*

Through zero-field, programmable step-by step heating; clean magnetic grains with lower blocking temperature lose their magnetization. Subsequently, the magnetized grains do not recover remanence by cooling the materials through zero fields. The temperature ranges, where rock material have no presence of ferromagnetism is known as Curie temperature and difficulties arises when there is alteration and transformation of new ferromagnetic materials during heating (Chen *et al.*,2017).

CHAPTER THREE

MATERIALS AND METHODS

3.1 Materials used for the field sampling

Figure 3.1 shows some of the representative southwestern Precambrian basement rock samples. The following materials were used during the field sampling exercise:

1. Compass clinometer
2. Global Positioning System (GPS)
3. Field note books
4. A geologic hammer
5. Measuring tape
6. A clinometer
7. A field bagand sacks
8. Topographical maps

3.2 Materials used for the laboratory analyses

The following equipment were used for laboratory analyses of the rock samples:Multifunctional kappabridge (MFK1-FA), Raman infrared spectroscopy, Scanning Electron Microprobe (SEM), Electron Microprobe Analysis (EMPA), X-ray diffractometry (XRD), X-ray refractometry (XRF), induced coupled plasma-mass spectrometer (ICP-MS), Portable gasoline drill, rock samples cutters, permanent magnet, hammer, alternating field (AF) and thermal (Th)demagnetizers, cryogneic magnetometer (DC-SQUID), JR5 spinner magnetometer, Impulse magnetizer, Vibrating Sample Magnetometer (VSM) and numerous workstations and softwares.

3.3 METHODS

Figure 3.2 illustrates the flowchart of the methods used in collecting and analysing the samples; whichwas divided into two (2), namely: Field sampling and Laboratory analyses.

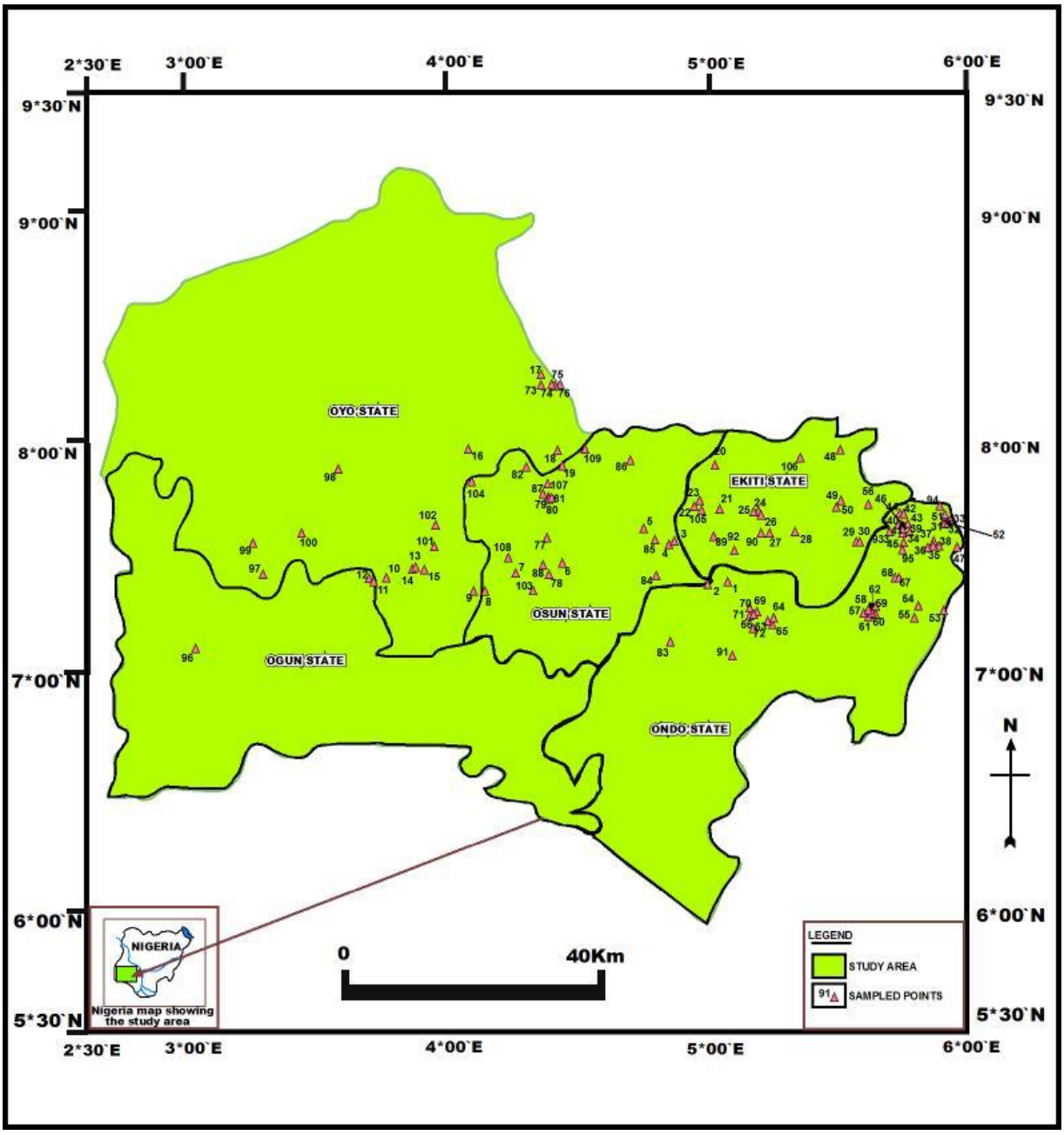

Fig. 3.1 Location map of the study area and sampled points

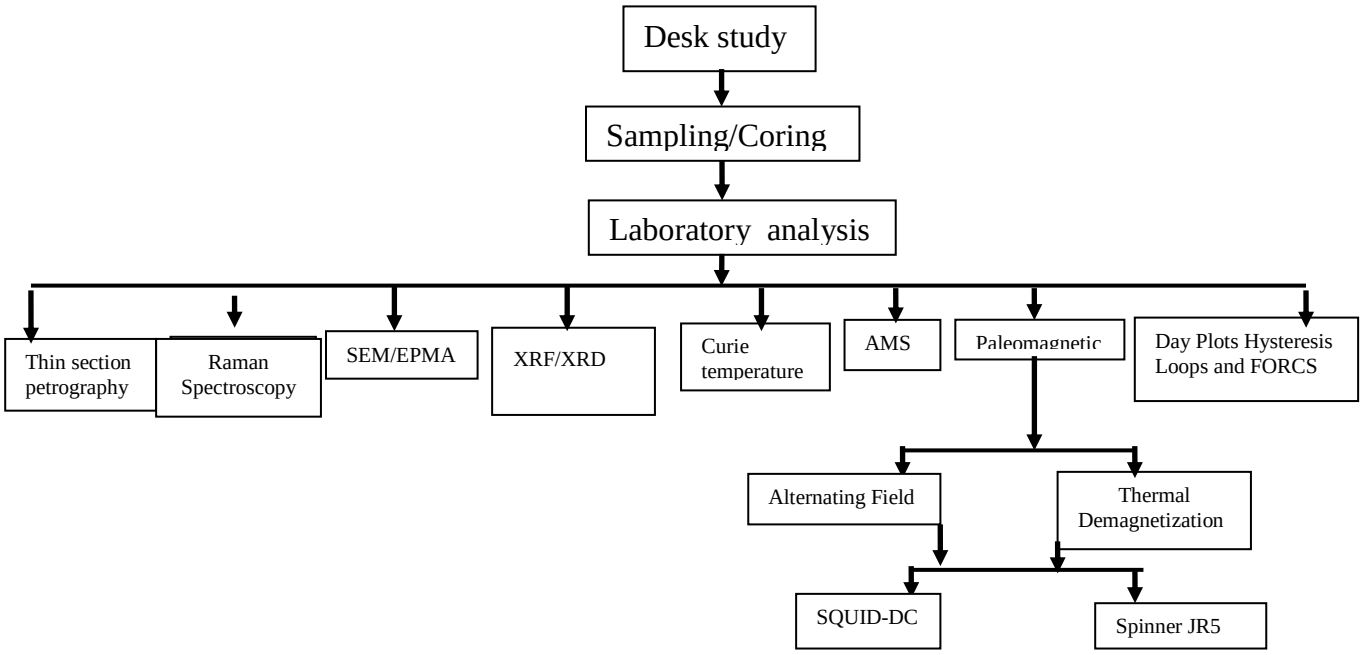

Fig. 3.2a. Interpreation flowchart

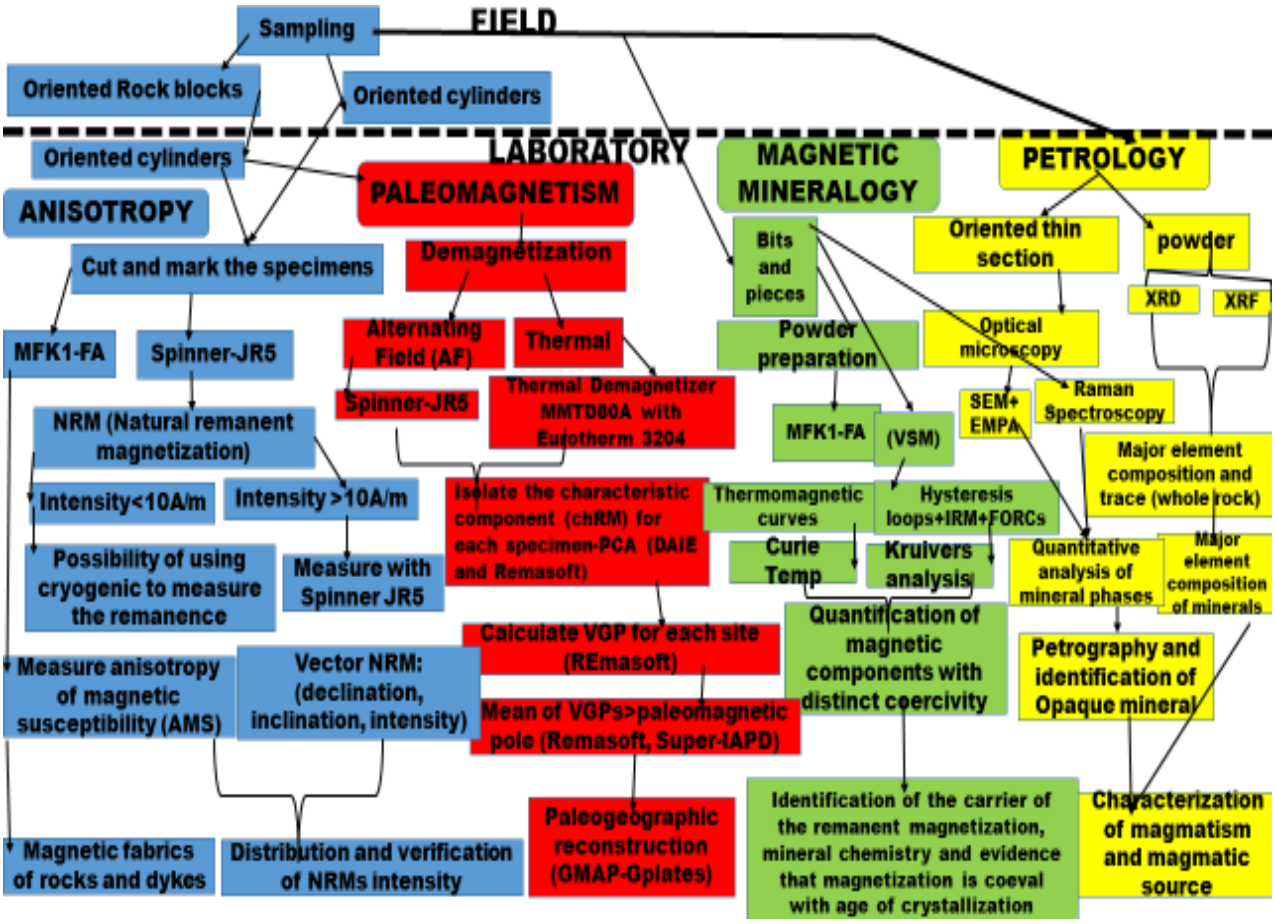

Fig. 3.2b. Flowchart of workflow

3.3.1 Paleomagnetic sampling

One hundred and ten (110) oriented block rock materials were sampled for baseline rock magnetic and for paleomagnetic evaluation of southwestern granitoids using handy rock machine driller affixed with water-cooled diamond bit (Fig. 3.3A). During the systematic rock sampling, about two to four rock material were sampled in a location (Fig. 3.3B) and traced with reference mark with arrows on top of the cylinder, the azimuth (angle between the geographic north and material reference mark) and plunge (angle between axis of cylindrical material and vertical) were recorded and marked on a field book for each location. The solar compass was used to cross-check if the azimuth acquired by magnetic compass, was correct, because some of the rocks had strong magnetization (caused by lightning strikes), which drew away the needle of magnetic compass.There was difficulty in drilling the rocks and most of the sampled oriented block samples were mapped and cut into cylindrical cores in the laboratory using the machine drill (Fig. 3.3C). The sampled rock materials were tagged as: CO ("Cyril Okpoli"), beginning with numerical digits (1, 2, 3…) and then using alphabets labels (A, B, C…) for the sampled location and drilled cylinder respectively. For example, block sample 9; CO-009A, CO-009B, CO-009C, etc… for block sample 10, etc…drilled cylinders from block samples area were assigned as CO-10A, CO-10B, CO-10C, etc. Norges Geologiske Undersokelse (NGU) that is Geological Survey of Norway built software 'IAPD2000' was used to input the field geographic coordinates and orientation dataset. Global Positioning System (GPS) was used to acquire the geographic coordinates and the local time that such rock materials were sampled; while the International Geographic Reference Field (IGRF) model software estimated the magnetic declination, solar azimuth and correct measured azimuths in the field, withreference to geographical north.

Sampled materials were brought to Paleomagnetic Laboratory, SOEST-HIGP and cut in the laboratory using standard protocols (Fig. 3.3D). Hence, the cylinder CO-10A were turned to three rock samples named CO-10A1 (underneath the mark), CO10A2, and CO-10A3 (upper mark). Figures 3.3E and 3.3F illustrate the coring of syenite dike and banded gneiss rock sample in the field respectively. The paleomagnetic standard specimen size was 2.2 cm in height and 2.5 cm in diameter for all the rock samples. The

sum of 1568 rock samples collected from 110 locations were utilized for paleomagnetic measurements.

Fig.3.3. (A) Sampling with a handy rock machine driller B: Orienting rock. (C) Drilled rocks. (D) cylindrical rocks. (E) Coring syenite dike. F: Banded gneiss rock sample

3.3.2 Laboratory Methods

Figure 3.2 shows the methodology flow chart used during the research studies. Raman infrared spectroscopy, XRD, SEM, EMPA, petrographic, paleomagnetic and chemical studies were carried out at the School of Ocean and Earth Science and Technology – Hawaii Institute of Geophysics and Planetology (SOEST-HIGP) Hawaii, Manoa, USA and Institute of Rock Magnetism (IRM) University of Minnesota, Department of Earth Sciences, Minneapolis, USA laboratories.

3.3.2.1 Micro-Raman spectroscopy

Granite (Akunu-akoko); biotite granite gneiss (Lanlate); Augen gneiss and banded gneiss (Ajibode UI, Igbatoro); banded gneiss (Imesi-Ekiti); porphyritic granite (Shasha-Akure); syenite (Iwo) and amphibolite (Ido-Ekiti) rock samples were hammered to bits and pieces and selected with strong permanent magnet in the laboratory because of their mineralogy and magnetic susceptibility.Tiny, unpolished grains of different iron titanium oxides concentrations were affixed on carbon tape attached to a glass slide for Raman spectra measurements. In addition to optical images, micro-Raman spectroscopy of various excitation wavelengths was used. At the University of Hawai'i, various instruments were used to capture Raman spectra. Spectra with 785 and 830 nm -Kaiser Optical Systems' micro-Raman system and Renishaw inVia microspectroscopy respectively were used for the study. The system consists of 785 and 830 nm Invictus diode laser, a Kaiser Holospec/Renishaw spectrometer, spectral range of 150–3300 cm^{-1}, Leica microscope with imaging capabilities, as well as an Andor CCD camera. The laser light was sent to the microscope via a 100-meter optical fibre, and the Raman pulse was sent to the spectrometer via a 100-meter optical fibre (Fig.3.4). A 50 objective lens fixed on the microscope in backscattering geometry was used to focus the laser spot and observe the signal.The spectrometer and microscope weree fixed through optical mirrors of different wavelengths and were operated using PRIOR workstation (via WiRE 3.2 software). The spectra were imported into MATLAB 7.4.0 and Grams/AI v8.0 for normalizing statistical analysis, background interference in each spectrum as well as baseline diffraction patterns i.e correction and peak fitting using Gaussian and Lorentzian geometries, Background correction was done using sixth-order polynomials in both cases. To obtain

principal components in the data collection, Principal Component Analysis (PCA) and Significant Factor Analysis (SFA) were employed. To avoid artifacts, similar specimens were stored; laser power had below 0.7 mW to prevent destruction of specimen; neutral density filters had a constant power of 675 μW; acquisition time was 60 s; spectrometer calibration before acquiring Raman spectra; and cyclohexane standard protocols were used (deFaria *et al*., 1997; Shebanova and Lazor, 2003b).This equipment was used to investigate the magmatic effect of maghemite on natural sample Raman spectra.

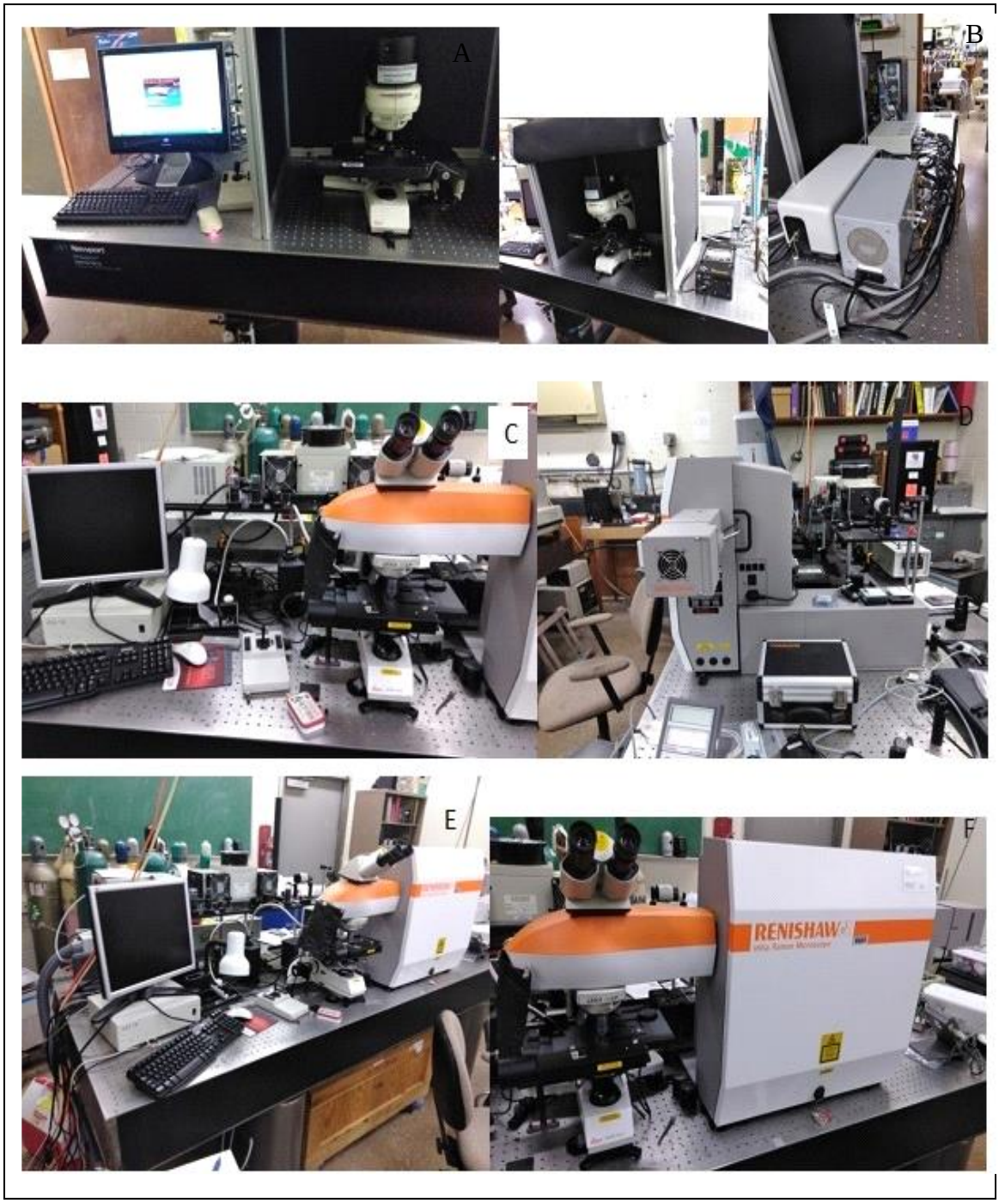

Fig. 3.4. A-B. Kaiser 785nm micro-Raman Microprobe system coupled with Invictus diode laser, C-F: Renishaw inVia micro-Raman system coupled with an 830 nm Invictus diode laser

3.3.2.2 Geochemistry (XRF AND ICP-MS)

Ejigbo biotite granite gneiss, Ikire granite gneiss, Iwaraja granite, Effon-Allaye quartzite, Ikare-Akoko migmatite gneiss, Akungba-Akoko banded gneiss, Iwo granodiorite and Gbongan migmatite granite gneiss were geochemically analysed among some selected samples from southwestern Nigeria. The rock samples were crushed into powdery form and analysed with XRF equipment. The XRF machine processes are as follows: knock out the inner orbital of the electron to excitation stage, detect and characterised their emissions and intensity and finally detect the intensities and elemental concentration. Thus, enabling the characterization of the probable sources and evolution of the southwestern Pan-African rocks. X-ray Refractometry (XRF) and Inductively Coupled Plasma Mass Spectrometer (ICP-MS) were carried out on the above named representative samples to characterize different lithologies and diverse geochemical signatures. The rock materials were mapped and collected in different units throughout the southwestern Nigeria granitoids. ICP-MS was used for elemental content of the samples while XRF provides information about elements in the rock samples.

3.3.2.3 Scanning Electron Microscopy and Electron probe Microanalyzer

Gneiss (Akunu-Akoko); granite (Iwaraja); biotite granite gneiss (Ikirun); charnockite (Akunu-Akoko) and granite (Etioro-Akoko) were used to describe the ferromagnetic minerals on the basis of their mineralogy and magnetic susceptibility. The polished thin sections were studied using SEM. Thus, SEM was employed in the Institute of SOEST-HIGP (Manoa, Hawaii, USA) to constrain the mineralogy of accessory minerals. SEM was used for imaging, qualitative analysis (only if equipped with an "EDS") and quantitative analysis (when equipped with an "EDS/WDS", Fig. 3.5). SEM and EPMA were applied, to characterize the specimen for: mineral identification; compositional information, microstructures/ deformation and compositional evolution of minerals.

The electron beam was attached to the magnetic lenses that allow interaction (in the vacuum) with the specimen, to variety of effects which are employed to aid identification and analyses. The solid state specimen can be placed as a grain/whole sample (size based on sample chamber size)/thin section. Sample in its entirety and polished part (especially

when quantitative data are sought) was used, and the whole rocks are imaged to deliver a "stereoscopic image".

Electron Probe Microanalyzer (EPMA) used for this study is primarily designed for quantitative analysis, whereas SEM and EPMA instruments have the same basic operating principle. They share several image-optimized components, particularly when high resolution images are required.The SEM used for this study has 3-D imaging capability, it allows the user to tilt the samples, while EPMA cannot be tilted. Therefore, the EPMA has many spectrometers of wavelength and dispersion that are not present in the SEM.

3.3.2.3.1 Sample preparation

For the quantitative analysis the samples were polished to remove cracks and pits. The rock polished section was done by means of special laps and diamond grit. 0.25 μm grit size yielded the best results. Thin layer of conductive carbon was used to transmit polarized light petrography without affecting the carbon coating. The beam was rastered in the coils (for slower speed and higher resolution) and over time the intensity of the current was changed.

3.3.2.4 XRD

Granite (Alagbaka); Gneiss (Owo-Ago-panu) and charnockite (Oda road Akure) were carefully chosen based on their mineralogy and magnetic properties. They were grounded into powder and formulated inside a sealed vacuum tube. Higher voltage ranging from 30-60 KV was applied, which heats the filament inside the tube and emitted several numbers of electrons. The applied high voltage accelerated the electrons which hits the copper target to produce x-rays. The x-rays were collimated and directed into powder specimen <10 microns. The x-ray signal was detected by the detector, and is then analyzed electronically to calculate the count rate. The x-ray scan was defined as the angle between the x-ray source, sample, and detector at a regulated rate between preset limits.

The result of the analyses was used to correlate the diffractogram magnetic phases of the minerals with that of SEM. During the experiment, different energies were observed in the XRD. It took a little time to sort out the pattern of the result of one phase only or the sum of more than one phase.

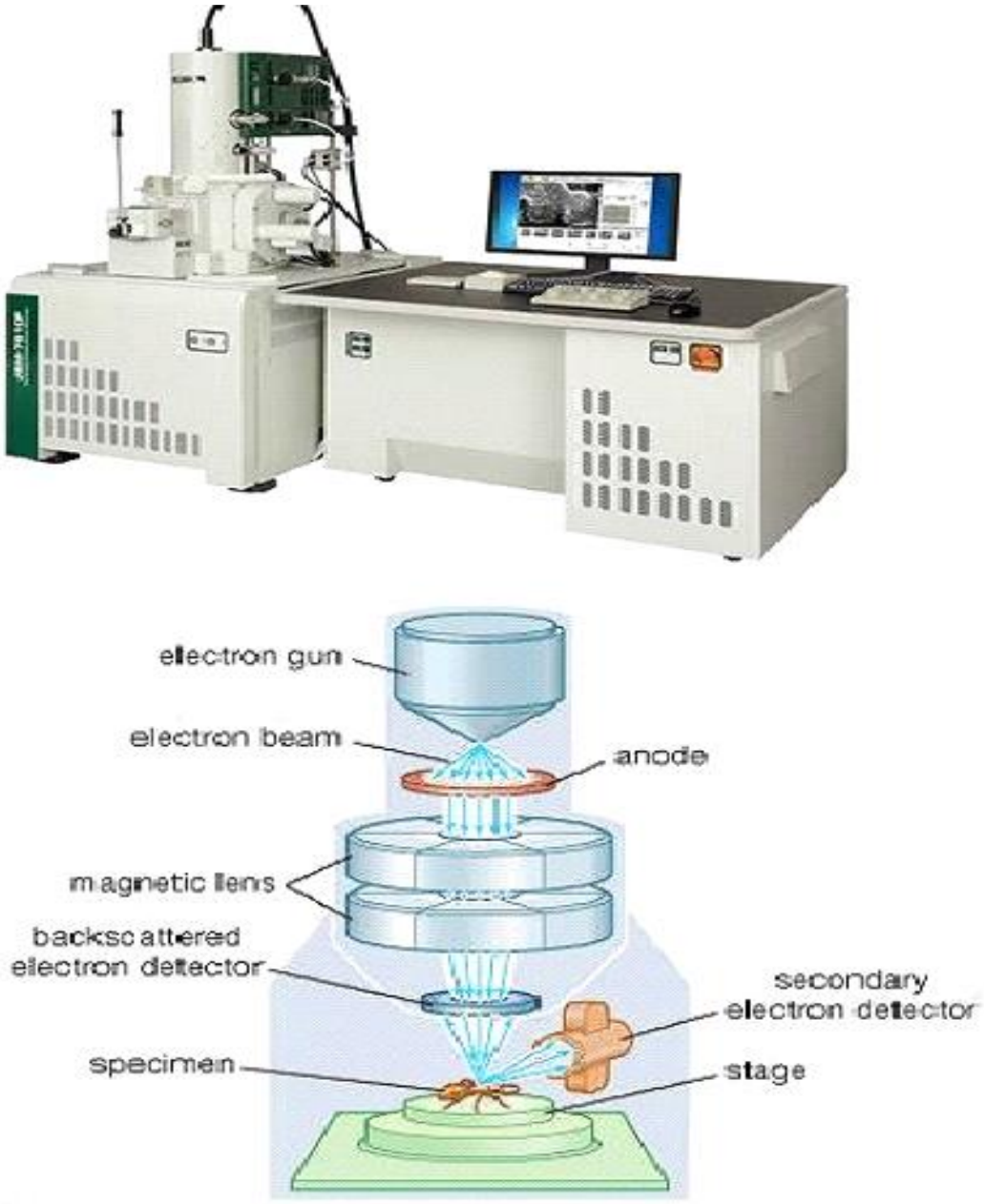

Fig. 3.5. SEM instrument, displaying the electron column, sample chamber, EDS detector, electronics console, and visual display monitors

3.3.2.5 AGICO MFK1-FA Kappabridge

3.3.2.5.1 Anisotropy of Magnetic Susceptibility (AMS)

Multifunctional kappabridge is a multifunctional petrofabric tool that was used in the laboratory to test the AMS (Fig. 3.6). AMS is a tensor that uses the equation: to relate the frequency of the applied field (H) to the acquired magnetization (M) of a substance. Mi = kijHj, where Mi (i= 1, 2, 3) represents the magnetization vector, Hj (j= 1, 2, 3) represents the magnetic field vector strength components, and kij (kij = kji) represents the second rank susceptibility components. The geometry of a symmetric tensor shows a directional difference.

Table 3.1 shows the coordinates and rock sample codes (CO1I, CO1G, CO1A, CO1O, CO2I, CO3I, CO3E, CO3IW, CO3A, CO3AO, CO4I, CO5I, CO6BA, CO6OA, CO7E, CO7IW, CO7I, CO8A and CO8I) used for the measurement of AMS. Core samples were measured for low-field (high sensitivity of phase determination) (300 Am^{-1} at 875 Hz) AMS using an AGICO MFK1- FA Kappabridge for spinning each specimen in 64 directions on three mutually orthogonal planes using an automatic rotator sample holder. Measurement at high field changes the magnetic domains of iron oxides.These softwares 'SUFAR' and 'ANISOFT 4.2' were used for acquisition and processing of the AMS data (AGICO, Czech Republic). Orient software was further used to process the magnetic foliation and lineation. K1, K2, and K3 establish the direction and degree of three primary orthogonal axes of the AMS ellipsoids; the amplitudes of such primary areas, for example, are utilized to calculate various parameters.T (shape parameter determining the magnetic susceptibility ellipsoid oblate/prolate geometry), P/ (corrected degree of magnetic anisotropy, i.e. magnetic susceptibility ellipsoid eccentricity), K (mean bulk susceptibility), P/ (corrected degree of magnetic anisotropy, i.e. magnetic susceptibility ellipsoid eccentricity), P/ (corrected degree (Jelinek, 1981; Tarling and Hrouda, 1993).

Fig.3.6. (a-b) multifuntional kappabridge (MFKI-FA) in Liquid Nitrogen and Argon gas environment

Table 3.1 Coordinates of rock sample codes used for AMS analysis

S/N	Coordinates		Sample codes	Location	Rock
1	7.37154	4.49456	CO1I	Ife	Gneiss
	7.29799	4.26398	CO1G	Gbongan	
	7.38161	5.5690	CO1A	Akunu-Akoko	
	7.38258	5.56925	CO1O	Okeagbe-Akoko	
2	7.23767	3.47201	CO2I	Ibadan	Aplite
3	7.23883	5.03494	CO3I	Igbara-Oke	Granite
	7.33593	4.52767	CO3E	Erin-Ijesha	
	7.33588	4.52701	CO3IW	Iwaraja	
	7.21282	4.84981	CO3A	Asejire	
	7.58697	4.05054	CO3AO	Abegundo Ogbomoso	
4	7.45485	4.23246	CO4I	Iwo	Diorite/syenite
5	7.25585	4.15447	CO5I	Ikire	Granite gneiss
6	7.16131	5.10061	CO6BA	BTO Akure	Charnockite
	7.16514	5.96141	CO6OA	Oda road Akure	
7	7.53501	4.18551	CO7E	Ejigbo	Granite 2
	7.33588	4.52701	CO7IW	Iwaraja	
	7.35666	4.51001	CO7I	Ilesha	
8	7.23011	5.42011	CO8A	Akungba-Akoko	Banded gneiss
	7.31511	5.45002	CO8I	Ikare-Akoko	

3.3.2.5.2 Thermomagneticof rocks

Table 3.2 show the coordinates and rock sample codes (CO1I, CO1E, CO1IW, CO1A, CO1O, CO1IL, CO2E, CO3G, CO4I, CO4A, CO5A, CO5I, CO6A, CO6I, CO7E, CO8A, CO8O, CO8I, CO8S, CO9I, CO9O and CO10I) used to measure the thermomagnetic properties of the rock specimen at SOEST-HIGP paleomagnetic laboratory. MFKI-FA were coupled with: CS-4, Nitrogen and Argon gases for thermomagnetic scales, the temperature varies from room temperature to 700 °C. For qualitative categorization of iron oxide mineralogy, MFKI-FA tests magnetic susceptibility as well as Curie temperature (Fig.3.6). Usually, 150 mg of rock fabric was heated to 700 °C in a 0.55 T external magnetic field.

The temperature rises from room temperature to 700 °C. With respect to temperature, the applied magnetic field (mass magnetization [Am^2kg^{-1}]) was determined. For Curie temperature testing, a progressive $20°Cmin^{-1}$ temperature increase to 700°C causes iron-oxide to lose its ferrimagnetic properties. The traces of the curve that show how the specimen restores its ferrimagnetic properties during heating and cooling are critical for identifying a certain iron-oxide material (Jelinek, 1981). Sharp fall in the magnetic susceptibility denote transformative behavior from ferromagnetic to paramagnetic minerals. Comparable heating and cooling curves are reversible and otherwise (irreversible) implying mineralogical transformations in the specimen during heating.

Table 3.2 Coordinates of rock sample codes used for thermomagnetic analysis

S/N	Coordinates		Sample codes	Location	Rock
1	7.23883	5.03494	CO1I	Igbara- Oke,	Granite
	7.33593	4.52767	CO1E	Erin-Ijesha,	
	7.33588	4.52701	CO11W	Iwaraja,	
	7.21282	4.8498	CO1A	Asejire,	
	7.53610	4.05054	CO1O	Ogbomoso,	
	7.58697	4.26356	CO1IL	Ilogbo-Osogbo	
2	7.45377	4.33949	CO2E	Effon-allaye	Quartzite
3	8.17508	4.21068	CO3G	Gbede	BIF
4	7.04012	5.06501	CO4I	Idanre,	Porphyritic Granite
	7.07551	3.22551	CO4A	Abeokuta	
5	7.23002	5.42001	CO5A	Akungba-Akoko	Banded gneiss
	7.31501	5.45011	CO5I	Ikare-Akoko	
6	7.23431	3.42997	CO6A	Ajibode UI	Augen gneiss
	7.13940	5.13761	CO6I	Igbatoro	
7	7.53511	4.18551	CO7E	Ejigbo	Biotite granite gneiss
8	7.38161	5.56577	CO8A	Akunu-Akoko	Charnockite
	7.38143	5.4556	CO8O	Okeagbe-Akoko	
	7.45485	4.23246	CO8I	Iwo	
	7.16587	5.14537	CO8S	Shasha Akure	
9	7.25585	4.15447	CO9I	Ikire	Granite gneiss
	7.12259	5.10704	CO9O	Okearo-Akure	
	7.38258	5.56925	CO9OK	Okeagbe-Akoko	
	7.36515	5.46454	CO9E	Erusu-Akoko	
10	7.14011	6.46001	CO10I	Igarra	Phylite

3.3.2.6 Shielded AF and Thermal Demagnetizer

Figures 3.7a shows the Thermal Demagnetizer MMTD80A coupled with programmable Eurotherm 3204 temperature controller. Thermal demagnetizer was used to demagnetized about 80 specimens for paleomagnetic analyses while the MOLSPIN shielded demagnetizer was used for demagnetization of specimens at peak fields up to 1000 Oersteds (1T) (Fig.3.7b).

Fig. 3.7. (a)Thermal Demagnetizer MMTD80A with Eurotherm 3204 temperature controller and(b) shielded Molspin Alternating Field demagnetizer

3.3.2.6.1 Demagnetization techniques

Granite (Okeagbe-Akoko, Ikire; Iyemi, Iyin-Ekiti, Igbara-Oke, Asejire); biotite granite gneiss (Ejigbo); gneiss (Ife); banded gneiss (Ajibode UI, Akungba-Akoko); augen gneiss (Ajibode UI); porphyritic granite (Erio-Ekiti, Akure), syenite (Iwo) were selected based on their mineralogy, magnetic susceptibility, and natural remanent magnetisation (NRM). A combination of alternating field (AF) and thermal (TH) demagnetization methods were employed. Their primary and secondary multi-remanence constituents can be measured using the equipment. Because constituent minerals obtained through different mechanisms have different coercivity spectra and blocking temperatures, these techniques were used. The coercivities of magnetic minerals are involved in AF demagnetization. The alternating field method entails exposing the specimen to increasing amounts of AF, with the waveform being sinusoidal and decreasing in magnitude linearly with time.It was used to extract remanence from grains whose coercivities were less than the peak demagnetizing area.Alternating magnetic field is fast treatment procedure likened to the thermal demagnetization method.Test of the natural remanent magnetization in determining the rock material is not a superimposition of several magnetic constituents and this was done by isolating the components of stable magnetization (ChRM).

The specimens were heated to a temperature below and near ferromagnetic mineral Curie temperatures in steps of 30 and 50 °C during step-by-step thermal (TH) demagnetization, and then allowed to cool in a zero magnetic field at room temperature. It gives magnetic grains blocking temperatures (Tb) that are lower than the temperature used to strip a portion of their normal remanent magnetization. Step by step, temperature ranges were measured, and residual magnetization and susceptibility were calculated.

Thermal cleaning was required because the Curie temperature assures that we can obtain the magnetic mineral that keeps the remanence by its unblocking temperature. The biggest disadvantages are the oxidation and change of magnetic grains during heat treatment, which affects their magnetic analysis and properties.The basic measurement of NRM yields the remanent magnetization recorded in rocks (declination, inclination, and total intensity). In the present study, the samples were AF demagnetized in 14 steps

following a sequence 2.5, 5, 7.5 10, 12.5, 15, 17.5, 20, 25, 30, 40, 60, 80 and 100 mT respectively. The thermal demagnetization was done on some selected samples in a sequence of 50°C, 100°C, 150°C, 200°C, 250°C, 300°C, 350°C, 400°C, 420°C, 440°C, 460°C,500°C,530°C, 550°C and 570°C respectively.

3.3.2.6.1.1 Analyses of remanent magnetization components

As soon as alternating field and thermal demagnetization have treated the specimen, the directions of the rock specimen are studied in order to isolate magnetic constituents. In this paleomagnetic study, stereographic and orthogonal projections were adopted. To characterize a stereographic projection direction, magnetization vector unit length tip was measured, the same sphere diameter aligned with the southern pole. They are the contact site with the equator plane sphere, usually referred to as open small circle. The geographic directions of the north, east, south and west were defined. Magnetic declination ranges from 0° (N direction) to 360° clockwise and from 0° at the edge of the equator plane, to 90° at the midpoint. AF and thermal dataset were analyzed with AGICO's Remasoft 3.0 program (Chadima and Hrouda, 2006) and Demagnetization analysis in excel DAIE-v2015 program (Sagnotti, 2013). Fisher (1953)'s statistics was employed to measure mean orientations.

3.3.2.7 Impulse magnetizer

Granite (Akungba-Akoko), banded iron formation (Gbede) were selected, to artificially increase their magnetism and monitor their magnetic characteristic behaviour. The samples were subjected to ASC Model IM-10 Impulse Magnetizer (Fig. 3.8) by first of all, demagnetizing and later impact an average of 1.5 T magnetization. The voltage was usually regulated with its knob in order to get the desired charging voltage shown on the charging voltmeter. This resulted to remagnetization of material in the 1 mof solenoid that posseses a strong magnetic field. The specimen was placed in the sample cavity until it touches the back of the cavity; by ensuring that the bottom of the holder assembles in the channel in the bottom of the cavity. The knob was adjusted to the precise desired charging voltage in an increasing order while the delay time was used to adjust the voltage and charging of the capacitors to a particular voltage. The voltage that was finally

used for each specimen, advanced asymptotically in the range of 30 to 60 s time period and observed through the digital meter. The averaged results were determined somewhat above the desired voltage, as the desired voltage advances at a rate of 0.5 V/s. TRIM and TRIGGER buttons were used to trim or trigger desired voltage. The knob was turned completely anticlockwise to switch–off the power. After acquiring the desired induced magnetization, the specimens were measured with the aid of Direct current-superconducting quantum interference device (DC-SQUID) or with the spinner magnetometer.

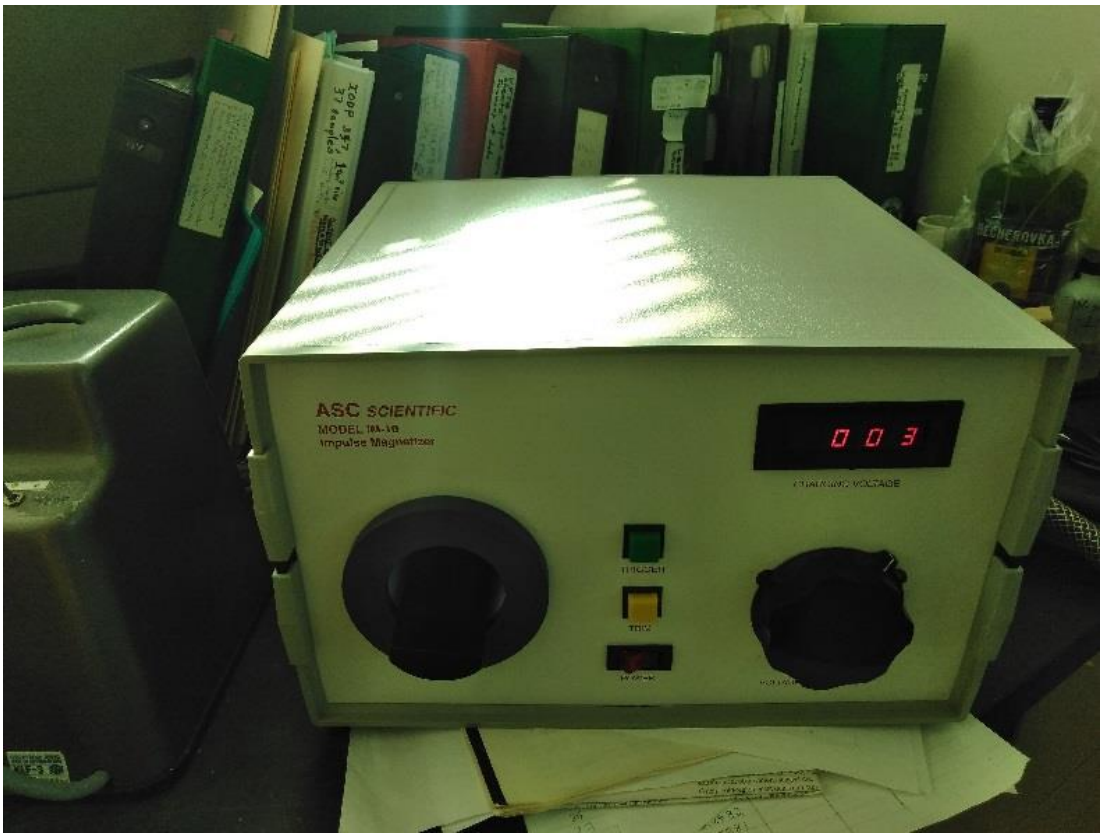

Fig. 3.8. Impulse Magnetizer

3.3.2.9 Molspin Spinner magnetometers

All the cored rock specimens were subjected to laboratory measurement of characteristic remanent magnetization (ChRM) for the aim of determining their magnetic properties with the aid of JR5 (Fig. 3.9). It makes use of cutting-edge microelectronic modules. It has two microprocessors that monitor the rotation speed of the specimen, signal gain, data acquisition, digital filtration, and the auto-position spinner. The magnetic interface was controlled by a serial channel RS232C provided by the workstation.

The key electronics board, the engine, the spinner assembly, the pick-up coils with preamplifier and triple permalloy shield, and the auto-position manipulator are all included in the JR5 (Fig. 3.9). For the power supply and serial channel of the workstation, it has a 15-pole and 9-pole socket. More so, it is equipped with LED colours signifying the position of the instrument. The colour that displayed green, yellow and red indicate: ready, processing of rock specimen and error condition respectively.

After demagnetizing the following rock specimens: granite, granite gneiss, gneiss, augen gneiss, banded gneiss, porphyritic granite, amphibolite, charnockite, coarse grained charnockite, foliated charnockite, quartzofeldspathic granite, quartzite, biotite granite gneiss, syenite, migmatite hornblende gneiss, aplite dyke, granodiorite, BIF, phyllite and diorite. The cored samples were spun on their own axis, resulting in time-varying magnetic flux with one or more stationary sensors. The magnetism component in the normal plane to the sample rotation axis is tested by the sensor. The rotary sensor compared and ranked the geomagnetic vector with a fixed direction (Collinson, 1983). The average sensitivity of the spinner magnetometer was dependent on the speed and sensitivity of the specimen deployed. During the measurements, the sensor (induction coil) was positioned inside the sample chamber and the signal output increased with respect to sample size of the rotation frequency and sensitivities peaked at 10^{-10} A m^2.

The program REMA5 processed the JR-5 spinner magnetometer measurement of characteristic remanent magnetization (chRM). The program tool yielded the text file with ext. [.TXT or PMD] which correspond to the pattern that was displayed in the monitor of the workstation [JR5], then, it was further subjected to advanced data interpretation with the aid of Remasoft and DAIE (Demagneitization Analysis in Excel

by Sagnotti, 2013). The geological file [GED] assumes same location of the Data file with input data option. The present directory uses program configuration file PARJR5.CFG that has calibrations constants and configuration parameters. Thus, an instance of missing file, it can be created automatically.

Table 3.3. Cored samples used for paleomagnetic analyses

Rock types	No. of samples collected in the field	No. of Recored Samples	No of samples analysed in the Lab.	Discarded samples
Granite	25	450	168	282
Granite gneiss	15	250	106	144
Gneiss	14	140	65	75
Augen Gneiss	2	20	6	14
Porphyritic Granite	11	110	41	69
Banded Gneiss	4	40	9	31
Amphibolite	2	20	7	13
Charnockite	15	150	46	104
Coarse grained Charnockite	1	18	6	12
Foliated charnockite	1	15	4	11
Qtzfeldspathic granite	1	19	6	13
Quartzite	5	50	23	27
Biotite granite gneiss	2	78	52	26
Syenite	1	23	14	9
Migmatite Hornblende Gneiss	1	14	8	6
Aplite dyke	2	49	21	28
Granodiorite	1	20	11	9
BIF	1	6	5	1
Phyllite	1	4	2	2
Diorite	1	11	6	5

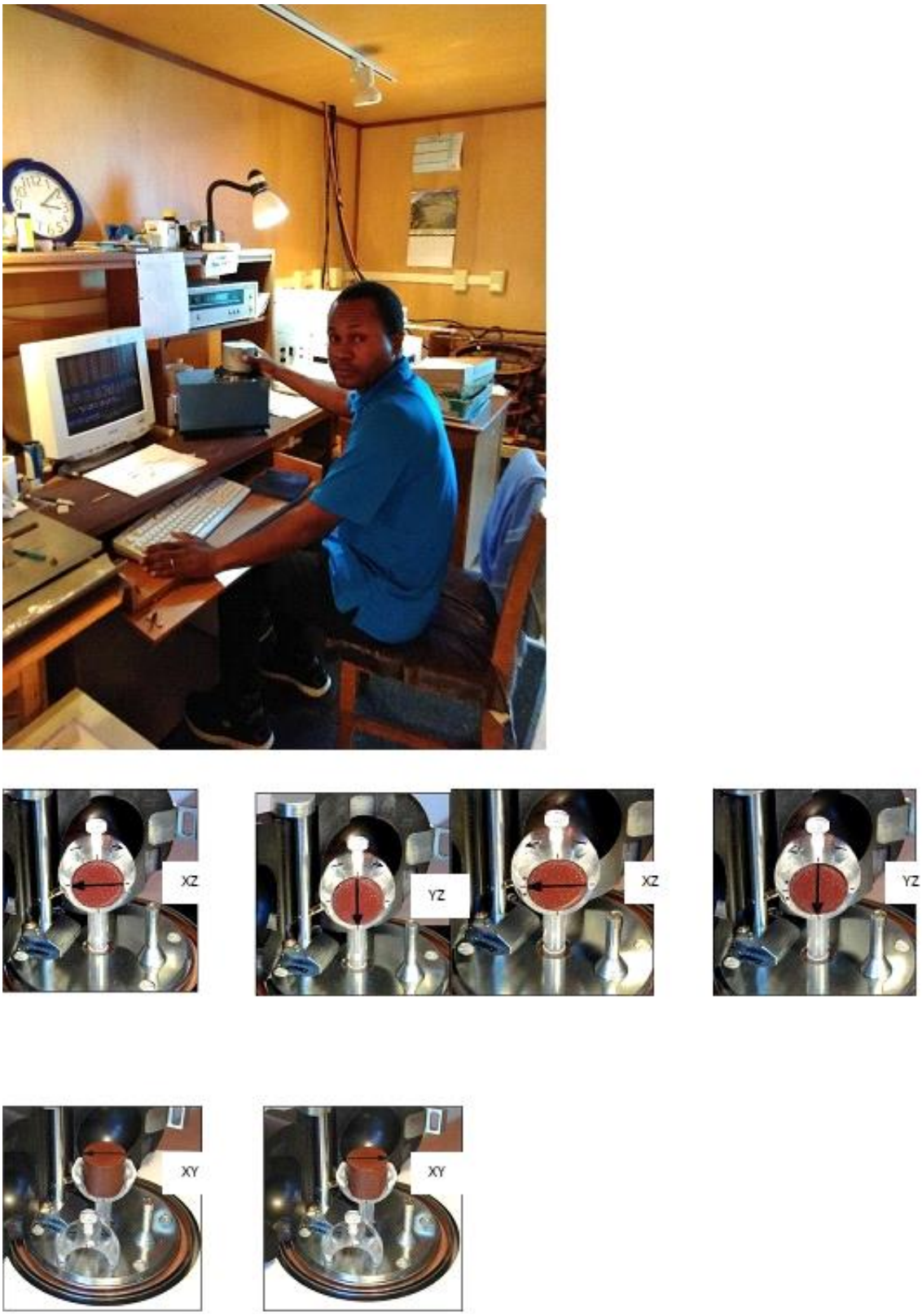

Fig. 3.9. Spinner magnetometer and its auto manipulations of six directions

3.3.2.9 Vibrating Sample Magnetometer (VSM)

Amphibolite (Ilesha), banded gneiss (Ikare-Akoko), biotite granite gneiss (Ikirun), charnockite (Akunu-Akoko), granite (Etioro-Akoko) samples were selected based on their mineralogical content and magnetic susceptibility. For magnetic hysteresis tests, the samples were split into smaller dimensions. Princeton Measuring Instruments - below are the parameters for the Vibrating Sample Magnetometer: The temperature range is 10 K to 1025 K, with a magnetic field of 0 T to 1.8 T and a sensitivity of $5X10^{-9}$ Am^2. A liquid helium cryostat was used in the MicroVSM, as well as a stepper motor that rotated and vibrated the samples. Temperature, area, and orientation are three independent variables that can be used to calculate magnetization. Low temperature transition and Curie point determinations were used to identify minerals using moment and remanence measurements as a function of temperature. It has a furnace that housed silvered double-walled glass tube and is spaced amid the poles of the electromagnet (Fig. 3.10).

Sample preparation and equipment settings: The specimen size was prepared to fit and housed by the pole pieces of the magnet; and power strip was switched on, that controlled the cooling water to the electromagnet. The MicroMag Controller power was cross-checked to ensure that the switch was on; subsequently it was noticed that the electromagnets began to cool as chilled water flows through them. The Bipolar Magnet Power Supply was switched on, which enabled the red colour power button on the two power stripson the left side of the workstation electronics. This allowed the vacuum pump to work; thus, opening the valve of the helium gas tank and its pressure was observed. Optimum pressure rate of 200-300 PSI/hour (pounds per quare inch per hour) was used and the vacuum gauge checked which displayed the pressure in the insulation space between the walls of the furnace tube. Immediately the pressure was less than about 50 millitor, the furnace current switch (heater) was turned on. The Enter key was pressed to select the setting and noted the samples whose high-field behavior were dominantly diamagnetic, the magnetic moment increased as the field decreased from its maximum. Centering, sensitivity and other settings: The SI units was used to select pre-defined sensitivity levels. The maximum applied field used for the hysteresis measurements was 1T, applied field and measured magnetic moment at the right- hand side was observed.

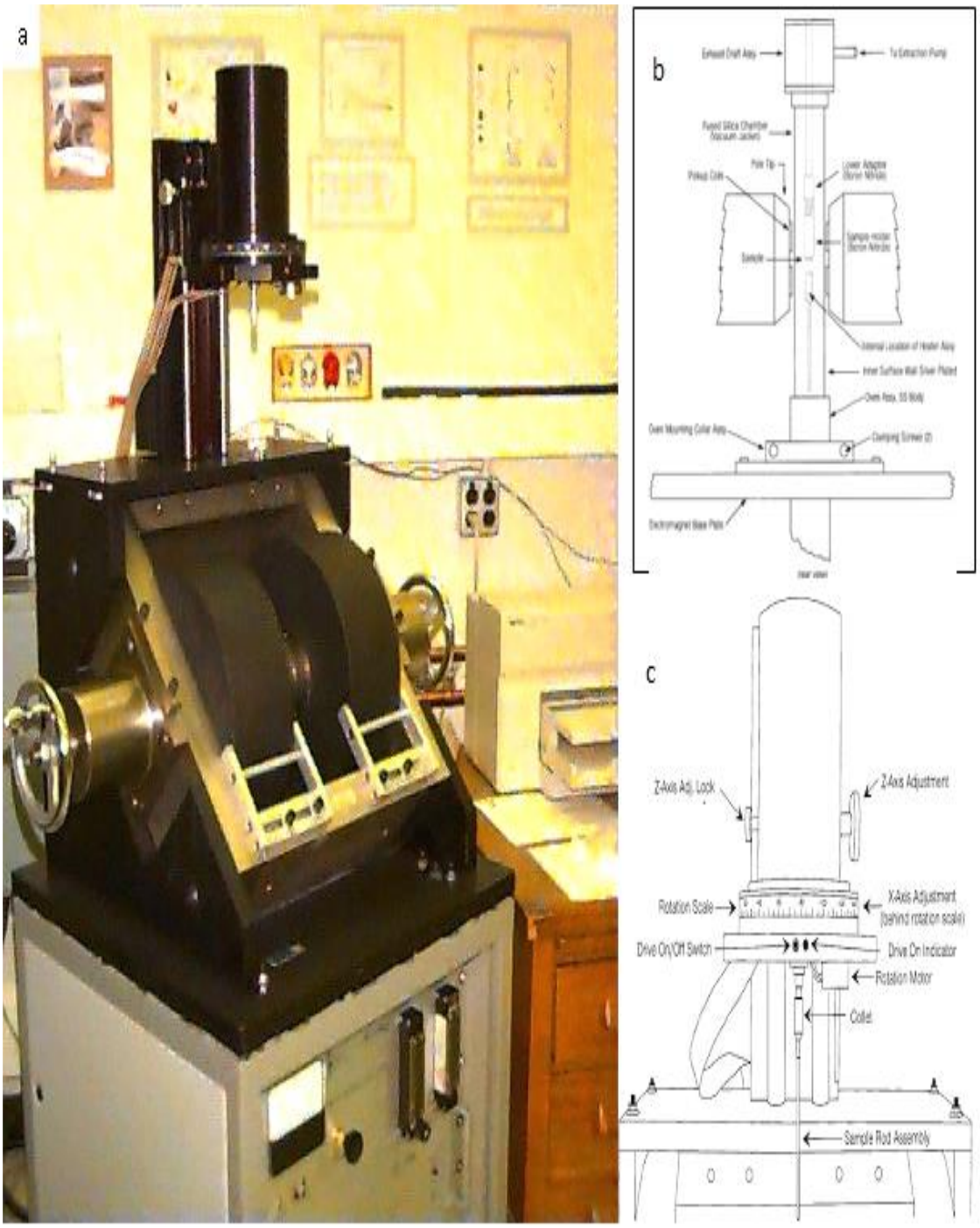

Fig. 3.10. (a) Vibrating sample Magnetometer (VSM), (b) schematic configuration with installed furnace and (c) vibration head locations of X-Y-Z knobs, Z-axis lock; and collet

The *Sensitivity* box in the menu (displayed on the left-side) was tapped and adjusted. The remanence experiments such as Hcr, the maximum moment was the saturation remanence. Longer averaging time was allowed, to give better signal/noise ratios and vibration amplitude was set to the relative value of 1.

Room-temperature measurements carried out include: 1. Direct moment vs Field (Hysteresis loop, first order reversal curves (FORC)). 2. Remanence curves (Hcr, IRM acquisition, DC demagnetization). VSM measurements were segmented into field, measurements of temperature and time-dependent magnetization, i.e. IRM acquisition curves, hysteresis loops and backfield curves respectively. Atleast 15min was used to determine hysteresis loop of 80 data points whereas other measurements were determined within temperature range of 190 – 800 °C.

Hysteresis curves were utilized to measure the magnetic domain structures of rocks under investigation (Dunlop, 2002b). The increased applied field, yielded equivalent magnetization and saturation which was termed saturation magnetization (Ms) whereas decreased field and magnetization resulted to zero sample remanent magnetization, which was termed saturation remanent magnetization (Mrs). The applied field was reversed which yielded nil susceptibility, as H was introduced into the field; zero field magnetization was generated, referred to as bulk coercive force (Hc). Applied field was increased in reversed order, which saturated the magnetization and decreased the remanent bulk coercive force (Hcr).

CHAPTER FOUR
RESULTS AND DISCUSSION

4.0 Preamble

Based on the objectives of this research work, the results will be discussed under the following subheadings: Raman Infrared Spectroscopy; petrofabric mineralogy which include X-Ray Fluorescence and Electron Probe Microanalyzer; Scanning Electron Microprobe (SEM); X-Ray Diffractometry (XRD); thermomagnetic (temperature dependence) that is Curie temperatures; Microstructural emplacement where Anisotropy of Magnetic Susceptibility (AMS) and geological models were created; paleomagnetic pole for continental drifts/ apparent polar wandering paths and Day plots, hysteresis loops and First Order Reversal Curves (FORCs) of rock remanence.

4.1 Mineralogical compositions and Raman Infra-red Spectroscopy result

Figure 4.1 revealed photomicrographs of of biotite granite gneiss under cross polars and plane polarized lights, the characteristic mapping of Raman infrared spectroscopy and individual measurements of biotite granite gneiss representative samples. Raman spectra were observed within the white matrix, pyroxene, opaque mineral pockets and diverse places around the mineral matrix. Maghemite Raman shift peaks are recorded at some points within the biotite granite gneiss and thin section petrography of all the rock units in the study area shows abundance of quartz, microcline and plagioclase as the major minerals that dominates the rock samples with other minor components such as hornblende, muscovite and the opaque minerals. Plagioclase, quartz, and microcline minerals were found to make up to 70% of the volume percentages of the rock in thin sections, with plagioclase being the most dominant mineral, followed by quartz, and microcline being the third most dominant mineral.Table 4.1 showed the results of 830 nm Raman microspectroscopy of biotite granite gneiss grains have 398.8 cm^{-1} and 663 cm^{-1} indicating weak spectra while that of 785 nm have 714.8 cm^{-1}, 720.4 cm^{-1} and 764.48 cm^{-}

[1] indicating strong peak bands respectively (Figs. 4.1) (Serna *et al*., 1982; deFaria, 1997; Chamritski and Burns, 2005; Hanesh, 2009).

Other bands at 515 cm^{-1} and 531.56 cm^{-1}, as well as a strong band at 519.5 cm^{-1} with a shoulder at 398.8 cm^{-1} and 663 cm^{-1} (Fig.4.3b); 785 nm laser excitation confirms that the peak found at 519 cm^{-1} and 521 cm^{-1} correlates to the granite (maghemite) structure. Raman shift point was recorded at 764.48 cm^{-1}, for the biotite granite gneiss which displays the fillings of plagioclase and additionally influencing the dendritic shapes of plagioclase and pyroxene, and, Raman shift positions precisely calculated.

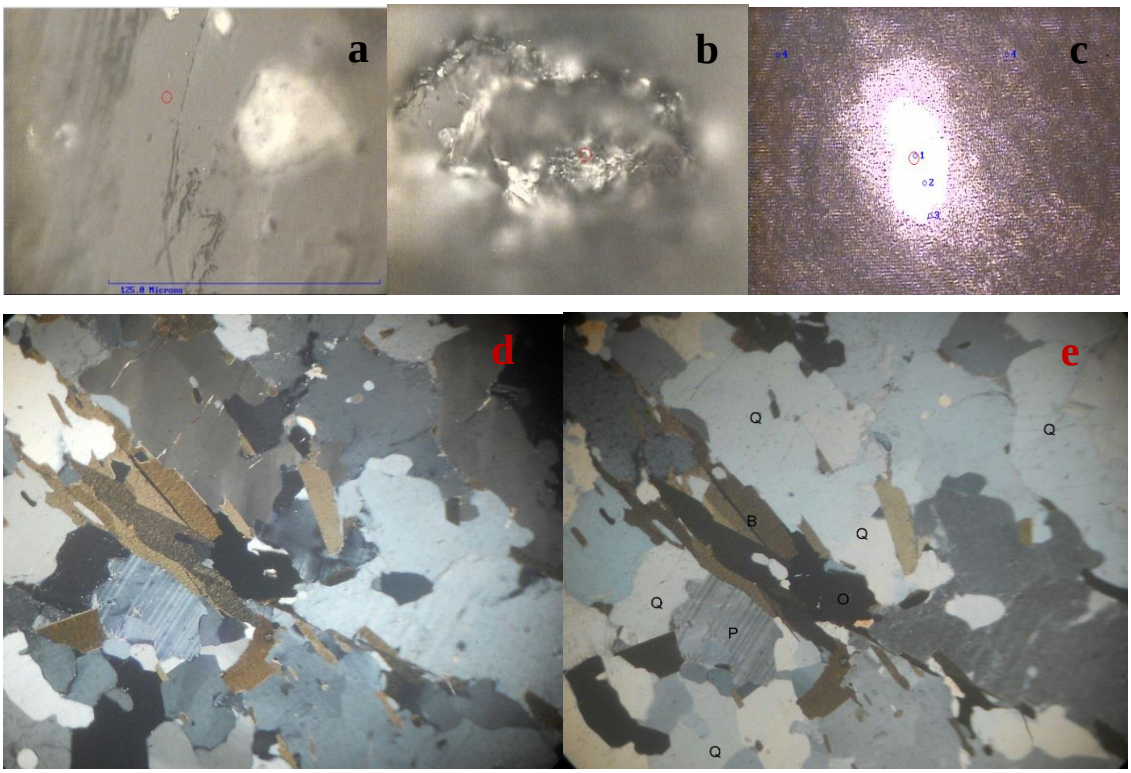

Fig. 4.1. (a-b) Raman maps and phase distribution of 2D map, ID lines and single point measurement studied on biotite granite gneiss (BGG). The BGG is surrounded by pyroxenes, quartz, plagioclase feldspars. The red circles indicate area of focus (c) Laser focus 2D mapping of BGG (numbers seen are points measurements in the rock sample) (d) Photomicrograph of biotite granite gneiss under PPL (e) Photomicrograph of biotite granite gneiss under XPL (Q quartz, P plagioclase, B biotite)

Table 4.1 Raman Spectra of Biotite granite gneiss, granite and charnockite for Maghemite

Raman Measurements	Biotite Granite Gneiss (785nm)	Biotite Granite Gneiss (830nm)	Granite (785nm)	Charnockite (785nm)
1	515.67 strong	398.8 weak	519 strong	519.95 strong
2	522.67 strong	519.1 strong	521 strong	717 weak
3	531.56 strong	521 strong	420 weak	1285.5 strong
4	714.8 weak	663 weak	710 weak	
5	720.4 weak			
6	764.48 weak			

Table 4.2 Interatomic potentials, estimated and observed properties, estimated and experimental wavenumbers for maghemite (Chamritski and Burns, 2005)

Short range interaction	Fe^{3+}–O^{2}	Fe^{2+}–O^{2-}	Fe^{3+}–O^{2-}	O^{3-}…O^{2-}	Shell Model		Fe^{3+}	Fe^{2+}–	O^{3-}										
***A* (eV)p(A)**	1102.4. 0.329	694.10.340	1102.4 0.329	22764. 143		*Y*(e)	4.97	2	-0.239										
***A* (eV)p(A)**	0	0	0	43		*K* (eVA^{-2})	805	301	60										
***A*(experiment)**	8.351		Types		Fe^{3+}			Fe^{3+}			Fe^{2+}			O^{2-}			O^{2-}		
		atomic coordinate	*xyz*	(Experiment)	0.125	0.366	-0.116	0.625	0.625	0.63	1	1	1	0.39	0.39	0.39	0.12	0.13	0.38
***A*(calculated)**	8.455	s *Pm3m*	*xyz*	(Estimated)	0.125	0.374	0.875	0.625	0.625	0.63	0.99	1	0.99	0.39	0.39	0.39	0.11	0.11	0.39
Observed ^{2} $_{-9}$$_{-25}$/cm^{1}		350		319	440	500		553	700										
Calculated/ cm^{-1}	212	356		362	440	493		523	695										
Sym species	T2(1)	T1	T2(2)		T2(3)	E	T2(4)		A1										
Activity	IR	Raman	IR		IR	Raman	IR		Raman										
Ions involved	Fe+O	Fe+O	Fe+O		Fe+O	Fe+O	Fe+O		Fe+O										
geometry	Broad		Broad				Broad												

The results of Raman shifts are: 398.8cm^{-1}, 521 cm^{-1} and 714.8 cm^{-1} signals in $P4_332$ mode, parallel swinging of the two tetragonal centres corresponds to polymorph Fe-O bond stretching,cubic $P4_332$ structure, and suggested change in the tetragonal symmetry in Table 4.2. These correlate with the Raman shifts of maghemite in Table 4.2 (Chamritski and Burns, 2005). This originates from Fe^{2-} , Fe^{3-} and O^{2-} which are the bond stretching in the **[**γ- Fe_2O_3] cubic $P4_332$/tetragonal$P4_12_12$ having transformation phase of magnetite spinel of α- Fe_2O_3 and γ- Fe_2O_3 polymorphs **(**Dunlop and Ozdemir, 1997**).** Kaiser microprobe of 785 nm recorded Raman peaks at 522.67 cm^{-1} and 714.8 cm^{-1}, 720.4 cm^{-1}, 764.48 cm^{-1} for maghemite mineral grains observed in biotite granite gneiss (Table 4.1).

Low temperature shortage causes oxidation of magnetite in magnetic moment, resulting in a reverse spinel structure with both Fe^{2-} and Fe^{3-}ions in tetrahedral postions (A) and octahedral (B) sites configuration were all factors that contributed to the presence of maghemite in the biotite granite gneiss (Dunlop and Ozdemir, 1997). Thus, figure 4.2 revealed a strength of 521 cm^{-1}, showing direct spatial similarity with the observed optical microscopy of the polarized light (Fig. 4.1d -e); but, when we have opaque coloured maghemite, the intensity is typically higher.

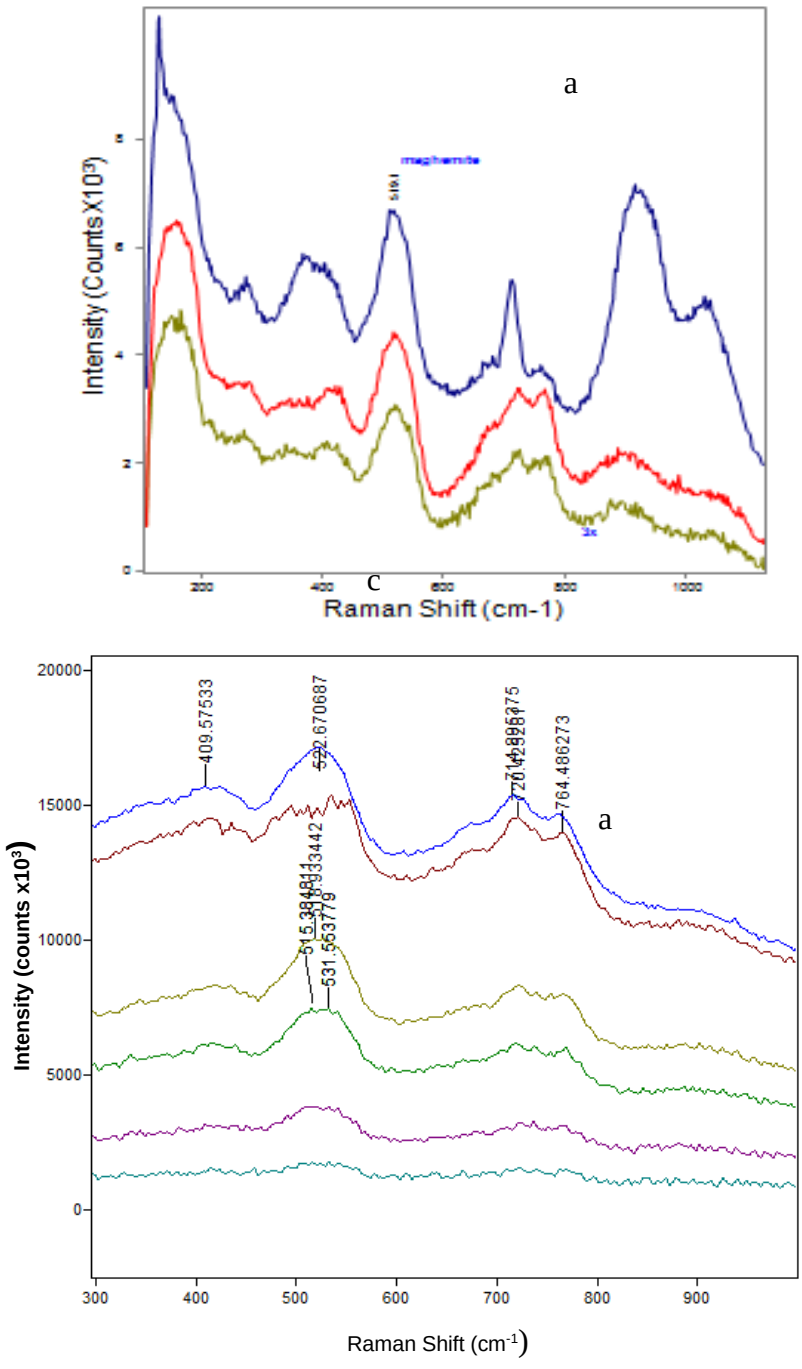

Fig. 4.2. (a-b) Biotite granite gneiss with 830nm In-Via Renishaw micro-Raman and Raman 785nm scaled 3x for clarity using 11mW 50X objective, 20sec. exposures and 5 accumulations

Figures 4.3 a-b revealed the characteristic mapping of Raman infrared spectroscopy and individual measurements of granite crystals as representative samples while figures 4.3c-d illustrated the photomicrograph of the granite. The main minerals in Granite are quartz, microcline and plagioclase, while minor minerals include hornblende, muscovite, and opaque minerals. Under plane polarized light, the quartz mineral in the rock samples was colourless, and it appears as subhedral prismatic crystals. Microcline is typified by polysynthetic twinning in two directions (cross-hatched), one according to albite law, and the other according to pericline law (monoclinic orthoclase/sanidine transformed to microcline) whereas plagioclase was distinguished by its polysynthethic twinning according to albite law. Biotite is brown, yellowish brown and reddish brown in the thin section. It is pleochroic occurring as plates and laths and showed elongation along foliation plane. However, muscovite is often seen as the platy brightly coloured minerals while hornblendes occur as a ferromagnesian mineral (Fig. 4.3c-d).

Several granite grains with variable colours were subjected to two excitation wavelengths of Raman microprobe disregarding configuration and cause of the 521cm^{-1} peak. The Raman mode at 519.1 cm^{-1} and 521 cm^{-1} corresponds to polymorph Fe-O bond stretching, cubic $P4_332$ structure which described the tetragonal distortion symmetry (Table 4.2). As shown in Figure 4.4, the intensity of the 521cm^{-1} spatial configuration correlate perfectly with the microscopy of the polarized light (Fig. 4.3c-d). These spectra were also noted by Serna *et al*., 1982; deFaria *et al*., 1997, Chamritski and Burns, 2005; Hanesh, 2009. The Raman shifts of 519 cm^{-1}, 522.67 cm^{-1}, 663 cm^{-1} and 714.8cm^{-1}are laser excitation wavelengths and not fluorescence induced. Chamritski and Burns (2005) in Tables 4.2 recorded that these bands appeared only for dark or opaque granite crystals when excited with Raman microprobe (785 and 830 nm) laser, even if the clear samples are less intense. Since the points are similar to those determined for maghemite lattice modes, Table 4.2 and these spectra correspond to translational lattice modes in maghemite geometry (Chamritski and Burns, 2005).

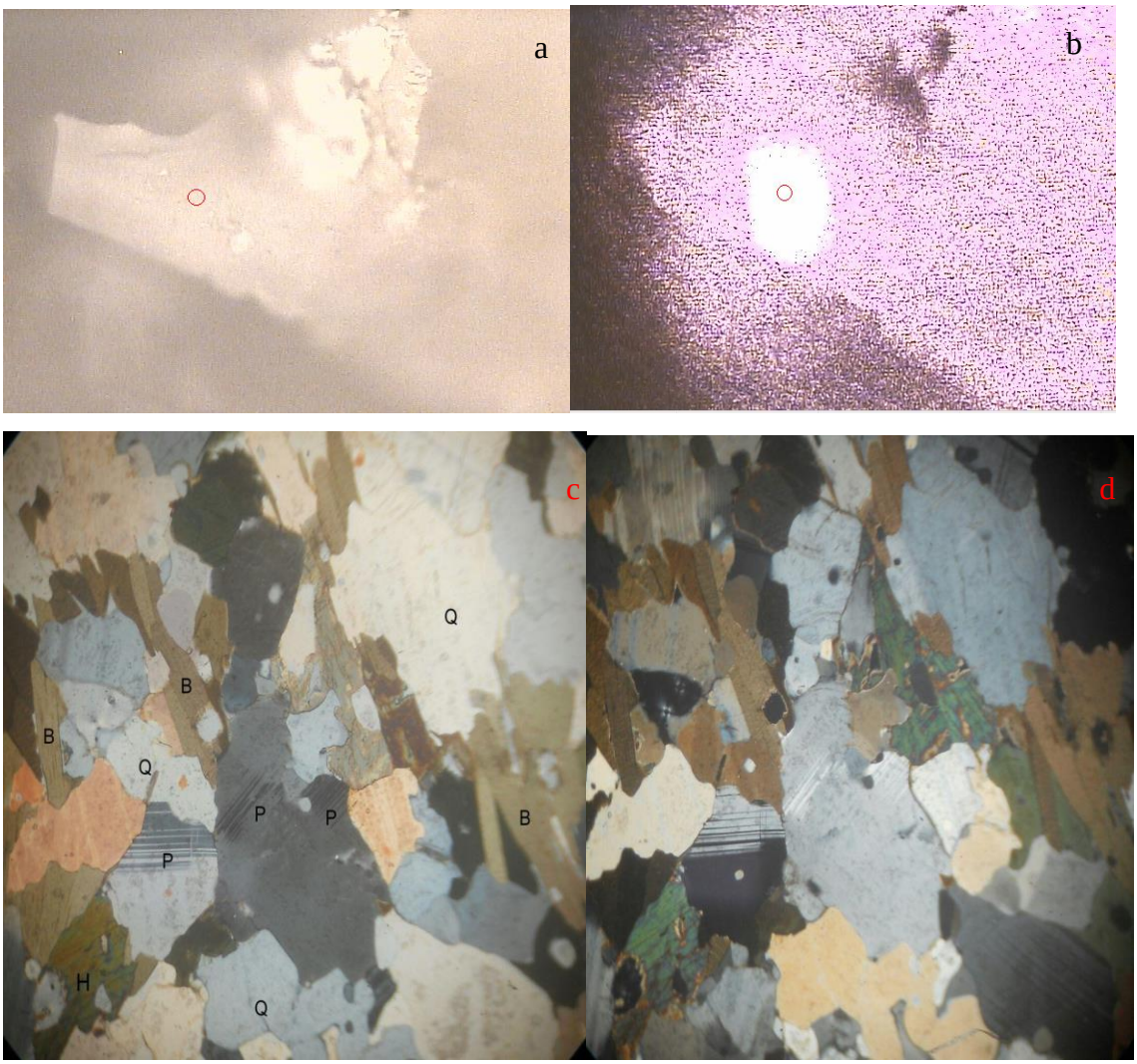

Fig. 4.3. (a-b)Raman maps and phase distribution of laser focused 2D map, ID lines and individual point measurement investigated on granite. Mineral observed in the granite are pyroxenes, quartz, plagioclase feldspars. The red circles indicate area of focus (c) Photomicrograph of Granite under PPL (d) Photomicrograph of Granite under XPL (Q quartz, B biotite, P plagioclase, H hornlende)

Additional maghemite points observed at 420 cm^{-1} within the granite and in the plagioclase feldspar caused a miscalculation in the Raman shift points. Raman fingerprints of pure granite were visible in spectra taken in the crystal's inner points as shown in Figure 4.4 as well as 521cm^{-1} excitation wavelengths having precise spatial and microscopy polarized light correlations (Figs. 4.3a-b).

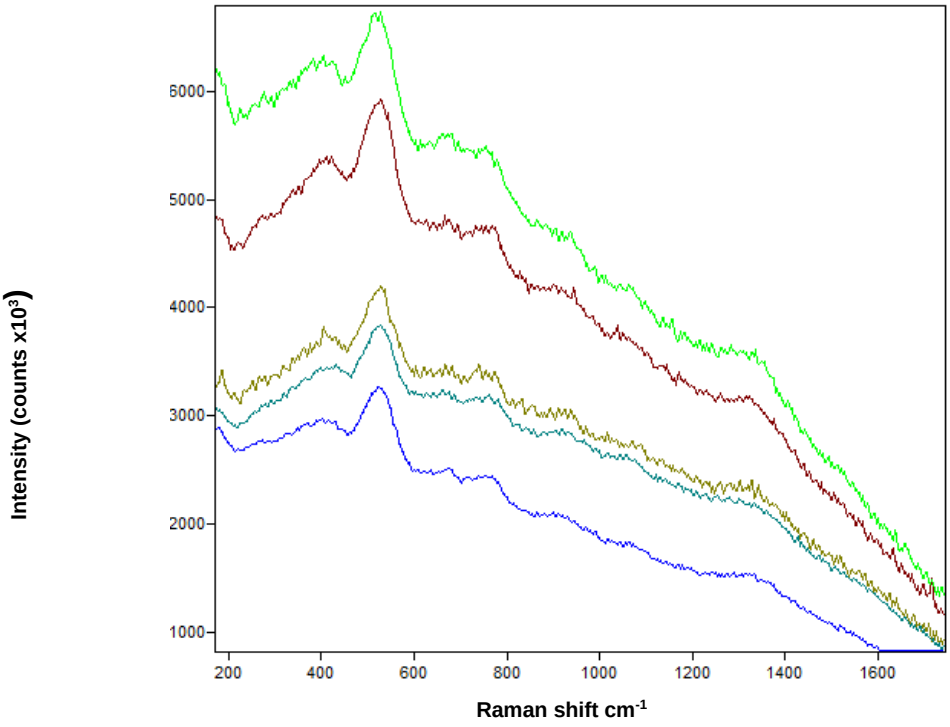

Fig. 4.4. Granite with 785nm Micro-raman microprobe all scaled 3x for clarity using 11mW 50X objective 20sec exposures and 1 accumulation

The charnockites were made up of orthopyroxene, clinopyroxene, plagioclase, and minor quartz and K-feldspar which exhibited its adakitic affinity (Fig.4.5). The charnockite in the southwestern Nigerian basement rocks showed assembly of biotite, clinopyroxene, orthopyroxene, K-feldspar, plagioclase, anti-perthite, quartz and maghemite. Figure 4.6 shows the Raman peaks of representative charnockite grains as it appears in the melting vein with the spectrum of glass in the charnockite grains, at 717cm^{-1}, and 1285.5cm^{-1}(Fig. 4.6). A strong band appears at 1285.5 cm^{-1} and may be due to rare earth elements fluorescence (Fig. 4.6). The maghemite mineral observed in charnockite exhibit predominantly fine-grains with high amount of K and low-K plagioclase and pyroxenes. Slavov *et al*., (2010) argued that molecular vibrations of Raman spectra were observed in nanoparticles of ferrofluids maghemite while Ma and Chen, (2018) and Nadeem *et al.* (2015) recorded such in synthetic maghemite. The result obtained by Raman microspectroscopy of southwestern Nigeria basement rocks was characterized and evolved by granulite-facies metamorphism of granitic rock.

Estimated Cartesian displacements illustrated the broad discrepancy among Raman bands mentioned in magnetite, maghemite, and hematite was characteristic of laser power and its heating effects, whereas the A_{1g} mode of Fe_3O_4 (670 cm^{-1}is only a mode of oxygen ion displacement. More so, the presence of non-stoichiometry of iron oxides caused secondary effects in Table 4.1 and 4.2. They are evidence of metasomatism and ductile deformation observed in the pectrography of the plagioclase crystal in charnockite rock. Biotite enclosed in clinopyroxene and orthopyroxene and its excitation wavelengths assembly points suggest being biotite, clinopyroxene, orthopyroxene, plagioclase, K-feldspar, quartz, and maghemite (Tubosun *et al*., 1984; Ferre *et al*., 2002).

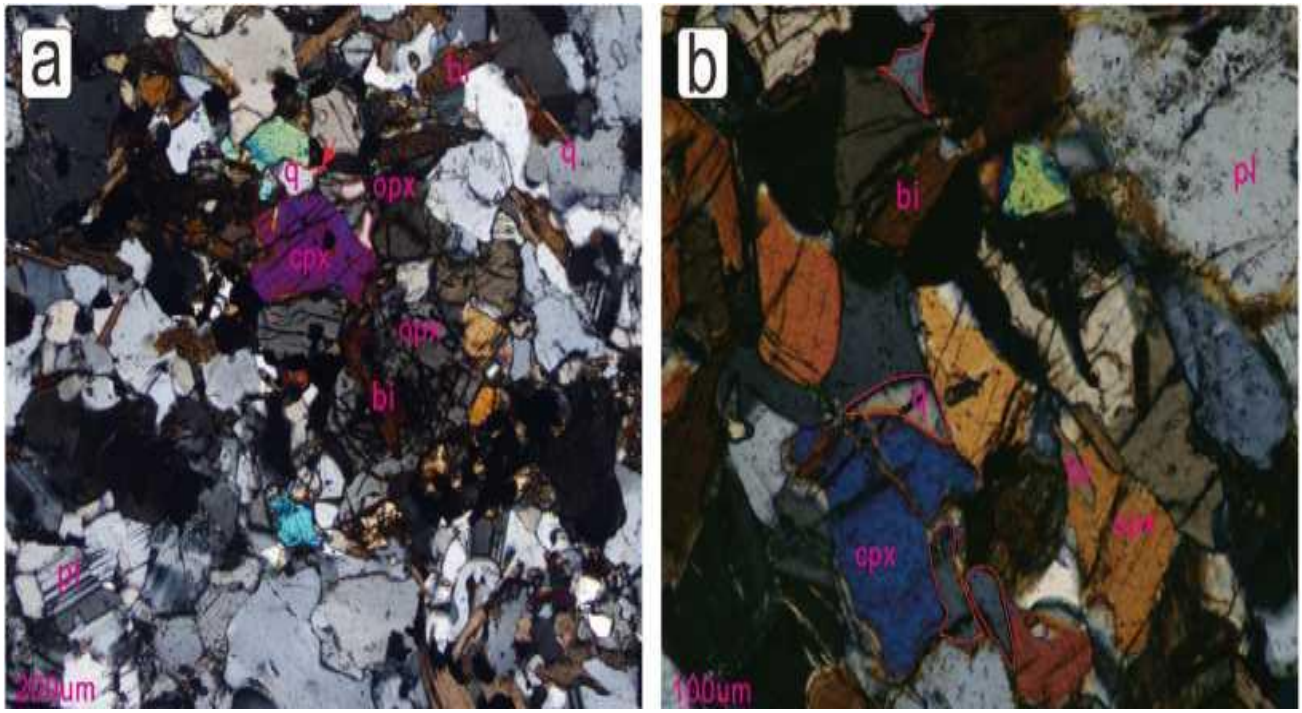

Fig 4.5. Photomicrograph of charnockite (a) PPL and (b) XPL (pl plagioclase, cpx clinopyroxene, bi biotite, q quartz, opx orthopyroxene)

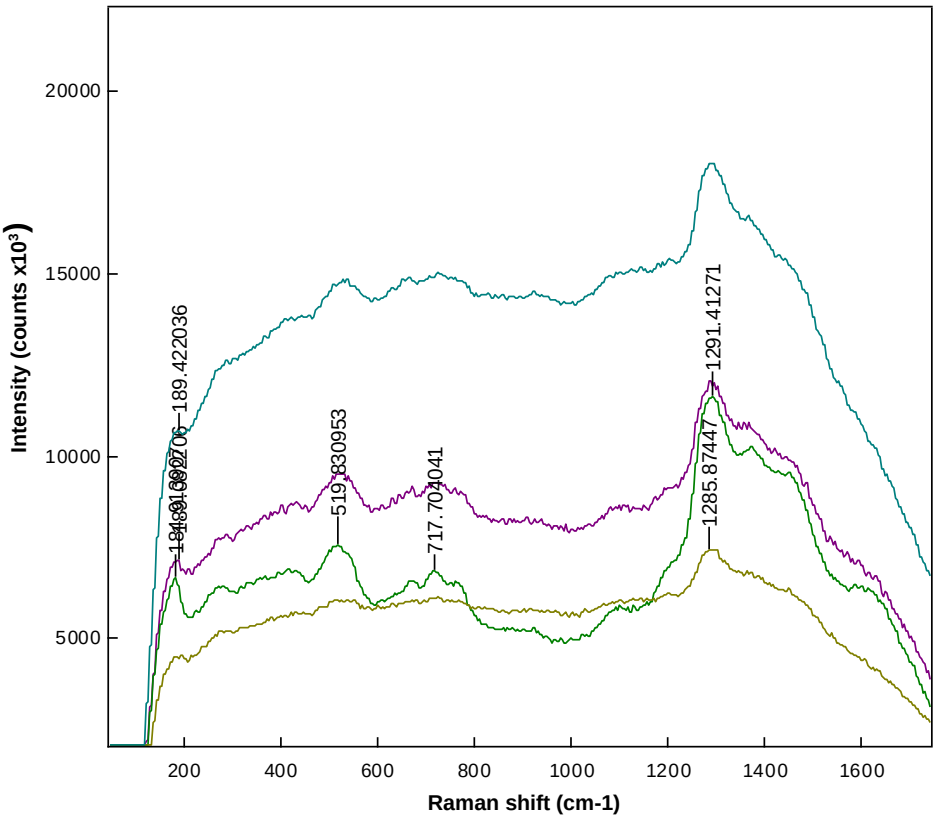

Fig. 4.6. Charnockite with 785 nm Micro-raman microprobe all scaled 2x for clarity using 11mW 50X objective 30sec exposures and 1 accumulation

4.1.1 Petrofabric Mineralogy

4.1.1.1 X-ray flourescence

Table 4.3 shows the results of X-ray refractometer recorded major and trace minerals in representative Precambrian rock samples from Southwestern Nigeria. The mean values of iron-oxides present in banded gneiss 1, granite gneiss 1, granite gneiss 2, granite, quartzite, migmatite gneiss 1, banded gneiss 2, granodiotite and migmatite gneiss 2 are 1.26, 1.08, 6.27, 1.94, 0.10, 0.71, 5.08, 6.91 and 7.34 percent respectively.

4.1.1.2 Electron Probe Microanalyzer Result

Table 4.3 shows spot analysis result of the percentage of maghemite (Fe_2O_3) present in the study area. Maghemite has a value of 74.6 % which suggested that tectonometamorphic process in the Precambrian rocks can be drawn to its metasomatic reactions encompassing reliable oxidised maghemite, having somewhat acidic fluid that has the capacity to modify the perthitic feldspar and andesine. Assuming that metamorphic and metasomatic processes are coeval within the study area, at that time, introduction of fluids may define the growth of prograde REE-rich-albite K-feldspar-biotite in the granitoids (Table 4.4). Therefore, the late formation of hydrothermal K-feldspar in the magmatic and metamorphic was likely to make it difficult to isolate the sodium-bearing fluids because of a deficient data set on pre-metamorphic protoliths in the study area**.** Clustered magmatic K-feldspar and albite discriminated in the granitoids because of their respective 0.04% and 0.09% values.This implies that granitoids vary regionally and locally. It's similar to disparities in magma oxidation states, as shown by Fe-Ti oxide variations in each surface (Table 4.4). Reduction and oxidation reactions and conditions of fluid pH were responsible for differentiation in iron-titanium oxide minerals. α-hematite is sensitive and replaceable to redox transformation than γ-maghemite. The granitoids are characterised with spread from positive to negative Eu-anomaly (from enriched to being depleted relative to REEs) albite Types I and II. The co-crystallization of hydrothermal K-feldspar and T2-albite supports the idea of fluid pH changes from acidic to neutral (45% Fosterite + 55% Enstatite), or decline in oxygen (O_2) (from hematite to magnetite stability). This demonstrates the formation of hematite and

magnetite occurrence as minute inclusions in purviews of reactive hydrothermal K-feldspar as well as modifications observed in basalts (Krasa and Herrero-bervera, 2005).

Table 4.3 Chemical analysis of granitoids from southwestern Nigeria (XRF)

Major/ Trace	Bgn eiss1	Gneiss 1	Ggn eiss2	Gran ite	Quart zite	Mgneiss1	Bg neiss2	gr.di orite	MG2
SiO_2	72.7	72.8	59.9	73.3	98.9	75.7	61.2	62.4	65.4
TiO_2	0.22	0.18	0.75	0.23	0.04	0.14	0.88	0.92	0.69
Al_2O_3	14.8	14.8	16.6	13.8	0.72	13	17.6	16.7	15.7
Fe_2O_3	1.26	1.08	6.27	1.94	0.1	0.74	5.08	6.99	7.34
MnO	0.01	0.01	0.09	0.03	0	0.02	0.15	0.1	0.13
MgO	0.41	0.32	3.03	0.34	0.07	0.22	1.73	1.99	1.89
CaO	0.4	0.7	5.15	1.36	0.02	0.86	4.8	2.59	2.69
Na_2O	3.34	3.85	4.12	3.66	0	3.25	5.53	2.33	3.4
K_2O	5.12	4.74	2.56	4.69	0.23	5.36	1.82	3.43	1.98
P_2O_5	0.28	0.29	0.25	0.06	0.01	0.07	0.3	0.29	0.04
LOI	1.25	1.11	0.51	0.5	0.01	0.42	51	1.41	0.71
Sum	99.79	99.88	99.23	99.91	100	99.78	99.6	99.15	100

Table 4.4 Electron Probe Microanalyzer result of maghemite from the study area in Granitoids (Granites and gneiss)

	Maghemite	K-Feldspar	Albite
F			0.02
Na_2O		0.76	10.89
SiO_2	0.3	63.24	67.29
MgO	8.4		0.25
MnO_2	0.9		
Al_2O_3	1.8	17.65	20.52
P_2O_5			0.03
Cl		0.05	
K_2O		15.39	0.49
CaO		0.03	0.16
TiO_2	13	0.02	
FeO		0.04	0.09
Fe_2O_3	74.6		
Total	99	97.19	99.72
%Albite		7	96.4
%Anorthite		0.1	0.8
% K Feldspar		92.8	2.8

4.1.1.3 Scanning Electron Microprobe

Mineralogical compositions of granitoids from the basement complex of Southwestern Ni -geria were studied using Scanning Electron Microscopy (SEM). Akunu gneiss, Iwaraja granite, Lanlate biotite granite gneiss, Ajibode banded gneiss and Okeagbe-Akoko charnockite predominantly recorded maghemite/magnetite, ilmenite, pyrite and poor (titano)magnetites, with differences in titanium (Ti), grain sizes content and configuration respectively (Fig. 4.7). Examinations of polished sections of samples from the southwestern Nigerian granitoids (Fig. 4.7A-F) exhibited grains of maghemite and magnetite (light grey); titanomagnetite (grey) magnetite (light grey); magnetite and titanomagnetite (striations of light grey); maghemite and titanomaghemite (grey); ilmenite observed between (white and grey) and pyrite observed between (white and grey) respectively.

Scanning electron microscope serves as a proxy in determining the diverse magnetic phases in iron titanium oxides present in the selected rock samples. Studies showed larger altered (titano)magnetite grains in the Akunu-Akoko gneiss, titanomagnetite in Iwaraja granite, phases of titanomagnetite and magnetite in Lanlate biotite granite gneiss with evidence of dehydration, maghemite and titanomaghemite in Ajibode banded gneiss, ilmenite in Okeagbe-Akoko charnockite and pyrite as seen in Erusu-AKoko granite gneiss (Fig.4.7 a-d). The Fe-Ti-O grains indicated transfomations of spinel rods, low-temperature oxidation reaction, precipitation of rock crystalline phases (exsolution) and dehydration due to tectono-metamorphic episodes observed in studied rock samples. The abundance of precursor magnetite was susceptible to transformation than the smaller magnetite grains resulting to the pronounced formation of maghemite and titanomaghemite in the rock samples. This result correlates with the arguments of Carporzen *et al*. (2006) that suggested tectono-metamorphism-related temperatures in the rock assemblage and heating of magnetite.

4.1.1.4 X-ray diffractometry

The magnetic minerals in the selected rock samples were investigated further using the XRD data (Fig. 4.8 a-c) to unravel the mineralogical phases found in the Alagbaka granite, Ago-panu Owo gneiss and Oda road charnockite. It demonstrates mainly the

silicate and pseudomorphs of magnetite phases. Figure 4.8 a-c showed pronounced spectra of silicate phase while the smaller spectra are pseudomorphs of magnetite (magnetite and maghemite). These results are consistent with that of the Raman spectroscopy, SEM and temperature dependence.

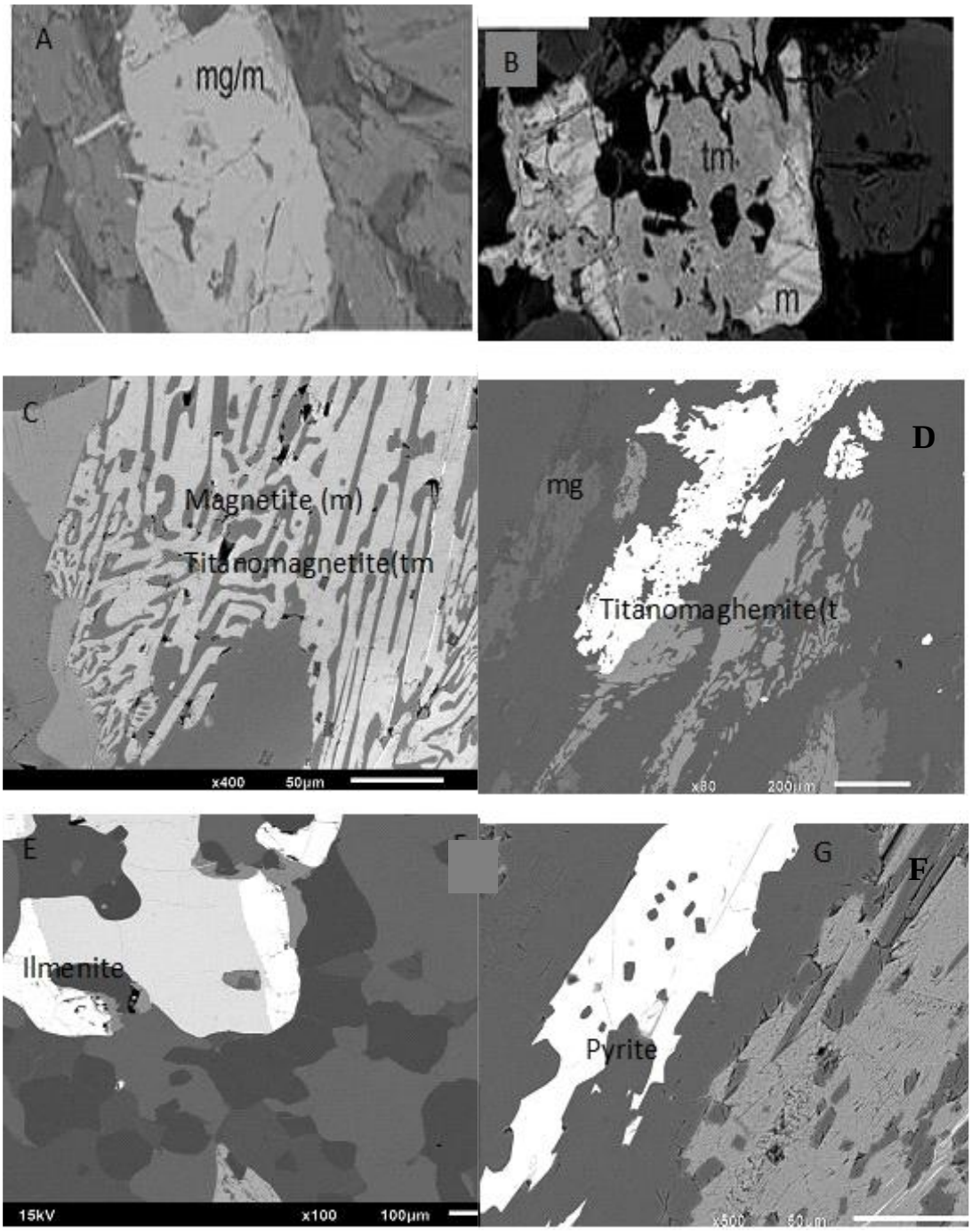

Fig. 4.7.SEM results of magnetic minerals (JEOLJSM-5900LV). (a) Altered magnetite (maghemite) of Akunu Akoko gneiss (scale:10 pm), (b) titano-magnetite of Iwaraja granite (scale:10 pm). (c) titano-magnetite and magnetite from dehydration of biotite in Lanlate biotite granite gneiss (d) titanomaghemite and maghemite of Ajibode banded gneiss (e) Ilmenite of Okeagbe-AKoko (f) Pyrite of Erusu-Akoko Charnockite

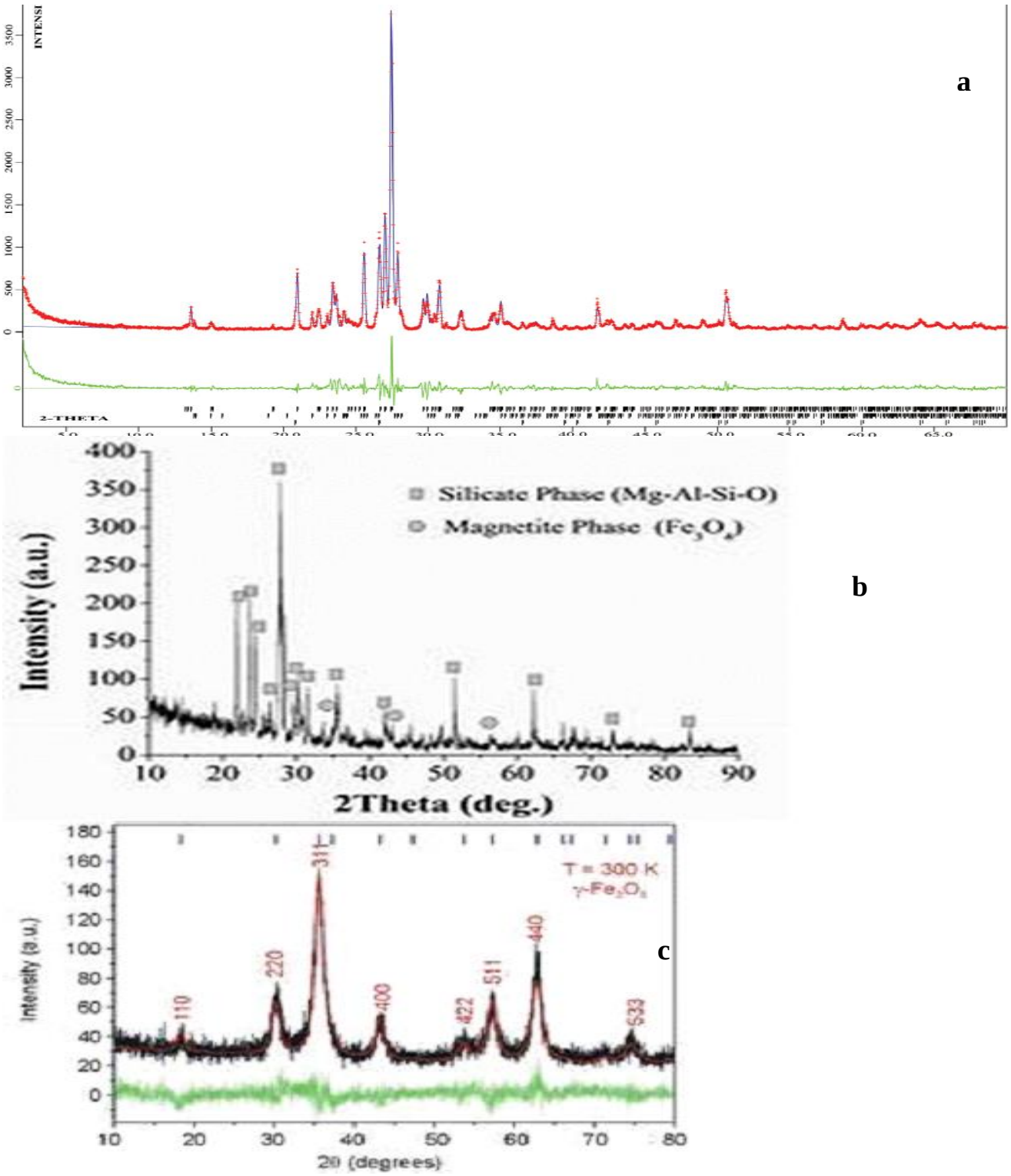

Fig. 4.8. XRD of some basement rocks at the study area (a) Alagbaka granite (b) Owo-Ago panu gneiss (c) Oda road Charnockite

4.2 Thermomagnetic (temperature dependence)

Temperature dependence was used to measure the magnetic indicators of the representative samples from southwestern Nigeria, which displayed normal Q values and variable behavior.There was predominance of maghemite iron oxide mineral in the rock samples, though the mineralogical stability differs because of the occurrence of poor magnetite and titanomagnetite magnetic phases (Figs. 4.9 to 4.12).The red colour curve is heating while the blue colour curve is cooling. The majority of granitoids in southwestern Nigeria exhibit a Hopkinson point in the heating cycle, indicating pseudo-single-domain and multidomain magnetite, with Curie temperatures in the 580 °C to 585 °C range (Dunlop and Ozdemir, 1997). While the magnetite mineral was 585 °C, the addition of titanomagnetite triggered the heating records of the low temperature magnetic period. When the Curie temperature of granitoids with a noticeable hump is between 450 °C and 600 °C, maghemite is produced. Magnetic susceptibility is reduced in samples with low magnetite content values around 400 °C, which is typical of paramagnetic conduct. Susceptibility versus temperature plots of granitoids of southwestern Nigeria of Granite, quartzite, banded iron formation, porphyritic granite, augen gneiss, banded gneiss, biotite granite gneiss, charnockite, granite gneiss and phyllite samples are shown in Figures 4.9 to 4.12. Representative granite samples (CO1I, CO1E, CO1IW, CO1A, CO1O, CO1IL) from Igbara-oke, Erin-Ijesha, Iwaraja, Asejire, Ogbomoso and Ilogbo-Osogbo, exhibited reversible heating and cooling curves bands (Fig. 4.9). Representative samples of Paleoproterozoic and Neoproterozoic granitoids from southwestern Nigeria showed extreme reversible heating and cooling curves during the measurements, which are characteristic of non-mineralogical transformations. The granite samples witnessed increase susceptibility around 220 °C, 280 °C, 300 °C,320 °C,340 °C, 380 °C,540 °C,580 °C,585 °C,600 °C (Fig. 4.9), which are characteristic of low-temperature titanomagnetite (maghemitization) occurence (Ade-Hall *et al.,* 1971; Sayab *et al.,*2021).They are indicative of hematite,poor (titano)magnetite and maghemite. The results show a decrease in sensitivity about 320 °C – 350 °C, which is linked to maghemite transposition. The development of new polymorphs of magnetite during heating was characterized by a cooling curve of high magnetic susceptibility.

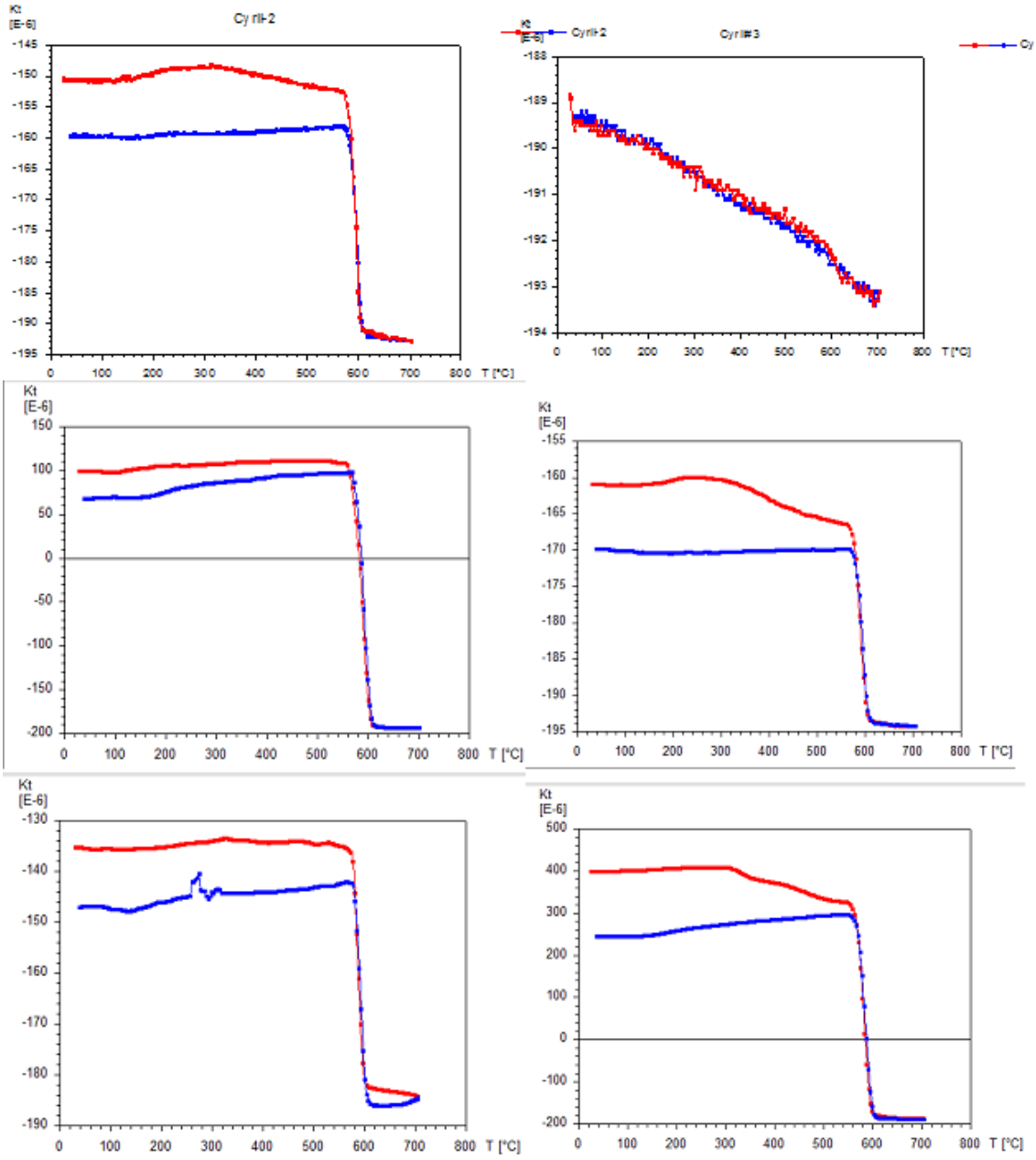

Fig. 4.9. Thermomagnetic curves of granites

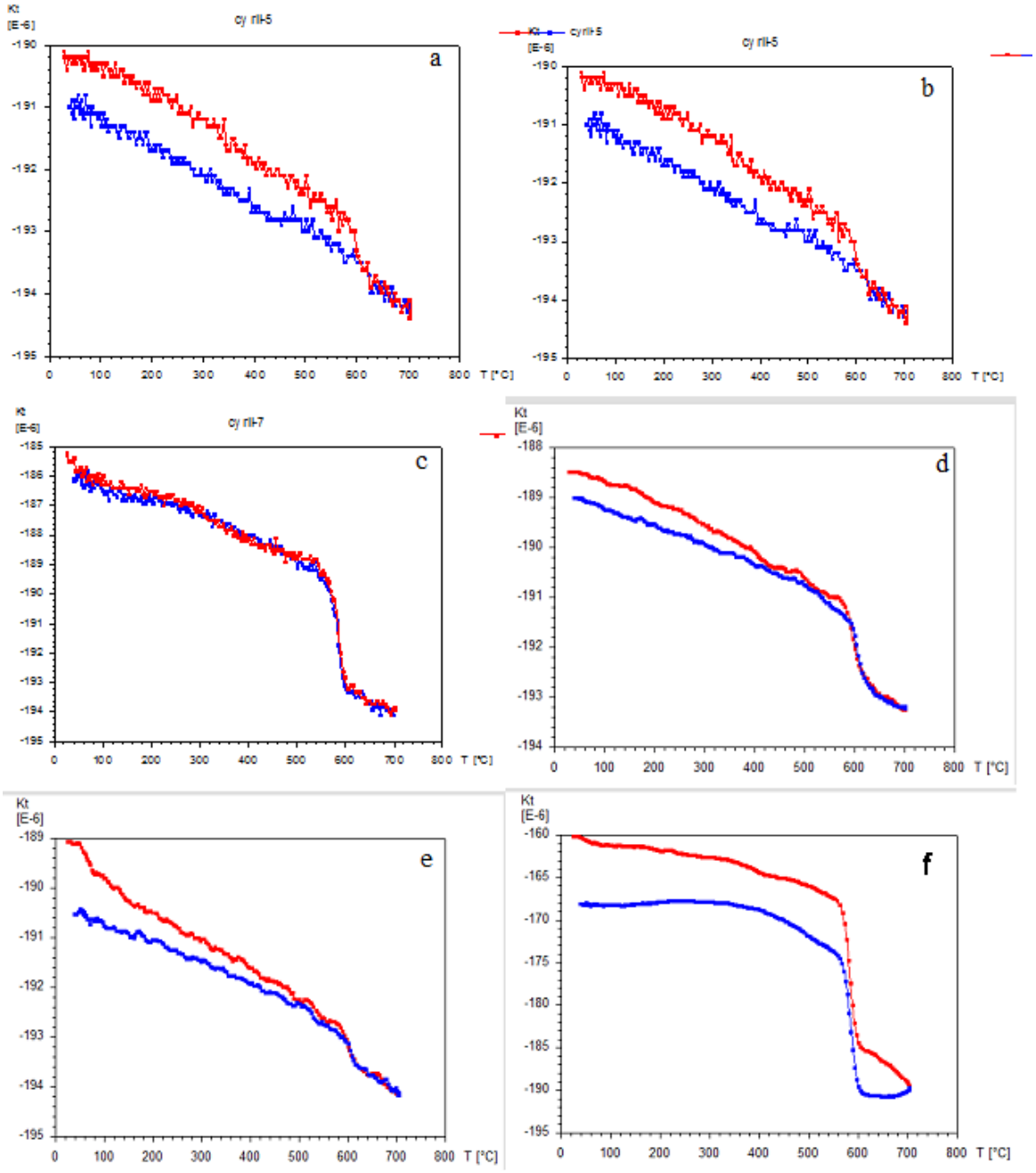

Fig. 4.10. Thermomagnetic curves of (a) Quartzite (b) Gbede BIF (c-d) porphyritic granite (e-f) Augen gneiss

Quartzite and banded iron formation (CO2E and CO3G) from Effon-Alaye and Gbede recorded increase susceptibility of 520 °C and 520 °C as well as 510 °C, 580 °C and 610 °C indicative of hematite, poor titanomagnetite and maghemite respectively (Fig. 4.10a and b).

Porphyritic granite representative samples (CO4I and CO4A) from Idanre and Abeokuta exhibited intense reversible heating and cooling curves typical of mineralogical magnetic phases observed in the heating measurements. The temperature dependence susceptibility values are 460 °C, 470 °C, 490 °C, 570 °C and 580 °C demonstrating magnetic character of poor titanomagnetite and maghemite (Fig. 4.10 c and d).

Augen gneiss representative samples (CO6A and CO6I) from Ajibode UI and Igbatoro show temperature dependence susceptibility values of 380 °C,400 °C, 500 °C, 580 °C and 600 °C indicating magnetic character of poor titanomagnetite and maghemite (Fig. 4.10e and f). During heating experiments, representative banded gneiss samples (CO5A and CO5I) from Akungba-Akoko and Ikare-Akoko demonstrate heating and cooling curves with high degree of reversibility, implying mineralogical phases. (Salminen *et al*., 2019).The temperature dependence susceptibility values are 520 °C and 610 °C as well as 180 °C,400 °C,530 °C and 590 °Cdemonstrating magnetic character of hematite, poor titanomagnetite and maghemite (Figs.4.11a and b).

Biotite granite gneiss representative sample (CO7E) from Ejigbo demonstrate intense reversible curves of heating and cooling, characteristic of mineralogical magnetic phases observed in the heating measurements. The temperature dependence susceptibility values are 380 °C and 585 °C demonstrating magnetic character of poor titanomagnetite and maghemite (Fig. 4.11c).

Phyllites representative sample (CO10I) from Igarra revealed intense reversible heating and cooling curves typical of non-mineralogical magnetic phases alteration observed in the heating measurements.The temperature dependence susceptibility values are 260 °C, 470 °C and 560 °C demonstrating magnetic character of hematite, poor titanomagnetite and maghemite (Fig. 4.11d)

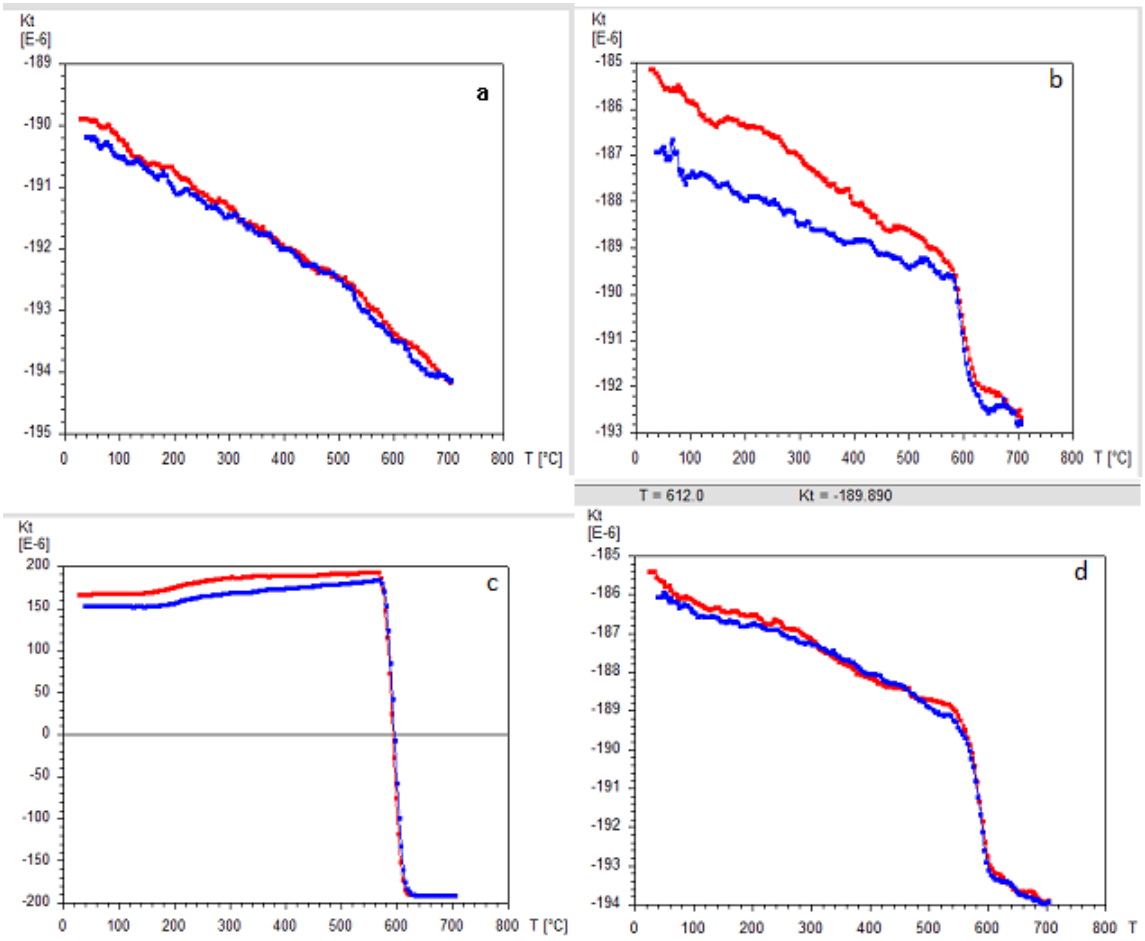

Fig. 4.11. Thermomagnetic curves of (a-b) Banded gneiss (c) Biotite granite gneiss (d) Phyllite

.

Charnockites representative samples (CO8A, CO8O, CO8I and CO8S) from Akunu-Akoko, Okeagbe-Akoko, Iwo and Shasha-Akure have intense reversible curves of heating and cooling typical of mineralogical magnetic phases observed in the heating measurements. The temperature dependence susceptibility values are 180 °C, 280 °C, 360 °C,400 °C,480 °C,560 °C and 585 °C demonstrating magnetic character of hematite, poor titanomagnetite and maghemite (Fig. 4.12a-d).

Granite gneiss samples (CO9I, CO9O, CO9OK and CO9E) from Ikire, Okearo-Akure, Okeagbe-AKoko and Erusu-Akoko indicate intense reversible curves of heating and cooling which is usual of non-mineralogical magnetic phases of transformation observed in the heating measurements. For this, the temperature dependence susceptibility values are 90 °C, 220 °C, 320 °C, 380 °C, 510 °C, 570 °C, 590 °C and 595 °C demonstrating magnetic character of hematite, poor titanomagnetite and maghemite (Fig. 4.12e-h). The mineralogical and non-mineralogical phases were classified based on kink/change in the curves; which suggested record of iron-oxide mineral (Salminen *et al*., 2019).

Most of the rock samples exhibited intense reversible heating and cooling curves typical of mineralogical magnetic phases observed in the heating measurements (e.g. granite, quartzite, banded iron formation, porphyritic granite, augen gneiss, banded gneiss, biotite granite gneiss, charnockite, granite gneiss and phyllite). In the first low-temperature calculation, there were two Verwey transformations, but only one Verwey transition in the second low-temperature measurement. The lower temperature transformation was already eliminated, and the higher temperature transformation is a few degrees lower than the initial low-temperature estimate (at 120 – 122 K). In the preliminary low-temperature measurement between 100 and 102 K, and the second low-temperature measurement about 122 K, the specimens reported further transformations. The interpreted rock specimen exhibited increased magnetic susceptibility values all through the second low-temperature measurement, which is related to the treatments during the first and are characteristic of non-mineralogical transformations during the measurements. There was a predominance of reversible curves of heating and cooling. More so, higher magnetic susceptibility throughout the cooling than the heating measurements, typical of formation

of maghemite for the duration of tectono-metamorphic episodes. As a result, the configuration and lattice of maghemite in these rock samples is slightly distorted (Dunlop and Özdemir, 1997). All the studied samples revealed reversibility behavior, having Hopkinson peaks and a thermomagnetic curve values of 560 °C, 580 °C, 585 °C, 590 °C, 595 °C, 610 °C, 620 °C, and 650 °C during the experiment; indicating SD, PSD/MD of titanomagnetite and maghemite. The recorded cooling measurements exhibited decrease of magnetic susceptibility around 320 °C and 330 °C which are typical of higher Ti content in poor titanomagnetite.

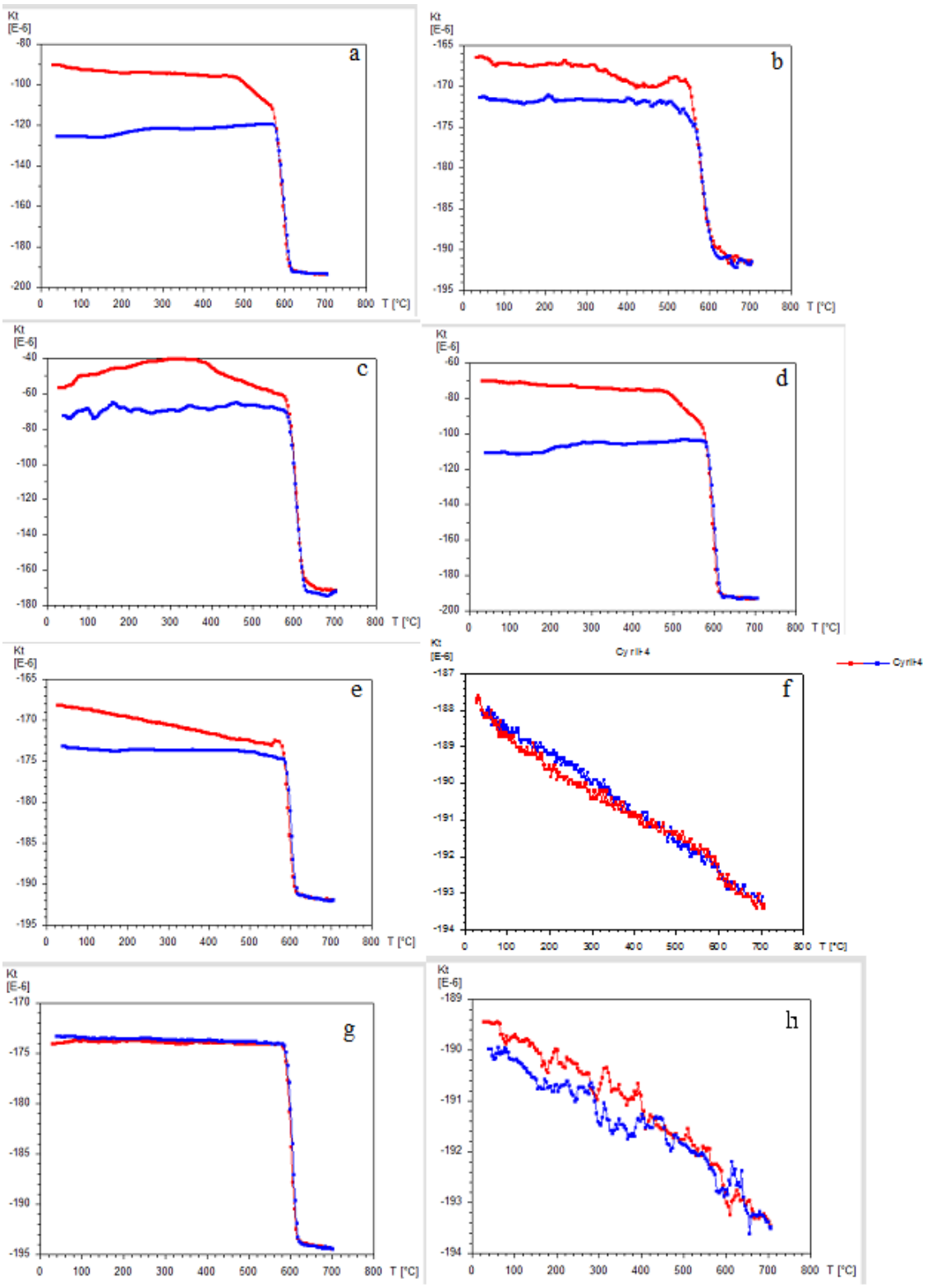

Fig. 4.12. Thermomagnetic curves of charnockites (a-d) and (e-h) Granite gneiss

4.3 Microstructural Emplacement

Anisotropy of Magnetic Susceptibility (AMS) was complementary to the understanding paleomagnetic characterisation to microstructural emplacement of Precambrian rocks of southwestern Nigeria. Figures 4.13 (a-i) show albite exsolution in microcline, plagioclase twinned and untwinned clusters, feldspar microcracks and microcracks healed with quartz, and elongate quartz established lineation and cut perpendicular to foliation and parallel to magnetic lineation; hornblende grains showed twinned and untwinned clusters, microcracks in feldspar and microcracks. The rock specimen had original north-south sinistral syn-D2 shearing structures that were obliterated at the end of dextral reactivation of the fault for the time of the D3 tectono-metamorphism, based on the observed N-S direction of magnetic foliation and lineation, as well as north-south S-shaped foliation. NNE-SSW to north-south to NNE-SSW (N0°E -N30°E) magmatic fabrics studied in the central Cameroun plutonic complex (Kwekam *et al.,* 2010). These microstructural emplacements took place between 580 and 552 Ma, and they correspond to the pluton emplacement at 576 Ma (Kwekam *et al.,* 2010). Detailed structural studies in the Precambrian mobile belt (PMB) and environs aided the understanding of its kinematic evolution, emplacement inferences of the southwestern Nigeria Basement rocks and correlated to central-eastern Cameroun and north-east Brazil.

Isoclinal folds, mylonitic foliation, and extended lineations all display the same NE-SW orientation, implying that the magnetic foliations and lineations correspond to the fracture orientation. Re-alignment of the structures was in synchrony with occurrence of mylonites. They were formed owed to the outcome of dextral activation of the Ife- Ilesha shear zone (IISZ) during the D_3 tectono- metamorphic event; making largely charnockite-granitoids to be rightly inclined (dextral). Conversely, there are presence of sinistral structures of mylonites with S-shape foliation (N12°E) orientation in IISZ. Tables 4.5 - 4.6 illustrate the aformentioned AMS of gneiss and aplite dyke which corresponds to Figures 4.14 - 4.15.

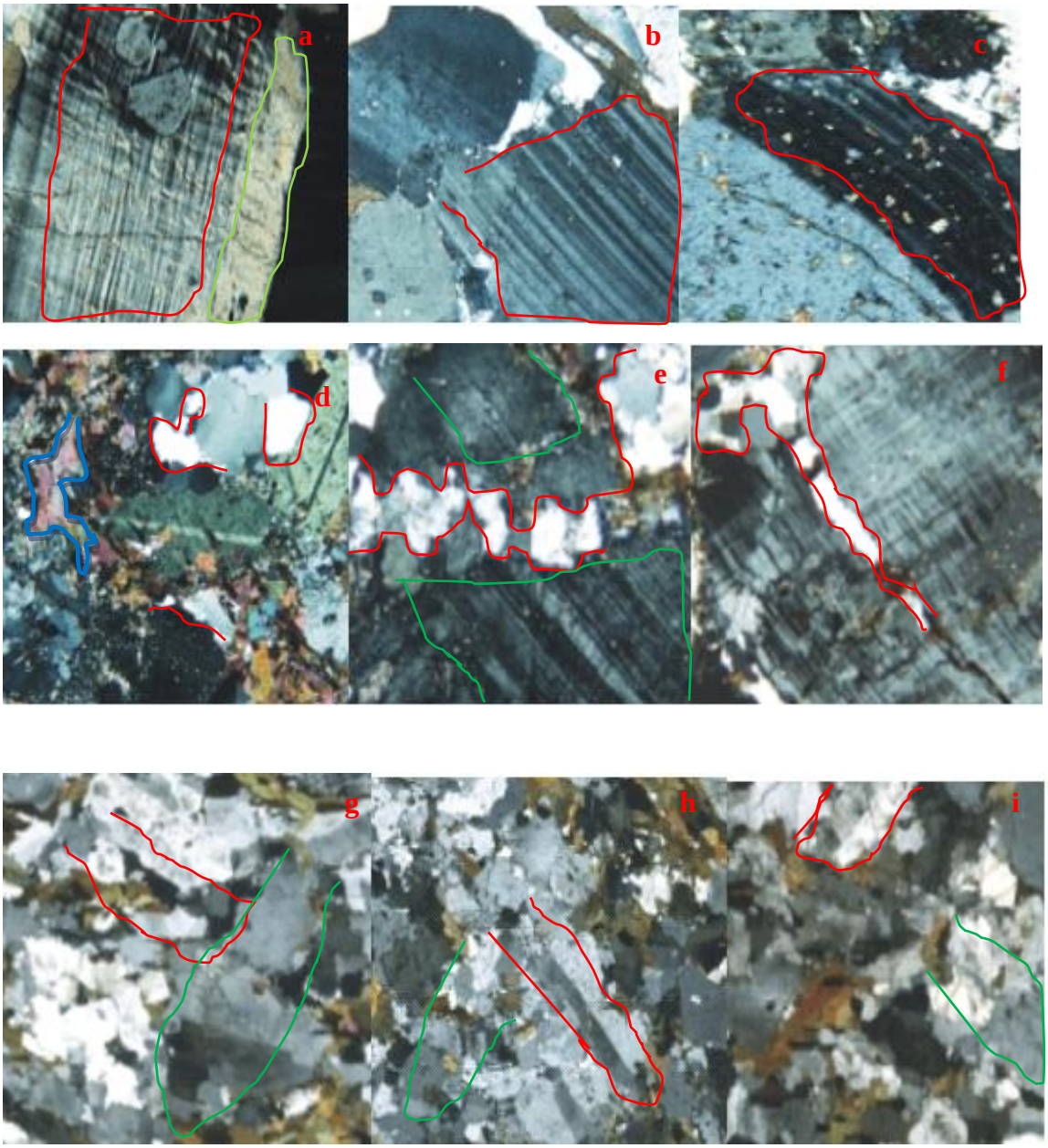

Fig. 4.13. (a-c) Granite gneiss exsolution (marked green of albite in microcline showing slight and strong bend with twin lamellae (marked red) in plagioclase; (d-f) Hornblende grains showing twinned and untwined cluster (marked green), microcracks in feldspar healed with quartz (marked red), microcracks in microcline (blue) and (g-i) Gneissic rock cut perpendicular to foliation (marked green) and parallel to magnetic lineation (marked red) and also cut parallel to foliation and lineation. As well as perpendicular to foliation and lineation. Strongly elongate quartz grains define the lineation

The orientation of NE-SW magnetic and stretched lineation has experienced minor plunge (<30°) subhorizontal transposed sheared blocks for anisotropy of magnetic susceptibility. These imply that sheared and mylonitized blocks are due to NE-SW directional thrust.

Table 4.5 and Figure 4.14 show gneiss representative samples (CO1I, CO1G, CO1A, CO1O) from Ife, Gbongan, Akunu-Akoko and Okeagbe-Akoko, have lowest and maximum mean bulk susceptibility (Km) values of 141 and 29,868; the shape parameter (T) have range of values from -0.78 to 0.73 indicating prolate and oblate ellipsoid; intensity parameter (P) have range of values from 1.039 - 1.302. The results of the maximum and minimum foliation and lineation range from 0.3 - 347 and 0.6 - 63.8 and 28.3 - 295 and 4.4 – 62, respectively. The foliation and lineation was trending NW-SE and NNE-SSW respectively (Fig. 4.14)

Table 4.5Anisotropy of magnetic susceptibility of Gneiss

Location	N	K(10^{-6} SI)	D1	L1	D3	L3	P	T
1	8	8349	347	33.1	109.9	40	1.064	-0.61
2	6	18.683	21.2	42.4	120.4	9.9	1.135	-0.28
3	8	9107	347	13	81.4	20.6	1.09	0.31
4	2	1693	345.5	48.6	94.6	16.1	1.046	0.71
5	6	1416	10.9	19.4	107.3	17.4	1.013	-0.31
6	6	29.868	20.3	45.6	121.5	10.7	1.145	-0.14
7	6	29.488	0.3	8.8	92.3	12.6	1.302	0.09
8	6	1785	345	35.9	125.4	46.8	1.057	0.37
9	10	1424	28	44.5	181	25.2	1.06	-0.28
10	7	22,366	4.3	8.5	96.5	14.1	1.229	0.53
11	7	1645	11	4.9	105.7	43.5	1.063	0.55
12	7	3962	11.7	0.6	102.7	61.5	1.171	0.09
13	6	219	231	63.8	28.3	23.6	1.09	0.51
14	6	153	199	31.1	73.2	43.5	1.072	0.65
15	6	141	193	45	42.8	40.8	1.039	0.64
16	6	2321	203	41.9	15.8	47.9	1.221	0.44
17	6	1600	161.9	22.7	39.3	52.3	1.078	0.73
18	6	9197	186	59.7	42.6	25	1.168	0.2
19	7	10189	213	46.4	85.9	29.5	1.195	0.41
20	7	2035	37.7	72	266	12.2	1.015	0.57
21	6	1253	192	4.1	282	6.5	1.018	0.27
22	8	2030	204	11.9	295	4.4	1.045	-0.78
23	6	5492	199	6	105.7	27.7	1.045	0.33
24	6	5514	191	1.1	98.8	49.2	1.054	0.11
25	6	4985	191	4	96.4	43.4	1.046	0.4
26	7	9324	346	9.9	94.8	62.5	1.051	0.03

N- No. of samples, K-Mean bulk susceptibility, D1- maximum magnetic susceptibility direction, L1- maximum linear degree of magnetic anisotropy, L3- minimum linear degree of magnetic anisotropy, D3- minimum magnetic susceptibility direction, P- Intensity of magnetic anisotropy, T -Shape parameter of magnetic anisotropy

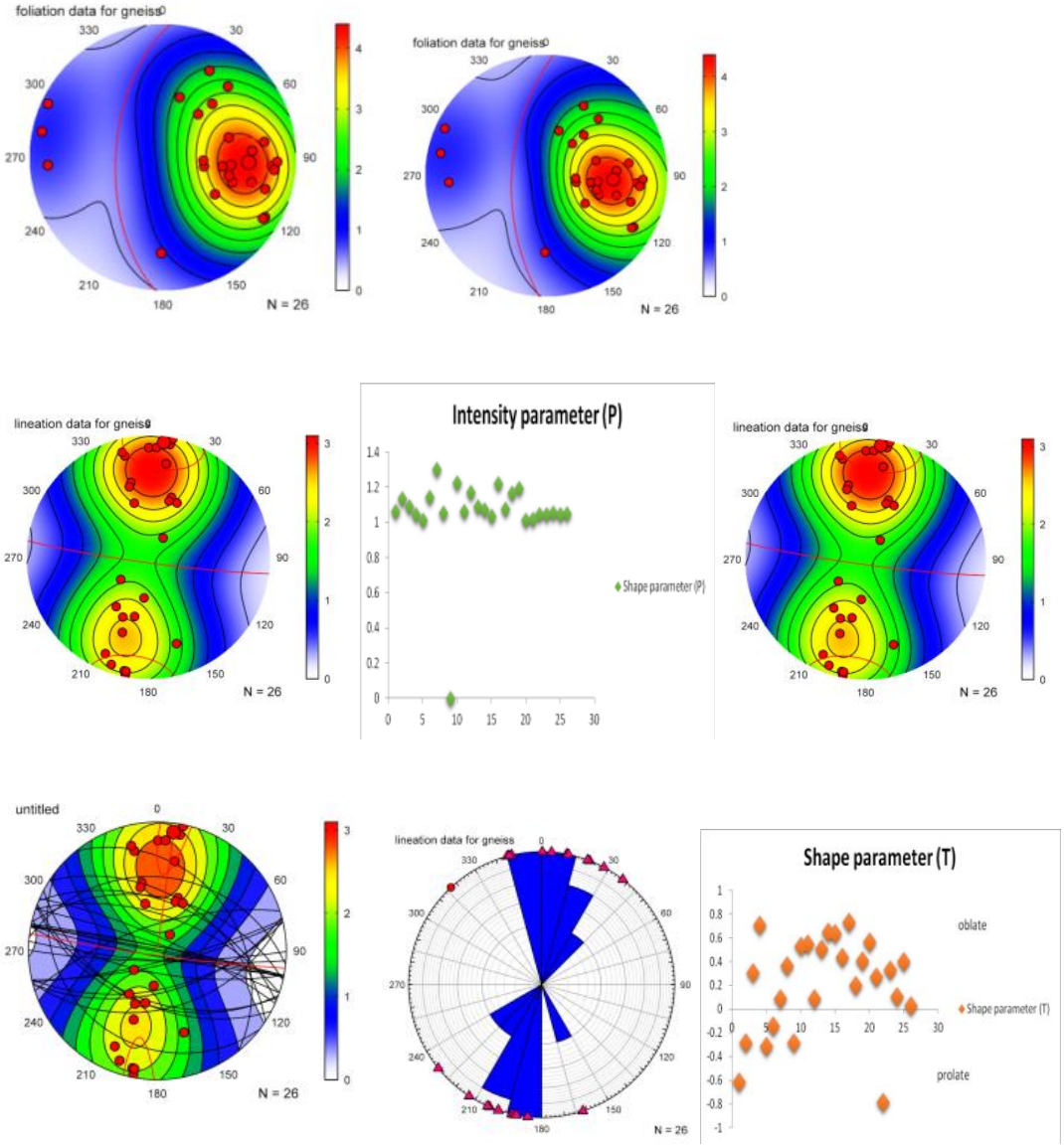

Fig. 4.14. Foliation (equidistant, stereographic, orthographic and equal area), Lineation (equidistant, stereographic and orthographic) and equal area circular histogram of Gneiss microstructures

Table 4.6 and Figure 4.15 show aplite dyke representative sample (CO2I) from Ibadan having lowest and maximum mean bulk susceptibility (Km) values of 20 and 8250; the shape parameter (T) have range of values from -0.32 to 0.6 indicating prolate and oblate ellipsoid; intensity parameter (P) have range of values from 1.013 - 1.512. The maximum and minimum foliation and lineation values are 32.5 - 350.8 and 13.4 - 80 as well as 39.7 - 297.1 and 3.6 - 43.2 respectively. The foliation and lineation was trending NE-SW and NNE-SSW respectively (Fig. 4.15)

Table 4.7 and Figure 4.16 show granite representative samples (CO3I, CO3E, CO3IW, CO3A, CO3AO) from Igbara-Oke, Erin-Ijesha, Iwaraja, Asejire and Abegundo Ogbomoso; have lowest and maximum mean bulk susceptibility (Km) values of 33 and 30233; the shape parameter (T) have range of values from -1.25 to 1.04 indicating prolate and oblate ellipsoid; intensity parameter (P) have range of values from 1.018- 1.174. The foliation and lineation was trending NW-SE and NNE-SSW respectively (Fig. 4.16). Table 4.7 reveals that the north-south and NNE-SSW granitoids witnessed shear markers by the older granites which correspond to D2 and D3 of the Cameroun and NE Brazil deformation phases, respectively (Fig.4.16).

Table 4.6 Anisotropy of magnetic susceptibility of Aplite dyke

Location	N	K(10^{-6} SI)	D1	L1	D3	L3	P	T
1	5	600	350.8	13.4	93.8	43.2	1.024	-0.12
2	6	20	297	45.7	47.9	19.5	1.512	0.58
3	6	702	68.3	65.9	269.3	22.7	1.013	-0.33
4	6	1496	35.2	22.4	297.2	18.6	1.099	0.6
5	6	4000	32.5	50.9	263.5	27	1.04	-0.32
6	6	8250	289	80	39.7	3.6	1.129	0.6
7	6	406	40.6	31.9	172.6	47.1	1.013	0.66
8	6	21	140.6	1.8	172.6	47.1	1.079	0.38

N- No. of samples, K-Mean bulk susceptibility, D1- maximum magnetic susceptibility direction, L1- maximum linear degree of magnetic anisotropy, L3- minimum linear degree of magnetic anisotropy, D3- minimum magnetic susceptibility direction, P- Intensity of magnetic anisotropy, T -Shape parameter of magnetic anisotropy

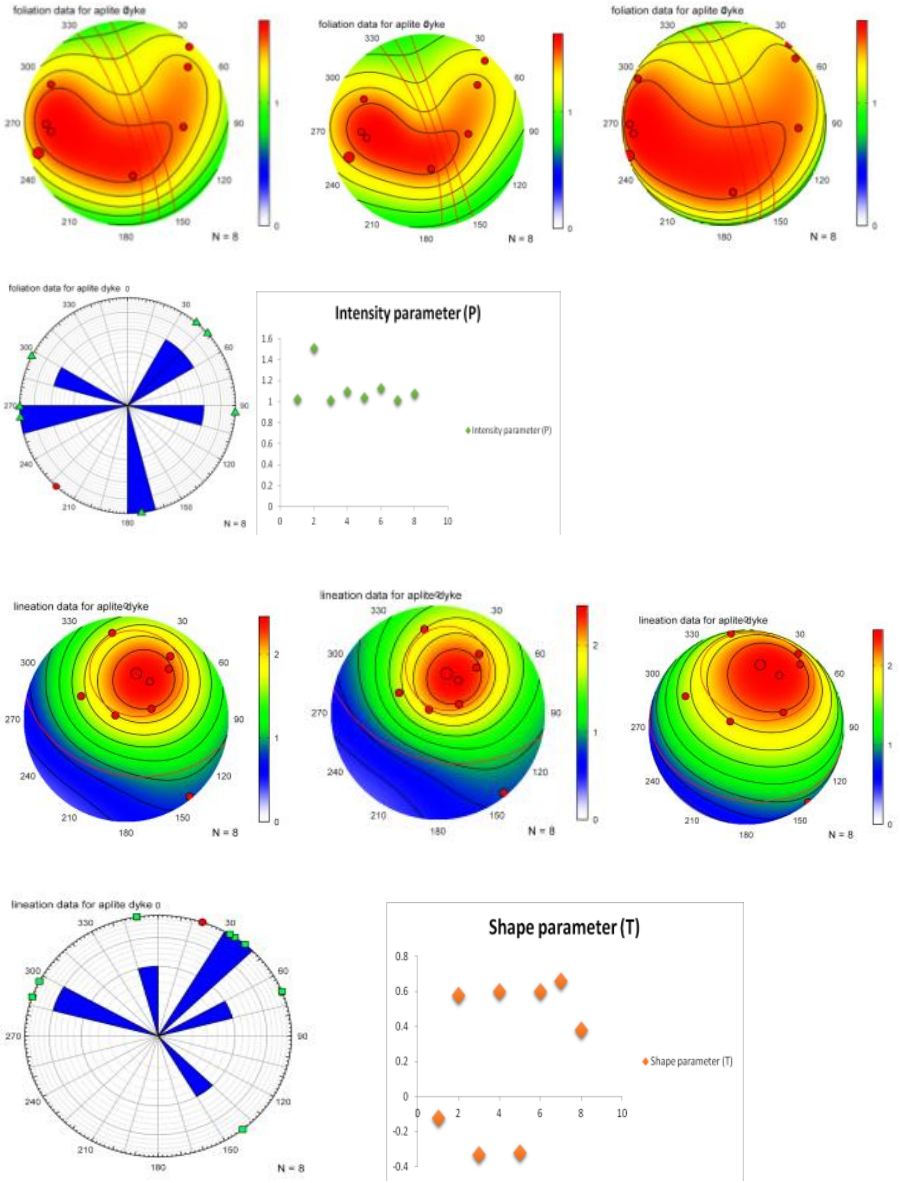

Fig. 4.15. Foliation (equidistant, stereographic, orthographic and equal area), Lineation (equidistant, stereographic and orthographic) and equal area circular histogram of Aplite dyke microstructures

AMS analysis have proven the synkinematic evolution of the charnockites-granitoids whereas the abundant D3 enclosing the traces of D2 markers are hard to unravel (Fig. 4.16). The granite is typified dominantly by NE-SW and N-S foliation directions, and a NNE-SSW lineation direction. The aforementioned orientations and formation of mylonitised blocks began in the N-S causing a sinistral shearing that modified the NNE-SSW and NE-SW emplacement directions of charnockite-granitoids plutons with an isochron of 613 and 590 Ma.

Table 4.8 and Figure 4.17 show diorite representative sample (CO4I) from Iwo, that haslowest and maximum mean bulk susceptibility (Km) values of 33 and 30233; the shape parameter (T) have range of values from -0.18 to 0.15 indicating prolate and oblate ellipsoid; intensity parameter (P) have range of values from 1.072 - 1.085. The maximum and minimum foliation and lineation values ranges from 101.7 - 93.6 and 70.6 - 62.8 as well as 353.5 - 205 and 6.3 - 1.3 respectively. The foliation and lineation was trending NW-SE and NNE-SSW respectively (Fig. 4.17)

Table 4.9 and Figure 4.18 show granite gneiss representative sample (CO5I) from Ikire, having lowest and maximum mean bulk susceptibility (Km) values ranging from 1632 - 26921; the shape parameter (T) have range of values from -0.09 to 0.75 indicating oblate and prolate ellipsoid; intensity parameter (P) have range of values from 1.035 - 1.158. The maximum and minimum foliation and lineation values ranges from 356 - 143 and 62.5 - 0.2 as well as 275 - 65.6 and 73.1 - 5.2 respectively. This imply that the direction trend NW-SE and NE-SW (Fig. 4.18)

Table 4.7 Anisotropy of magnetic susceptibility of Granite

Locations	N	K(10^{-6} SI)	D1	L1	D3	L3	P	T
1	6	11016	83.2	81.9	324	4	1.174	-23
2	6	2846	239	85.9	125	1.6	1.05	1.04
3	7	1450	68.5	30.8	299	47.1	1.038	0.57
4	6	12708	85.8	62.2	294	25	1.064	-0.41
5	6	920	228	68.4	116.9	7.9	1.019	-0.25
6	6	750	35.6	63.7	267	17.4	1.019	-1.25
7	6	13190	40.3	39.4	305	7.5	1.146	0.62
8	6	9644	49.4	32.2	310	14.7	1.055	0.56
9	6	9731	54.6	43.2	323.2	1.5	1.05	0.2
10	6	6272	252	62.4	7.7	13	1.05	0.2
11	6	17910	141.3	44.6	48.4	2.9	1.188	0.41
12	6	10926	123	61.6	21	6.4	1.139	0.37
13	6	12270	328.5	60.7	207.1	11.5	1.115	0.83
14	8	30233	335	65.5	225	8.9	1.24	0.62
15	7	18580	351.1	35.2	82.8	2.4	1.236	0.39
16	6	11498	206	80	323	4.5	1.087	0.87
17	6	1776	89	9.2	358.7	2.2	1.12	0.62
18	7	5292	89	53.3	306	30.9	1.043	-0.18
19	6	1140	187	14	319	69.5	1.052	0.27
20	6	60	221	26.4	351	52.3	1.066	0.37
21	6	1310	191	2.9	99.6	10.1	1.04	-0.26
22	7	190	197	14.9	287	0.8	1.05	0.19
23	6	1631	358.9	61.4	203	26.5	1.044	-0.16
24	6	1631	197	4.4	104.2	25.2	1.026	-0.06
25	7	710	4.2	7	232	79.8	1.027	0.19
26	6	528	347	16.3	88.7	35.1	1.018	0.12
27	6	140	23.4	11	215	78.8	1.048	0.02
28	6	14	128	18.1	228	27.5	1.025	-0.68
29	6	2128	223	0.4	132	17.3	1.045	-0.1
30	6	343	188	26.3	313	49	1.064	-0.22
31	6	2144	19.4	51.3	114.1	3.7	1.037	-0.06
32	7	2617	37.8	13.1	129.3	6.4	1.059	-0.5
33	6	2021	37.1	18	128.2	3.4	1.056	-0.9
34	6	33	60.1	37.1	170	24.1	1.035	-0.42
35	6	48	31.5	13.2	191	76	1.024	0.25
36	6	47	17.8	3.9	149.6	84.1	1.036	0.5
37	6	2366	29.9	0.9	299	58.1	1.089	-0.51
38	6	284	28.5	10.1	120.7	11.9	1.038	0.1
39	7	4190	221	5.3	127.2	32.1	1.059	-0.63

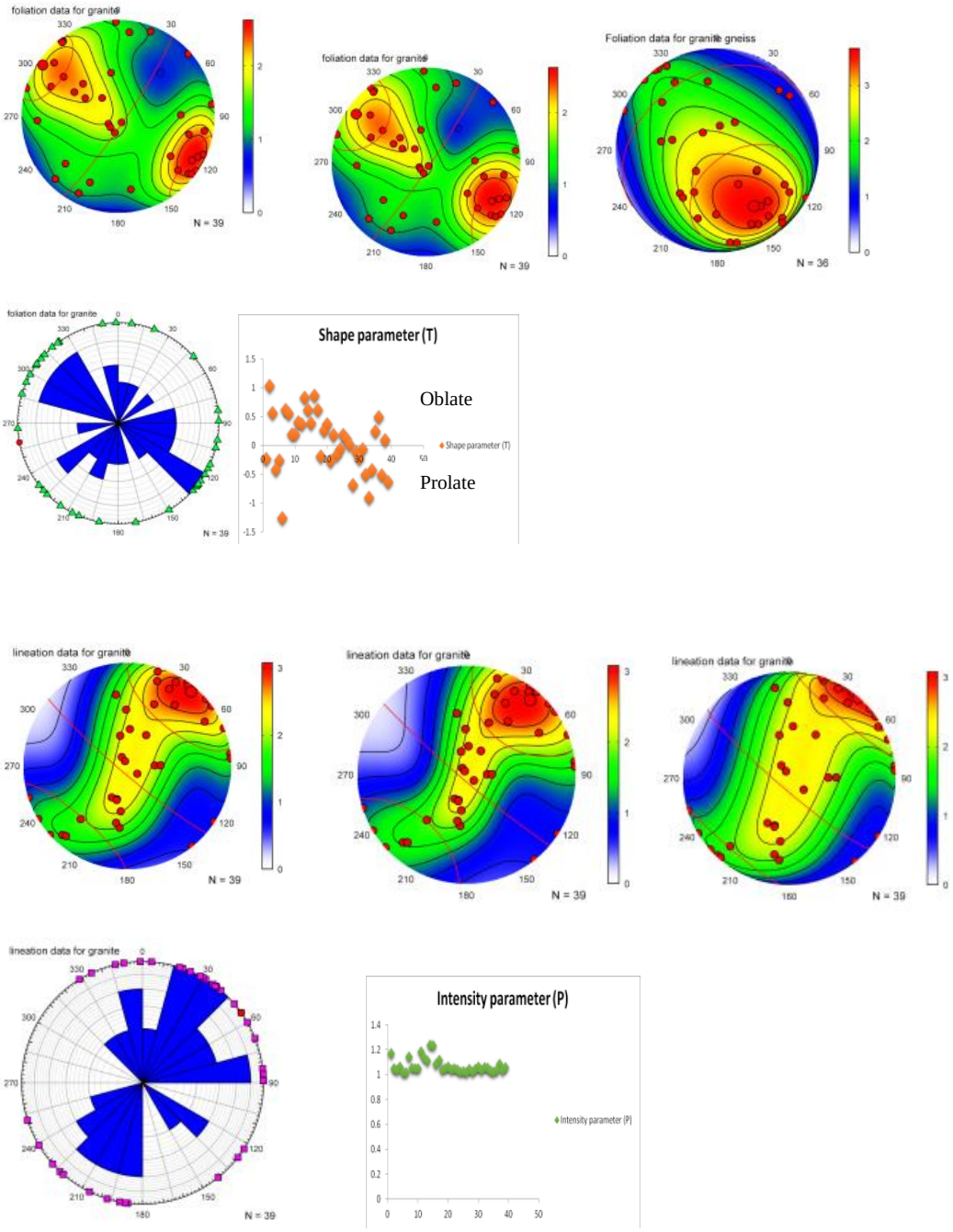

Fig. 4.16. Foliation (equidistant, stereographic and equal area), Lineation (equidistant, stereographic and orthographic) and equal area circular chart of Granite 1

Table 4.10a and b and Figure 4.19 show charnockite representative samples (CO6BA, CO6OA) from BTO Akure and Oda road Akure, having lowest and maximum mean bulk susceptibility (Km) values of 5641 and 10059. The azimuth/plunge of foliation and lineation values ranges from 29 - 253 and 2 - 34 as well as 223 - 247 and 5.24 respectively. This suggested that charnockite was trending NW-SE and NE-SW (Fig. 4.19). The shape parameter (T) have range of values from -0.01 to 1.29 indicating prolate and oblate ellipsoid while intensity parameter (P) have range of values from 1.06 - 1.75 (Fig. 4.20 a-b).The initial D2 shearing and synchronous reactivation of D3 N49°E trending fault around isochron age of 552 and 580 Ma were witnessed within the granodiorites and charnockites and D3 markers are observed (Figs. 4.19 and 4.21).

The non-existence of D2 markers in migmatite gneiss was due to solid state deformation products of the southwestern Nigeria plutons. Prevalence of NE-SW plunging fold axes revealed that shearing was responsible for the deformation and less flattening indices. These events (shearing and deformation) reoriented the fold axes towards the shear behavior; resulting to the formation of asymmetric folds which are evidence of D_3.

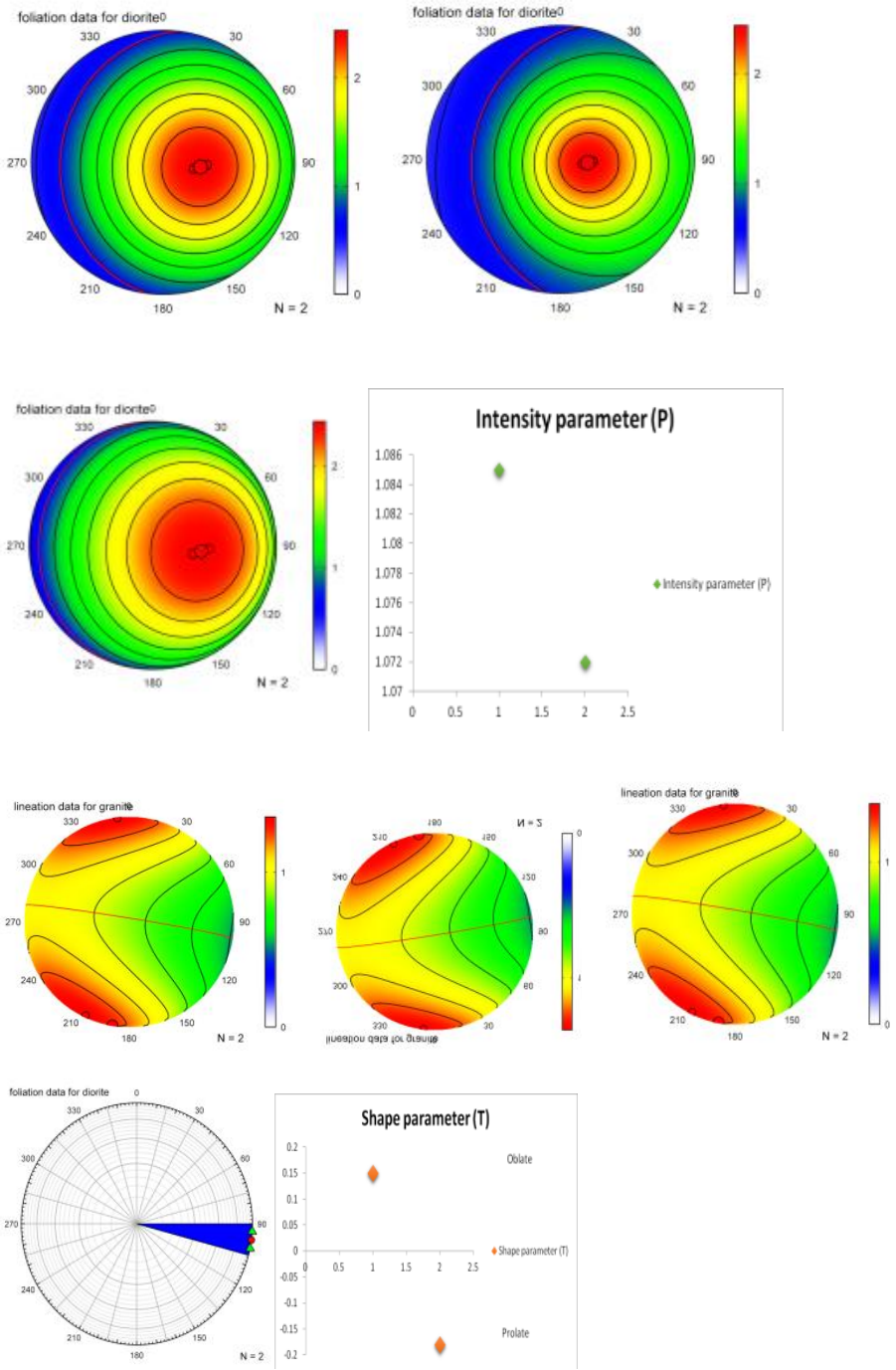

Fig. 4.17. Foliation (equidistant, stereographic, orthographic and equal area), Lineation (equidistant, stereographic and orthographic) and equal area circular chart of diorite

Table 4.8Anisotropy of magnetic susceptibility of Diorite

Location	N	K(10^{-6} SI)	D1	L1	D3	I3	P	T
1	9	6641	205	10.3	93.6	62.8	1.085	0.15
2	7	4467	353.5	6.3	101.7	70.6	1.072	-0.18

N- No. of samples, K-Mean bulk susceptibility, D1 maximum magnetic susceptibility direction, L1 maximum linear degree of magnetic anisotropy, L3 minimum linear degree of magnetic anisotropy, P Intensity of magnetic anisotropy, T Shape parameter of magnetic anisotropy

Table 4.11 and appendix 1 showed granite representative samples (CO7E, CO7IW, CO7I) from Ejigbo, Iwaraja and Ilesha, which have lowest and maximum mean bulk susceptibility (Km) values of 247 and 12856; the shape parameter (T) have range of values from 0.3 to -0.35 indicating prolate and oblate ellipsoid. Intensity parameter (P) have range of values from 1.3 – 2.0 (Fig. 4.22 c-d). The azimuth/plunge of foliation and lineation values ranges from 6 - 350 and 29 - 78 as well as 223 - 247 and 5 - 24 respectively. This suggested that granite was trending NNE-SSW and NNW-SSE (Fig. 4.22) and intensity parameter (P) have range of values from 1.3 – 2.0 (Appendix 2).

Banded gneiss representative samples (CO8A and CO8I) from Akungba-Akoko and Ikare-Akoko, having lowest and maximum mean bulk susceptibility (Km) values ranges from 20.4 to 39.4; the shape parameter (T) have range of values from -0.72 to 0.7 indicating prolate and oblate ellipsoid (Table 4.13 and Fig. 4.21). The foliation and lineation ranges from 84 - 205 and 1 - 68 as well as 5 - 361 and 15 - 80 respectively. This imply the banded gneiss was trending NNE-SSW and NNW-SSE (Fig. 4.21) and intensity parameter (P) have range of values from 7.5 - 17.6 (Appendix 2).

Table 4.9Anisotropy of magnetic susceptibility of Granite gneiss

Location	N	K(10^{-6} SI)	D1	L1	D3	L3	P	T
1	6	1632	335	4.9	65.6	11.3	1.11	0.06
2	8	2823	14.3	62.5	275	5.2	1.158	-0.32
3	8	21629	356	9.4	261	29.4	1.158	0.33
4	7	26921	343	8.3	107.8	5.6	1.076	0.75
5	8	13480	201	22.3	105.7	11.5	1.102	-0.09
6	6	16017	218	1.4	122.8	73.1	1.035	0.46
7	6	16005	258	0.2	167.1	13.9	1.062	0.26
8	6	15460	258.2	42.2	135.8	30.4	1.066	0.04
9	7	15269	314	57.6	127.8	32.3	1.066	0.41
10	6	18238	164	36.6	93.7	53	1.052	0.41

N- No. of samples, K-Mean bulk susceptibility, D1- maximum magnetic susceptibility direction, L1- maximum linear degree of magnetic anisotropy, L3- minimum linear degree of magnetic anisotropy, D3- minimum magnetic susceptibility direction, P- Intensity of magnetic anisotropy, T -Shape parameter of magnetic anisotropy

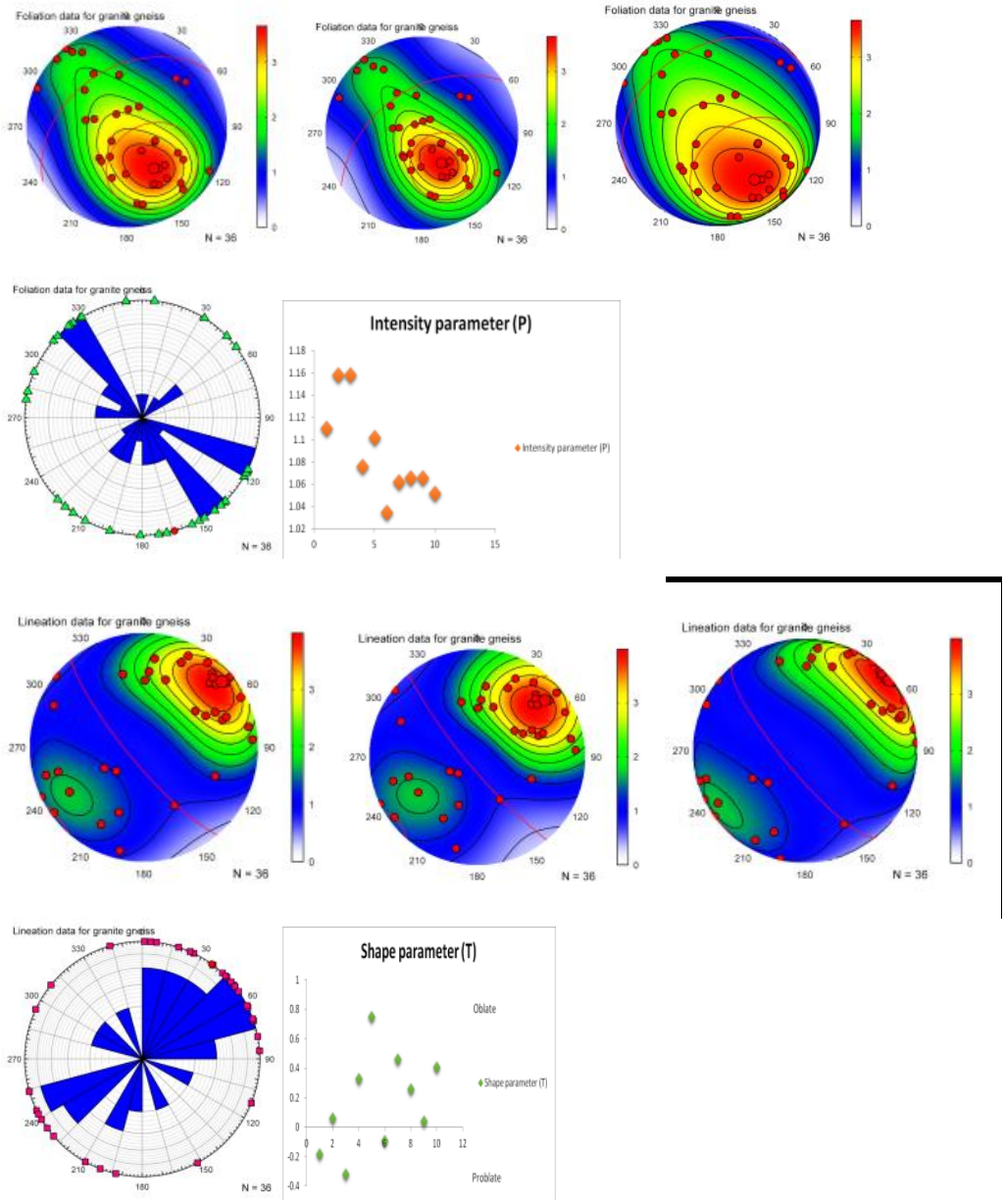

Fig. 4.18. Foliation (equidistant, stereographic and equal area), Lineation (equidistant, stereographic and orthographic) and equal area circular chart of Granite gneiss

Table 4.11 and appendix 1 show granite representative samples (CO7E, CO7IW, CO7I) from Ejigbo, Iwaraja and Ilesha, which have lowest and maximum mean bulk susceptibility (Km) values of 247 and 12856; the shape parameter (T) have range of values from 0.3 to -0.35 indicating prolate and oblate ellipsoid. Intensity parameter (P) have range of values from 1.3 – 2.0 (Fig. 4.22 c-d). The azimuth/plunge of foliation and lineation values ranges from 6 - 350 and 29 - 78 as well as 223 - 247 and 5 - 24 respectively. This suggested that granite was trending NNE-SSW and NNW-SSE (Appndix 1) and intensity parameter (P) have range of values from 1.3 – 2.0 (Appendix 2).

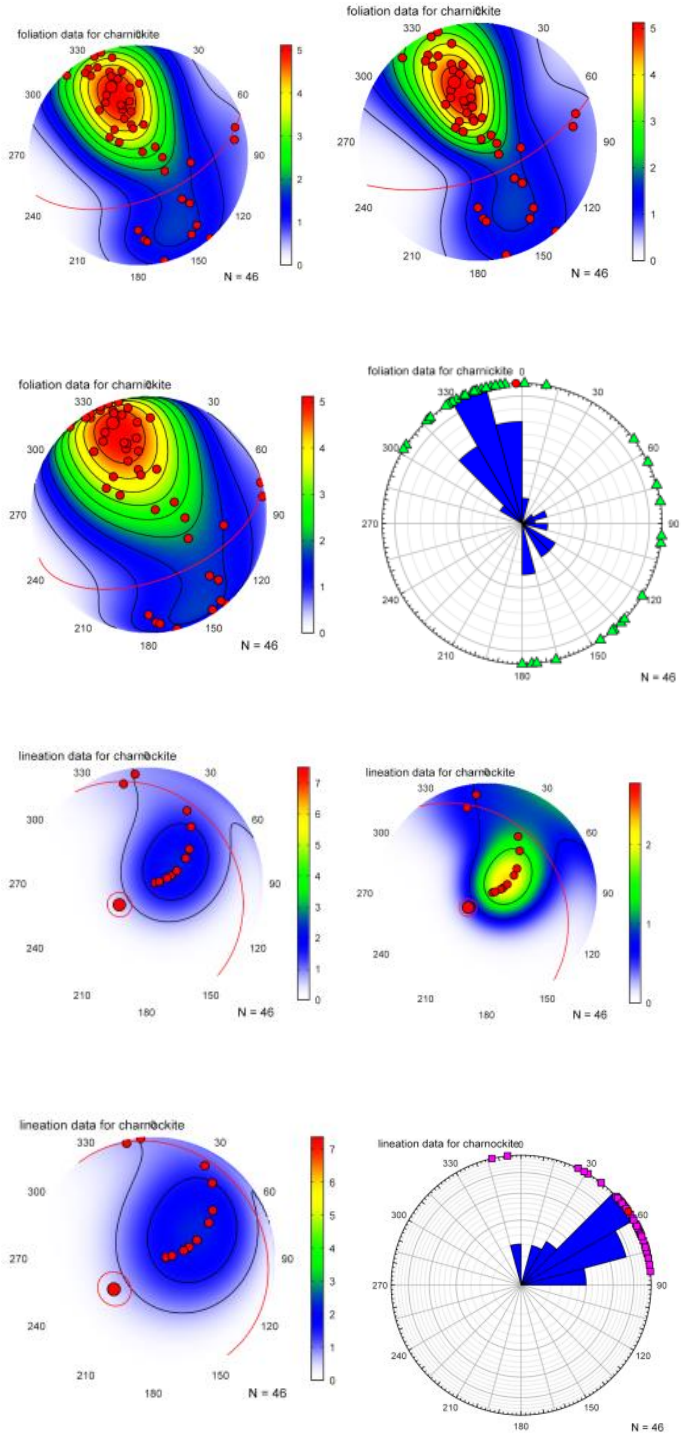

Fig 4.19. Foliation (equidistant, stereographic and equal area), Lineation (equidistant, stereographic and orthographic) and equal area circular chart of Charnockite

Table 4.10a.Anisotropy of magnetic susceptibility of Charnockites

K(10^{-6}SI)	KI	K2	K3	P	L	F	T	K1 /Azimuth/plunge		K3 /Azimuth/plunge	
29167	35243	28982	23277	1.51	1.2	1.25	0.06	228	16	318	3
54990	69261	52836	42872	1.62	1.3	1.23	-0.13	229	21	139	0
26717	31772	26389	21991	1.44	1.2	1.2	-0.01	211	25	341	54
17644	20710	16824	15399	1.34	1.2	1.09	-0.4	206	14	98	50
53119	63163	54273	41921	1.51	1.2	1.29	0.26	246	6	343	51
50863	63256	50268	39065	1.62	1.3	1.29	0.05	230	34	353	38
32900	40911	29944	27846	1.47	1.4	1.08	-0.62	232	4	53	86
28845	34710	28411	23415	1.48	1.2	1.21	-0.51	234	9	121	67
25072	30202	23437	21576	1.4	1.3	1.09	-0.27	51	2	317	64
25745	31680	24491	21091	1.5	1.3	1.16	0.23	57	7	304	73
20637	23844	20965	17102	1.39	1.1	1.23	-0.12	218	15	347	67
14750	18193	14274	11784	1.54	1.3	1.21	0	227	12	95	72
17850	21058	17660	14833	1.42	1.2	1.19	-0.5	227	14	64	76
10059	12252	7367	8558	1.43	1.3	1.09	-0.61	245	5	349	70
15192	18884	13846	12847	1.47	1.4	1.08	-0.01	247	4	341	50
36109	40357	35913	32058	1.26	1.1	1.12	-0.93	38	3	302	65
34133	39428	31604	31366	1.26	1.3	1.01	0.3	233	18	329	17
18948	21668	19391	15786	1.37	1.1	1.23	-0.02	230	6	135	43
53345	59342	53069	47621	1.25	1.4	1.11	-0.07	29	19	133	36
55473	71781	53340	41299	1.74	1.3	1.29	-0.42	228	18	332	38
31448	39101	29252	25991	1.5	1.2	1.13	-0.06	84	5	176	24
25163	30283	24659	20546	1.47	1.3	1.2	0.19	235	16	140	18
29131	36900	29423	21070	1.75	1.2	1.4	-0.08	242	15	335	13
12484	14623	12265	10564	1.38	1.2	1.16	-0.16	237	14	330	10
33040	39395	32071	27653	1.42	1.2	1.16	0.05	73	25	180	32
10584	12764	10515	8473	1.51	1.2	1.24	0.05	72	27	174	22
20657	24250	20576	17144	1.41	1.2	1.2	0.09	231	7	328	43
16541	19994	16497	13132	1.52	1.2	1.26	-0.01	228	11	339	61
27108	31287	26890	23148	1.35	1.1	1.16	-0.05	51	2	319	45
39689	46840	39067	33160	1.41	1.3	1.18	-0.22	239	18	351	49
21314	23734	20917	19292	1.23	1.2	1.08	-0.27	254	23	1	35
13944	16552	13063	12217	1.29	1.3	1.07	-0.36	256	17	166	1
19223	21943	18681	17044	1.41	1.2	1.1	-0.28	243	18	341	21
13112	15684	12463	11188	1.34	1.4	1.11	-0.74	250	5	340	1
16377	19069	15825	14237	1.41	1.3	1.11	-0.54	75	3	345	9
38889	47450	35297	33741	1.45	1.2	1.05	0.07	244	15	341	25

Table 4.10b.Anisotropy of magnetic susceptibility of Charnockites continued

K(10^{-6}SI)	KI	K2	K3	P	L	F	T	K1 /Azimuth/plunge		K3 /Azimuth/plunge	
35922	39714	47440	28782	1.25	1.1	1.08	0.32	240	15	146	14
46152	41450	24656	30428	1.41	1.3	1.18	-0.33	67	4	336	2
26216	53511	23651	37504	1.38	1.1	1.26	0.3	234	13	327	12
23059	32520	31891	21474	1.36	1.1	1.45	-0.15	167	17	74	9
32399	26930	16438	18596	1.43	1.1	1.27	0.06	174	14	81	12
16483	19337	21990	28974	1.51	1.1	1.1	0.57	243	11	340	34
21013	23329	18867	13674	1.41	1.2	1.2	-0.98	258	9	10	67
21743	27551	47032	17720	1.06	1.2	0.57	-0.06	81	11	345	29
56417	66779	21433	18810	1.46	1.5	1	0.01	248	9	351	57

K-Mean bulk susceptibility, K1 maximum magnetic susceptibility direction, K2intermediate magnetic susceptibility, K3minimum magnetic susceptibility, P Intensity of magnetic anisotropy, L Linear degree of magnetic anisotropy, F Planar degree of magnetic anisotropy

Banded gneiss representative samples (CO8A and CO8I) from Akungba-Akoko and Ikare-Akoko, having lowest and maximum mean bulk susceptibility (Km) values ranges from 20.4 to 39.4; the shape parameter (T) have range of values from -0.72 to 0.7 indicating prolate and oblate ellipsoid (Table 4.13 and Fig. 4.21). The foliation and lineation ranges from 84 - 205 and 1 - 68 as well as 5 - 361 and 15 - 80 respectively. This imply the banded gneiss was trending NNE-SSW and NNW-SSE (Fig. 4.21) and intensity parameter (P) have range of values from 7.5 - 17.6 (Appendix 2).

Therefore, the evolution of granitoids was caused by amalgamation of pure and simple shearing; resulting to synchronous emplacement of D_2 tectono-metamorphism (Tables 4.5 - 4.12). The Pan- African granites demonstrated dextral S-type potassic-feldspar porphyries and megacrysts (Figs. 4.18-4.20), suggestive of sinistral r-type cycle of megacrysts and porphyries for the period of dextral shearing (Njonfang *et al*., 2008). The witnessed sheared planes recorded the orientation of the primary stress r_1= N92E; since $r_1$persists for the period D2 and D3 deformations. The reopening of dextral D3 tectonism is of isochron age of 564 and 558 Ma or <572 Ma (Njonfang *et al*., 2008; Salminen *et al*., 2019). Similar age was given in Pan-African granites evidenced with the mylonitisation.

Table 4.11 Anisotropy of magnetic susceptibility of Granite

K(10^{-6}SI)	KI	K2	K3	P	L	F	T	K1	Azimuth/ plunge	K3	Azimuth/ plunge
9143	10826	9033	7569	1.4	1	1.19	0	247	6	350	64
7673	8621	7752	6646	1.3	1	1.17	0.18	246	5	345	60
8294	9449	8253	7180	1.3	1	1.15	0.01	232	23	335	29
12856	14408	13192	10970	1.3	1	1.2	0.35	227	24	337	37
247	5974	4310	3208	1.9	1	1.34	-0.1	246	10	102	78
7171	10019	6565	42929	2	2	1.33	-0.2	242	13	116	68
12057	15867	11383	8921	1.8	1	1.28	-0.2	230	9	96	77
8731	11203	8123	6886	1.6	1	1.18	-0.3	223	14	6	73

K-Mean bulk susceptibility, K1 maximum magnetic susceptibility direction, K2 intermediate magnetic susceptibility, K3 minimum magnetic susceptibility, P Intensity of magnetic anisotropy, L Linear degree of magnetic anisotropy, F Planar degree of magnetic anisotropy

Sheared zones and foliations; subhorizontal lineations and triaxial orientations are parallel prolate ellipsoids defined by AMS. Subhorizontal lineations and triaxial formation was as a results of strike-slip and compressional system (Kwekam *et al.*, 2010), leading to moderate NE-SW lineation and their respective foliations directions. Mylonitisation in NW-SE margins of the IISZ, dips and steeps the charnockites and the Pan-African (Older) granites to same orientation. Thus, a marginal orogenic, compressional low-angle fold-and-thrust belt and an interior belt regulated by transpressive high-angle faults flank the transition zone between the charnockites and the Older granites. (Kwekam *et al.*, 2010). The introduction of intrusives, post collisonal granitoid motions, and metacratonic evolution and cratonic boundary around Congo craton, which is related to southwestern Nigerian Precambrian rocks, were suggested by Kwekam *et al.* (2010) and Liegeois *et al.*, (2003) models.

Table 4.12 Anisotropy of magnetic susceptibility of Banded gneiss

N	Km(10^{-6}SI)	KID*	KKII*	K3D*	K3I*	E12	E23	E31	P%	L%	F%
4	25	323	33	195	44	55.4	15	12.7	7.5	1.2	6.3
5	39.4	339	47	172	43	38.5	14.9	11.2	12.5	2.8	9.4
4	29.7	5	33	194	57	37.4	16.9	12.2	9.6	2.7	7.1
4	25.6	296	25	189	33	37.3	22.8	15.3	10.1	3.4	6.5
4	26	337	42	205	36	32.9	32.9	19.2	12.4	6.4	5.6
4	24.8	351	29	91	16	19.7	19.7	16	11.2	8.5	2.4
4	24.2	196	15	84	54	40.9	40.9	11.9	17.6	3.7	13
4	31.2	267	80	165	1	26.1	26.1	13.5	14.8	6.8	7.6
4	20.4	35	21	190	68	11.9	11.9	10.2	10.7	8.9	1.5

Km-Mean bulk susceptibility, KID* maximum magnetic susceptibility direction, KKII*intermediate magnetic susceptibility, K3D*minimum magnetic susceptibility, K3I*maximum magnetic susceptibility magnitude, E12 intermediate magnetic susceptibility, E23 minimum magnetic susceptibility direction, E31minimum magnetic susceptibility direction, P% Intensity of magnetic anisotropy, L% Linear degree of magnetic anisotropy, F% Planar degree of magnetic anisotropy

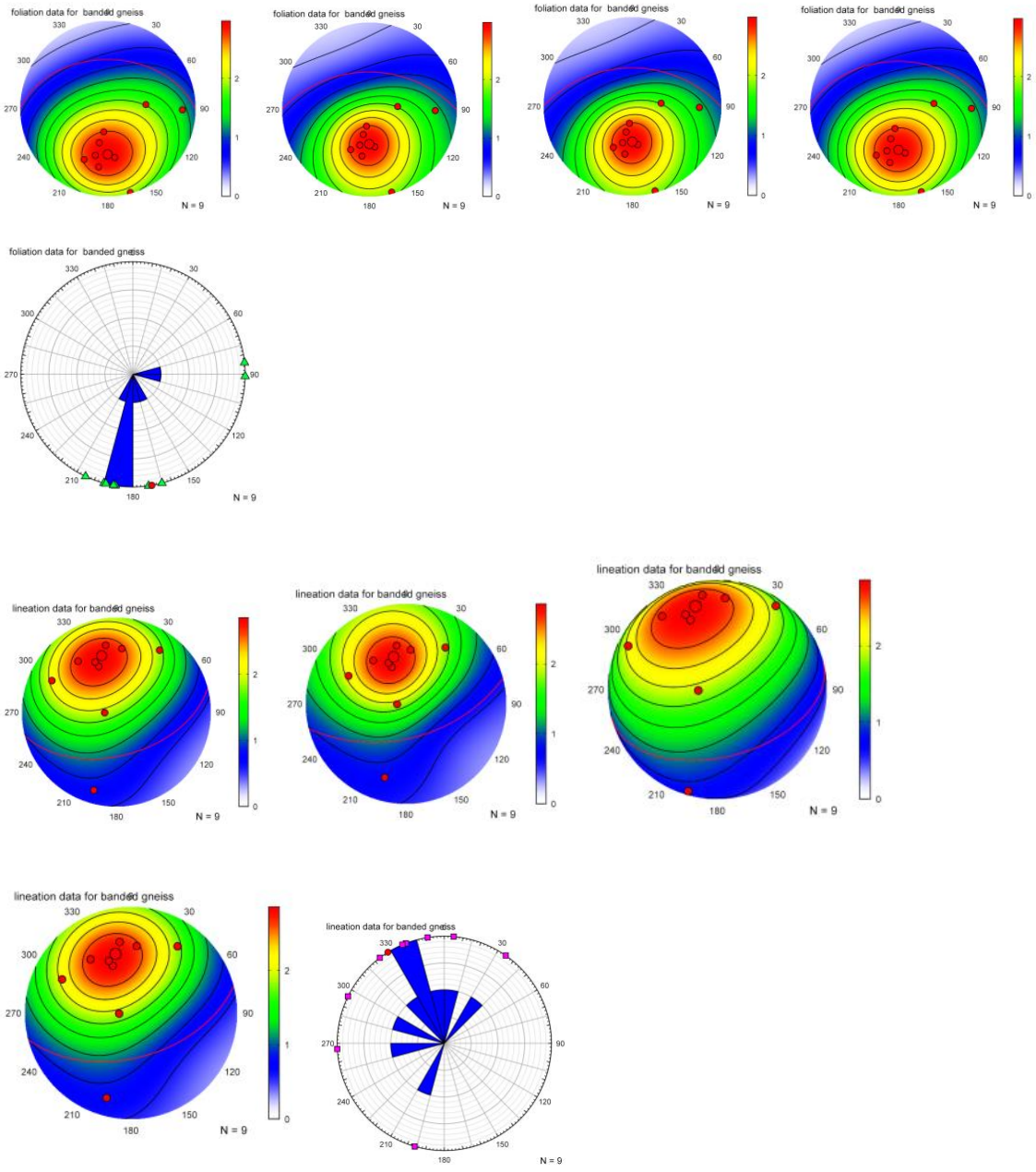

Fig. 4.20. Foliation (equidistant, stereographic, orthographic and equal area), Lineation (equidistant, stereographic and orthographic) and equal area circular histogram of Banded gneiss

4.3.1 Evolution of the tectono-metamorphic rocks and Implications for emplacement of the plutons

Due to sinistral (left-sided) pull-apart motion, the plutonic rocks emplacement (intrusion of igneous rock) was caused by the activation of pull-apart basin that dips to the shear zone. The syn-kinematic (geologic process occurring tectonic activity) emplacement of the charnockite-granitoids sinistral pull movement led to opening up of fractures in the Precambrian basement complex of Nigeria. This synchronous emplacement of the plutons in the southwestern Nigeria was around 600 and 613 Ma which typifies D2 pull movement (Toteu *et al.*, 2001; Ngako and Njonfang, 2011; Kwekam *et al.*,2010).

The indent related shear zone determines a post-deformational diverging grid system with a variable shaped E-W belt model. Deformation of the Dahomeyan-Pharusian belt documented initial medium pressure-low temperature (MP-LT) and medium pressure-high temperature (MP–HT) metamorphism between 650-625Ma (Rahaman, 1988) U-Pb ages of gneiss and granite gneiss, and is analogous to syn-deformation evolution of the NW Cameroon, whereas the suture zone demonstrated nappe (large-scale recumbent folds, fault plane shearing and imbricate thrust stacks). Therefore, leading to over-thrusting of MP-LT and MP-HT greenschist-amphibolites (Fig. 4.21) into the San-Francisco Congo craton (SFCC). The extreme conditions of clayey rocks (as lubricants) reduce frictional resistance and high pressure fluids acting on lithostatic pressures thus permitting fracturation and ultramylonites/cataclasites. Thrust sheets of the orogenic wedge was hinged on gravitational sliding which resulted to formation of oblique-slip, compressive forces, shortening of the basement. Basement and superficial nappes forms thick- thin skinned styles and large scale overthrust. The duplexes of nappe are characterized with the suturing of the several folds, thrust fault and underthrust around tectonic units.

The model suggested three-plate deformations affecting: the SFCC, the eastern Saharan block (ESB), and the western African craton (Fig. 4.22 a-d) (Trans-Saharan-Central African/CAFB and Brasiliano western Gondwana belts). The ESB and the northern boundary of the SFCC, previously classified as a basin and range block, became

deformed in the N-S. (for the period of back arc extension to subduction, Fig. 4.22a). Following the Saharan rigid prong penetration to the SFCC active boundary about 640 and 580 Ma, this deformation resulted in strike-slip tectonics (Fig. 4.22b) and violent collisions within Cameroon and north-western blocks. The tectono-metamorphic episodes documented in this active domain are: i) thickening of the crust ii) coupled strike-slip-lateral wrench movements (indent), and iii) $N70^0$ to EW oriented sinistral-lateral wrench movements. The structural dynamics demonstrated deformation of active Trans-Saharan and West African cratons at isochron age of 630 Ma, whereas SW and SE Nigeria basement complex were dominantly oriented by NE-SW stress up to 590 Ma. There are records of NW-SE regional clockwise rotation signifying late tectono-metamorphism that constrained predominantly by West African Craton (WAC).

The strike-slip tectonics occurred due to the following reasons: (1) inflexible indenter stronger than indented margin. Subduction through intense seismicity and volcanism permits the proposed rheological phase and active margins that are weaker than passive margins; (2) due to a volume constraint, the denser lithospheric mantle was removed from the indenter to allow penetration into the opposite margin. Furthermore, indenter penetration caused local delamination by inducing differential shortening of the lithospheric mantle (light and deformable) and lithospheric mantle (inflexible and denser) in the indented plate (Fig. 4.22b, c, d). These fundamental tectono-metamorphisms indicated that the asthenosphere vast masses, rather than the crust, were likely to ascend, causing large-scale melting at the front of the merging plates. Batholith intrusions cause these abundant crustal melting processes and partial dismemberment of the colliding plates in southwestern-southeastern Nigeria may explain intense reactivation and partial melting. Only the most extreme metamorphic isograds resulted in partial rock melting, indicating both powerful and widespread phenomena as well as low severity and geographic zoning. Currently, these areas typically showed a Pan-African imprint and the crustal evolutions that go with it.

Between 591 and 576 Ma, the Borborema domain of NE Brazil witnessed various stretched plutons is constrained by active deformation within dextral transcurent shear

zones in the NE-SW, NNE-SSW, and N-S directions, showing their syn-kinematic emplacement(Neves and Mariano, 1999). The emplacement of plutons in early sinistral and late dextral kinematic conjugate settings in Cameroon, SE Nigeria, and NE Brazil corresponds to Ngako and Njonfang's (2011) Pan-African tectonism in Western Gondwana.

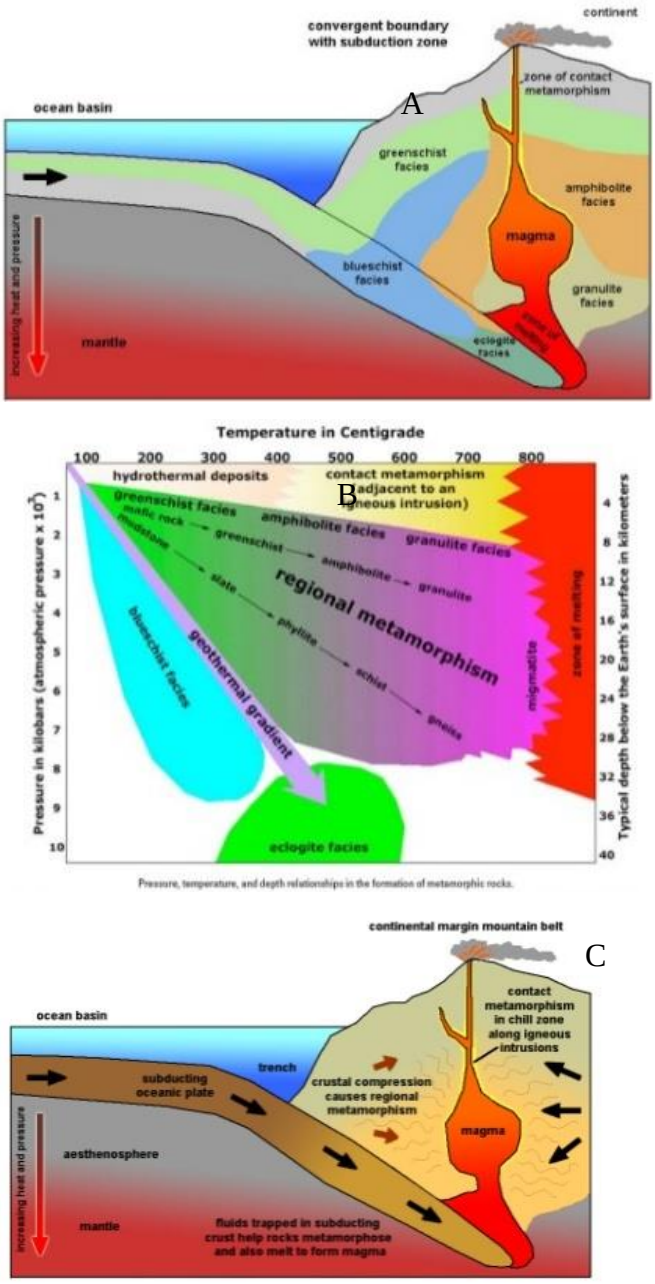

Fig. 4.21. (A) Model showing tectono-regional metamorphism relationship: ridges and rift valleys- described by intense geothermal gradients contact and metamorphosed ocean floor. (B - C) Regions of magmatic movement; volcanic - plutonic complexes: greenschists amphibolites granulites. Regions of thickening of the crust and orogeny: greenschists amphibolites (MP+LT and MP+HT) granulites (HP+HT) and type B eclogites. Modified after: http://www.geologyin.com/2016/01/ html

The results show that regional synkinematic location of granite plutons is restricted by NE-SW active shear zones that run from west to east Cameroon, SW to SE Nigeria, and Borborema, and is Pan-African.

The following are the tectono-metamorphic history of the Ifewara-Ilesha schist belt
Tectonic, magmatic and sedimentary episodes

A.1.Subduction and back-arc extension

A.2. Active margin volcanism IISZ

A.3.Volcanic sediments (metasediments)

A.4. Regional basic to intermediate plutonic suite dominates syn-tectonic plutonism. (0.600-0.630Ga)

B.1.Horizontal shortening (F2 upright to recline), thrusting and exhumation of Ilesha-Ifewara Mylonite and ultramylonites segments derived from mid-mantle along deep listric faults (pure and simple shear deformation). Retrogression of the Ilesha-Ifewara MP-LT and MP-HT and extensive migmatization.

B.2.Increasing delamination of lithospheric mantle and uprise of hot asthenosphere versus the collisional orogens of crust.

C 1. Orogenic collision between ESB prong and the SFCC; crust redoubling/flat lying S1 foliation.

C.2. Burial and metamorphism of SW granitoids (MP-LT and MP-HT) greenschist amphibolites facies (footwall).

C.3. Retrogression (Paleoproterozoic) trench-related greenschist amphibolites facies (hanging wall).

C.4. Early phases of delamination of the lithospheric mantle.

D.1. Wrench movements following prong, pull-apart basin.

D.2. Advanced delamination and lithosphere mantle owing to indentation

D.3. Extensive melting and granitization of crust causing break-up of the ESB, the active margin reactivated Pan African structures (D4 or D3) dextral shear along IIFZ.

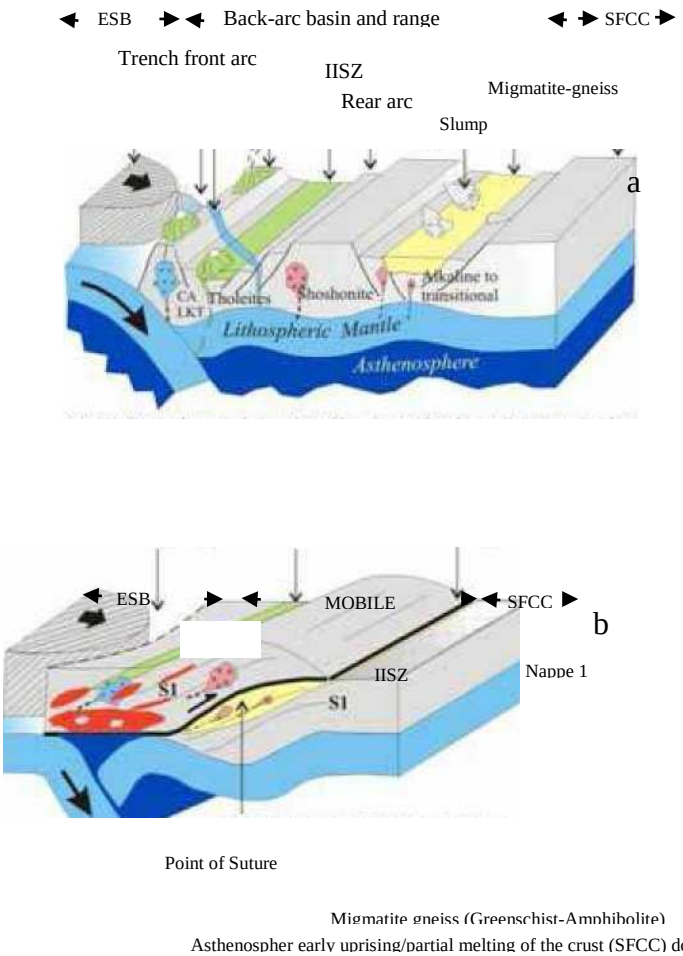

Fig. 4.22. (a) Pre-orogenic setting: subduction/back-arc basin (1 - 0.640Ga),(b) Phase D1: crustal redoubling and thickening-early thrusting/nappe 1 (0.640 - 0.630Ga) (Modified after, Ngako and Njonfang, 2011)

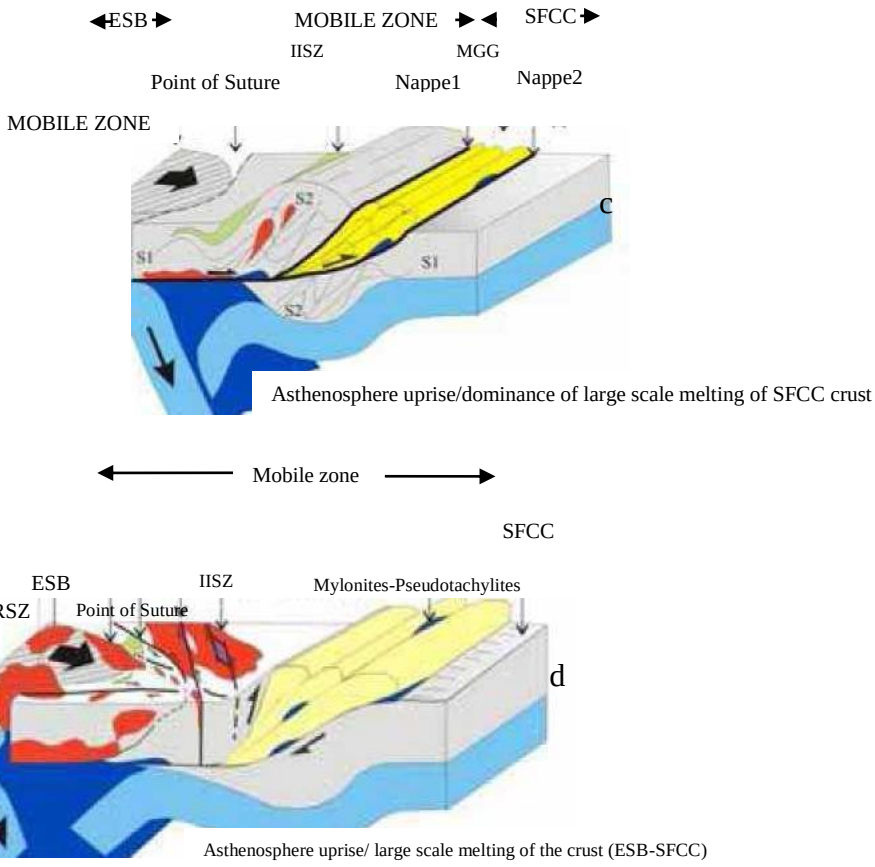

Fig. 4.22. (c) Phase D2: Crustal shortening and thickening-upright to recline fold/Nappe 2 (0.600Ga), (d) Phase D: Conjugate wrench movement at the prong front (0.585 - 0.580 Ga) (Modified after, Ngako and Njonfang, 2011)

4.4 PALEOGEOGRAPHIC RECONSTRUCTION USING PALAEOMAGNETIC RESULTS

4.4.1 Alternating field and thermal demagnetizations

The alternating field demagnetization of rock specimens yielded Median Destructive Field (MDF) result varying from 110-480 mT. The granitoids demonstrate minor transformation in the direction of NRM and fast decline in intensity for the period of lower steps of demagnetization followed by a stable remanence at higher levels of demagnetization. Low MDFs and unstable NRMs characterised the measured samples. The non-stability of secondary magnetization was witnessed in Fe-Ti oxide granitoids (Appendix 3) where the planes are close to the stable magnetization. Zijderveld,(1967) vector plots of AF and thermal demagnetization data show a wide range of behavior. Decay toward the origin with AF demagnetization was observed for many samples, but in some specimens, few modifications or a trend away from the origin occurs with AF or thermal demagnetization until temperatures >500 °C are peaked. Some specimen with higher MDF values always possess smaller modified angles in the NRM and large coercivity. The oxidation of pyroxene and plagioclase minerals in the measured rock in the course of the deformation process contributes to the formation and magnetization of secondary minerals. Few samples from thermally demagnetized specimen with Fe-Ti-oxide minerals demonstrate stable intensity and inclination up to 600°C. It thus reveals reliable NRM components representing high blocking temperature magnetic minerals of 560 °C to 580°C such as magnetite.

4.4.1.1 Occurrence of Exsolved Maghemite in whole rock Analysis

Results exhibited preliminary records of exsolved maghemite in silicate, plagioclase and pyroxene minerals in the southwestern Nigeria Precambrian gneiss and granitoids. These iron oxides are seen in the pyroxene and plagioclase minerals showing good magnetic stability (Fig. 4.23a, b and c). Thus, accomplishing the prerequisite of a reliable recorder of the old geomagnetic fields.

The laboratory measurement of one hundred and ten sites, mean declination and inclination generated largely remagnetised and few magnetically stable, reliable and

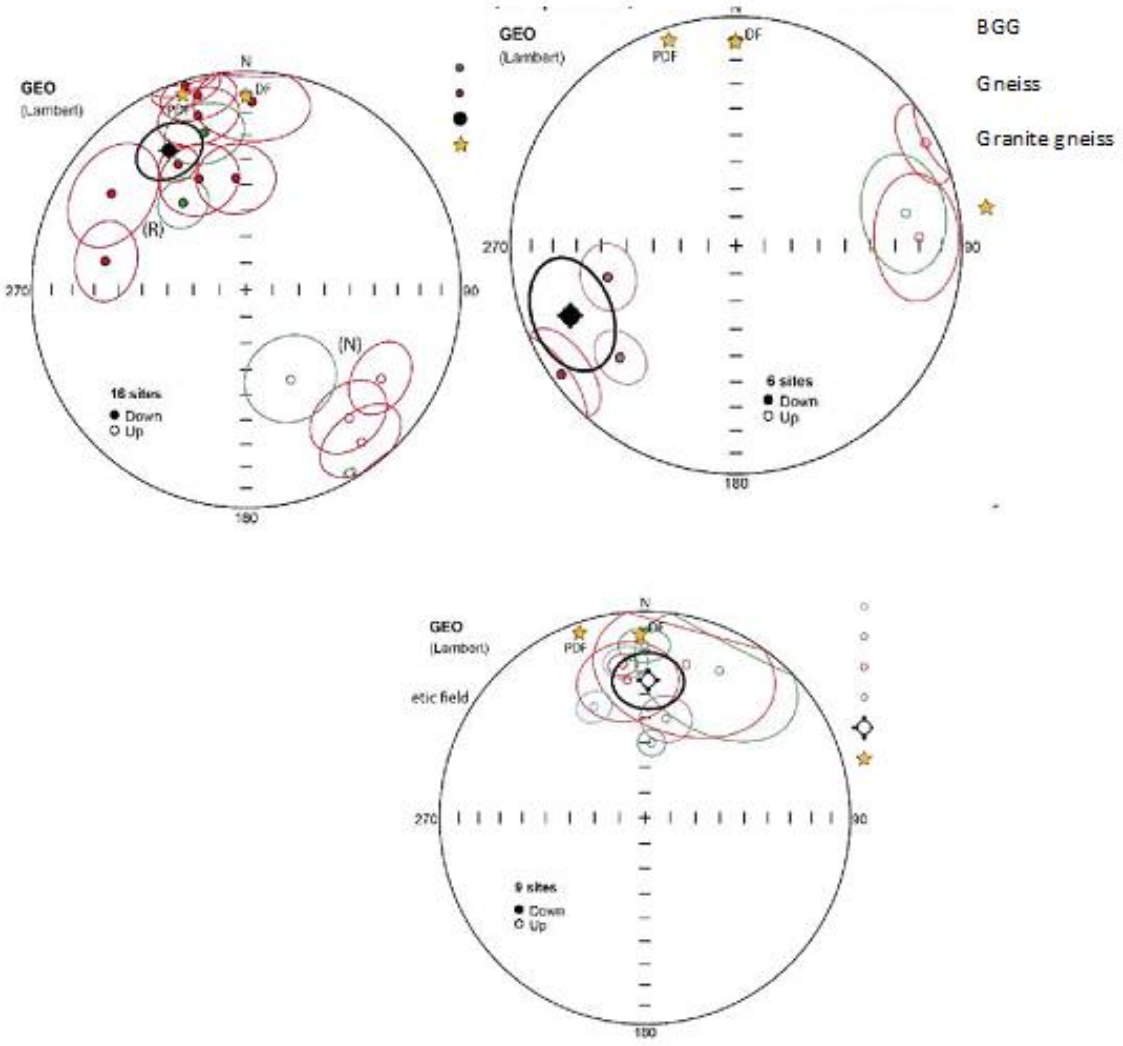

Fig. 4.23. Site mean directions of biotite granite gneiss (green colour), gneiss (red colour) and granite gneiss (black colour).

relatively coherent result respectively. Majority of the rock specimens used for paleomagnetic and Rock magnetic studies were discarded in most of the sites due to their magnetic instability and incoherency in the treated specimens.This is due to their probable secondary overprints on the rock specimen due remagnetization of the Southwestern Precambrian Basement rocks. Thus, further study treatments were carried out on the sites that demonstrated stability in their rock magnetic and paleomagnetic characters. On a stereographic projection, the results of alternating field and thermal demagnetization treatments from southwestern Nigerian Paleoproterozoic/Neoproterozoic rocks with paleomagnetically positive sites (Fig. 4.23) showed their mean declination and inclination directions, as well as their respective statistical parameters (Tables 4.13 and 4.14). Granitic rocks from all over Africa are graded as having a northwesterly declination and a relatively steep inclination (NW NRM). The W remanence was recognised as a predominant paleomagnetic orientation of the Precambrian period for the southwestern Nigeria granitoid rocks, while the northwest direction refers to the tilt-corrected paleomagnetic direction of 650 ±150 Ma. The west NRM direction witnessed the corrected tilt directions of Pan African rocks distributed in southwestern Nigeria. The northwesterly NRM was obtained during secondary remanent magnetization.Two of the sites are NW remanence rocks created by W remanence, while the others are NW remanence rocks. The rock specimens (granitoids) from these sites belong to Paleoproterozoic (Eburnean) and Neoproterozoic (Pan-African) (Table 4.15 and the references).

Table 4.13.Alternating field demagnetization results

Site	coordinates	PCA	VGP Lat	VGP long	Paleolatitude	Age(Ma)	N	Dec	Inc	α95	dp	dm
1	7.35N 4.43.5E	Anchored NRM to 40mT	47.3	93.4	5.9	600±150	6	43	12	0.8	0.4	1
3	7.24N 5E	Anchored 40mT to 100mT	-36	45.5	32.6	600±150	5	141	52	1.2	1.1	2
6	8.17.5N 4.21E	Anchored NRM to 15mT	41.2	295	-21	600±150	4	131	-38	1.6	1.1	2
7	7.43.7N 4.57E	Anchored NRM to 30mT	45	318	-34.6	600±150	6	141	-54	0.4	1.6	2
11	7.133N 5.13.7E	Anchored 40mTto 100mT	25.4	289	-15.5	600±150	7	115	-29	0.2	0.1	0
16	7.25.6N 4.15E	Anchored NRM to 100mT	-38	86.4	1.6	600±150	8	128	3.2	0.1	0.1	0
21	7.27N 3.55E	Anchored NRM to 100mT	-62	296	-3.9	600±150	7	26	-7.8	0.8	0.4	1

Table 4.14.Thermal demagnetization results

Site	Coordinates	PCA	VGP lat	VGP Long	Paleol atitude	Age (Ma)	N	Dec	Inc	α95	dp	dm
7	7.43.7N 4.57E	Anchored 40mT to 57mT	0.9	86.4	-8.2	600±150	7	-90	-16	1.1	0.6	1
8	7.38N 5.57E	Anchored 40mT to 57mT	-33	75.5	-12.6	600±150	6	-54	-24	1.9	1.1	2
13	7.36.5N 3.27E	Anchored 30mT to 57mT	158	-21	-10.8	600±150	5	158	-21	0	0	0
15	7.37N 4.49.5E	Anchored 30mT to 57mT	46.8	-23	-11.9	600±150	6	47	-23	0.5	0.3	1
19	7.23N 3.43E	Anchored NRM to 50mT	42.1	28.6	15.2	600±150	7	42	29	0	0	0

Plotted in Figure 4.23 are the reversed, normal and mixed site mean directions for the Pan African orogenies (Paleoproterozoic to Neoproterozoic). African paleomagnetic pole location (120.6, *0* = 47.1, Tables 4.13 and 4.14) calculated from the rock specimen data as reported by Van der Voo, (1990). The field direction during this time varied only slightly. During magnetization and remagnetization of the SW Nigeria granitoids, the magnetic field directions were slightly different from the documented Mid to Late Paleozoic direction. Principal component analysis (PCA) were done to get the best fitted line after the demagnetizations of sites 1,3,6,7,11,16, 21 as well as 7,8,13, 15. As a result, mean directions of site 13 from the southwestern Nigeria granitoids largely exhibit fair precision (κ> 5.0).

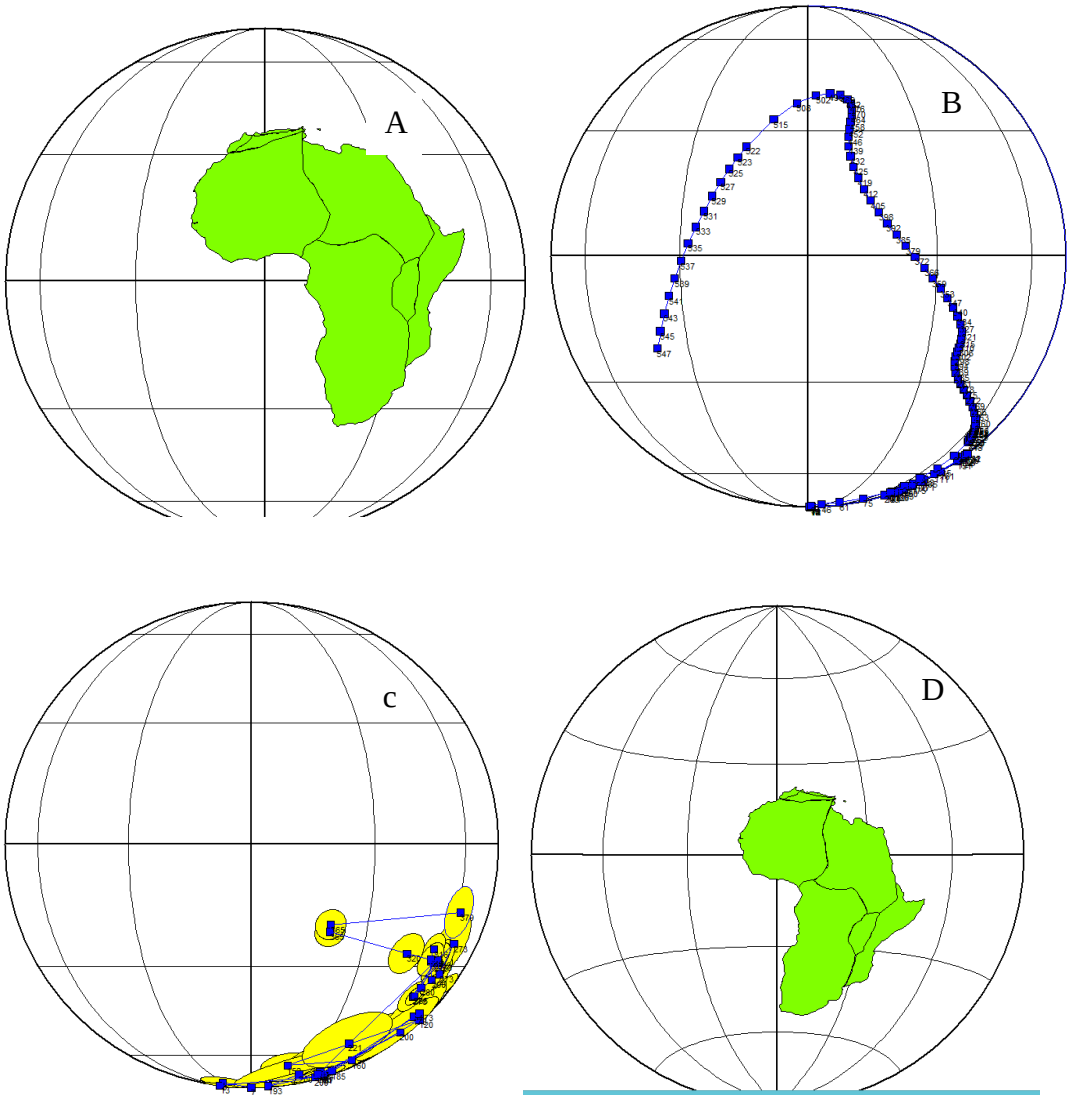

Fig. 4.24. (A) African craton displayed in present position. (B)Spline Apparent pole wandering APW of Africa pole, (c)VGP reconstruction of Africa database (D)fit (lat=0.0, long=151.60, angle=27.50) with Africa, taking account of the opening of the south Atlantic. (C) The 'corrected' NAM positioned according to pole 5 in VGP file \data\VGPs\Africa-NW Africa_2012

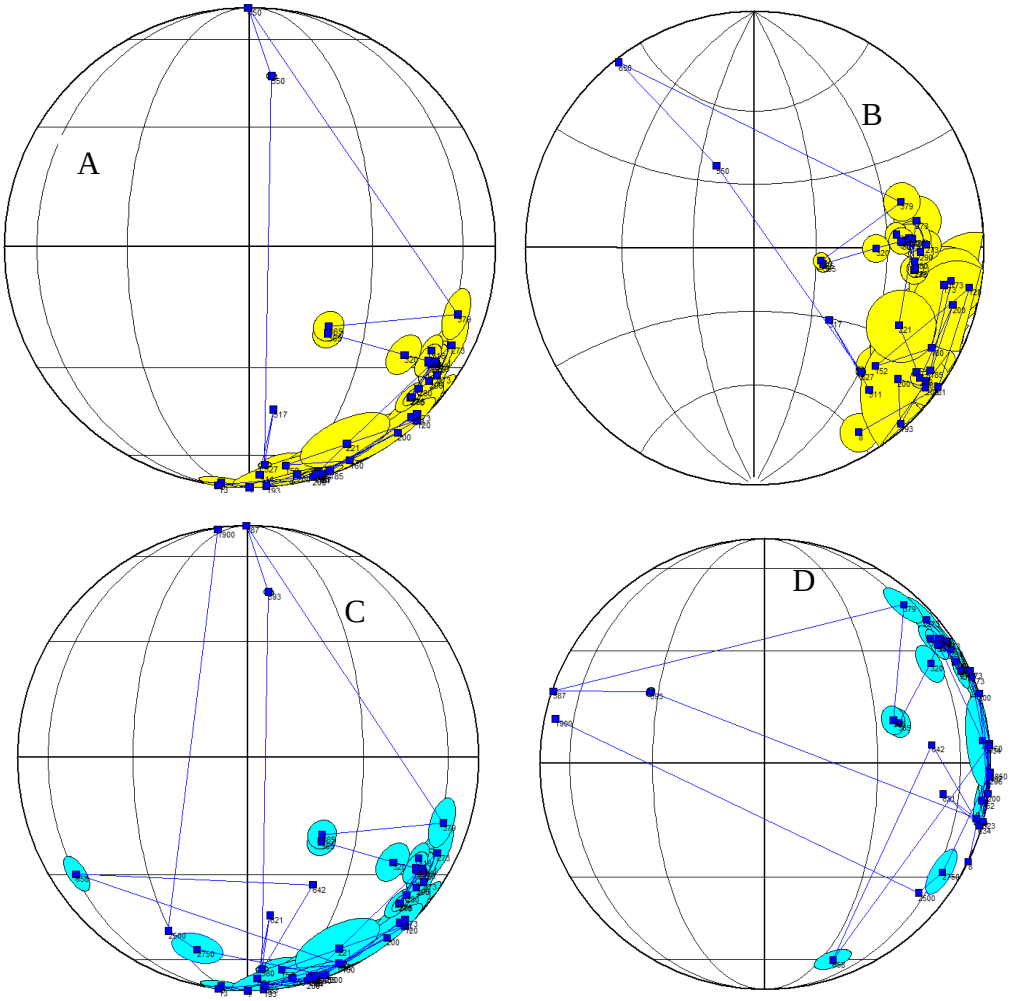

Fig. 4.25. (A) Plotted new VGP from SW Nigeria (B) Reconstructed VGP for SW Nigeria Merged with NW Africa, (c) VGPs stereogram of Southwestern Nigeria shield (d) Reconstructed to present Coordinates

Tables 4.13 and 4.14 show the calculation of virtual geographic pole (VGP), paleolatitude declination, inclination, alpha 95%, confidence dp, dm (the great circle path from site to pole and perperdicular respectively)(McElhinny and McFadden, 1990). The results revealed that the field direction during this time varied only slightly. The area has been tectonically moved as a result of post-magnetization causing the Nigerian shield magnetic direction to be deviated from an original primary direction. Corrected results (Tables 4.16 and 4.17 and Figs. 4.24- 4.25) do not improve the conformity between the African poles and the estimated pole from the Nigerian shield because of remagnetization, thus making it spurious. Evaluating root mean (RM) data from granitoid units is usually difficult since such units generally yield directions with poor RM accuracy. Further, tilt estimates can only be approximate, when distinct geological criteria demonstrate folding and faulting cannot be correlated to the unit. When evaluating the pole position for the SW Nigerian shield, errors due to (1) the large elliptical confidence was defined for the pole position, (2) recognized tilt events, and (3) the streaked great circle distribution of reversed, normal and mixed Remanent magnetization (RM) directions toward the Pan African events must be examined. Because the pole was poorly constrained, the data can accommodate several possible interpretations. First, the unit may have gained an RM orientation during long-term cooling compared to steady African cooling, and magnetic acquisition in the gneiss may have taken place over long stretches of time, during which reversals in the Earth's magnetic field direction occurred. Both polarities may have been recorded in individual sample owed to varying blocking temperatures. Perhaps, the field direction changed slightly during this period, then a deflection along a great circle toward the polarity which the earth’s field sustained for the shortest length of time, would be observed. Such a deflection, where changes in the field direction are represented by angular limits of mean directions from Van der Voo *et al.,* (1990) and percentages represent the relative time the earth’s field spent in each polarity. These results in conjunction with demagnetization data suggest that the geomagnetic field was represented by both polarities (reversed dominating) during the magnetization of the southwestern Nigeria granitoids.

The paleomagnetic results of some representative sites from southwestern Nigeria basement complex are illustrated in demagnetization behaviours (Figs. 4.26 - 4.30). There were more positive records of AF measurements than thermal measurements in treatment of secondary remanence magnetization components from most of the granitoids. Generally, most of the granitoid specimens demonstrate two components: (1) Present crust's magnetic field revealing viscous component direction at the sampling site (D = 10°, I = 74°); (2) low NNE- SSW- component direction, and/or (3) inclination oriented steeply downward and NNE-NNW declination. NNE-SSW shallow component was considered as IISZ direction (Adeoti and Okonkwo, 2017) while NNE-NE which typifies the primary magnetization and secondary remagnetization respectively (Salminen *et al*., 2018).

At least three explanations for the observed SW Nigeria paleopole position exist, these are: present position acquired magnetic remanence; NW thrust to after RM acquisition brought the SW craton to its present position, or the southwestern Nigeria acquired its magnetization and was transported to the northeast >1000 km by a left-lateral transcurrent fault system, and was later thrust to the northwest to the present location of the body.The magnetic fabric exhibited by the SW Nigeria granitoids closely approximates the mineral fabric, suggesting that both were acquired during the four deformational (D1, D2, D3 and D4) events which have affected the body. Results indicate that the RM was acquired during magnetite recrystallization or cooling from metamorphic temperatures (~600°C) to maghemite. RM acquisition in the gneiss seems to have happened over a comparatively long period of time, with reversed, mixed and normal polarities represented in the magnetic signature of the unit.

4.4.1.2 Paleomagnetic pole magnetic components

Application of AF and thermal treatments cleaned the secondary magnetization components at 8–10 mT and temperatures above 150 °C. A shallow S-SW components was acquired on sites 1,3,6,7,11,16,21 and 7, 8, 13, 15, 19 respectively (Tables 4.13 and 4.14). McFadden and McElhinny (2000) technique was used to calculate the mean direction through great circles demagnetization patterns and the sampled sites displayed preserved W-SW component directions.

After inverting site mean directions that were isolated in the other sites, Figure 4.23 revealed that S-SW lie near the NE components. The results are compared to the positive site baked reversal test (McFadden and McElhinny, 1990) parameters, which reflect normal and reverse polarities of the same averaged magnetic field. For each location, the calculated mean direction and VGPs, as well as its corresponding paleomagnetic pole for southwestern granitoids, were obtained (Tables 4.13 and 4.14). Figures 4.24 to 4.25 demonstrated the reconstructed virtual geographic poles (VGPs) stereogram of southwestern Nigeria to the present coordinates which lies close to the equator. The evident polar wandering path of Precambrian rocks in southwest Nigeria was caused by the effects of the mantle and superplumes. The acquired conjugate poles lie towards SW-NE at 304.8°E and 61.8°S directions (dp = 5.4, dm = 10.7); which was relatively at mean direction of 305.1^0E and 64.5°S (dp = 2.3, dm = 4.5).

Table 4.15 Tectono-metamorphic history of Nigerian Shield Modified after Ferre *et al*. (2002)

Collision phases	Tectono-metamorphic episodes	Radiometric dates	Tectonics/ Time	Tectonic setting	Isotherms
D_1 medium-low temps Shear zones NNE-SSW strike-slipS_4-L_4	Higher greenschist-lower amphibolite Bioti-Choritel-Muscovites within leucosomes granite pegmatite dikes	550±5Ma Argon-Argon, Amphibolite; Rubidium-Strontium, Biotite-WR; granites-migmatite gneiss	D_o 650 Ma	Initial collision Δt≈5My convergence rate ≈5cm/yr	
D_2 High temp. Shear zones N-S oblique-slip S_3-L_3	Low pressure granulite-amphibolite Biotite granite within leucosomes Hornblende biotite granites	585±10 Ma U-Pb zircon; granitoid-migmatite gneiss	D_1 640 Ma	Collision& crustal thickening Thermal rebound→pervasive melting. Energetic sink →Crust thicken. Lower crust failure→ strike-slip	
D_3 Ductile stretching facile dips S_2 N-S horizontal L_2	medium-low temps granulite Opx, mesoperthite, Sill Amp in leucosomes biotite granite, granitoid-, charnockites	615± 10 Ma U-Pb zircon; granitoid-diatexites, charnockites	D_2 615 Ma	Oblique collision& crustal thickening Thermal rebound→pervasive melting. Energetic sink →Crust thicken. Lower crust failure→ strike-slip	
D_4 Ductile flat-lying S_1 E-W horizontal L_1	High pressure granulite, Ky+Rut-Ilm-Qtz, Opx in leucosomes	640±20 Ma U-Pb zircon, fayalite-carrying monzonite	D_3 580 Ma	Oblique collision& crustal thickening	
			D_4 550 Ma	Cooling slow exhumation. Transcurrent fault	

Table 4.16 Isochron ages of Nigerian shield

LOCATION/ROCK TYPE	Ma	OROGENIC EVENTS	ISOTOPE METHOD	REFERENCES
Idanre porphyritic granite SW	587		U-Pb	1
Idanre massive charnockite SW	593		U-Pb	1
Idanre gneissic charnockite SW	580	Neoproterozoic (Pan-African)	U-Pb	1
Akure porphyritic granite SW	621		U-Pb	1
Akure gneissic charnockite SW	634		U-Pb	1
Ikerre Ekiti charnockite SW	623		U-Pb	1
Ile-Ife granite gneiss SW	1850	Paleoproterozoic	U-Pb	2
Ile-Ife grey gneiss SW	2300	Paleoproterozoic (Eburnean)	U-Pb	2
Ibadan aplite SW	2750		Rb-Sr	3
Odo-Ogun gneiss SW	2500		U-Pb	4
Igbetti augen gneiss SW	1900	Paleoproterozoic	Rb-Sr	2
GeoloGranitoids scattered around	600	Neoproterozoic	U-Pb	6
Granitoids scattered around	2000	Paleoproterozoic	U-Pb	6
Granodiorite scholllen	2153±6.5	Paleoproterozoic (Eburnean)	U-Pb	5
Granulitic mylonitic granodioritic orthogneiss	2095±14		U-Pb	5
Patchy graniodioritic migmatite	655.7±8.2		U-Pb	5
Felsic dyke	572.4±8.1		U-Pb	5
Hornblende biotite mafic meta tonalite	643.7±9.8		U-Pb	5
Hornblende granodioritic orthogneiss	610±9.4	Neoproterozoic (Pan-African)	U-Pb	5
Biotite-hornblende orthogneiss	560±5.8		U-Pb	5
Migmatite biotite granodioritic orthogneiss	617±09		U-Pb	5
Migmatite SE	605±28		U-Pb	6
schist SE	665±16		U-Pb	6
Iwo Quartz Potassic Syenite	642 ± 6	Pan-African	U-Pb	7

References:1, Tubosun *et al*. (1984); 2, Rahaman (1988); 3, Oversby (1975); 4, Pidgeon *et al*. (1976); 5, Rahaman *et al*. (1991); 6, Ekwueme and Kroner (1998); 7, Adetunji *et al*.(2018)

4.4.1.3 Southwestern Nigeria paleomagnetic pole age

Maghemite and poor end member of magnetite minerals bear the NRM in the southwestern Nigeria Precambrian rocks from which can also deduced that the crystallized secondary minerals formed through a hydrothermal modification of the iron-bearing silicates. During the end of the magmatic stage and initial cooling, they are incorporated into the pyroxenes and plagioclase. Sulfide oxide growth, on the other hand, is characteristic of a hydrothermal imprint formed after granitoid crystallization in a greenschist. Both maghemite and poor magnetite end member have similar remanence despite their unblocking temperatures being considerably modified. Hence, giving credence to the fact that the magnetization was obtained for the period of hydrothermal imprint, the occurrence of hydrothermal fluid presumably washed subsequent primary remanence in these granitoids.

The introduction of hydrothermal fluids occurred at a temperature well above the Pb–Pb closure, which corresponds to the age of the magnetic pole in southwestern Nigeria (~ 571 Ma). Granitoids emplaced over 700 Ma were not reliant on high-level hydrothermal emplacement in unmetamorphosed southwestern Nigerian Precambrian rocks, implying a Pan-African episode. Meanwhile, evidence on magnetic susceptibility anisotropy shows that the Pan African nappe was thrust south of southwestern Nigeria (Table 4.18), linking hydrothermal markings to fluid exchange at the nappe's base. Thus, the Pb–Pb date, which is younger than the 620 Ma U–Pb acquired from a deformed metabasite, can provide the thrust a better constrain age (Van Schmus et al., 2008). As a result, 620 Ma was proposed as the magmatic rock's crystallization period rather than the tectonic event's age. The 571 Ma periods, on the other hand, proposed retrograde metamorphism at the nappe's base.The metamorphism ranges from amphibolite-granulite and retrograde greenschist facies towards north to base of nappe respectively in Nigeria.

Table 4.17 Paleomagnetic results (AF) for Southwestern Nigeria granitoids

Site	coordinates	PCA	VGP Lat	VGP long	Paleolatitude	Age(Ma)	N	Dec	Inc	α95	dp	dm
1	7.35N 4.43.5E	Anchored NRm to 40mT	47.3	93.4	5.9	600±150	6	43	12	0.8	0.4	0.8
3	7.24N 5E	Anchored 40mT to 100mT	-36	45.5	32.6	600±150	5	141	52	1.2	1.1	1.6
6	8.17.5N 4.21E	anchored NRM to 15mT	41.2	295	-21	600±150	4	131	-38	1.6	1.1	1.9
7	7.43.7N 4.57E	Anchored NRM to 30mT	45	318	-34.6	600±150	6	141	-54	0.4	1.6	2.2
11	7.133N 5.13.7E	Anchored 40mT to 100mT	25.4	289	-15.5	600±150	7	115	-29	0.2	0.1	0.2
16	7.25.6N 4.15E	Anchored NRM to 100mT	-38	86.4	1.6	600±150	8	128	3.2	0.1	0.1	0.1
21	7.27N 3.55E	Anchored NRM to 100mT	-62	296	-3.9	600±150	7	26	-7.8	0.8	0.4	0.8

Table 4.18 Paleomagnetic results (Thermal) for Southwestern Nigeria granitoids

Site	Coordinates	PCA	VGP lat	VGP Long	Paleol atitude	Age (Ma)	N	Dec	Inc	α95	dp	dm
7	7.43.7N 4.57E	Anchored 40mT to 57mT	0.9	86.4	-8.2	600±150	7	-90	-16	1.1	0.6	1.1
8	7.38N 5.57E	Anchored 40mT to 57mT	-33	75.5	-12.6	600±150	6	-54	-24	1.9	1.1	2
13	7.36.5N 3.27E	Anchored 30mT to 57mT	158	-21	-10.8	600±150	5	158	-21	0	0	0
15	7.37N 4.49.5E	Anchored 30mT to 57mT	46.8	-23	-11.9	600±150	6	47	-23	0.5	0.3	0.5
19	7.23N 3.43E	Anchored NRM to 50mT	42.1	28.6	15.2	600±150	7	42	29	0	0	0

Site, Coordinates- Latitude and Longitude of sampling site; Pol., Polarity of isolated direction; NRM-normal,reversed, mixed polarity; PCA Principal component analysis using using Kirschvink, 1980; VGPlat/VGPlong, pole's latitude/longitude of the pole ; Paleolatitue (Using IAPD); Age Ma Isochron age; N, number of (sites)/samples/specimens; * denotes the number used to calculate mean value; Dec, declination; Inc, inclination; a95, the radius of the 95% confidence cone in Fisher (1953) statistics; (dp, dm), precision parameter;.A95,oval of radius of the 95% confidence cone of the pole; K, Fisher (1953) precision parameter of pole

4.4.1.4 Southwestern Nigeria Pan African apparent polar wander path (APWP)

The southwestern Nigeria pole offers valuable Pan African event constraint to the APWP of the Congo craton. Six out of the seven Van Der Voo (1990) criteria were met: (1) U-Pb dating of amphiboles represent age of metamorphism and its thermal magnetization; (2) the secular variation was still averaged despite the remagnetization, which make some of the rock samples to be discarded; (3) all isolated sites with coherent NRM and PCA were subjected to progressive AF and thermal treatments; (5) Pan-African tectono-metamorphic process impacted the southwestern Precambrian rocks at 570 Ma, thus resetting the remanence; (6) southwestern Nigeria pole did not match younger poles of the Congo craton inside the African plate;(7) Effective reversal test of SW site mean directions, which typifies natural, reverse, mixed polarities in a single averaged magnetic field. The aforementioned criteria are the baked/fold contact test in the *Q*-index classification of van Der Voo used in determining the APWP. SW Nigeria pole (600±150Ma) dataset not available for Gondwana in the 750-450 Ma period (Rahaman, 1988; Tubosun *et al.*, 1984; Ferre *et al.,* 2002; Table 4.19). More so, the African craton of the Nigeria sector was recalculated using Tables 4.17 to 4.19 to generate the new virtual geographic poles (VGPs) that reconstructed VGP for southwestern Nigeria to the present pole. As a result, the southwestern Nigerian pole was employed to pinpoint the paleogeographic position of the Precambrian rocks in the southwest. The remagnetization event that influenced meta-sediments and intruding syenites in SW Nigeria was dated at some point during a coeval remagnetization episode of Pan African greenschist metamorphism. (Meert *et al.,* 1995; Salminen *et al.,* 2019).

Table 4.19 Recalculated paleomagnetic results

CLPOL	DEC	INC	a95	GLAT	GLON	PLAT	PLON	Dp	Dm	AGE
IPG	42.6	11.7	0.8	47.3	93.40'	93.40'	7.40'	0.4	0.8	587
C	141.3	52	1.2	-35.7	35.7	45.50'	7.20'	1.1	1.6	593
GC	131.1	-38	1.6	41.2	41.20'	295	8.17	1.1	1.9	580
PG	141	-54	0.4	45	45	317.50'	7.44	1.6	2.2	621
AU	114.5	-29	0.2	25.4	25.40'	288.90'	7.13	0.4	0.2	634
ISD	161	65	200.7	7.48'	4.12	-33	19.50'	261	324	642
SY	235	34	5	7.40'	4.10'	-29.9	300.60'	3.3	5.7	658
AC	158	20.4	71.4	7.25	5.19	-61.8	56.4	39	74.9	634
IC	-3	-10	142.1	7.29	5.13	-77.3	18.90'	73	144	623
AIGG	344.2	-12	8.5	7.63	4.76	-69.3	54.60'	4.4	8.6	1850
IG	341.2	-4.7	6.4	7.49	4.55	-68.8	67.60'	3.2	6.4	2300
IA	16.3	-41	6.5	7.38	3.95	-55.3	337.10'	4.8	7.9	2750
OG	25.1	-45	159.6	7.53	3.31	-47.9	329	129	203	2500
IAG	351.6	29.5	90.5	8.73	4.13	79.2	315.6	55	100	1900

CLPOL:Idanre porphyritic granite, charnockite, gneissic charnockite, Akure porphyritic granite, gneissic charnockite, Iwo syenodiorite, syenite, Akure charnockite, Ikere Charnockite, Ilesha granite gneiss, Ile-Ife grey gneiss, Ibadan aplite, odo ogun gneiss, augen gneiss

4.4.1.5 Demagnetization behaviours

For samples of the same site CO-17 subjected to thermal treatments have secondary remagnetization averagely 70% at 300–500°C the remainder of the signal was washed up to 570°C (Fig. 4.27). Up to 500 °C the rest of the samples retains >50% of the magnetization is lost (e.g., CO-008, CO-013 in Figs. 4.27 and 4.28). The temperature unblocking revealed two distinct elements, one with natural polarity against N and the other towards NNW and NE. The second specimen has a low unblocking temperature and was fully cleaned up to 300 °C, while the northerly specimen reported magnetization up to intermediate unblocking temperatures (580 °C), which is referred to as characteristic remanent magnetization (*ChRM*). Thus, regardless of NRM decrease for the first 300 samples; large percentage of the samples were treated to remove secondary remanence (Chen *et al.*,2017).

When secondary remanence was cleaned from room temperature to about 300 °C to 400 °C, stable paleomagnetic directions and their components are not well demonstrated. As a result, the remaining samples were handled because their magnetization was cleaned from room temperature to 580 °C with N to NE and linear directions. The great circle that corresponds to these migrations converges at declination/inclination =3.5°/58°(maximum angle of deviation of 2.1°). Just one part per sample was achieved at Site 74, which is fully cleaned up to 580 °C. Site 74 reveals a sharp drop in magnetization up to 300-400 °C (e.g., CO-74B in Fig. 4.30).*ChRM* cleaning with AF and thermal treatment about 500 °C characterizes ChRM plunging towards NE with inverse polarity (9 samples), while normal polarity was cleaned at 300-400 °C with S and W orientations.

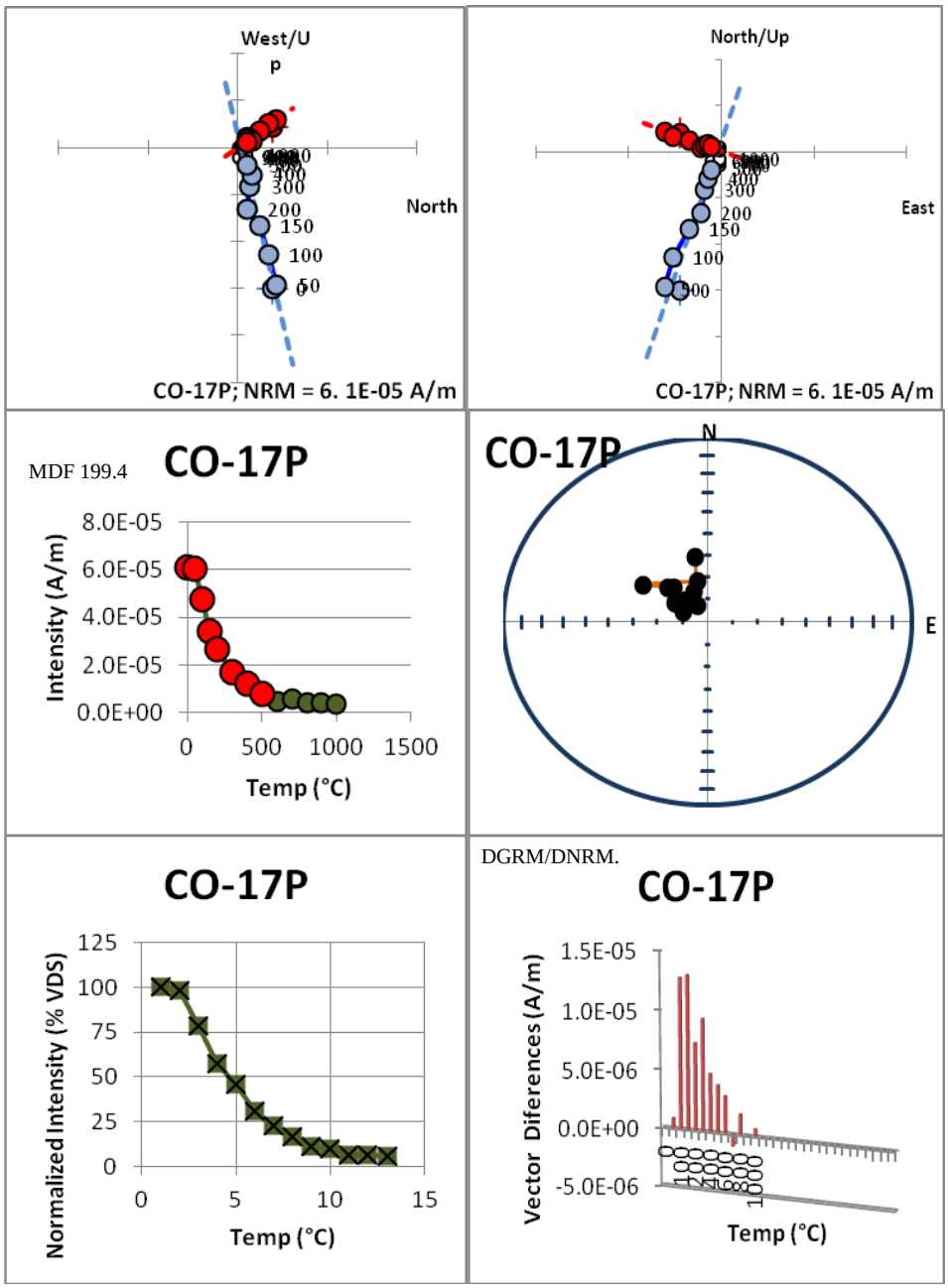

Fig. 4.26. Alternate field demagnetization of zijdervield orthogonal vectorization

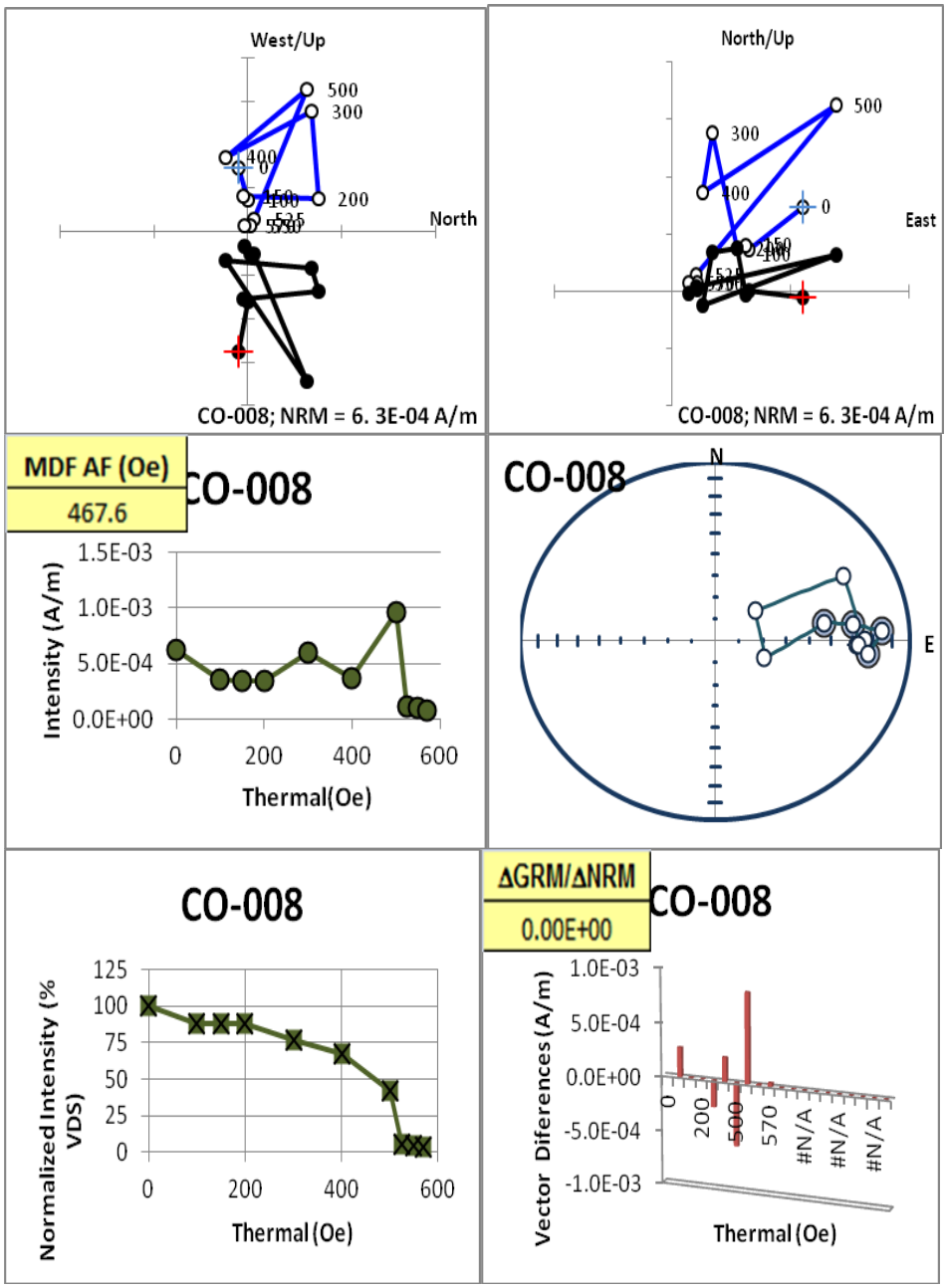

Fig. 4.27. Thermal demagnetization showing zijdervield orthogonal

These treatments demonstrate linear to intermediate directions to the origin pointing to its stability because of its demagnetization at 150 mT and >500°C for median destructive field temperature; whereas the samples recorded difficulty in aligning its component to the origin. These non-alignments occurred because of remagnetization of samples at 300-400 °C, that rendered the measurement of a *ChRM* to fit the great circle. Examples of the stereographic projections witnessed cluster of directions with low inclination towards E, a common line with the great circles (Fig. 4.28) as well as second cluster falls towards NW ~80° with reversed polarity and the most of the sites showed mixed polarities as apparent polar wander (as observed for sample CO-013).

In comparison to the ferrimagnetic one, the samples have a low paramagnetic effect, as shown by the similarities of the curve before and after slope correction. CO-008 sample was decomposed into two overlapping modules with Median Destructive Fields (MDF) ranging from 30-40 to 60-70 mT, as well as a third higher coercivity segment (*MDF* ~ 467 mT).

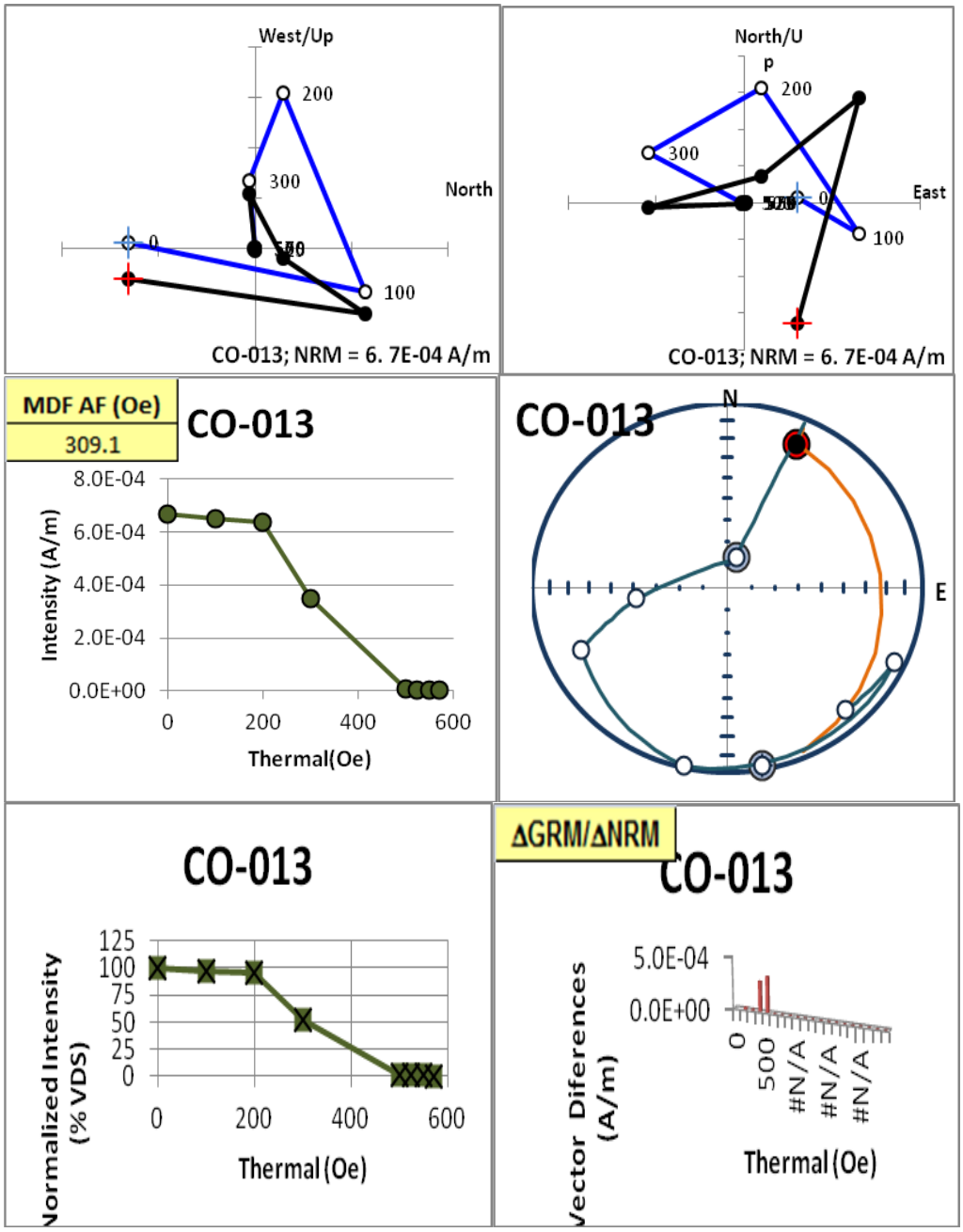

Fig. 4.28. Thermal demagnetization showing zijdervield orthogonal vectorization

There were 23 components in the thermal treatment, with component A to be demagnetized at 200. The viscous remanence of the current geomagnetic field (PGF) has an intermediate temperature dimension B, which was isolated at 100—400°C and was not found in either the PGF or the ChRM.

The clustering at the geographic coordinate revealed intermediate temperature components, while the high temperature cleaning end points of certain samples from sites/locations 1, 4, and 6 are not linear to the origin and ChRM was isolated using the remagnetization loop process. Specimens with high temperature components are typically separated at 400–530 °C because increasing magnetic susceptibility >530 °C contributes to chaos in remanent directions (Fig. 4.28). Tilt correction and mean directions added to ChRM were grouped with an increasing precise parameter, implying a 95% confidence rating, according to the fold test's success (McElhinny and McFadden, 2000; Salminen *et al.,* 2019). Therefore, the ChRM at high temperatures was most likely a primary remanence.The corresponding paleomagnetic poles of the ChRM from southwestern Nigeria shield is shown in detail on Tables 4.16 and 4.17.

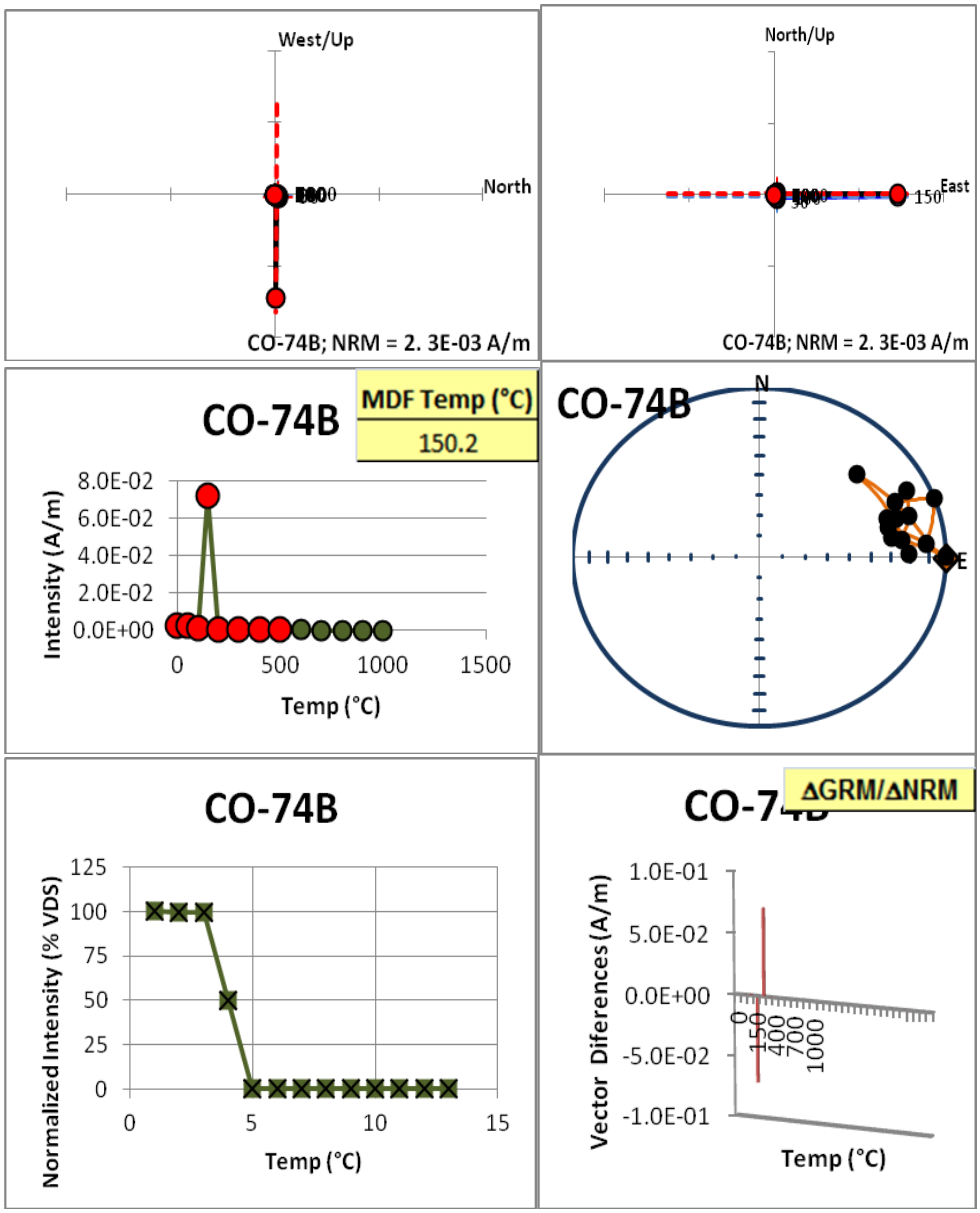

Fig. 4.29. AF demagnetization showing zijdervield orthogonal vectorization

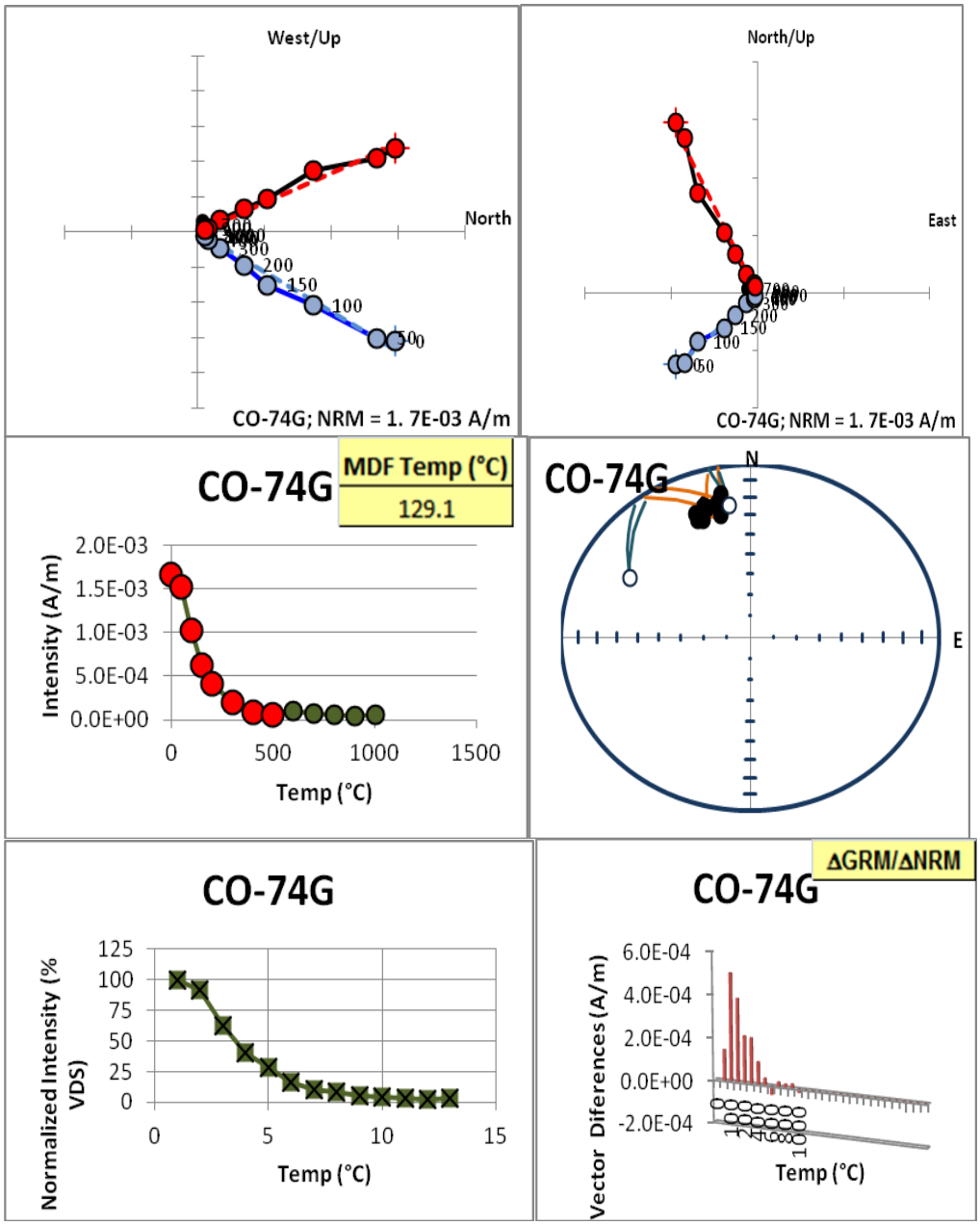

Fig. 4.30.AF demagnetization showing zijdervield orthogonal vectorization

4.4.1.6 Remagnetization age

Sites/locations 1 - 8 having an intermediate unblocking temperature of 100—400 ℃, witnessed perfect dispersed clustering in geographic coordinate after tilt correction. This implies remanence imprint after folding. Majority of the sites were unable to isolate the intermediate temperature component due to its remagnetization. The corresponding imprint on the paleomagnetic pole situated at 85.1°N, 183.0°E with α95=10.1° (*dp*=12.7, *dm*=8.0) in geographic coordinates, are very similar to the basement system of Precambrian poles of southwestern Nigeria. Therefore, this overprint was considered to be remagnetization in Pan-African times. In Nigeria's Eastern basement complex, NE Brazil, Central Cameroon, and much of the west Gondwana crustals provinces, different remagnetization has been observed. Tables 4.18 and 4.19 summarized the relationships between available geologic model isochron ages, tectonometamophic history, and crustal evolution model that support acrretional model for Paleoproterozoic and Neoproterozoic rocks with consistent older model isochron age in support of significant involvement of Archean felsic crust in their orogeny and suggested that southwestern Nigeria's tectonometamophic history and crustal Nigerian active margins and Trans Saharan belt utilized U–Pb geochronological data (Table 4.19) to infer the magmatism that occured from 670 to 545 Ma (Kalsbeek *et al*., 2012 and this study) for the overriding plate of Benino-Nigerian Shield. The age of ultra-high pressure metamorphic eclogites from the passive margin of the West African Craton subducted to mantle depths recently restricted the timing of crustal deformation to 600±150 Ma. The lower plate (West African Craton) and upper plate (Benino-Nigerian Shield) both experienced east-plunging continental subduction, which pushed the flanking passive margin to >90°.This suggests that granitoids subducted between 670 and 610 Ma, resulting in the crystallization of the Pharusian oceanic plate, while igneous rocks associated with arc magmatism include the hornblende-biotite granodioritic gneiss, dated at 610.6 9.4 Ma. Pan-African granites older than 610 Ma predate non-subduction-zone deformation. The Benino-Nigerian basement complex was formed by continental arc, according to a geochemical dataset and Sr–Nd isotopic kinematics application to the 670–610 Ma migmatite-gneisses.

Northeast Brazil witnessed a reworked granitoids- diatexites at 620–610 Ma which differ from the Benino-Nigerian basement complex So far, igneous rocks from the Benino-Nigerian basement complex have been dated as being younger than 670 Ma, while detrital zircon grains from sedimentary deposits have revealed 780 Ma Neoproterozoic magmatism. On the basis of Nd isotopes and bulk-rock geochemistry, this early stage of magmatism was well described along the African part of the West Gondwana Orogen that has a juvenile environment (Berger et al., 2011), while the Central Brazil juvenile arc documented Neoproterozoic evolution of the 4000-km long West Gondwana Orogen for the duration of the Tonian and Cryogenian periods (950–750 Ma) (Matteini et al., 2010). Most of these rocks recorded remagnetization of the granitoids which are inclined to be transformed in later period. The majority of these rocks recorded remagnetization of granitoids that are prone to transformation in the future. A granitic batholith intrusion lies to the north of the study field, and its active thermal fluid invaded the Archean migmatite gneiss extensively in the Neoproterozoic. This could explain the intermediate temperature overprint that results. After the Eburnean, the southwestern Nigerian basement complex has been subjected to numerous tectonic activities. At least four events of deformation were observed in the paleomagnetic result (Table 4.16).

The antipodal conviction limit of the normal and reversed ChRM directions passes the C type inversion test, indicating that the ChRM components maintained their primary remanence before tilting. The reversal alternative is found in the lower part of the southwestern Precambrian rocks, while the upper part has a normal polarity. The paleomagnetic samples in the study area experienced predominantly normal reversal than reverse polarities. On the other hand, site's 6 ChRM directions were isolated by intersecting constraints of remagnetization circles and reversed polarities in view of the high temperature endpoints trend (Fig. 4.23c).

All of the Pan-African magnetic poles are plotted on an equal-area stereo-projection, showing that they were all located around a narrow circle of relative rotation of local micro-blocks within the southwestern Nigeria basement complex. The fault blocks in the southwestern Nigeria basement complex are well formed, with active faulting driving

these micro-blocks around vertical axis rotation, causing Pan-African paleomagnetic directions, especially declination, to become variable in different parts of the province.
Syenite dikes and associated NW-mafic dikes was situated at moderate NW downward direction (ChRM) assigned as Component A. It consists of 16 sites/locations having felsic and NW mafic dikes that couldn't isolate syenite after alternating field demagnetization. All through AF treatments, diverse unstable magnetization directions were witnessed for some granitoids site. This indicates that the area experience both polarities.

In component B, two sites recorded NS-potassic syenite dike with a northern ChRM direction. Likewise, thermal treatments could not isolate the same rock component that recorded it within the normal pole of southwestern Nigeria basement (granite) acquired near the NS-felsic and aplite dikes.

In component C, two sites of the Precambrian grey gneiss revealed low downward inclination, plunging SW(Fig. 4.23). Remagnetization of grey gneiss by component B (granite) was due to its close association. Micro-granitoid (quartzofelspathic) dikes specimen observed in Component C was isolated by MOLPIN-AF or thermal treatments, which has mixing characteristics not recorded in the other dikes of syenitediorite. Polarities of normal (N) and reverse (R) were observed.

4.4.1.7 Geochronological and paleomagnetic mechanisms

On the emplacement of dikes in southwestern Nigeria basement complex, a fast cooling was documented from U-Pb dating on zircons to reveal their age of crystallization. The growth of granitic magma (750 – 850°C) with temperature closure >900°C; possess a robust geochronometer that differ with the constituent minerals in the closure. Conjugate use of U-Pb and ^{40}Ar-^{39}Ar dating do characterize and identify superimpositions of tectono-metamorphic episodes in cratonic setting (Tavares, 2015); because amphibole (**Tc**= 450 – 500°C), muscovite (**Tc**= 450°C),and biotite (**Tc**= 300°C) have lesser temperature closure than U-Pb scheme on zircon (**Tc** >900°C). Matching U-Pb and ^{40}Ar-^{39}Ar ages for the same rock implies a fast cooling mechanism. Thus, relative minerals possessing separate

closure temperatures can be used to calculate the rate of cooling (°C. Ma^{-1}) of country rocks under study.

Limited information on geochronological data, were available for the Southwestern Basement rocks. Recent studies on dating in Iwo area by Adetunji *et al.*, (2018) (Fig. 4.31) provided robust U-Pb isochron ages for the western Nigeria domain (Fig. 4.31) (Table 4.19). Examples of the robust ages are: Ibadan Aplite -2750Ma (Oversby (1975), felsic dyke - 572.4±8.1 Ma (Ganade *et al*., 2016) and Iwo Syenite 642±6Ma, (Adetunji *et al.*, 2018). The recently dated rocks have ages of 642±6Ma on whole rock, which cannot be considered as consistently stable. Large Rb-Sr ages (aplite/gneiss) ranging from 3000 – 1800 Ma typifies Paleoproterozoic resetting in southwestern Nigeria basement complex (Trans Saharan orogenic belts and Eburnean event). Non-existence of young aged rock does not imply lack of tectono-metamorphic episodes, as felsic dike swarm emplacement in the study area, recently dated at 572.4±8.1 Ma and 642±6Ma (Adetunji *et al*.,2018). The lack of these ages was owed to the thermal diffusion in rocks which was difficult and non-efficient mechanism in massive granitoids. Amphibole having temperature closure of ~501 °C, probably be the finest geochronometer in dating key NRM having strong equal blocking temperatures. Biotite ages of ~300 °C may typify ages of high temperature deformations, representative of secondary NRM.

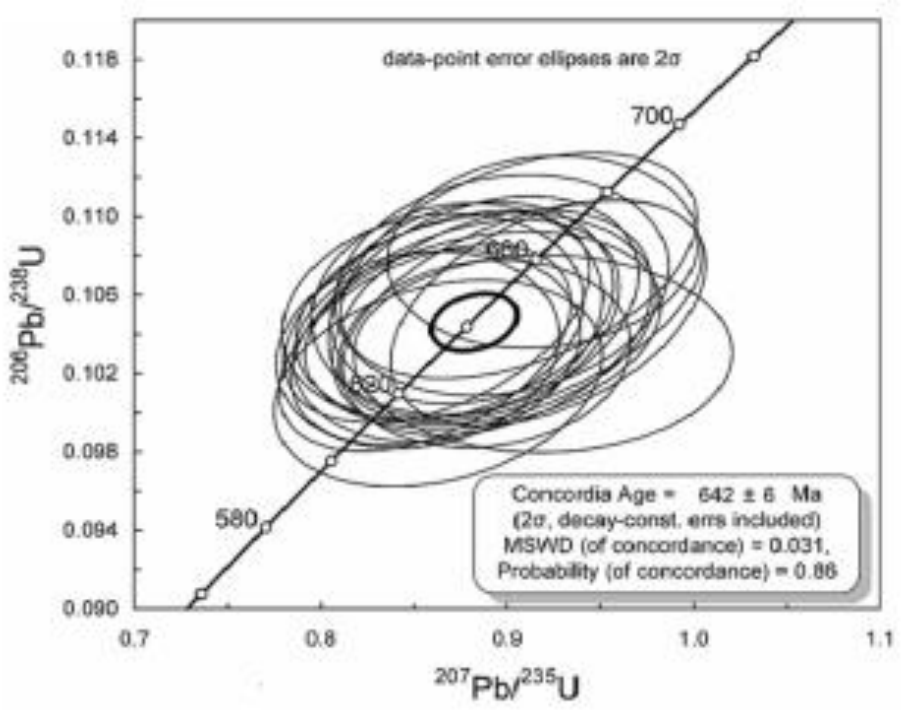

Fig. 4.31. Recent concordia plot of uranium-lead zircon data of Iwo syenite, southwestern Nigeria (Adapted from Adetunji *et al*., 2018)

4.5 Day plots, hysteresis loops, First Order Reversal Curves (FORCs)

By characterizing the rock using hysteresis analyses and calculations, it was shown that the geometry of hysteresis loops within southwestern Nigeria basement rocks have maghemite as a dominant phase with evidence from their wasp-waisted behavior (Fig.4.32). This suggest occurrence of multiple magnetic carriers (Dunlop and Özdemir, 1997; Chen *et al.* ,2017). The granitoids, on the other hand, had typical Median Destructive Field (MDF) parameter values (0.3–0.5), indicating SD, PSD, and MD grains of magnetite components. They have lower Q values ranging from 0.7 to 14 (dimensionless indicator of anelasticity). The magnetic carriers of the samples are PSD and MD domains of various sizes. The intensity of remanence of both the ARM and IRM decay curves tested indicate strong Q values for NRM with similar IRM decay curves. Large remanent magnetization values caused by lightning or other high fields, such as Carporzen *et al* (2005) suggested tectono-metamorphism. Biotite granite gneiss grains have single population of magnetic carrier (SD) and other samples have rapid intensity decay rate of remanence, then ARM/IRM, implying that the magnetization evolved thermally.

Amphibolite, banded gneiss, biotite granite gneiss, granite and charnockite rock specimens recorded evidence of SD, PSD and MD domain maghemite, with non-mineralogical transformations during the measurements (Fig. 4.32).Heterogeneity in the magnetic mineralogy of studied samples in terms of distinct grain sizes and its coerciveness typifies PSD and MD magnetite. Moreso, magnetic behavior of exceptional maghemitization are owed to episodes of Pan–African orogenies. The effects of pressure-temperature (PT) are characterized by larger maghemite and (titano)magnetite grains. Also, magnetic grains are found within the PSD domain, implies that the NRM carriers may be a combination of fine and large grains sizes within SD and MD.

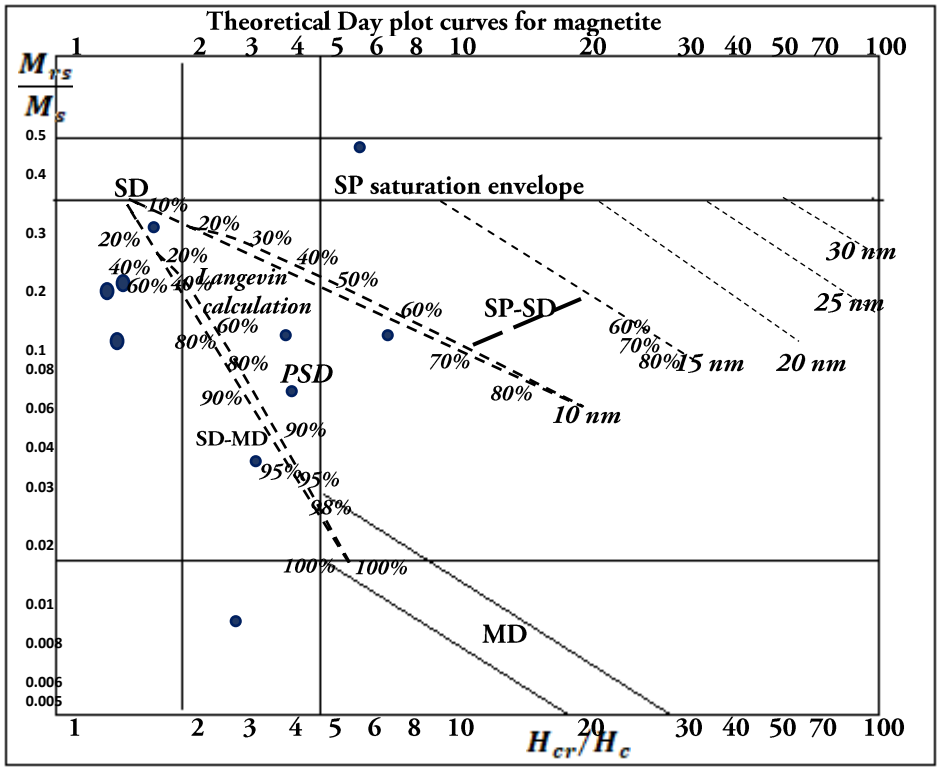

Fig 4.32. SD, PSD and MD plot of the study area (after Day plot *et al*. 1977)

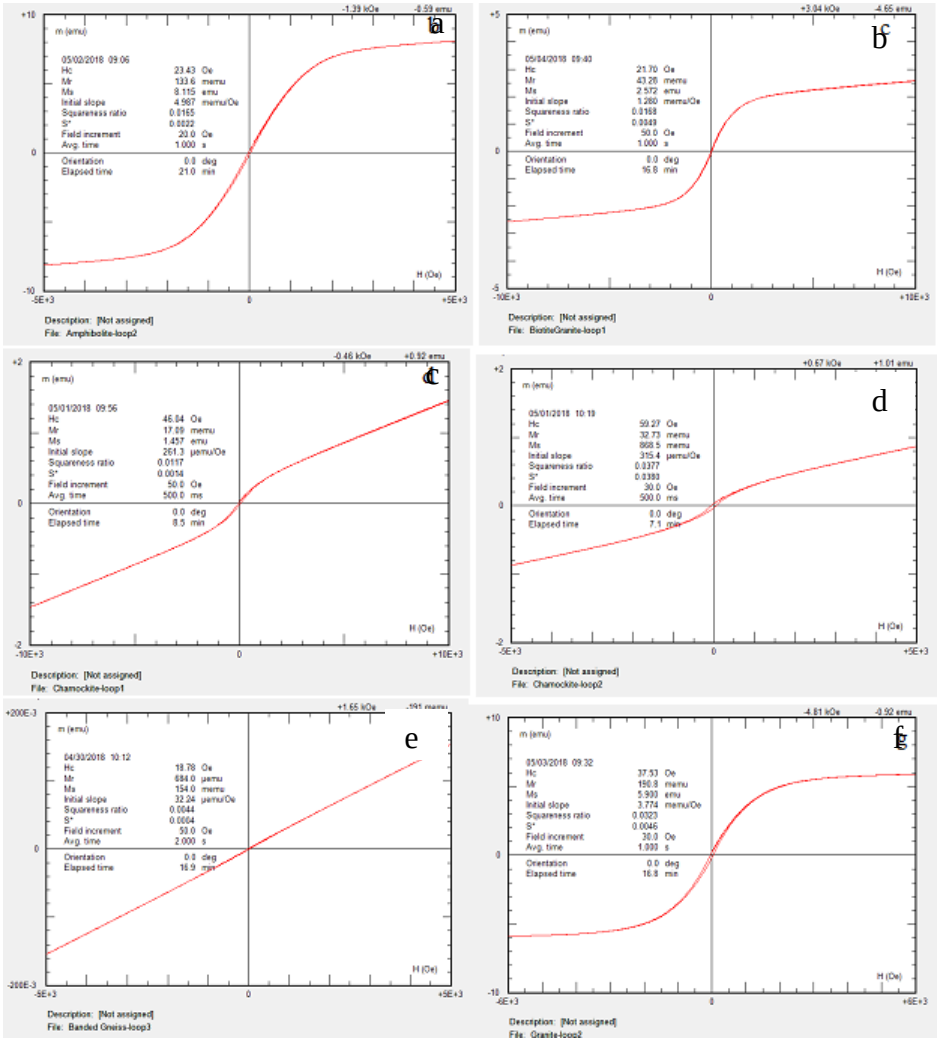

Fig. 4.33. Narrow waisted hystersis loops of (a) Amphibolite (b) biotite granite gneiss (c-d) charnockite (e) banded gneiss (f) granite

Vast majority of the examined rock samples confirmed clues of maghemitization during the measurement, due to the tectono-metamorphic history of the rock (Fig. 4.33a). The distinction of stoichiometric and non-stoichiometric of maghemite grains; magnetite grains were affected by tectono-metamorphic impacts of Pan–African orogenies. Because normal remanence intensity measurements show a metamorphic-related magnetization component carried by magnetite, which is an associate of the Pan-African events that made the lowest temperature to reset the direction of magnetization of magnetite (580 °C), this was the case. Furthermore, it was clear from Ivanov (2005)'s impact model that the center of the core, with a minimum radius of 15 km, was placed at temperatures above 700°C, which would have lasted for tens of thousands of years after the periods in deeply buried host rocks. Pan–African orogenies' tectono-metamorphic effect on magnetite grains; may be attributed to stoichiometric and non-stoichiometric maghemite grains differences. Since normal remanence strength values show a metamorphic-related magnetization portion borne by magnetite, which is an associate of the Pan-African events that made the minimum temperature to, reset the direction of magnetization of magnetite (580 C), this was the case. Furthermore, it was clear from Ivanov (2005)'s impact model that the center of the nucleus, with a minimum radius of 15 km, was put in temperatures above 700°C, which would have lasted 10-100’s thousands of years after the periods in deeply buried host rocks. This correlates with the works of Ferre *et al*., (2002) on increased temperature gradients demonstrated across the core.

Figure 4.33(b, c) suggests confirmation of maghemite, titanomagnetite and hematite as the most important magnetic minerals in the samples as demonstrated by temperature controlled magnetic susceptibility curves (n = 12).

Figure 4.34 demonstrate dominance of maghemite on the IRM acquisition curves (higher than 80% of total magnetization). Two populations noticed in the maghemite typifies variable mineralogical and grain size proportions of rock samples, identifiable with the aid of statistical analysis (Kruiver *et al.*,2001). Presence of high coercivity magnetite component assigned as C_{HMag} have large maghemite population values between 43 and 97% of the magnetization. They are described by a mean $B_{1/2}$ = 63.2 mT and saturation of

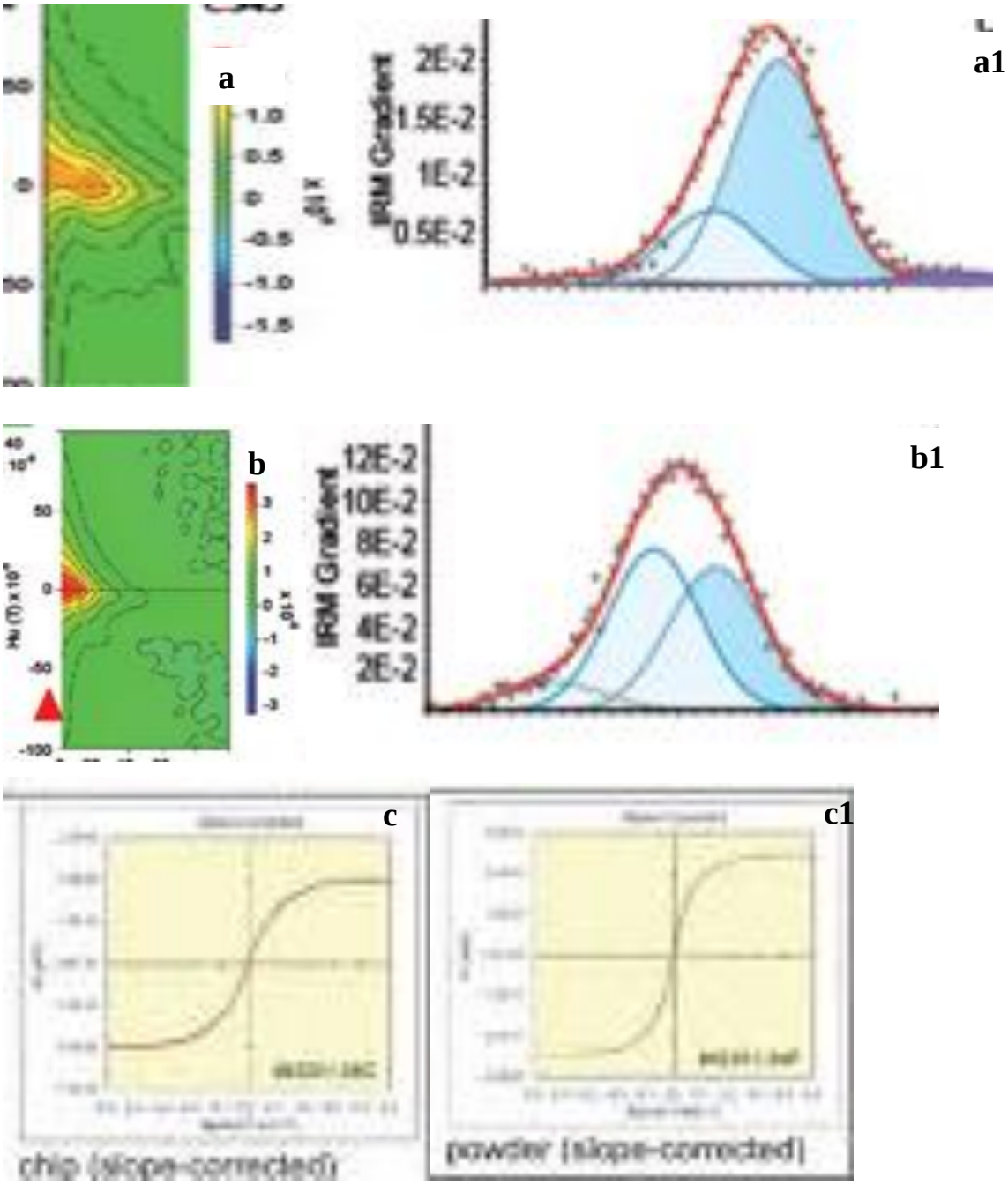

Fig. 4.34. (a) FORC diagrams of PSD behavior; (b) linear and Gaussian cumulative measurements respectively having dominance of decreasing magnetic grain size of maghemite and hematite and (c) Examples of chip and powder specimen for hysteresis loops after applying correction to a linear gradient of paramagnetism

4×10^{-4}, 1.23×10^{-1} A/m (mostly between 10^{-3} and 5×10^{-2} A/m) of medium coercivity and SIRM respectively. Secondly, presence of medium coercivity magnetite component assigned as C_{HMag} have maghemite-like population with lower mean coercivity (mean $B_{1/2}$ = 25.9 mT; which can characterize ~ 47% of the magnetization with variable SIRM between 7×10^{-4} and 5.3×10^{-2} A/m. High coercivity hematite component designated as C_{hem} represents higher coercivity, having a mean of $B_{1/2}$ = 490 (Appendix 6). Averagely, 4% of the total magnetization was traceable to hematite with uneven distributions. Categorically, hematite-like pattern agrees to 1–2% population of the samples magnetization, yet some samples are characterized with more than 20% of magnetization. A low coercivity component designated as C_{LMag} have mean $B_{1/2}$ = 6.4 mT which indicates that it has mean of 7% on the total magnetization that suggests coarse-grained magnetite.

In contrast, plots produced by the bulk of the IRM data for granite (a) that correspond to single magnetic components, typical of low coercive force (Hc) ferromagnetic material, exhibited low B1/2 values suggesting the field at which half of the IRM saturation was maximum (18–25 mT). The specimens were treated to direct current magnetic fields of 3.0, 0.4, and then 0.12 T in three orthogonal directions, resulting in a suite of multiple IRMs. Figures 4.35 and 4.36 show the IRM component decay curves for granite (a), with the primary magnetic process having a low coercive force (0.112 T) in the soft fraction and a strong spectrum up to 585 °C.

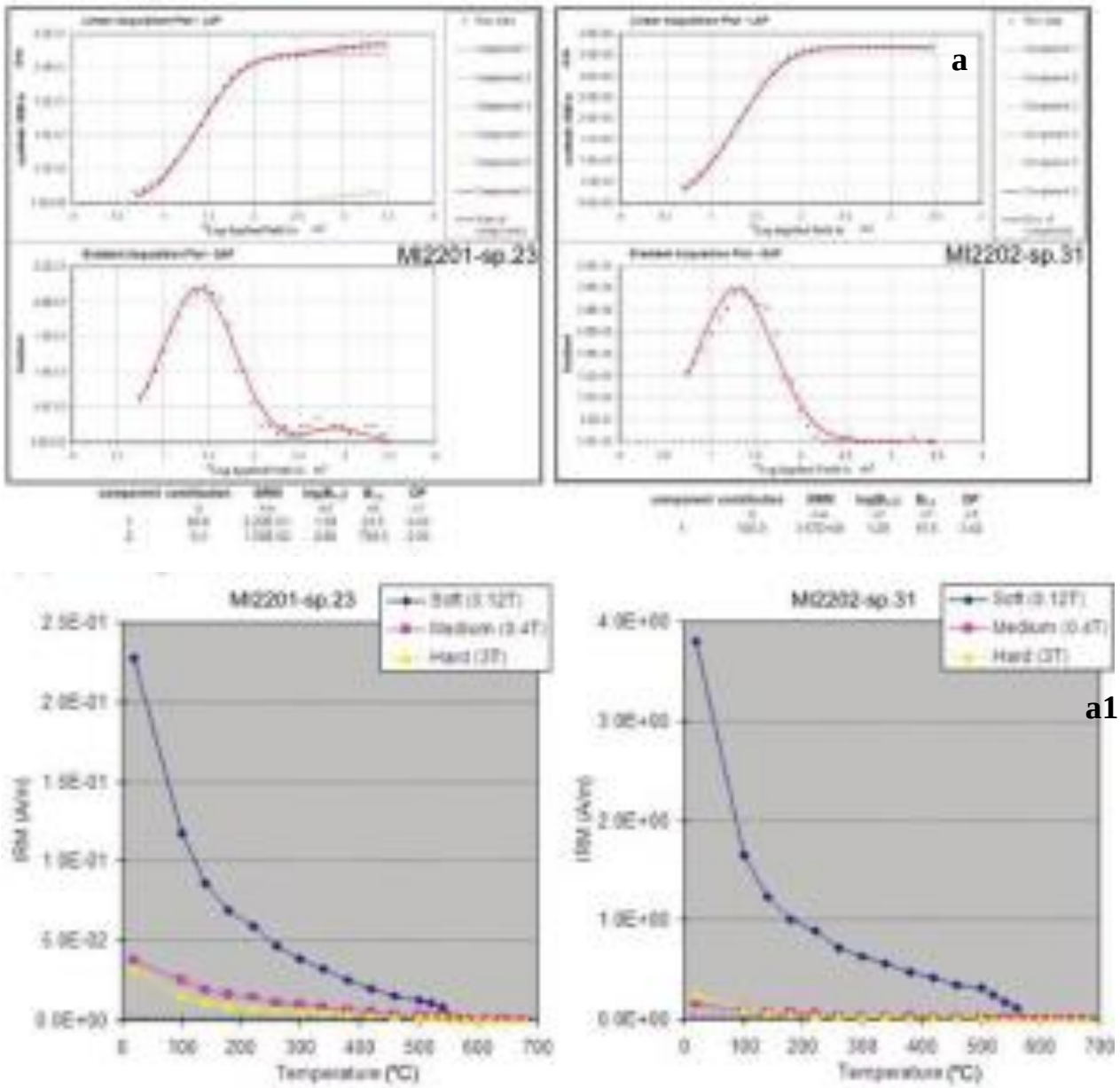

Fig. 4.35. Linear acquisition plot, gradient of acquisition plot and thermal demagnetization of isothermal remanent magnetization obtained dc fields of 3 T for (a, a1) granite. Specimens were treated with AF demagnetizer at 100 mT

Comparatively, low $B_{1/2}$ values implying the field at which half of the IRM saturation was peaked (18–25 mT) illustrate plots generated by bulk of the IRM data for granite (a) corresponding to single magnetic components, representative of low coercive force (Hc) ferromagnetic mineral. Suiteof multiple IRMs were generated by the application of direct current magnetic fields of 3.0, 0.4 and then 0.12 T on the specimens in three orthogonal directions. Figures 4.35 and 4.36 demonstrate the decay curve of the IRM components for granite (a) with the dominant magnetic phase having low coercive force (<0.12 T) in the soft fraction and broad spectrum up to 585°C. This confirms that maghemite and low (titano)magnetite are the carriers of the high-TUB (unblocking temperatures) part of remanence. The intrusive aplite rock's mild and hard fractions range from $0.12 < Hc < 0.4$ T and $0.4 < Hc < 3.0$ T respectively.

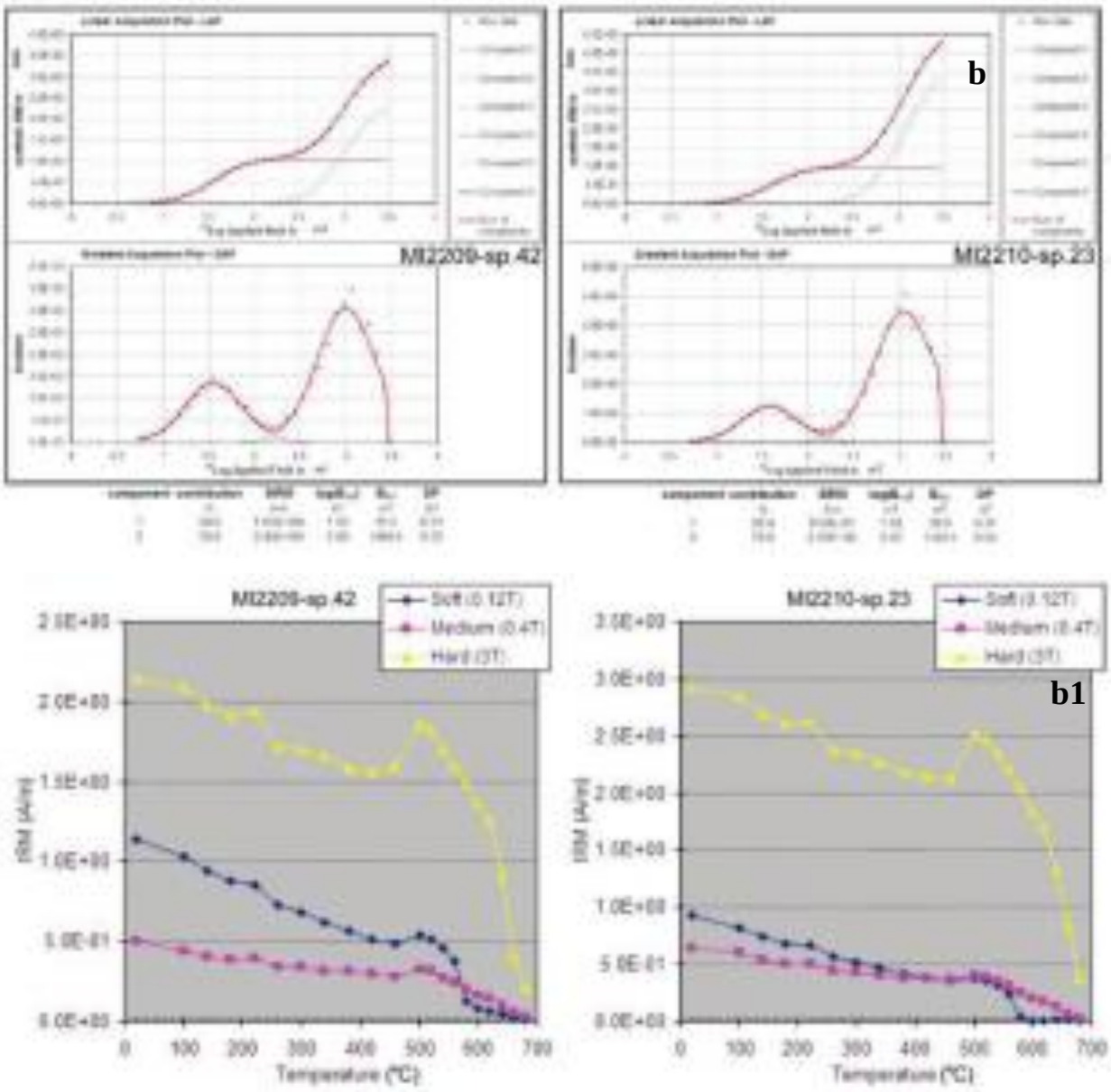

Fig. 4.36. Linear acquisition plot, gradient of acquisition plot and thermal demagnetization of isothermal remanent magnetization obtained dc fields of 3 T (b, b1) aplite intrusive rock. Specimens were treated with AF demagnetizer at 100 mT

The mild and hard fractions of altered granite range from TUB 580 °C to TUB 680 °C, respectively; representative of SD-size magnetite and hematite (Fig.4.36). Inside the MD and SD-sized hematite, the mild and rough components of the intrusive rock ranged between TUB< 680 °C and TUB <680 °C, respectively.

Figure 4.37 shows the First order reversal curves of amphibolite, biotite granite gneiss, banded gneiss, charnockite and granite respectively.The FORC diagrams indicate the presence of interacting singledomain (SD), no interaction (PSD) and vertical spread (MD) particles. The vertical spread in maghemite does not interact strongly like magnetite. Amphibolite and biotite granite gneiss suggest MD behaviour because of the vertical spread at Bu=0. Banded gneiss Peak at Bu=0, which demonstrate, that the peak was close to 0 with very low Bu. Super-paramagnetic (SP) particles associated with MD grains, as observed in banded gneiss. Charnockite and granite demonstrate that the sample was different with small vertical spread in comparison to others (Chen *et al.,* 2017; Zhao *et al.,* 2017). The specimens recorded no interactions, but showed the presence of PSD grains.

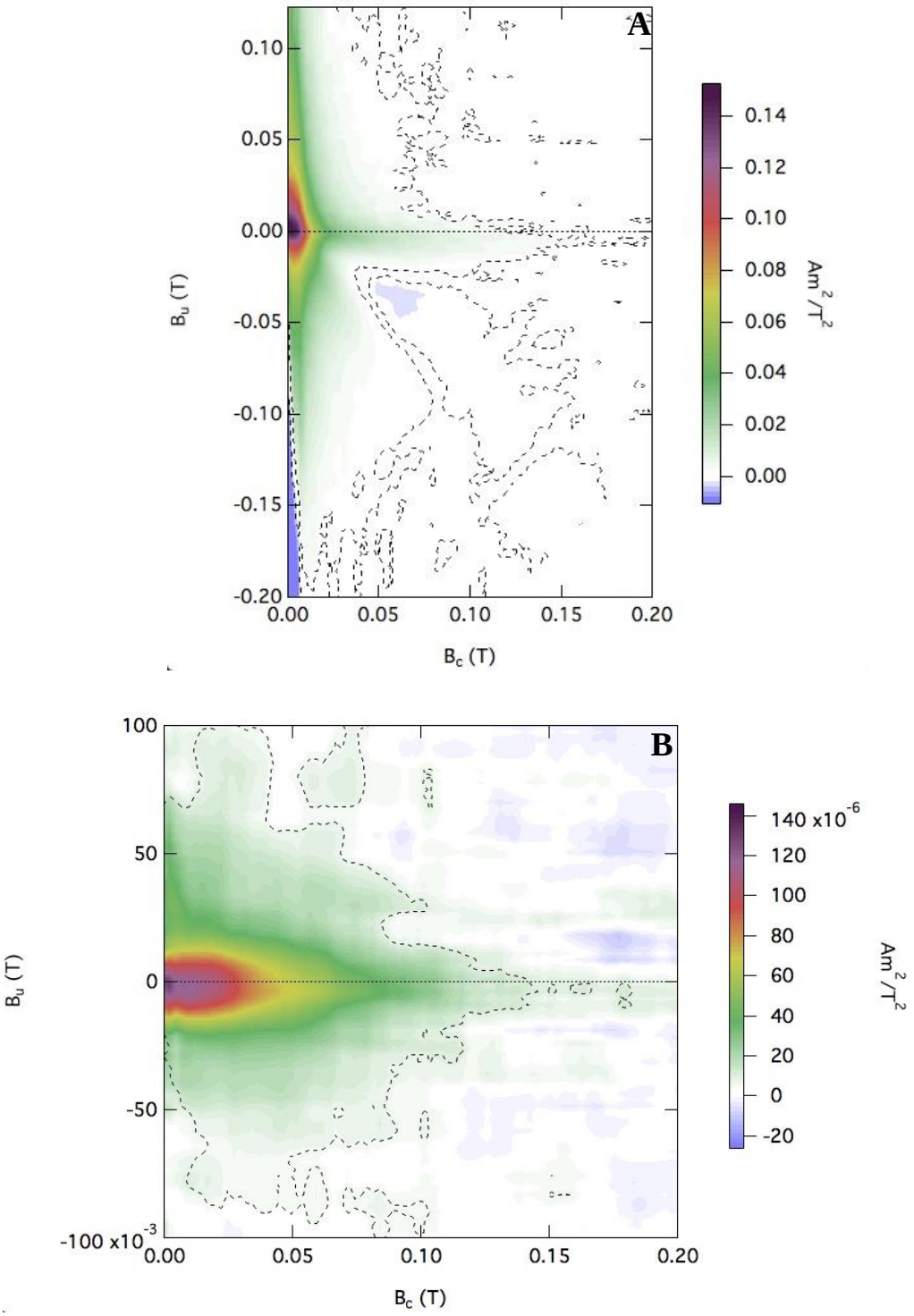

Fig. 4.38: First Order Reversal Curves (FORCs) (A) Amphibolite (B) Banded Gneiss

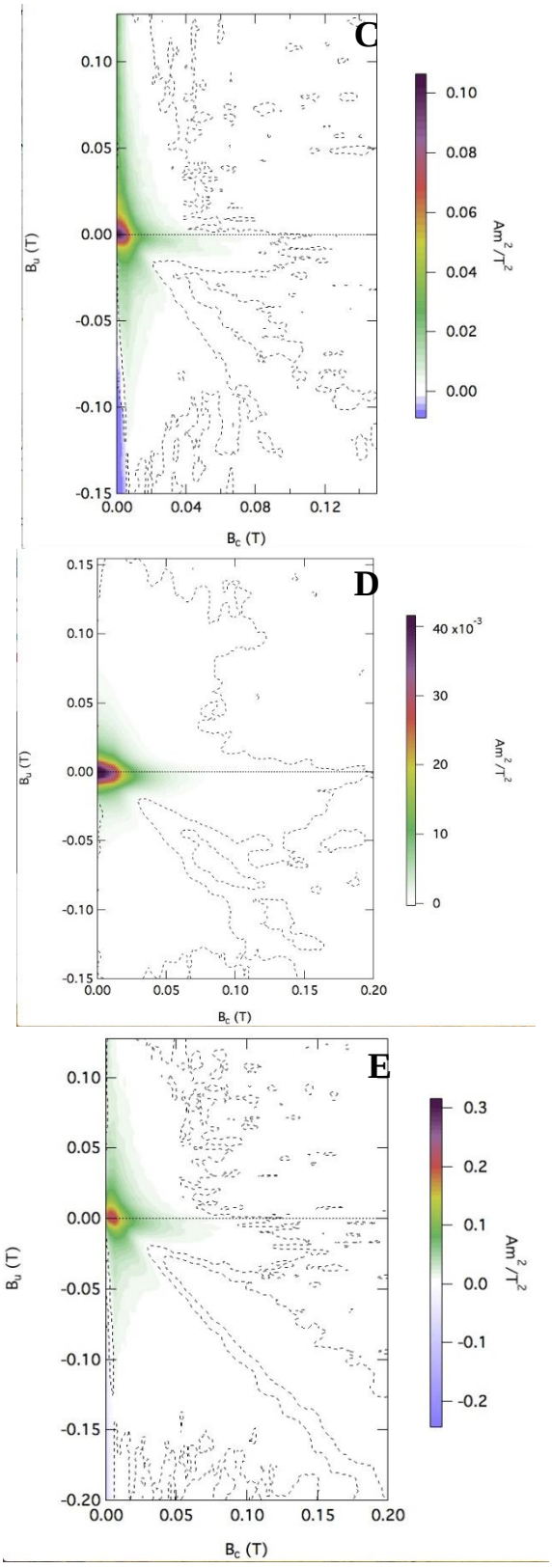

Fig. 4.38. First Order Reversal Curves (FORCs) (C) Biotite granite (D) Charnockite (E) Granite

4.6 DISCUSSIONS

4.6.1 Rock magnetic characterisation of the Precambrian Basement rocks of southwestern Nigeria

The plagioclase, pyroxene, orthopyroxene, clinopyroxenes and opaque minerals in most of the Precambrian Basement rocks of the study area revealed pseudomorphs of Fe-Ti-O bond stretching, and the lattice and shape are well distributed. Metasomatism and ductile deformation is observed in plagioclase mineral. Maghemite fine grains with a content of potassium plagioclase and pyroxene evolved from granulite facies metamorphism of granitic rock. The result of this study are in agrrement with Raman spectroscopy by Ma and Chen (2018) and Nadeem (2015), where synthetic maghemite was used in their study and the result showed that the calculated and observed data were the same; while Slavov *et al*. (2010) argued that molecular vibrations of Raman spectra were observed in nanoparticles of ferrofluids maghemite. The calculated and observed Raman spectra were different due to the low laser power and heating effects. Weak Raman spectra from the Precambrian Basement rocks were 398.8, 663, 714.8, 720.4, 764.48, 426, 710,717 cm^{-1} and strong Raman spectra were 519.1,521, 515.67,522.67,531.56,519.96,1285.5 cm^{-1} and were compared with the previous works of Chamritsi and Burns (2005) and they corresponded accordingly. The aforementioned calculated Raman spectra did not perfectly align with previous studies of Serna *et al*. (1982), deFaria *et al*. (1997); Chamritski and Burns (2005) and Hanesh (2009) because the Cartesian and estimated results were done manually which could introduce significant error. The XRF results and their suitability for paleomagnetic studies for Fe_2O_3 having 7.34, 6.99, 6.27, 5.08 wt. % of migmatite gneiss, granodiorite, granite gneiss and biotite granite rocks of the study area implied the stability of these specimens for paleogeographic reconstruction.

The SEM results revealed the non-suitability of some of the Precambrian Basement rocks for paleogeographic reconstruction, but were well suited for magnetic rock characterisation of type II and III content. The precursor magnetite was prone to the alteration from magnetic grains resulting in the pronounced formation of maghemite in the study area. The magnetic domain phases configuration in the study area were PSD, MD, SP and SD predominantly. The study area has witnessed several episodes of orogenies that have altered the pure iron oxides, documented for the paleomagnetic

records. Tectono-metamorphism, hydrothermal imprints of the early, mid and later episodes of Pan-African orogenies resulted in remagnetisation of the rocks (Salminen *et al.*, 2019; Baldim and Oliveira, 2021). Thus, the maghemite did not interact perfectly as the magnetite observed in most rock samples, thus implying the impacts of tectonometamorphism. Most of the different classes of Precambrian rocks in southwestern Nigeria generated pseudo-single domain (PSD), multi-domain (MD) and superparamagnetic behaviours (Roberts *et al.*, 2017) because of the modification of the primary magnetite to other types of iron oxides. Thus, the stability of the geomagnetic field vector of the rocks has been transformed/modified, which led to setbacks of secular variations of most of the treated rock specimens. The presence of primary magnetites in some of the granitoids, especially the gneisses, generated reliable, stable, and coherent mean directions used to reconstruct the apparent polar wandering paths of the continent.

The XRD result showed quartz, microcline, pyroxene, iron oxide minerals in the granitoids, and the result implied that magnetite; minor magnetite/maghemite minerals carry the magnetic grains with sporadic appearances and they occurred because of the tectonometamorphic episodes. The EPMA revealed the late formation of hydrothermal K-feldspar in the magmatic and metamorphic rocks, which made it difficult to isolate the sodium-bearing fluids because of insufficient dataset on pre-metamorphic protoliths in the study area. Reduction and oxidation reactions and conditions of fluid pH were responsible for differentiation in Fe-Ti-O minerals. Redox transformation of α-hematite is sensitive and replaceable than γ-maghemite. The granitoids were characterised by the spread from positive to negative Eu-anomaly (from enriched to being depleted relative to REEs); albite Types I and II demonstrate the formation of hematite and magnetite occurrences as minute inclusions in purviews of reactive hydrothermal K-feldspar as well as modifications observed in basalts in the works of Krasa and Herrero-bervera (2005). The growth of maghemite/(titano)magnetites was consistent with the foliation pattern; however, they are characterised by the hydrothermal mineral fluid of the regional Pan African event. This suggested that they documented the formation of Type I magnetites when the metamorphism peaked; whereas, Type II magnetites suggest retrograde metamorphism that revealed grain matrix reactions during the prograde metamorphic

path. The thermomagnetic dependence of the rocks samples from the study area were consistent with the paleomagnetic results and showed shoulder type reversible heating and cooling Curie temperature curves. Poor magnetite and titanomagnetite magnetic phases are typical of pseudo-single, multi-domain and single-domain decreasing order of paramagnetic behaviour. The Precambrian Basement rocks witnessed the non-mineralogical transformation of hematite, poor titanomaghemite, titanomagnetite in low-temperature maghemitization (Nutman *et al.*, 2017; Roberts *et al.*, 2017), which implied that the lattice and shape were well distributed. Decrease of magnetic susceptibility around 360-500 ºC is an example of higher titanium in poor titanomagnetite, suggesting that the pseudomorphs of magnetite having high magnetic susceptibilities influenced the generated regional magnetic anomalies detected in the southwestern Nigerian Precambrian rocks. The predominance of maghemite/titanomagnetite in southwestern Nigeria granitoids developed either in the course of diagenesis (Type III), prograde metamorphism (Type II), or peaked metamorphism (Type I). There are two isolated records of maghemite growth phases: (1) Primary maghemite blebs are incorporated inside Type II prograde magnetites, and (2) maghemite veinlets developing within ilmenite, obviously cutting syn-peak transversely to post-peak metamorphic garnet and greenschist- amphibolite facies, respectively.

4.6.2 Delineation of Orogenic events in Precambrian Basement rocks of southwestern Nigeria

Within the southwestern Nigerian Precambrian Basement Complex, virtually all the Pan-African granitoids demonstrate intense magnetic susceptibility (having subhorizontal magnetic lineation direction), which is comparable to the adjoining shear zones as measured by Anisotropy of Magnetic Susceptibility (AMS) (Bina and Henry, 1990 and reference therein; Raposo and Gastal, 2009). The result of the AMS implied that it is deficient in the post-magmatic collision. During late magmatism, regional stressed-field led to the formation of diorite, granite, and a large amount of maghemite/(titano)magnetite were crystallised. Constant intrusive magma along sheared zones, local thrusting recorded type II magnetites during the Precambrian. According to this model, the Ifewara-Ilesha terrane moves north along the western frontier, extending

to the Saharan metacraton. During late-magmatic stages in southwestern Nigeria, the Granite 1 magnetic fabric was not exposed to a stressed regional zone. The model is assumed due to the migmatite-gneiss Basement's conjugate rigidity and the late tectonism's young intrusive (Salminen *et al.,* 2019). Recent occurrences in the Gneissic complex's fault network evolution typified significant faults distinct from the main structure, and the successive fault generations are characterised by intense fractures favouring substantial weathering observed by a reasonable decrease in the magnetic susceptibility mean. Magnetic fabric deformation in the Granite gneiss is seen around NNE–SSW faults; while the magnetic fabric in granite had clear NW–SE faults. The deformation suggests that the faults have separate progressions and may not be linked by the same conjugated network. As shown by the NNE- SSW faults characteristics, the north-south II shear zone-blocking resulted in fault activity moving to another fault network. The NW–SE fault system is primarily late Pan-African in origin and is linked to the tectonometamorphism of the Pan African occurrence that occurred between 575 and 555 Ma to the east.

Therefore, the evolution of granitoids was made possible by fusing high-temperature shearing in the N-S direction, resulting in the synchronous emplacement of D2 tectono-metamorphism. Njonfang *et al*. (2008) argued that the Pan-African granites demonstrated dextral S-type potassic-feldspar porphyries and megacrysts, suggestive of a sinistral r-type cycle of megacrysts and porphyries for the period of dextral shearing. The same type of event was witnessed in the study area, having orientation of the sheared planes of the primary stress r_1= N92E; since r_1 persists for the period D2 and D3 deformations. The reopening of dextral D3 tectonism, known for ductile thrusting, shallow dips S2 in the N-S direction, and horizontal L2 is of isochron age of 564 and 558 Ma or <572 Ma. Similar age was given in Pan-African granites, evidenced with the mylonitisation. Subhorizontal lineations and triaxial formation resulted from strike-slip and compressional systems suggested by Njonfang *et al*., 2008; Kwekam *et al.,* 2010; Salminen *et al*., 2019, leading to moderate NE-SW lineation and their respective foliations directions. Kwekam *et al.* (2010) and Liegeois *et al.,* (2003) evolutionary models of Congo craton exhibited post-collisional granitoid intrusive. The aforementioned evolutional trends imply that the study area recorded S3-L3 and oblique slips. The deformation and tectonometamorphism

in the Precambrian Basement Complex of southwestern Nigeria are: D0 =650 Ma, D1 =640 Ma, D2 = 615 Ma, D3 = 580 Ma and D4 =550 Ma. The studies also suggest that the study area underwent four deformational events. The second phase of deformation in the pull-apart basin emplaced charnockite- granitoids around 600 and 613 Ma. Consequently, a marginal orogenic, compressional low-angle fold-and-thrust belt and an interior belt regulated by transpressive high-angle faults flank the transition zone between the charnockites and the Older Granites around Ifewara-Ilesha shear zone. The extreme conditions of clayey rocks (as lubricants) reduce frictional resistance and high-pressure fluids acting on lithostatic pressures, thus permitting fracturation and ultramylonites/cataclasites. Gravitational sliding and suturing of thrust faults and underthrust, folds due to the hinged orogenic wedge thrust sheets led to the formation of oblique-slip, compressive forces, shortening of the basement superficial nappes (thick-thin-skinned styles and large scale overthrust) in Ifewara- Ilesha Shear Zone (IISZ), which differ from the rest of the study area. Ife-Ilesha shear zones were overprinted with (MP-LT and MP-HT) amphibolite-greenschist facies. Pseudotachylytes, which have never been described before in southwest Nigeria, are local intrusions within the narrow Ifewara fault zone. Pseudotachylytes are black, fine-grained to glassy rocks, similar in appearance to tachylytes (glassy basaltic rocks), after which they are named. They were supposed to have occurred due to partial melting of rocks caused by more extreme cataclasis. The evolution model characterised plagioclase and biotite fission and replacement by epidote, sericite, chlorite, and titanite. TThe introduction of intrusives post-collisional granitoid motions, metacratonic evolution and cratonic boundary around Congo craton correlated to southwestern Nigerian Precambrian Basement rocks. The E-W belt model in the shear zone determined a post-deformational diverging grid system of the Dahomeyan-Pharusian belt typified with medium pressure-low temperature and medium pressure- high-temperature metamorphism between 650-625Ma (Rahaman, 1988). U-Pb ages of gneiss and granite gneiss are analogous to the syn-deformation evolution of the NW Cameroon. As a result, the San-Francisco Congo craton (SFCC) is being over-thrust with greenschist-amphibolites (Chaves, 2021; Baldim and Oliveira, 2021; Percival *et al.*, 2021). Evolution and strain analysis of the shear zone, which is characterized by an NNE plunging fold and mylonitization stretched lineation. The

evolution model of ESB and SFCC led to shear–associated early folds (asymmetrical, open-close) and late folds (tight-isoclinal) as well as dextral strike-slip tectonics that resulted in the progressive mylonite to ultramylonite. The events suggested that the Central Hoggar Belt, which is part of the Pan-African Trans-Saharan mobile belt, has regionally related shear zones and San Francisco Congo craton (SFCC), where appreciable dextral strike-slip motions were witnessed along these major thrust faults.

The paleogeogeographic reconstruction of the paleomagnetic results of individual site orientation of the magnetic is characteristic of geomagnetic field record that averaged the overall sites of the study area, which produce the secular geomagnetic variation. Thus, this suggested that the Pan African granitoids from Southwestern Nigeria shield possessed primary NRM. As a result, there has been a significant divergence of arguments on the Pan -African paleomagnetic dataset. Few paleomagnetic data sampled in the study area passed a fold test and was considered a stable/reliable specimen; however, most sites have gone through episodes of remagnetisation. The Pan African granitoids, especially gneiss, granite and biotite granite gneiss, showed coherent paleomagnetic direction with 100% declinations. This result implies that insufficiently consistent datasets in Pan-African paleomagnetic directions in the Precambrian Basement Complex of southwestern Nigeria. The southwestern Nigeria pole does not coincide with younger poles for the Congo Craton for the African Plate.

Low unblocking temperatures associated with dikes and most of the rocks in the study area represent remagnetisation typified with random directions. In the baked contact test, the final phase of metamorphism and intrusions with high susceptibility values were documented. Low temperatures show unstable grains that are prone to remagnetisation, and those high temperatures ~580 ºC represent stable grains and rarely remagnetise. These finer magnetite grains with SD are stable with high relaxation times, whereas the MD grains are known for their low stability and relaxation time. Robust isochron ages of the Precambrian Basement Complex of southwestern Nigeria from Paleoproterozoic to Neoproterozoic Trans Saharan orogenic belt of Rb-Ar (Aplite/gneiss) 3000-1800 Ma. The emplacement of younger dike swarms around 572.4±8.1 Ma and 642±6 Ma ((Tugume *et al.,* 2013; Ganade *et al.,* 2016; Adetunji *et al.,* 2018). Amphibole, biotite,

hornblende could allow thermal diffusion due to closure temperature (460- 500 ºC) for primary and secondary magnetisation and agreement of U-Pb (300 ºC) and Ar-Ar (> 900 ºC) for same rock type suggest rapid cooling historyand the emplacement of dikes in the study area. The apparent Polar Wandering Path (APWP) was due to plate motion and true polar wander caused by internal geological processes (mantle convention). The continental drift starts from the South Pole and move towards the North Pole, later progresses towards the equator in an elbow-shape path. The Precambrian paleomagnetic typifies present geomagnetic field because it did not pass fold test of granitoid which are inclined to be altered. There is evidence of pronounced reverse, normal and mixed polarities in the study area. On amphibole grains from Precambrian rocks, 206Pb/207Pb techniques dated both metamorphism and magnetic resets at 571 ±6 Ma. The normal and reverse polarities found in late Neoproterozoic granitoids are coeval with the paleopole at 304.80E and 61.80S (dp = 5.4, dm = 10.7), which meet the fifth criteria of Van der vool (1990). These pole and certain primary-poles of the Congo Craton suggests an elbow-shaped apparent polar wandering path ranging from 593 to 547 Ma at the fading phases of the Pan African tectono-metamorphism which the previous works of Kalsbeek *et al.* (2013); Tugume *et al.* (2013); Lofty (2015); Chaves (2021); Sayab *et al.* (2021) in Precambrian terrain suggested.

Maghemite, titanomaghemite and hematite dominate the samples in decreasing order of magnetic susceptibility. The Fe-Ti-O is divided into two populations with diverse proportions. Maghemite (high coercivity, low susceptibility, large grains) is abundant, with a magnetisation of 43-97%. The second maghemite population has medium coercivity, intermediate magnetic susceptibility with a mixture of fine and large grains having 47% of magnetisation of Saturated Isothermal Remanent Magnetization (SIRM). Hematite has higher magnetisation, low susceptibility with 4-20% of magnetisation. Magnetite has a low coercivity, higher magnetic susceptibility, finer grains and represents 7% of magnetisation in the study area. The ChRM reside in the magnetite while the major unblocking temperature component of ChRM in the southwestern Nigeria Precambrian rocks is maghemite and titanomagnetite. The rocks recorded hard and medium fractions of SD-sized magnetite and hematite temperatures of 500 ºC - 680 ºC. The applications and limitations of the hysteresis loops were ambiguous due to mineral composition in

rock specimens, grain sizes, internal stress and magnetic interactions. Detail information on switching and interacting fields in hysteresis loops, i.e. FORCs aided characterisation of the domain phases. Interacting and non-interacting closed peak structure of SD; intermediate between MD and SD demonstrated closed and open peak contours of PSD; coarse grains parallel with Hu axis in MD and SP manifested when relaxation and averaging times correspond and Hu axis parallel and analogous to MD but behave like SD on cooling in its exponential nature due to relaxation time (Roberts *et al.,* 2000; Pike *et al.,* 2001). The implication of these MD>PSD>SD decreasing order in FORCs results imply a complex system of orogeny that is difficult to generate coherent and stable mean directions of secular variation of paleomagnetic datasets on a regional scale of the orogenic belt in the southwestern Nigeria Precambrian Basement Complex rocks.

CHAPTER FIVE
CONCLUSIONS AND RECOMMENDATIONS

5.1 CONCLUSIONS

This study involves petrology, geochronology nd paleomagnetism to characterise the space-time framework of Pan-African rocks within the Rodinia supercontinent.

For the Raman infrared spectroscopy of maghemite, simulated atoms, phonon energies, and their eigenvectors were estimated, revealing a decrease in maghemite sequence symmetry and an increase in the estimated and observed Raman-active phonons.In the course of heating, the uniqueness of magnetite and maghemite transformations; describes the rise in the Raman spectra of maghemite through estimation and observations of analogous wavenumbers of magnetite pseudomorphs that revealed its atomic origin. For instance, individual specimen of biotite granite gneiss, granite and charnockite have maghemite at strong peak spectra 519,521, 522.00 cm^{-1} and 1285.5 and weak shoulder Raman spectra at 398.8, 663, 710 and 717cm^{-1} with 830 and 785nm infra-red raman spectroscopy.

The chemical analysis of the major and trace minerals of some Precambrian rocks of southwestern Nigeria showed that iron-oxides present in biotite granite gneiss, gneiss 2, gneiss, granite, quartzite, migmatite gneiss 1, banded gneiss, granodiotite and migmatite gneiss have values of 1.26, 1.08, 6.27, 1.94, 0.10, 0.71, 5.08, 6.91 and 7.34 and electron microprobe analysis quantitatively showed that maghemite present in most of the granitoids recorded 74.6%.

The magnetic ferric-oxide was in intimate intergrowth with ilmenite which occured both in megascopic grains and minute oriented lamellae. Absence of hydrated minerals revealed that maghemite formation was a hypogene process, which occurred after

chemical closure of the iron oxide formation in the country rocks. Confinement of this oxidation process to the oxide bodies seems to be due to inter-grain diffusion and some sort of fluid conduction to the oxide bodies owing to rheological variations between them and the Precambrian rocks. Early processes of exsolution due to late magmatic oxidation generated some of the ilmenite along with precursor magnetite, the latter being subsequently oxidized to maghemite during the main oxidizing event. Incorporation of minor cations in maghemite could have stabilized it against structural inversion to hematite, and ilmenite remained stable during the oxidation of the spinel.

XRD recorded silicate and magnetite phases in the representative rock samples. The Precambrian rocks especially the granitoids revealed quartz, microcline feldspar, pyroxene, iron oxide. The pseudomorph of the magnetite phase was dominated by the maghemite. The temperature dependence (Curie temperature) of the representative Precambrian rocks of southwestern Nigeria unraveled the magnetic behavior of various rock samples studied.Granite rocks recorded 220 °C, 280 °C, 300 °C, 320 °C, 340 °C, 380 °C, 540 °C, 580 °C, 585 °C, 600 °C which implies the presence of hematite, poor (titano)magnetite and maghemite. Quartzite and banded iron formation increase susceptibility of 520 °C and 520 °C as well as 510 °C, 580 °C and 610 °C indicative of hematite, poor titanomagnetite and maghemite. Porphyritic granite 460 °C, 470 °C, 490°C, 570 °C and 580 °C demonstrating magnetic character of poor titanomagnetite and maghemite. Augen gneiss measurements recorded Curie temperature range from 380 °C, 400 °C, 500°C, 580 °C and 600 °C indicating magnetic character of poor titanomagnetite and maghemite. Banded gneiss documented 520 °C and 610 °C as well as 180 °C,400°C ,530 °C and 590 °C demonstrating magnetic character of hematite, poor titanomagnetite and maghemite. Charnockites show strong reversibility of mineralogical curves for heating and cooling recorded Curie temperature of 180 °C, 280 °C, 360 °C, 400 °C, 480 °C, 560 °C and 585 °C demonstrating magnetic character of hematite, poor titanomagnetite and maghemite. Phyllites range from 260 °C, 470°C and 560 °C demonstrating magnetic character of hematite, poor titanomagnetite and maghemite

The southwestern Precambrian rocks Paleoproterozoic/Eburnean basement: the orthogneiss has been dated at 1850 Ma using the U–Pb LA-ICP-MS process on zircon (Rahaman, 1988). The orthogneiss became somewhat gneissified during Pan-African tectono-metamorphism, and its zircons recrystallized into thin rims dated at 580 Ma, implying the time of pluton intrusion, like the elliptical study of the gneissic charnockite pluton (580 Ma). Reactivation of the Pan-African tectonics on the migmatite gneiss protolith (Eburnean graniticpluton) were not affected in numerous sites. Ifewara- Ilesha terrane, feature with granite pluton has been dated at 587 Ma.Geochemical and isotopes parameters have revealed that the Paleoproterozoic/Eburnean orthogneiss and the granite plutons represent same lithospheric source, while the Paleoproterozoic/Eburnean source became molten all throughPan-African event. Conversely, the geochemical and isotope character of Granite having alkali-calcic and large negative Nd, correlated with Pan-African tectono-metamorphism around Ifewara-Ilesha terrane, west of the shear zone (Adeoti and Okonkwo, 2017).

The appearance of various magnetic fabrics on the investigated representative rock samples showed the presence of various pluton assemblages. The Pan-African orogeny may have caused collisional magnetic fabric in the Paleoproterozoic/Eburnean gneissic pluton.The syenodiorites intrusivesfound within southwestern Precambrian belong to the Saharan metacraton, dated 642±6 Ma exhibit secondary thrusts known as syn-thrust.Moreso, they are correlated to large motions that occurred in the course of Ifewara-Ilesha shearing.The regional stressed field of granite gniess intrusion revealed its magnetic fabric in the shear zone owed to late emplacement of magmatic structures,look like that of granite. Since the plutons were formed by local distensions caused by motions along shear zones, this suggests that the Ifewara-Ilesha shear zone has been active for a long time.The Granite plutons isolated from the granite gneiss having its magnetic fabric lyingsubvertically to magnetic lineation; witnessed correlation to primary fabric to magma emplacement, which suggested the distension conditions reported by this plutonthroughout its late-magmatic evolution. Noticeable strong weathering of the rocks revealed sharp decrease of mean magnetic susceptibility, whichis owed to the late faults. The research documented two consecutive generations of faults. Firstly, NNE–SSW

orientation having pronounced influence on the magnetic fabric in the granite gneiss pluton. Secondly, NW–SE direction which do not influence remarkable magnetic fabric. The second one, obliterated the second phase of shearing especially at the shear zone, with the introduction of late Pan-African massifs, probably correlated to the southwestern Nigeria Pan-African tectono-metamorphism as well as Hoggar ranging from 575 and 555 Ma.

For the first time in southwestern Nigeria Precambrian rock; AMS revealed the internal configuration of magnetic fabrics bereft of detail structural macroscopic markers and mapping. The calc-alkaline and high-potassic feldspars in the granitic plutons suggested late tectonic emplacement due to dextral transpressive NE-to ENE.The tectonically controlled plutonemplacement along the IISZ correlate perfectly with Ediacaran high-K alkaline granitoids next to the sheared area of Patos (NEBrazil). These findings support West Gondwanas Pre-Mesozoic reconstruction hypothesis of the calc-alkaline Patos Shear zonethatconnects to the shear zone of Central Cameroon.

Conjugate fault motions down the N50°E resulted in the formation of the Precambrian mobile belt (PMB): concurrent main N-S sinistral shearing configurations with the anti-clockwise D2 activation, which were nearly annihilated by the D3 collision stage; and a secondary NE-SW concurrent dextral shearing configurations with the clockwise D3 movement. The Ifewara-Ilesha plutons were formed as a result of the reactivation of D2 collision along NE-SW and East-West fracture schemes, which resulted in the development of pull- apart structures. Dextral shear marker mechanism in mylonites and ultra-mylonites, as well as the southern and northern protomylonitization of the southwestern Nigeria basement, were all documented during the D3 collision stages and reallignement of both the PMB and its plutons respectively. Active shear zones influenced the kinematic regional emplacement of granitoids in Nigeria basement complex which correlate with the eastern to central Cameroun and NE Brazil. The Pan African mobile belt connects the marginal orogenic, low-angle fold and thrust compressive belt, and the high-angle transpressive fault belt.

The paleomagnetic pole positions of some Precambrian rocks in southwestern with respect to the orogenic events revealed true polar wander paths towards the equator during the assemblage of Rodinia supercontinent. The rocks demonstrated primary and secondary remagnetizations (normal, reversed and mixed polarities) and stability established by representative rocks of biotite granite gneiss, granite gneiss and syenite.

Amphibolite, biotite granite gneiss, granite, granite gneiss, charnockite, and banded gneiss all showed ferromagnetic grains in pilot magnetic experiments. In the decreasing order of magnetic grain size, linear acquisition plot (LAP), gradient acquisition plot (GAP), and thermal demagnetization of isothermal remanent magnetizations (IRM) with linear and gradient treatment showed the predominance of maghemite and hematite. The theoretical Day plot of magnetite, backfield remanence/hysteresis loops and first order reversal curves (FORCs) displayed SD-MD, SP-SD; MD, PSD, SP grains and narrow-waisted loops respectively.

5.2 RECOMMENDATIONS

It is recommended for future research work to study full geomagnetic vector studies on volcanic rocks for paleointensity, secular variation, excursions in Jos Plateau Nigeria.
This kind of study should be extended to regional tectonic and structural studies using multifunctional kappabridge in the laboratory to assess the microstructures and micro fabrics of any rock type. For example, lava studies can be done using dykes to investigate AMS that will give full structural dynamics and susceptibility tensors.

Future research work should also be extended to other basement complexes in Nigeria for detail Precambrian research. Multi-disciplinary approaches using numerical, seismic, paleomagnetic dataset, Fourier Transform Infrared (FTIR) spectroscopy, Raman Spectroscopy, SEM, geochronology and geochemical analysis of cored and powder samples, geared towards understanding the geodynamics of Nigeria rocks.

5.3 Contributions to Knowledge

Raman infrared spectroscopy have shown fingerprinting on specific iron-oxide

responsible for the character of the Precambrian Basement rocks which have never been utilized in the past. Preliminary microstructural- Anisotropy of Magnetic Susceptibility (AMS) of cored rock samples of southwestern Nigeria Precambrian Basement were determined in the laboratory which correlated with the dextral transpression, strain partitioning and the Ifewara-Ilesha shear zone system with the Central Cameroun and NE Brazil in this study but differ with the other Precambrian Basement rocks. Thermomagnetic- Curie temperatures and scanning electron microscopy of the studied rocks have revealed the first ever behavior of the southwestern Precambrian Basement rocks due to presence of maghemite, hematite, magnetite, ilemenite and pyrite.

Continental drifts/Apparent polar wandering paths and the pole positions of the southwestern Precambrian rock in the Pan- African orogenies demonstrated regional remagnetisation of the granitoids in the Trans- Saharan province, which suggested high mantle activity, a true polar Wander drifts towards the equator and the amalgamation of the Rodinia supercontinent.

This research work has contributed in the usage of magnetic hysteresis phases (Linear Acquisition Plot (LAP), Gradient Acquisition Plot (GAP), and thermal demagnetization of Isothermal Remanent Magnetizations (IRM) with linear and gradient treatment) to determine the decreasing order of magnetic grain size caused by the predominance of maghemite and hematite. The theoretical Day plot of magnetite, backfield remanence/hysteresis loops and First Order Reversal Curves (FORCs) in this study unlocked the single domain-multi domain, superparamagnetic, pseudo-single domain grains due to narrow- waisted loops of the Precambrian basement rocks.

REFERENCES

Abdelsalam, M. G., Liegeois, J. P. and Stern, R. J. 2002. The Saharan Metacraton. *Journal of African Earth Sciences* 34 (3-4): 119-136.

Abubakre, O. K., Sule, Y. O., and Muraina R. A. 2009. Exploring the potentilas of tailings of Bukuru Cassiterite deposit for the production of Iron ore pellets. *The journal of Minerals and mineral characterization and engineering.* Michigan.8(5):359-366.

Ade-Hall, J. M., Palmer, H. C., Hubbar, T. P. 1971. The magnetic and opaque petrological response of basalt to regional hydrothermal alteration. *Geophysical Journal of Royal Astronomical Society* 24: 137–174.

Adeoti, B. and Okonkwo, C.T. 2017. Structural evolution of Iwaraja shear zone, Southwestern Nigeria. *Journal of African earth sciences* 131:117-127.

Adetunji, A., Olarewaju V. O, Ocan O. O, Macheva L. and Ganev V. Y. 2018. Geochemistry and U-Pb zircon geochronology of Iwo quartz potassic syenite, southwestern Nigeria: Constraints on petrogenesis, timing of deformation and terrane amalgamation, *Precambrian Research* 307: 125–136.

Ajaikaiye, D. E. 1989. Densities of Rocks within the Nigerian Younger granite. In Kogbe, C. A. (Ed.): *Geology of Nigeria.* Elizabeth Publishers.

Ajibade, A. C. and Wright, J. B. 1989. The Togo-Benin-Nigeria shield: evidence of crustal aggregation in the Pan African belt. *Tectonophysic*s 65:125-129.

Ajibade, A. C. 1976. Provisional classification and correlation of the schist belts in Northwest Nigeria. In: Kogbe, C.A. (ed) *Geology of Nigeria*. Elizabethan Publication Company., Surulere, Lagos, Nigeria. 85-90.

Ajibade, A. C. 1988. Structural and tectonic evolution of the Nigerian basement with special reference to NW Nigeria. *In International Conference on Proterozoic Geology Tectonics High-Grade Terrains (Ife, Nigeria).*

Anike, L.O., Umeji, A.C. and Onyeagocha, A.C. 1990. Geology and Geochemistry of the Muro banded-iron formation, SW Plateau state, Nigeria. *Journal of Mining and Geology*26: 21-26.

Attoh, K., Hawkins, D., Bowring, S. and Allen, B. 1991. U-Pb zircon ages of gneisses from the Pan-African Dahomeyide orogen, West Africa. *EOS Transactions of the American Geophysical Union* 72: 299.

Attoh, K., Dallmeyer, R. D. and Affaton, P. 1997. Chronology of nappe assembly in the Pan-African Dahomeyide orogen, West Africa: evidence from 40Ar/39Ar mineral ages. *Precambrian Research* 82 (1-2): 153-171.

Baldim, M.R. and Oliveira, E.P., 2021. Northeast Sao Francisco craton and West-Congo craton linked before the Rhyacian (2.10-2.04 Ga) orogeny: Evidences from provenance and U-Pb ages of supracrustal rocks from The Rio Capim greenstone belt, Serrinlia Block, *Precambrian Research* 352: 105985

Berger, J., Caby, R., Liégeois, J. P., Mercier, J. C. C. and Demaiffe, D. 2011. Deep inside a Neoproterozoic intra-oceanic arc: growth, differentiation and exhumation of the Amalaoulaou complex (Gourma, Mali). *Contribution Mineralogy Petrology* 162:773–796

Besse, J., Courtillot, V., 2002. Apparent and true polar wander and the geometry of the geomagnetic field over the last 200 Myr. *Journal of Geophysical Research: Solid Earth*107: EPM 6-1-EPM 6-31.

Bina, M., and Henry, B. 1990. Magnetic properties, opaque mineralogy and magnetic

anisotropies of serpentinized peridotites from ODP hole 670A near Mid-Atlantic ridge. *Physics of the Earth and Planetary Interiors* 65: 88–103.

Bispo-Santos F., D'Agrella-Filho, M.S., Trindade, R. I. F., Elming, S., Janikian, L., Vasconcelos, P.M., Perillo, B.M., Perga, I., da Silva, J.A., Barros, M. A. D. A. 2012. Tectonic implications of the 1419Ma Nova Guarita mafic intrusives paleomagnetic pole (Amazonian Craton) on the longevity of Nuna, *Precambrian Research* 196-197:1-22, DOI:10.1016/j.precamres.2011.10.022

Black, R., Caby, R., Moussine-Pouchkine, A., Bayer, R., Betrand, J. M., Boullier, M. M., Fabre, J. and Resquer, A. 1979. Evidence for late Precambrian plate tectonics in West Africa. *Nature* 278 (5701): 223-227.

Black, R. L., Latouche, J., Liegeois, Caby, R. and Bertrand, J. M. 1994. Pan-African displaced terranes in the Tuareg shield (central Sahara). *Geology* 22 (7): 641-644.

Black, R. and Liégeois, J. P. 1993. Cratons, mobile belts, alkaline rocks and continental lithospheric mantle: The Pan-African testimony. *Journal of Geological Society* London. 150: 89–98.

Borradaile G. J. and Craig, A**.** 1987. Relationship between magnetic susceptibility and strain in laboratory experiments Tectonophysics, 133 (1-2): 121-135.

Brookfield, M. E. 1993. Neoproterozoic Laurentia-Australia fit. *Geology*, 21 (8): 683-686.

Brown, L. L and McEnroe, S. A. 2015. 916 Ma Pole for southwestern Baltica: palaeomagnetism of the Bjerkreim-Sokndal layered intrusion, Rogaland Igneous Complex, southern Norway *Geophysical Journal International* 203: 567–587.

Butler, R. 1992. *Paleomagnetism.* Blackwell Scientific, Cambridge, 319 p.

Caby R, Betrand, J. M. L and Black, R. 1989. Pan-African ocean closure and continental collision in the Hogger-Iforas segment, central sahara. (Kroner A ed.) *Precambrian plate tectonics*Elsevier Amsterdam. 407-437.

Caby, R. 2003. Terrane assembly and geodynamic evolution of central–western Hoggar: a synthesis. *Journal of African Earth Sciences* 37: 133–159

Caby, R. and Boesse J. M. 2001. Pan-African Nappe System in South-West Nigeria: 'Ife lle-llesha Schist Belt.*Journal African. Earth Sciences*,33 (2). 21 I-225.

Caen-Vachette, M. and Umeji, A. C. 1983. Whole-rock Rb–Sr dating of two monzogranites in southern Nigeria and their implications on the age of the Pan-African orogenic cycle. *Journal of African Earth Sciences* 1: 339–342.

Canon-Tapia, E. and Herrero-Bervera, E. 2009. Sampling strategies and the anisotropy of magnetic susceptibility of dykes, *Tectonophysics* 466(1-2): 3-17.

Carporzen, L., Gilder, S. A., Hart, R. J. 2006. Origin and implications of Verwey transitions in the basement rocks of the Vredefort meteorite crater, South Africa. *Earth Planetary Science Letters* 251: 305–317.

Chadima, M. and Hrouda, F. 2006. Remasoft 3.0 a user friendly paleomagnetic data browser and analyser. *Travaus Geophysiques* 27: 20-21.

Chamritski, I. and Burns, G. 2005. Infrared- and Raman-active phonons of magnetite, maghemite, and hematite: A computer simulation and spectroscopic study. *Journal of Physical Chemistry B* 109: 4965–4968.

Chaves, A.D.O. 2021. Columbia (Nuna) supercontinent with external subduction girdle and concentric accretionary collisional and intracontinental orogens permeated by large igneous provinces and rocks. *Precambrian Research* 352: 106017.

Chen,L. D. Heslop, A. P., Roberts,L., Chang, X., Zhao, H. V., McGregor,G., Marino, L., Rodriguez-Sanz,E. Rohling, J. and Palike H. 2017. Remanence acquisition efficiency inbiogenic and detrital magnetite andrecording of geomagneticpaleointensity, *Geochemistry Geophysics. Geosystem*., 18, doi:10.1002/2016GC006753.

Collinson, D. W., 1983. *Methods in Rock Magnetism and Palaeomagnetism: Techniques and Instrumentation*. New York: Chapman & Hall.

Condie, K. C. 2002a. Breakup of a Paleoproterozoic Supercontinent. *Gondwana Research,* 5 (1): 41-43.

_____, 2002b. The supercontinent cycle: are there two patterns of cyclicity? *Journal of African Earth Sciences* 35 (2): 179-183.

Cooray, I. G. 1974. *The charnockitic rocks of Nigeria*. Pitchamutu volumes. Banglandese university, India, 5073p.

D'Agrella-Filho, M. S., Trindade, R. I. F., Queiroz, M. V. B., Meira, V. T., Janikian, L., Ruiz, A. S. and Bispo-Santos, F. 2016. Reassessment of Aguapeí (Salto do Céu) Paleomagnetic pole of the Amazonian Craton and implications for Proterozoic supercontinents. *Precambrian Research* 272: 1-17.

Dada, S. S. 2008. Proterozoic evolution of the Nigeria-Boborema province. *Geological Society, London, Special Publications* 294 (1): 121-136.

Dada, S. S. 1998. Crust-forming ages and Proterozoic crustal evolution in Nigeria: a reappraisal of current interpretations. *Precambrian Research* 87: 65–74.

Dada, S. S. 2006. Proterozoic evolution of Nigeria. In: Oshin, O. (Ed.), *The Basement Complex of Nigeria and its Mineral Resources* (A Tribute to Prof. M. A. O. Rahaman). Akin Jinad & Co., Ibadan, 29–44.

Dada, S. S., Lancelot, J. R., Briqueu, L., 1989. Age and origin of the annular charnockitic complex at Toro, Northern Nigeria: U–Pb and Rb–Sr evidence. *Journal of African Earth Sciences* 9: 227–234.

Dada, S. S. and Respaut, J. P. 1989. La monzonite a` fayalite de Bauchi (bauchite), nouveau te´moin d'un magmatisme syntectonique panafricain au nord du Nige´ria. *Comptes Rendus de l'Acade´mie des Sciences* Paris 309: 887–892.

Dada, S. S., Tubosun, I. A., Lancelot, J. R., and Lar, A. U. 1993. Late Archean U–Pb age for the reactivated basement of Northeastern Nigeria. *Journal of African Earth Sciences* 16: 405–412.

Dalziel, I. 1997. Neoproterozoic-Paleozoic geography and tectonics: Review, hypothesis, environmental speculation. *GSA Bulletin* 109 (1): 16-42.

Day, R., Fuller, M. and Schmidt, V. A. 1977. Hysteresis properties of titanomagnetites:grain size and compositional dependence. *Physics of the Earth Planetary Interior* 13: 260-267.

De Waele, B., Johnson, S. and Pisarevsky, S. 2008. Palaeoproterozoic to Neoproterozoic growth and evolution of the eastern Congo Craton: Its role in the Rodinia puzzle. *Precambrian Research 160* (1-2): 127-141.

deFaria, D. L. A., Silva, S. V., and deOliveira, M. T. 1997. Raman microspectroscopy of some iron oxides and oxyhydroxides. *Journal of Raman Spectroscopy* 28: 873–878.

Deynoux, M., Affaton, P., Trompette, R. and Villeneuve, M. 2006. Pan-African tectonic evolution and glacial events registered in Neoproterozoic to Cambrian cratonic and foreland basins of West Africa. *Journal of African Earth Sciences* 46 (5): 397-426.

Dunlop, D. J. 2002a. Theory and application of the Day plot (Mrs/Ms versus Hcr/Hc). Theoretical curves and tests using titanomagnetite data. *Journal of Geophysical Research* 107.http://dx.doi.org/10.1029 /2001J B000486.

_, 2002b. Theory and application of the Day plot (Mrs/Ms versus Hcr/Hc), application to data for rocks, sediments and soils. *Journal of Geophysical Research* 107. http://dx.doi.org/10.1029/2001JB000487.

Dunlop, D.J. and Özdemir, Ö. 1997. *Rock Magnetism*: Fundamentals and Frontiers. Cambridge University Press, New York/London/Cambridge, 573 pp.

Eagles, G. 2007. New angles on South Atlantic opening. *Geophysical Journal International* 168 (1): 353-361.

Ekwueme, B. N. and Kro¨ner, A. 1998. Single zircon evaporation ages from the Oban Massif, southeastern Nigeria. *Journal of African Earth Sciences* 26: 195–205.

Eludoyin, O.M., Adelekan, I.O., Webster, R. and Eludoyin, A.O. 2013. Air temperature, relative humidity, climate regionalization and thermal comfort of Nigeria. *International journal of climatology* 34(6) https://doi.org/10.1002/joc.3817

Evans, M.E., 1976. Test of dipolar nature of the geomagnetic field throughout Phanerozoic time *Nature* 262,676-677

Evans, D. A. D., 2009. The palaeomagnetically viable, long-lived and all-inclusive Rodinia supercontinent reconstruction. *Geological Society, London, Special Publications* 327 (1): 371-404.

Ferre, E., Gleizes, G. and Caby, R. 2002. Obliquely convergent tectonics and granite emplacement in the Trans-saharan belt of Eastern Nigeria: a synthesis, *Precambrian Research* 114: 199-219.

Ferre, E., Gleizes, G., and Caby, R. 2002. Obliquely convergent tectonics and graniteemplacement in the Trans-Saharan belts of Eastern Nigeria: a synthesis.*Precambrian Research* 11: 199-219.

Ferre´, E., De´le´ris, J., Bouchez, J. L., Lar, A. U. and Peucat, J. J., 1996. The Pan-African reactivation of contrasted Eburnean and Archaean provinces in Nigeria: structural and isotopic data. *Journal of the Geological Society* London 153: 719–728.

Fisher, R., 1953. Dispersion on a sphere. *Proceedings of Royal Society* 217: 295–305.

Ganade, C. E., Cordani, U. G., Agbossoumounde, Y., Caby, R., Basei, M. A. S., Weinberg, R. F. and Sato K. 2016. Tightening Ne Brazil and Nw Africa connections: New U –Pb/Lu-Hf zircon data of a complete plate tectonic cycle in the Dahomey belt of the West Gondwana orogen in Togo and Benin.*Precambrian research* 276, 24-42.

Gehring, A. U., Fischer, H. Louvel, M., Kunze, K. and Weilder P. G. 2009. High temperature stability of natural maghemite: a magnetic and spectroscopic study. *Geophysical Journal International* 179, 1361–1371doi: 10.1111/j.1365-246X.2009. 04348.x

Geoffroy, L., Callot, J. P., Aubourg, C. and Moreira, M. 2002. Magnetic and plagioclase linear fabric discrepancy in dykes: a new way to define the flow vector using magnetic foliation https://doi.org/10.1046/j.1365-3121.2002.00412.x

Goscombe, B., Hand, M. and Gray, D. 2003a. Structure of the Kaoko Belt, Namibia:

progressive evolution of a classic transpressional orogen. *Journal of Structural Geology* 25 (7): 1049-1081.

Goscombe, B., Hand, M. and Gray, D. 2003b. The Metamorphic Architecture of a Transpressional Orogen: The Kaoko Belt, Namibia. *Journal of Petrology* 44 (4): 679-711.

Gower, C. F. 1996. The evolution of the Grenville Province in eastern Labrador, Canada. *Geological Society, London, Special Publications* 112 (1): 197-218.

Grant, N. K. 1978. Geochronology of the Precambrian basement complex rocks from Ibadan southwest Nigeria. *Earth and planetary science letters* 10: 19-38.

Gray, D. R., Foster, D. A., Meert, J. G., Goscombe, B. D., Armstrong, R. Trouw, R. A. J. and Passchier, C. W. 2008. A Damara orogen perspective on the assembly of southwestern Gondwana. *Geological Society, London, Special Publications* 294 (1): 257-278.

Halls, H. C. 1978.The use of converging remagnetization circles in *paleomagnetism*. *Physics of the Earth and Planetary Science* 16: 1-11.

Hanesh, M. 2009. Raman spectroscopy of iron oxides and (oxy)hydroxides at low laser power and possible applications in environmental magnetic studies *Geophysical Journal International* doi: 10.1111/j.1365-246X.2009. 04122.x 177: 941–948

Hanson, R. E., 2003. Proterozoic geochronology and tectonic evolution of southern Africa. *Geological Society, London, Special Publications* 206 (1): 427-463.

Hartstra, R. L. 1982. Grain size dependence of initial susceptibility and saturation magnetization-related parameters of four natural magnetites in the PSD-MD range. *Geophysical Journal of the Royal Astronomical Society* 71: 477–495.

Henry, B., Merabet, N., Derder, M.E.M., Bayou, B. 2004. Chemical remagnetizations in the Illizi basin (Saharan craton, Algeria) *Geophysical Journal International* 156: 200–212

. Herrero-Bervera, E., Canon-Tapia, E., Walker, G. P. L. and Guerrero-García, J. C. 2002. The Nuuanu and Wailau giant landslides: insights from paleomagnetic and anisotropy of magnetic susceptibility (AMS) studies.*Physics of the Earth and Planetary Interiors* 129 (1-2): 83-98

Hirdes, W. and Davis, D. W. 2002. U-Pb zircon and rutile metamorphic ages of Dahomeyan garnet-hornblende gneiss in southeastern Ghana, West Africa. *Journal of African Earth Sciences* 35 (3): 445-449.

Hoffman, P. 1991. Did the Breakout of Laurentia Turn Gondwanaland Inside-Out? *Science* 252: 1409-1412.

Hyodo H and Dunlop, D. J. 1993. Effect of anisotropy on the paleomagnetic contact test for a Grenville dike. *Journal of Geophysical Research* 98 (B5): 7997-8017.

International Geological Timescale 2002. International Stratigraphic Chart, Remane, J. Cita, M.B. Dercourt, J. Bouysee, P. Repetto, F. Faure-Muret, A (eds.),International Union of Geological sciences: International Commision on Stratigraphy, Paris, 2002

Ivanov, B. A. 2005. Numerical modeling of the largest terrestrial meteorite craters. *Solar System Research* 39: 381–409.

Jelinek, V. 1977. The statistical theory of measuring anisotropy of magnetic susceptibility of rocks and its applications. Brno, *Geopfyzika*1-88.

Jelinek, V.1981. Characterisation of the magnetic fabric of rocks. *Tectonophysics*79, 63-

John, T., Schenk, V., Haase, K., Scherer, E. and Tembo, F. 2003. Evidence for a Neoproterozoic ocean in south-central Africa from mid-oceanic-ridge-type geochemical signatures and pressure-temperature estimates of Zambian eclogites. *Geology* 31 (3): 243-246.

Kalsbeek, F., Affaton, P., Ekwueme, B., Freid, R. and Thranea, K. 2012. Geochronology of granitoid and metasedimentary rocks from Togo and Benin, West Africa: comparisons with NE Brazil. *Precambrian Research* 196–197: 218–233.

Kalsbeek F., Ekwueme B.N., Penayec, J. de Souzad, Z.S., Thranea K. 2013. Recognition of Early and Late Neoproterozoic supracrustal units in West Africaand North-East Brazil from detrital zircon geochronology *Precambrian Research* 226, 105– 115

Key, R., Liyungu, A., Njamue, F., Somwe, V., Banda, J. Mosley, P. and Armstrong, R. 2001. The western arm of the Lufilian Arc in NW Zambia and its potential for copper mineralization. *Journal of African Earth Sciences* 33: 503-528.

Kirschvink, J. L. 1980. The least-squares line and plane and the analysis of palaeomagnetic data. *Geophysical journal of Royal Astronomical Society*. 62 (3): 699–718

Klein, E. L. and Moura, C. A. *V.* 2008. Sao Luis Craton and Gurupi Belt (Brazil): possible links with the West African Craton and surrounding Pan-African belts. *Geological Society, London, Special Publications* 294 (1): 137-151.

Krása, D. and Herrero-Bervera, E. 2005. Alteration induced changes of magnetic fabric as exemplified by dykes of the Koolau volcanic range. *Earth and Planetary Science Letters* 240 (2): 445-453.

Kröner, A., Ekwueme, B. N. and Pidgeon, R. T. 2001. The Oldest Rocks in West Africa: SHRIMP Zircon Age for Early Archean Migmatitic Orthogneiss at Kaduna, Northern Nigeria. *Journal of Geology* 109: 399–406.

Kruiver, P. P., Dekkers, M.J. and Heslop, D. 2001. Quantification of magnetic coercivity components by the analysis of the acquisition of curves of isothermal remanent magnetization *Earth and planetary science letters* 189: 269-276.

Kuster, D., 1995. Rb–Sr isotope systematics of muscovite from Pan-African pegmatites of Western and Northeastern Africa. *Mineralogy and Petrology* 55: 71–83.

Kwekam, M., Liegeois, J. P., Njonfang, E., Affaton, P., Hartmann, G. and Tchoua, F. 2010.origin and significance of the Fomopea Pan-African high-K calc-alkaline.*Nature*:79-95.

Langereis C.G., Linssen J.H., Mullender T.A.T., Zijderveld J.D.A. 1989. Demagnetization. In: *Geophysics*. Encyclopedia of Earth Science. Springer, Boston, Massachusetts. https://doi.org/10.1007/0-387-30752-4_23

Lar, U. A. 1988. Ge´ochronologie U-Pb sur zircons et monazites de l'encaissant (orthogneiss, migmatite) du Complexe charnockitique de Toro (Nigeria). unpublished MSc Thesis. 93 p., Universite´ des Sciences et Techniques du Languedoc, Montpellier.

Liégeois, J. P., Latouche, L., Boughrara, M., Navez, J. and Guiraud, M., 2003. The LATEA metacraton (Central Hoggar, Tuareg shield, Algeria): behaviour of an old passive margin during the Pan-African orogeny. *Journal of African Earth Science* 37: 161–190.

Lindsley, D. H. 1976. The crystal chemistry and structure of oxide minerals as exemplified by the Fe-Ti oxides. In D. Rumble III, Ed., Oxide Minerals, 3, p. L1–

L60. *Reviews in Mineralogy*, Mineralogical Society of America, Chantilly, Virginia.

_____1991. Experimental studies of oxide minerals. In D.H. Lindsley, Ed., Oxide Minerals: Petrologic and magnetic significance, 25, p. 69–106. *Reviews in Mineralogy*, Mineralogical Society of America, Chantilly, Virginia.

Lofty, H.I. 2015. Early Cretaceous counterclockwise rotationof Northeast Africa within the equatorial zone:Paleomagnetic study on Mansouri ring complex,Southeastern Desert**,** Egypt, *NRIAG Journal of Astronomy and Geophysics* 2015, http://dx.doi.org/10.1016/j.nrjag.2015.01.001

Lowrie, W. 2007. *Fundamentals of Geophysics* 2nd Edition, Cambridge University Press, New York, USA, 374p.

Lowrie, W. and Fuller M. 1971. On the alternating field demagnetization characteristics of multidomain thermoremanent magnetization in magnetite, *Journal of Geophysical Research***,** 76**,** 6339– 6349.

McElhinny M. W. and McFadden, P. L. 2000. "*Paleomagnetism, Continents and Oceans,"* Academic Press, International Geophysics Series, San Diego, 73: 382p.

Ma, J. and Chen, K. 2018. Origin of unusual thermomagnetic behaviors in maghemite. Journal of *Physics and Chemistry of Solids* 112: 88–93.

Magnetic hysteresis (Retrieved on 5/15/20 electricalacademia www.theoretica.us)

Matteini, M., Junges, S. L., Dantas, E. L., Pimentel, M. M. and Bühn, B. 2010. In situ zircon U–Pb and Lu–Hf isotope systematic on magmatic rocks: insights on the crustal evolution of the Neoproterozoic Goiás Magmatic Arc, Brasília belt, Central Brazil. *Gondwana Research*. 17: 1–12

McCurry, P. and Wright, J. B. 1971. On place and time orogenic granite plutonism. *Geology society of American Bullettin*, 82: 1476-1713.

McElhinny, M. W., McFadden, P. L., and Merrill, R.T., 1996. The time averaged field 0-5 Ma. *Journal of Geophysical research* 101, 25, 007- 25,027, doi: 10.1029/96JB01911

McElhinny, M. W. and Senanayake, W. E. 1982. Variation in the geomagnetic dipole 1: the past 50000 years. *Journal of Geomagnetism and Geoelectricity* 34: 39–51.

McEnroe, S.A., Brown, L.L., Robinson, P. 2004. Earth analog for Martian magnetic anomalies: remanence properties of hemo-ilmenite norites in the Bjerkreim-Sokndal intrusion, Rogaland, Norway. *Journal of Applied Geophysics* 56: 195–212.

McFadden, P. L. and McElhinny, M. W. 1990. Classification of the reversal test in palaeomagnetism. *Geophysical Journal International* 103 .3: 725–729.

Meert, J. and Lieberman, B. 2008. The Neoproterozoic assembly of Gondwana and its relationship to the Ediacaran-Cambrian radiation. *Gondwana Research* 14: 5-21.

Meert, J., Van der Voo, R. and Ayub, S. 1995. Paleomagnetic investigation of the Neo-proterozic Gagwe lavas and Mbozi complex, Tanzania and the assembly of Gondwana. *Precambrian Research* 74: 225-244.

Miller, R. B. and Paterson, S. R. 1999. In defense of magmatic diapirs. J*ournal of structural Geology* 21: 1161 – 1173.

Moores, E. M. 1991. Southwest U.S.-East Antarctic (SWEAT) connection: A hypothesis. *Geology* 19. 5: 425-428.

Muxworthy, A. R., Dunlop, D. J. and O'zdemir, O' 2003. Low-temperature cycling of isothermal and anhysteretic remanence: Microcoercivity and magnetic memory, *Earth Planetary Science Letters*205**:** 173–184.

Nadeem, K., Krenn H. and Szabó D. V. 2015. Memory effect versus exchange bias for maghemite nanoparticles *Journal of Magnetism and Magnetic Materials* 393: 239–242.

Neves, S. P., Bruguier, O., Bosch, D., da Silva, J. M. R. and Mariano, G. 2008. U-Pb ages of plutonic and metaplutonic rocks in southern Borborema Province (NE Brazil): Timing of Brasiliano deformation and magmatism. *Journal of South American Earth Sciences* 25.3: 285-297.

Nigerian Geological Survey Agency (NGSA) 2010. Geological map of Nigeria 1:250,000, Abuja Nigeria.

Ngako, V. and Njonfang, E. 2011. *Plates Amalgamation and Plate Destruction, the Western Gondwana History, Tectonics*, Damien, C. (Ed.), ISBN: 978-953-307-545-7, InTech, Available from:http://www.intechopen.com/books/tectonics/plates-amalgamation-and-plate-destruction-the-westerngondwana-history.

Njonfang, E., Ngako, V., Moreau, C., Affaton, P. and Diot, E. 2008. Restraining bends inhigh temperature shear zones: the ''Central Cameroon Shear Zone", CentralAfrica. J*ournal of African Earth Science.* 52: 9-20

Nutman A. P.,Bennett, V.C. and Friend, C.R.L.,2017. Seeing through the magnetite: Reassessing Eoarchean atmospherecomposition from Isua (Greenyyyuyuland) 3.7 Ga banded iron formations*Geoscience Frontiers*8: 1233-1240

Nzenti, J. P., Barbey, P., Macaudiere, J. and Soba, D. 1988. Origin and evolution of the Late Precambrian high-grade Yaounde gneisses (Cameroon). *Precambrian research* 38: 91-109.

Obaje, N. G. 2009. *Geology and Mineral Resources of Nigeria.* Lecture Notes in Earth Sciences Springer Verlag, Berlin, 221p

Obiora, S. C. 2005. *Field Descriptions of Hard Rocks with examples from the Nigerian Basement Complex* (1st ed.) Snap Press (Nig.) Ltd. Enugu, 14p.

_____2008. *Geology and Mineral Resources of the Precambrian Basement Complex of Nigeria*. A talk presented at the National Geophysical Research Institute, Hyderabad, India on 25th November 2008 as a CSIR- TWAS Postdoctoral Fellow.

Odeyemi, I. 2005. A review of the ororgenic events in the Precambrian basement of Nigeria, West Africa. *International journal of earth sciences* Springer Berlin/Heidelberg, 70.3: 897-909.

Okonkwo, C. T. and Ganev, V. Y. 2012. U-Pb zircon geochronology of the Jebba granitic gneiss and its implications for the Paleoproterozoic evolution of Jebba area, southwestern Nigeria. *International Journal of Geoscience* 3: 1065–1073.

Oloche, O. B., Sirajo, M. Z., Suleiman, I. Y and Onche, E. 2009. Characterization of Koton-Karfe iron ore pellets for pig iron production in Nigeria, *Nigerian journal of clinical practice* 15. 2: 89-96.

Oniku, A. S., Osazuwa, I. B. and Meludu, O. C. 2008. Determination of emplacement direction of Zaria granite batholith using anisotropy of magnetic susceptibility (AMS) method *Nigerian journal of Physics* 20.1:189-197

Onyeagocha, A.C. and Ekwueme, B.N., 1990. Temperaturepressure distribution patterns in metamorphosed rocks ofthe Nigerian Basement Complex a preliminary analysis. *Journal African Earth Sciences* 11: 83-93.

Opdyke, N.D. and Channell, J.E.T. 1996. Magnetic Stratigraphy.San Diego, CA: Academic Press.

Osazuwa, I. B., Meludu, O. C., and Oniku, A. S. 2008. Preliminary studies on temperature dependence of magnetic susceptibility of some rocks within the northwestern part of northen Nigeria basement complex. *Nigerian journal of Physics* 20.1: 198-205

Oversby, V. M. 1975. Lead Isotopic Study of Aplites from the Precambrian Basement Rocks near Ibadan, Southwestern Nigeria. *Earth Planet. Science Letters*. 27: 177-180.

Oyawoye, M. O. 1964. The Geology of the Nigeria Basement Complex, Journal of. *Nigeria Mining Geoogy and Meteorological Society*1. 2: 87-102

_____ 1972. *The basement complex of Nigeria in African geology* edited by T. F. J Dessau Vagie and Whiteman. University of Ibadan Press 66-102

Percival, J.J., Konopacek, J., Eresland, R., Slama, J., De Campos R.S., Battisti, M.A., and Bitencourt, M.D.F. 2021. Preorogenic connection of the foreland domains of the Kaoko-Dom Feliciano- Gariep orogenic system. *Precambrian Research* 354: 106060

Pidgeon, R. T., Van Breemen, O. and Oyawoye, M. O. 1976. Pan-African and earlier events in the Basement Complex of Nigeria, *Proceedings of 25th International Geological Congress Sydney* Australia. 3: 667.

Pisarevsky, S. A., M. T. D. Wingate, C. M. Powell, S. Johnson, and D. A. D. Evans,

2003. Models of Rodinia assembly and fragmentation. *Geological Society, London, Special Publications,* 206 (1): 35-55.

Rahaman, M. A. 1976. Review of the Basement Geology of Southwestern Nigeria. In: *Geology of Nigeria* (Kogbe, C. A. ed.) Elizabethan Publication Company Lagos, 41- 48.

_____1988. Recent advances in the study of the Basement Complex of Nigeria. In: Oluyide, P.O., Mbonu, W.C., Ogezi, A.E., Egbuniwe, I.G., Ajibade, A.C., Umeji, A. C. (Eds.), *Precambrian Geology of Nigeria*. Geological Survey of Nigeria special publication, pp. 11–41.

Rahaman, M.A., Tubosun, I.A., Lancelot, J.R. 1991. U-Pb geochronology of potassic syenites from SW Nigeria and the timing of deformation events during the Pan African Orogeny. *Journal African Earth Sciences* 13:387-395

Rahaman, M.A.O., Ajayi, T.R., Oshin, l.O. and Asubiojo. E.O.L, 1988. Trace clement geochemistry and geotcctonic setting of lle-llcsha Schist Belt. *Precambrian. Geology of Nigeria,* L 241-256.

Rahaman, M. A. O. and Ocan. O. O. 1978. On Relationship in the Precambrian Migmatite Gneiss of Nigeria.*Journal of Mining and Geology.* 15.1: 23-30.

Raposo, M. I. B. and Gastal M. C. P.,2009. Emplacement mechanism of the main granite pluton of the Lavras do Sul intrusive complex, South Brazil, determined by magnetic anisotropies *Tectonophysics* 466: 18–31

Reshetnyak, M. Y. and Pavlov, V. E. 2016. Evolution of the dipole geomagnetic field. Observations and models. *Geomagnetism and Aeronomy* 56: 110-124.

Roberts, A. P., Pike, C. R. and Verosub, K. L. 2000. First-order reversal curve diagrams: anew tool for characterizing the magnetic properties of natural samples. *Journal ofGeophysicalResearch.* 105: 28461-28475

Roberts, A. P., Almeida, T. P., Church, N. S., Harrison, R. J., Heslop, D., Li, Y., Muxworthy A.R.., Williams, W., Zhao, X. (2017). Resolving the origin ofpseudo-single domain magneticbehavior. *Journal of Geophysical Research: Solid Earth*, 122, 9534–9558.https://doi.org/10.1002/2017JB014860

Rogers, J. J. W. and Santosh, M. 2002. Configuration of Columbia, a Mesoproterozoic Supercontinent. *Gondwana Research* 5. 1: 5-22.

Rogers, J. J. W. 1996. A History of Continents in the past Three Billion Years. *The Journal of Geology* 104. 1: 91-107.

Rohrbach, A., Ballhaus, C., Golla-Schindler, U., Ulmer, P., Kamenetsky, V. S., and Kuzmin, D. V. .2007 Metal saturation in the upper mantle. *Nature* 449: 456–458.

Sagnotti, L. 2013. Demagnetization Analysis in Excel (DAIE). An open source workbook in Excel for viewing and analysis in demagnetization data from Plaeomagnetic discrete samples. *Annals of Geophysics* 56. 1: 0114.

Salminen, J., Klein, R. and Mertanen, S. 2018. New rock magnetic and paleomagnetic results for the 1.64 Ga Suomenniemi dyke swarm, SE Finland. doi: https://doi.org/10.1016/ *Precambrian Research* 2018.01.001.

Salminen J, Klein, R and Mertanen, S., 2019. New Rock magnetic results for the 1.64 Ga suomenniemi dyke swam, SE Finland *Precambrian Research* 329: 195-210

Sayab, M, Lahtinen, R., Koykka, J., Holtta P., Karinen, J., Niiranen, T. and Levaniemi, H. 2021. Improved resolution of Paleoproterozoic orogenesis: multidirectional

collision tectonic in the sodankyla belt of northern Finland *Precambrian Research* 359: 106193

Serna, C. J., Rendon, J. L. and Iglesias, J. E.1982. Infrared surface modes in corundum-type microcrystalline oxides. *Spectrochimica Acta Part A: Molecular Spectroscopy* 38. 7: 797-802.

Shebanova, O.N. and Lazor, P. 2003a. Raman spectroscopic study of magnetite ($FeFe_2O_4$): a new assignment for the vibrational spectrum. *Journal of Solid State Chemistry* 174: 424–430.

_____,2003b. Raman study of magnetite (Fe3O4): laser-induced thermal effects and oxidation. *Journal of Raman Spectroscopy* 34: 845–852.

_____,2003c. Vibrational modeling of the thermodynamic properties of magnetite (Fe3O4) at high pressure from Raman spectroscopic study. *Journal of Chemical Physics* 119: 6100–6110.

Slavov, L., Abrashev, M.V., Merodiiska, T., Gelev, Ch., Vandenberghe, R.E., Markova-Deneva, I., Nedkov, I. 2010. Raman spectroscopy investigation of magnetite nanoparticles in ferrofluids, *Journal of Magnetism and Magnetic Materials* doi:10.1016/j.jmmm.2010.01.005

Snelling, N. J., 1964. Age Determination Unit. *Institution of Geological Science*. Annual Report, 30–40.

Stacey, F.D. and Banerjee, S.K. 1974**.** The Physical Principles in Rock Magnetism.Amsterdam: Elsevier, 195 pp

Stern, R. J. 2008. Neoproterozoic crustal growth: The solid Earth system during a critical episode of Earth history. *Gondwana Research* 14.1-2: 33-50.

Studfile 2016. Characterization of magnetic hysteresis. www.studfile.net

Tack, L., Wingate, M. T. D., De Waele, B., Meert, J., Belousova, E., Griffin, B., Tahon, A. and Fernandez-Alonso,M. 2010. The 1375 Ma "Kibaran event" in Central Africa: Prominent emplacement of bimodal magmatism under extensional regime. *Precambrian Research* 180. 1-2: 63-84.

Tarduno, J. A., and Mamajek E.E. 2014. Detecting the oldest geodynamo and attendant shielding from the solar *Physics of the earth and Planetary Interiors*, 233, 68-87.

Tarling, D. H. and Hrouda, F. 1993. *The Magnetic Anisotropy of Rocks*; Chapman and Hall, London, 213p

Tavares, F. M. 2015. Evolução Geotectônica do Nordeste da Província Carajás. Tese de Doutorado, Instituto de Geociências, Universidade Federal do Rio de Janeiro, 115p.

Toteu, S. F, Penaye, J., and Djomani, Y. P. 2004. Geodynamic evolution of the Pan-African belt in central Africa with special reference to Cameroon. *Canadian Journal of Earth Sciences* 41: 73-85.

Toteu, S. F., Van Schmus, R. W., Penaye, J. and Micharda, 2001. New U-Pb and Sm-Nddata from North-Central Cameroon and its bearing on the Pre-Pan-Africanhistory of Central Africa. *Precambrian. Research* 108: 45-73.

Tougarinov, A. I., Knorre, K. G., Shanin, L. L., Prokofieva, L. N., 1968. The geochronology of some Precambrian rocks of southern West Africa. *Canadian Journal of Earth Sciences* 5: 639–642.

Trompette, R. 1994.*Geology of Western Gondwana (2000-500 Ma). Pan-African-Brasiliano aggregation of South America and Africa*. Balkema, A.A., Rotterdam, 350p.

Tubosun, I. A., Lancelot, J. R., Rahaman, M. A., Ocan, O., 1984. U -Pb Pan African ages of two charnockite-granite association from southwestern Nigeria. *Contribution to Mineralogy and Petrology* 88: 188-195.

Tugume, F., Nyblade A., Julià, J., van der Meijde, M.,2013. Precambrian crustal structure in Africa and Arabia: Evidence lacking forsecular variation*Tectonophysics* 609: 250–266

Usui, Y., Tarduno, J.A., Watkeys, M., Hofmann, A., Cottrell, R.D., 2009. Evidence for a 3.45-billion-year-old magnetic remanence: Hints of an ancient geodynamo from conglomerates of South Africa. *Geochemistry, Geophysics, Geosystems* 10,Q09Z07.

Valeriano, C. M., Pimentel, M. M., Heilbron, M., Almeida, J. C. H., and Trouw, R. A. J. 2008. Tectonic evolution of the Brasilia Belt, Central Brazil, and early assembly of Gondwana. *Geological Society, London, Special Publications,* 294. 1: 197-210.

Van Der Voo, R., 1990. The reliability of paleomagnetic data. *Tectonophysics* 184. 1:1–9.

van Schmus, W. R., Oliveira, E. P., da Silva Filho, A. F., Toteu S. F., Penaye, J. and Guimaraes, I. P. 2008. Proterozoic links between the Borborema Province, NE Brazil, *and* the Central African Fold Belt. *Geological Society, London, Special Publications* 294.1: 69-99.

Veikkolainen, T., Pesonen, L., Korhonen, K. 2014c. An analysis of geomagnetic field reversals supports the validity of the Geocentric Axial Dipole (GAD) hypothesis in the
Precambrian. *Precambrian Research* 244: 33-41.

Weil, A. B., Van der Voo, R., Mac Niocaill, C. and Meert, J. G. 1998. The Proterozoic supercontinent Rodinia: paleomagnetically derived reconstructions for 1100 to 800

Ma. *Earth and Planetary Science Letters*, 154. 1-4: 13-24.

Wingate,M. T. D.and Giddings, J. W. 2000. Age and paleomagnetism of the Mundine Well dyke swarm, Western Australia: implications for an Australia-Laurentia connection at 755 Ma. *Precambrian Research* 100: 335-354.

Wingate, M. T. D., Pisarevsky, S. A. and Evans, D. A. D. 2002. Rodinia connections between Australia and Laurentia: no SWEAT, no AUSWUS? *Terra Nova* 14. 2: 121-128.

Zedgenizov, D. A., Kagi, H., Shatsky, V. S. and Sobolev, N. V. 2004. Carbonatitic melts in cuboid diamonds from Udachnaya kimberlite pipe, Yakutia; evidence from vibrational spectroscopy. *Mineralogical Magazine* 68: 6173.

Zhao, X., Roberts,A. P., Heslop, D.,Paterson, G.A., Li, Y., and Li, J. 2017. Magneticdomain state diagnosis using hysteresisreversal curves, *Journal of Geophysical Research: Solid Earth* 122: 4767–4789, doi:10.1002/2016JB013683.

Zijderveld, J. D. A., 1967. *A.C. demagnetization of rocks: analysis of results*. In: Collinson, D.W., Creer, K.M. (Eds.), Methods in Paleomagnetizm. Elsevier, Amsterdam, 254–286.

Zinin, P. V., Huss, G. R., Sharma, S. K., Krot, A. N., and Bonal, L. 2007. Raman spectroscopic study of Roosevelt County (RC) 075 chondrite. 8th Lunar and Planetary Science Conference, *Lunar and Planetary Science* XXXVIII, League City, Texas. LPI Contribution no. 1338, p. 2223.

APPENDIX 1

Foliation (equidistant, stereographic, orthographic and equal area), Lineation (equidistant, stereographic and orthographic) and equal area circular chart of Granite 2

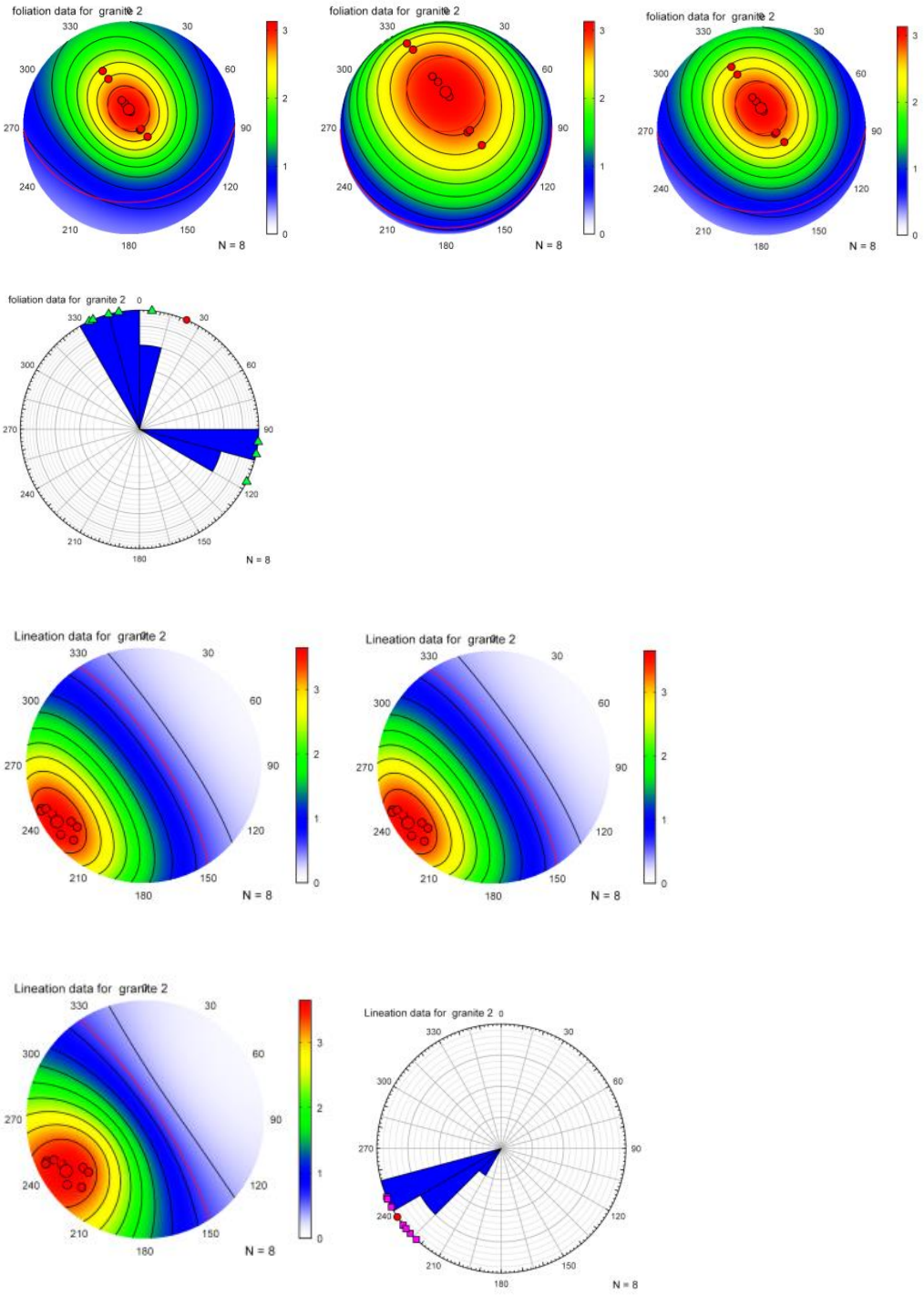

APPENDIX 2

(a-b) Intensity (P) and shape parameter for Charnockite, (c-d) Intensity (P) and shape parameter for Granite 2 and (e-f) Intensity (P) and shape parameter for Banded gneiss respectively

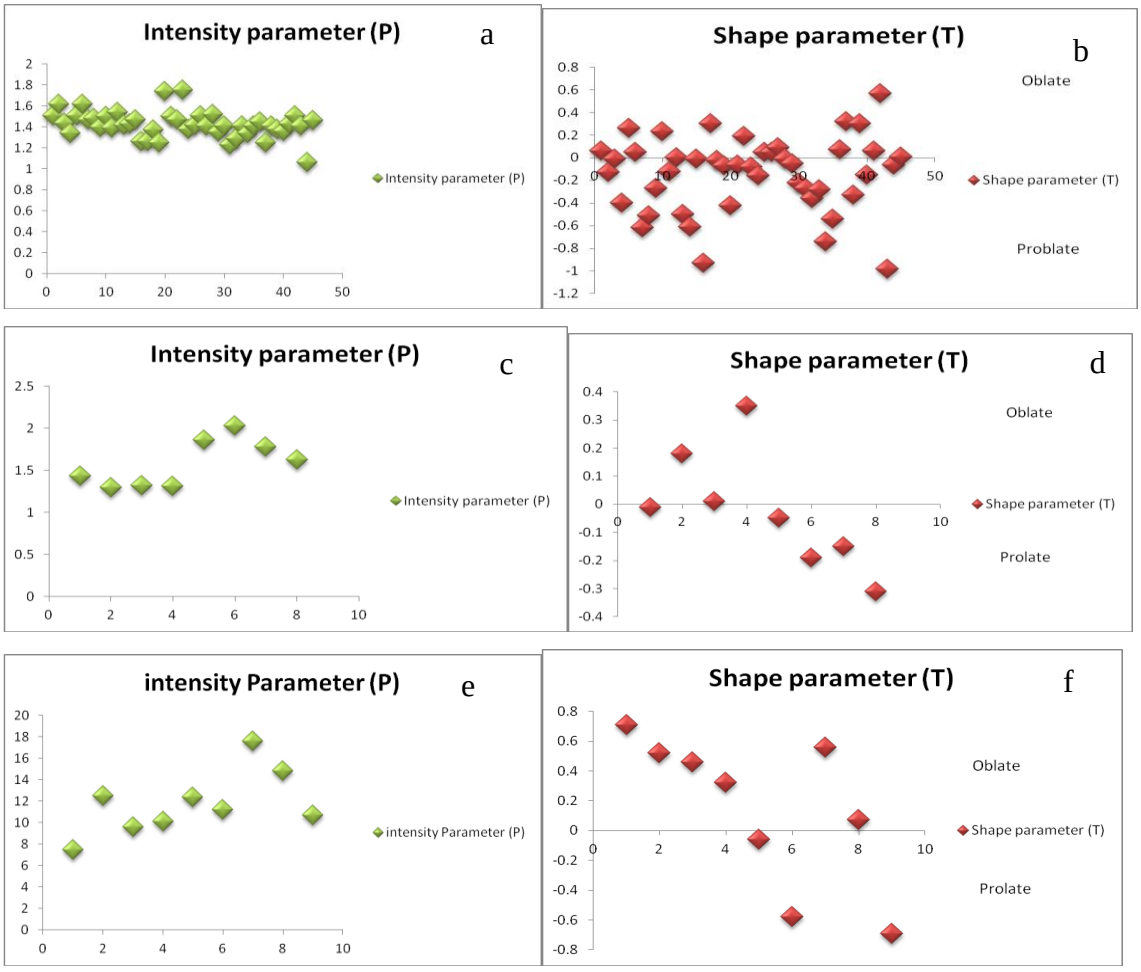

APPENDIX 3

Representative Zijderveld orthogonal directions using Remasoft (Chadima and Hrouda,2003**)**

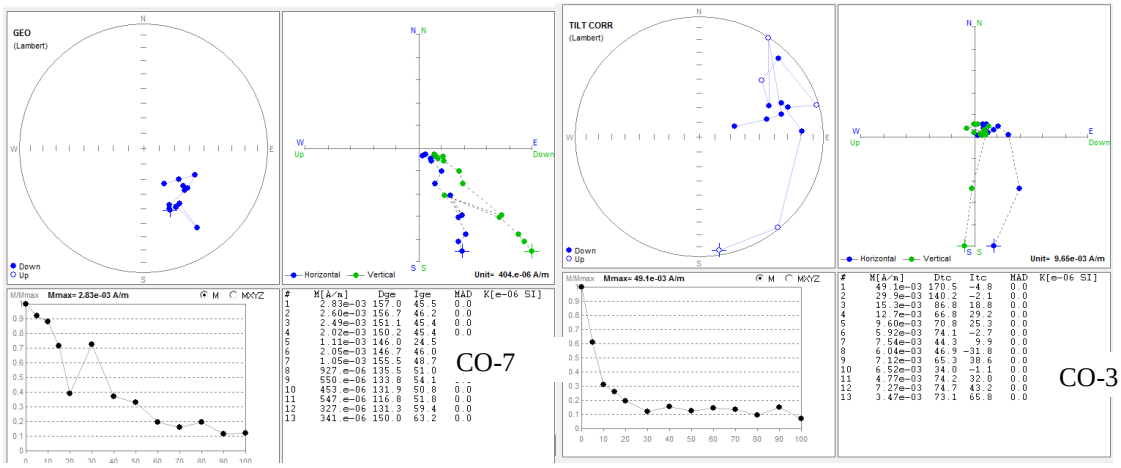

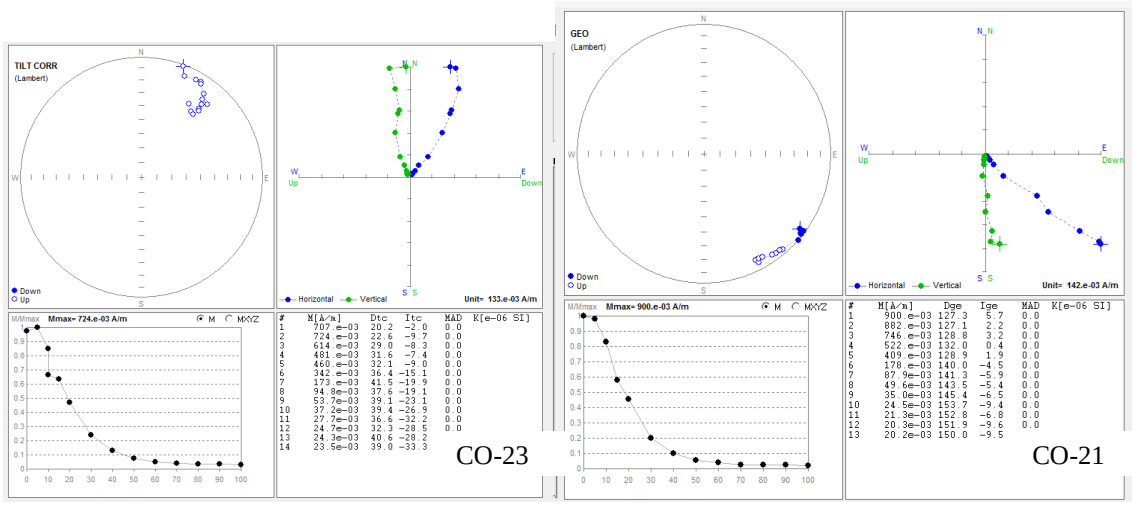

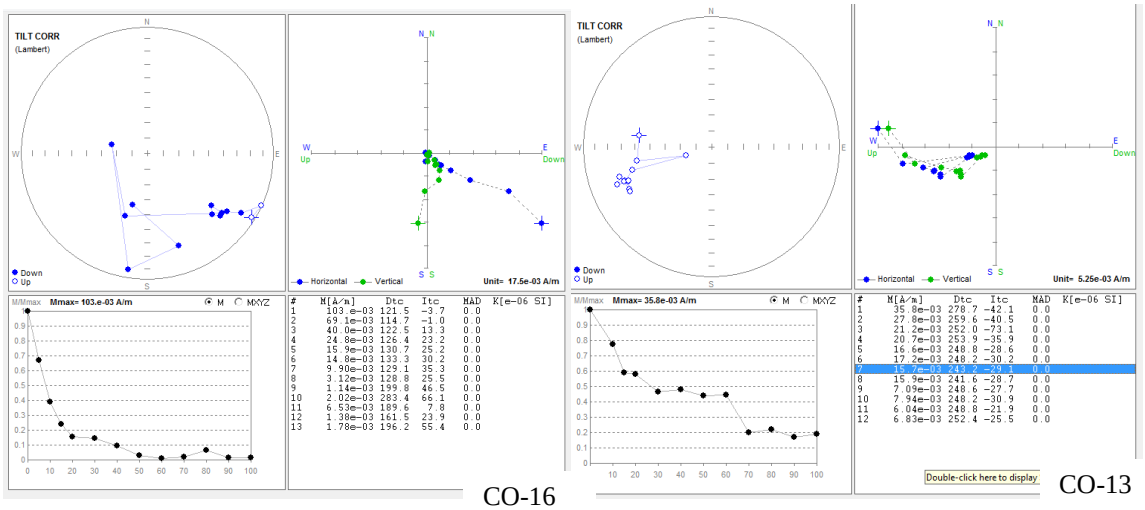

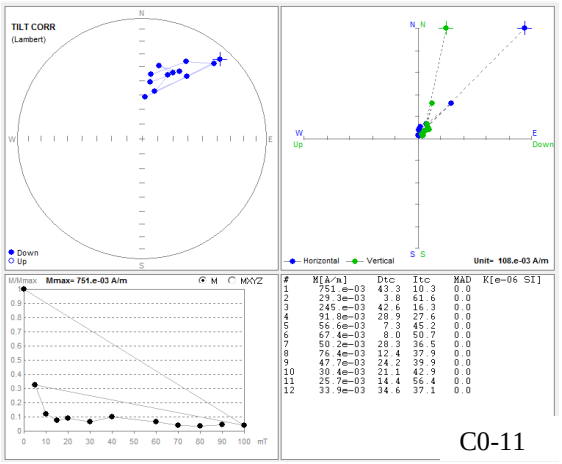
TILT CORR
(Lambert)
N
W
E
S
Down
Up
N N
W
Up
E
Down
S S
Horizontal
Vertical
Unit= 108.e-03 A/m
M/Mmax
Mmax= 751.e-03 A/m
M
MXYZ
0 10 20 30 40 50 60 70 80 90 100 mT
M[A/m] Dtc Itc MAD K[e-06 SI]
1 751.e-03 43.3 10.3 0.0
2 29.3e-03 3.8 61.6 0.0
3 245.e-03 42.6 16.3 0.0
4 91.8e-03 29.9 27.6 0.0
5 56.6e-03 7.3 45.2 0.0
6 67.4e-03 8.0 50.7 0.0
7 50.2e-03 28.3 36.5 0.0
8 76.4e-03 12.4 37.9 0.0
9 47.7e-03 24.2 39.9 0.0
10 30.4e-03 21.1 42.9 0.0
11 25.7e-03 14.4 56.4 0.0
12 33.9e-03 34.6 37.1 0.0

C0-11

APPENDIX 4

Chemical analysis of granitoids from southwestern Nigeria (ICPMS)

Major& Trace	Bgn eiss	Gneiss 2	Ggn eiss	Gra nite	Quart zite	Mgn eiss	Bgn eiss	gr.dio rite	MG
A/CNK	1.26	1.16	0.88	1.02	2.52	1.02	0.89	1.36	1.24
Cs(ppm)	6.3	6.7	1.9	7.6	0.4	3.8	2.8	6	1.5
Rb	358	250	71	294	8.9	183	73	168	106
Ba	426	476	1035	681	24	339	606	1137	345
Pb	10	12	17	25	0.9	36	18	20	15
Sr	79	101	860	157	1	109	610	266	259
Y	3.2	5.8	17	39	9.1	11	37	37	40
Th	14	7.3	6.5	28	3.3	28	7	15	15
U	4	4.6	1.4	12	0.6	3.9	1.7	3.2	1.3
Zr	104	85	133	204	47	108	296	336	318
Hf	3	2.5	3.4	6.1	1.2	3.9	6.8	8.3	7.9
Nb	4.8	5.9	9.2	24	2.6	9.6	19	19	15
Ta	0.8	1	1.1	3.4	2.2	2.6	1.7	1.9	1.3
Zn	48	24	56	41	2.1	15	76	78	76
Cu	1.6	3	46	2.3	5.3	0	13	29	20
Ni	2.5	1.5	22	7.3	0.6	1.2	7.2	30	33
Sc	4	6.5	17	5.3	3.8	6	21	17	17
V	11	6.6	138	11	2.2	7	94	76	84
Cr	6.7	3.3	34	4	1.4	2.4	7.1	70	60
Co	8	7.6	25	14	13	16	17	22	24
Ga	27	26	20	24	1.9	16	23	24	33
La	24.96	20.54	34.61	50.25	12.34	44.1	35.8	62.49	55.6
Ce	49.57	41.38	65.14	96.46	21.01	84.17	82.24	125.53	106
Pr	6.47	4.68	7.39	10.58	2.69	9.04	11.06	15.09	12.7
Nd	23.36	15.9	26.78	35.31	9.09	28.42	43.37	54.28	42.6
Sm	4.27	3.1	4.81	7.1	1.69	4.79	8.79	9.74	6.87
Eu	0.32	0.31	1.17	0.71	0.2	0.65	2.01	1.65	1.16
Gd	2.62	2.11	3.96	6.3	1.48	3.48	7.65	7.83	5.81
Tb	0.28	0.27	0.56	1.03	0.24	0.46	1.16	1.2	0.94
Dy	0.93	1.09	2.86	5.84	1.31	2.13	6.18	6.26	5.87
Ho	0.11	0.17	0.58	1.19	0.28	0.35	1.22	1.22	1.34
Er	0.29	0.43	1.5	3.24	0.76	0.94	3.3	3.3	3.88
Tm	0.03	0.06	0.24	0.53	0.12	0.15	0.53	0.53	0.64
Yb	0.21	0.37	1.49	3.53	0.75	0.94	3.31	3.31	4.26
Lu	0.03	0.05	0.22	0.58	0.11	0.15	0.49	0.49	0.65

APPENDIX 5

Representative Geographic coordinates of sampled sites and rock types.

S/N	Longitude	Latitude	Locations
1	7.23.883	5.03.494	IGBARA OKE GRANITE
2	7.24.088	5.00.118	OWENA PORPHYRITIC GRANITE
3	7.33.593	4.52.767	ERIN IJESA GRANITE38
4	7.33.588	4.52.701	ERIN IWARAJA IJESA GRANITE
5	7.37.154	4.49.456	IFE GNEISS
6	7.29.799	4.26.398	GBONGAN
7	7.25.585	4.15.447	IKIRE APOMU ROCK
8	7.21.281	4.8.498	ASEJIRE GRANITE
9	7.21.733	4.06.981	EGBEDA GRANITE
10	7.23.767	3.47.200	APATA IBADAN MUDEGBO QUARTZITE
11	7.23.427	3.43.005	OMI- ADIO GRANITE
12	7.23.430	3.42.997	AJIBODE AUGEN GNEISS
13	7.27.685	3.53.934	AJIBODE BANDED GNEISS
14	7.27.684	3.53.934	AGBOWO OYO-RD GRANITE
15	7.27.249	3.54.998	IKWABA GRANITE
16	7.58.713	4.05.064	IYEMI
17	8.17.508	4.21.068	GBEDE BIF
18	7.58.697	4.05.054	ABOGUNDE OGBOMOSO GRANITE
19	7.53.610	4.26.356	ILOGBO OSOGBO RD GRANITE
20	7.45.377	4.33.949	EFFON ALAAYE PSAMMITE
21	7.41.988	4.53.306	ITAORE QUARTZITE RIDGE
22	7.43.723	4.57.301	ERIO EKITI PORPHYRITIC GRANITE
23	7.44.049	4.59.829	IYIN EKITI GRANITE
24	7.40.724	5.10.411	ODO EKITI AMPHIBOLITE
25	7.40.801	5.11.161	IYIN EKITI QUARTZOFELDSPATHIC GRANITE
26	7.40.314	5.11.648	FEDPOLY RD ADO EKITI
27	7.36.804	5.14.688	ADO IMESI RD
28	7.36.814	5.20.663	AGBEWA STR ALONG FEDPOLY RD CHARNOCKITE
29	7.33.678	5.34.434	IMESI EKITI BANDED GNEISS
30	7.33.678	5.34.434	IMESI EKITI BANDED GNEISS
31	7.38.161	5.56.577	AKUNU CHARNOCKITE
32	7.38.161	5.56.60	AKUNU GRANITE GNEISS
33	7.38.258	5.56.90	AKUNU GREY GNEISS
34	7.38.258	5.56.925	OKEAGBE GRANITE GNEISS
35	7.32.061	5.52.049	GRANITE GNEISS
36	7.32.087	5.51.224	PEGMATITE
37	7.33.126	5.52.310	BANDED GNEISS

APPENDIX 5

Representative coordinates of sampled sites and rock types continued

S/N	longitude	Latitude	Locations
38	7.31.947	5.53.288	GRANITE
39	7.38.143	5.45.56	OKEAGBE CHARNOCKITE
40	7.38.336	5.45.25	OKEAGBE CHARNOCKITE
41	7.36.515	5.46.454	ERUSU GRANITE GNEISS
42	7.40.549	5.45.38	OYIN GRANITE
43	7.38.142	5.45.562	OKEAGBE CHARNOCKITE
44	7.40.549	5.45.38	OYIN QUARTZITE
45	7.34.216	5.46.9	ARIGIDI OKEAGBE RD CHARNOCKITE /GRAN-GNEISS
46	7.36.515	5.46.454	ERUSU GRANITE
47	7.42.42	5.58.39	PORPHYRITIC GRANITE
48	7.58.06	5.58.032	FINE GRAINED &COARSE GRAINED CHARNOCKITE
49	7.43.15	5.59.17	GREY GNEISS
50	7.42.36	5.58.32	FOLIATED CHARNOCKITE
51	7.4	5.56	GNEISS
52	7.39	5.55	GRANITE GNEISS
53	7.16.36	5.5.34	GREY GNEISS
54	7.17.45	6.5.50	GRANITE
55	7.14.46	6.4.6	PHYLLITE NEAR IGARRA
56	7.24.721	5.43.633	ETIORO GNEISS
57	7.16.721	5.37.657	OWO-AGO PANU GNEISS
58	7.16.587	5.14.519	AKURE PORPHYRITIC GRANITE
59	7.16.589	5.14.519	AKURE PORPHYRITIC GRANITE
60	7.16.587	5.14.537	SHASHA AKURE CHARNOCKITIC GRANITE
61	7.16.587	5.14.537	SHASHA AKURE CHARNOCKITIC GRANITE
62	7.16.606	5.14.541	SHASHA AKURE GRANITE GNEISS
63	7.13.940	5.13.761	IGATORO AKURE AUGENGNEISS
64	7.14.010	5.14.223	IGBATORO OPP CUSTOM CHARNOCKITE
65	7.132.938	5.13.737	IGBATORO AUGEN GNEISS
66	7.15.377	5.10.863	ALAGBAKA DOME GRANITE
67	7.24.747	5.43.615	AYEGUNLE OKA GNEISS
68	7.24.721	5.43.633	ETIORO GNEISS
69	7.16.131	5.10.061	BTO AKURE CHARNOCKITE
70	7.17.559	5.09.135	FUTA GRANITE
71	7.16.514	5.9.614	ODA ROAD CHARNOCKITE
72	7.12.259	5.10.704	OKEARO IDANRE ESTATE GRANITE
73	8.15.06	4.21.291	GRANITE GNEISS
74	8.15.564	4.21.404	BANDED GNEISS
75	8.16.227	4.23.387	AMPHIBOLITE
76	8.16.82	4.23	GRANITE

APPENDIX 5

Representative coordinates of sampled sites and rock types continued

S/N	Longitude	Latitude	Locations
77	7.45.48.5	4.23.24.6	IWO SHEET CHARNOCKITE
78	7.25.56.4	4.24.39.2	IWO SHEET CHARNOCKITE
79	7.46.03.4	4.24.30.1	IWO SHEET BANDED GNEISS
80	7.46.09.6	4.24.30.1	IWO SHEET GRANITE GNEISS
81	7.46.09.6	4.25.24.5	IWO SHEET GNEISS
82	7.53.5	4.18.55	EJIGBO MIGMATITE BIOTITE GNEISS
83	7.08	4.52	ILE-OLUJI MIGMATITE BIOTITE GNEISS
84	7.25	4.49	IPERINDO GRANITE GNEISS
85	7.34.5	4.48.5	IROBU GRANITE GNEISS
86	7.55	4.42	IKIRUN GRANITE GNEISS
87	7.46	4.23	AWO CHARNOCKITE
88	7.27.4	4.41.5	IFEWARA QUARTZITE
89	7.35	5.02	QUARTZITE EFFON ALAYE
90	7.36	5.12.5	PORPHYRITIC GRANITE
91	7.04	5.06.5	IDANRE PORPHYRITIC GRANITE
92	7.31	5.05.5	IGBARA ODO MIGMATITE GNEISS
93	7.35	5.43.5	OGBAGI MIGMATITE HORNBLENDE GNEISS
94	7.42	5.54	AJOWA MIGMATITE GNEISS
95	7.31.5	5.45	IKARE MIGMATITE GNEISS
96	7.07.55	3.22.55	ABEOKUTA PORPHYRITIC GRANITE
97	7.25.5	3.17.55	IGBOORA AMPHIBOLITE
98	7.52.1	3.56	OYO BIOTITE GRANITE GNEISS
99	7.33	3.15.50	TAPA BIOTITE GRANODIORITE
100	7.36.501	3.26.55	LANLATE BIOTITE GRANITE GNEISS
101	7.32	3.56.501	MONIYA MIGMATITE GNEISS
102	7.38	3.57.55	IKEREKU GNEISS
103	7.29	4.32.501	IFE GNEISS
104	7.49	5.04	IJERO EKITI GNEISS
105	7.42.10	5.00.501	ERIO EKITI PORPHYRITIC GRANITE
106	7.5.551	5.21	AIYEDE EKITI PORPHYRITIC GRANITE
107	7.48.101	5.23.512	OSIN EKITI CHARNOCKITE
108	7.3	5.14.203	IKERE EKITI PORPHYRITIC GRANITE
109	7.58	5.33.511	OKE-AKO EKITI GRANITE GNEISS

APPENDIX 6: Magnetic mineralogy

Sample	low coercivity component				low coercivity component				High coercivity component				Hematite component			
Granite	contr %	SIRM, A/m	B1/2 Mt	DP log mT	contr %	SIRM, A/m	B1/2 Mt	DP log mT	contr %	SIRM, A/m	B1/2 Mt	DP log mT	contr %	SIRM, A/m	B1/2 Mt	DP log mT
1	45	1,25E-03	10	12,00	91	9,80E-02	31,6	0,32	0				0			
2	9	1,00E-02	6,3	0,38	43	3,00E-02	28,2	0,28	7	2,00E-04	56,2	0,4	34	9,50E-04	281,8	0,30
3	10	1,00E-02	10,0	0,40	80	8,00E-02	37,2	0,33	57	4,00E-02	79,4	0,28	14	4,00E-04	1584,9	0,20
4	5	9,00E-03	4,0	0,50	29	5,30E-02	28,2	0,35	66	1,23E-01	69,2	0,30	10	1,00E-02	316,2	0,30
BGG/Sample|																
1	10	4,00E-03	10,0	0,45	10	4,00E-03	20,0	0,25	90	3,55E-02	42,7	0,33	0			
2	5	1,80E-03	10,0	0,40	2	7,00E-04	20,0	0,50	85	3,30E-02	66,1	0,32	0			
3	3	7,00E-05	1,8	0,50	41	1,60E-02	30,2	0,28	97	2,23E-02	58,9	0,38	0			
4	4	1,50E-03	2,5	0,90	44	1,50E-02	28,2	0,28	74	2,70E-02	79,4	0,35	20	7,30E-03	794,3	0,38
5	10	4,00E-03	8,9	0,35	47	5,20E-02	22,4	0,27	46	1,80E-02	63,1	0,27	3	1,00E-03	316,2	0,3
6	7	1,50E-04	3,2	0,80	46	1,10E-03	17,8	0,30	93	2,00E-03	39,8	0,33	0			
7	9	1,00E-02	5,6	0,30	41	7,50E-03	25,1	0,30	43	4,80E-02	52,5	0,28	1	1,00E-03	251,2	0,1
8	8	2,00E-04	3,2	0,20	28	1,50E-02	28,2	0,28	46	1,10E-03	83,2	0,25	0			